Design and synthesis of inhibitors of the non-canonical NF-κB pathway for the treatment of prostate and pancreatic cancer.

A thesis submitted to the University of Strathclyde

for the degree of Doctor of Philosophy

by

Chris West

2016

Strathclyde Institute of Pharmacy and Biomedical Sciences

University of Strathclyde

Glasgow

Declaration of authenticity and author's rights

This thesis is the result of the author's original research. It has been composed by the author and has not been previously submitted for examination which has led to the award of a degree.

Signed:

Date:

Acknowledgements

There are many people to whom I owe enormous thanks and without whom this work may have never happened.

Firstly, my thanks go to my supervisor Professor Simon Mackay for the opportunity to work within his research group and for his support and guidance throughout my PhD in helping me to develop my research skills. Also to Professor Nick Tomkinson; for the years of invaluable problem sessions and encouragement which have proved so beneficial to me. My heartfelt thanks to you both.

I would like to thank all the members, past and present, of Simon's research group who have so graciously and ably assisted me during my studies in so many ways: Ms Aisha Alsfouk, Dr Nahoum Anthony, Dr Jessica Baiget, Dr Giacomo Berretta, Dr Dave Breen, Dr Chris Lawson and Dr Jude Huggan. Also to those in our write-up room, particularly Mr Tony Vassileiou and Dr Murray Robertson, who have contributed to making this such an enjoyable place to work.

My thanks must also go to Mr Craig Irving and Mrs Pat Keating for NMR and mass spec analysis, to Mrs Louise Young and Ms Gráinne Abbott for their help with my biochemical assays, and to all the members of the biology team who have provided me with data. A huge thank you to you all for your invaluable contributions.

A massive thank you to my parents who have supported me through all my studies. I am truly thankful for all your love and encouragement over these many years.

Finally, my greatest thanks must go to my devoted wife Laura, who has patiently endured my eternal studentship, has been a constant encouragement and who has removed more commas from this work than I thought possible! There are no words to say how grateful I am for everything you have done so I will simply say "thank you".

Table of Contents

Table of Figures

List of Abbreviations

^{13}C NMR	**Carbon nuclear magnetic resonance**
^{1}H NMR	**Proton nuclear magnetic resonance**
B:	**Generic base. Behaves as a proton acceptor/lone pair donor**
Boc	**Di-*tert*-butyl dicarbonate**
DEPTQ	**distorsionless enhancement by polarization transfer including the detection of quaternary nuclei**
DMF	***N,N*-Dimethylformamide**
DMSO	**Dimethylsulfoxide**
DMSO-*d6*	**Deuterated dimethylsulfoxide**
dppf	**Diphenylphosphinoferracene**
dtbpf	**Di-*tert*-butylphosphinoferracene**
ESI	**Electrospray ionisation**
FTIR	**Fourier transform infrared spectroscopy**
HBA	**Hydrogen bond acceptor**
HBD	**Hydrogen bond donor**
HMBC	**Heteronuclear Multiple-Bond Correlation spectroscopy**
HRMS	**High resolution mass spectrometry**
HSQC	**Heteronuclear Single Quantum Correlation spectroscopy**
IC_{50}	**50% of maximal inhibitory concentration**
***J*MOD**	***J*-modulated spin echo**
LC-MS	**Liquid chromatography - mass spectrometry**
LRMS	**Low resolution mass spectrometry**
NIK	**NF-κB-inducing kinase**
NIS	**N-iodosuccinimide**
SAR	**Structure-activity relationship**
S_NAr	**Nucleophilic aromatic substitution**
TFA	**Trifluoroacetic acid**
THF	**Tetrahydrofuran**
TLC	**Thin layer chromatography**
TPSA	**Topological polar surface area**
UV	**Ultra-violet**

Abstract

The dysregulation of the transcription factor NF-κB has been linked with multiple pathologies including cancers, inflammatory diseases and autoimmune conditions. Under basal conditions, NF-κB is held in an inactive state in the cytosol. Upon stimulation, in response to cellular stress, NF-κB translocates to the nucleus where it is able to activate gene expression. These genes include a number of pro-inflammatory cytokines, growth factors and pro-survival genes.

Targeting specifically the non-canonical NF-κB pathway with small molecule inhibitors has been suggested as a possible therapeutic intervention for prostate and pancreatic cancers. The non-canonical NF-κB pathway is highly dependent on the enzyme NF-κB-inducing kinase (NIK). This kinase is responsible for the phosphorylation of the downstream kinase IKKα which, in turn, phosphorylates the p100 protein. Proteolytic processing of p100 releases the NF-κB subunit p52 which dimerises with RelB to form the NF-κB protein complex.

This project involves the design and synthesis of small molecule inhibitors of IKKα and NIK as potential prostate and pancreatic anti-cancer compounds. A series of amidopyridines were shown to be selective inhibitors of IKKα over the related isoform IKKβ and an SAR study identified some compounds with single digit nanomolar potency against IKKα and some with greater than 500-fold selectivity for IKKα over IKKβ. Development of NIK inhibitors showed substituting the 4-position of a pyrrolopyrimidine scaffold with a 6-substituted indoline provided sub-micromolar potency against NIK. SAR was carried out on both ring systems leading to synthesis of a known NIK inhibitor which was shown to have potent cellular activity and tractable pharmacokinetic properties but poor selectivity over a wider panel of kinases. Further development led to a compound which retained good potency against NIK but with a far superior off-target profile compared to the known NIK inhibitor.

1. Introduction

Cancer is a collective name for over 100 malignant diseases involving abnormal cell growth with the potential to spread into surrounding tissues.[1] In 2012, approximately 14.1 million new cases of cancer occurred globally, resulting in around 8.2 million deaths. This accounts for nearly 15% of all human deaths.[2]

In 2000, Douglas Hanahan and Robert Weinberg published a seminal paper entitled "The Hallmarks of Cancer", in which they proposed that each of the multitude of observable pathologies could be assigned to one of six categories: tissue invasion and metastasis; limitless replicative potential; sustained angiogenesis; evasion of apoptosis; self-sufficiency in growth signals and insensitivity to anti-growth signals.[3] This was followed in 2011 with a refined view which added the two emerging hallmarks of reprogramming energy metabolism and evading immune destruction, and proposing that underlying all these hallmarks are two "enabling characteristics" -namely tumour promoting inflammation and genomic instability.[4]

An appreciation of these hallmarks provides two main things. Firstly, it helps to simplify a vastly complex topic and aid understanding of how certain cancers exert their influence and how it might be best to treat them. Secondly, it provides insight into how to determine the importance of a potential target within the cancer setting and what assessments would be appropriate to prove this. This means that before a biological target can be chosen for cancer treatment, it must first be shown to have some effect on one or more of these hallmarks. Once this has been demonstrated then there must also be some way to quantify the effect of up or downregulating this target.

1.1. Introduction to pancreatic cancer

Pancreatic cancer is the 12th most commonly diagnosed type of cancer worldwide, with an estimated 338,000 new cases each year.[5] Pancreatic cancers are broadly placed into two categories: endocrine and exocrine, with exocrine tumours being considerably more common. The early stages of pancreatic cancer are often asymptomatic and thus the disease is generally advanced when diagnosed.[6] Symptoms vary at later stages between endocrine and exocrine tumours. Exocrine tumours often result in very vague symptoms such as stomach or back pain and weight loss and are therefore difficult to diagnose. More

serious symptoms can be diabetes, blood clots and jaundice. Endocrine tumours are sometimes easier to diagnose as, in around a third of cases, the tumour produces hormones. The symptoms experienced differ based on the hormone produced. There are five main classes of endocrine tumour: insulinomas; gastrinomas; somatostatinomas; VIPomas and glucagonomas.[7]

The difficulty in diagnosing pancreatic cancer arises because there are no well assessed biomarkers for which to test. Two markers which are screened for are carcinoembryonic antigen (CEA) and carbohydrate antigen 19-9 (CA19-9), however these markers are unreliable and care must be taken in interpreting results.[8,9] As blood tests are not reliable, they are usually followed up with ultrasound, CT or MRI scans, endoscopy or laparoscopy.[10]

Generally, due to the fact that pancreatic cancer is normally diagnosed in the latter stages, there are very limited treatment options currently available; and those treatments given are often palliative rather than curative. In the case of most stage 1 (localised tumour less than 2 cm diameter) and some stage 2 (localised tumour greater than 2 cm diameter) or endocrine tumours, a curative surgery may be attempted. For more advanced cancer, surgery may still be used to relieve symptoms either by removing some of the tumour or by inserting a stent to unblock the bile duct - a common side effect of pancreatic cancer.[11,12] Radiotherapy is rarely used as a treatment for pancreatic cancer but is occasionally used - again usually for relief of symptoms. Another treatment that is available is chemotherapy, using either gemcitabine or 5-fluorouracil, but, again because of late diagnosis, this is usually only for around 6 months. These are discussed further in section 1.1.1.

1.1.1. Current chemotherapeutic interventions in pancreatic cancer

1.1.1.1. Gemcitabine

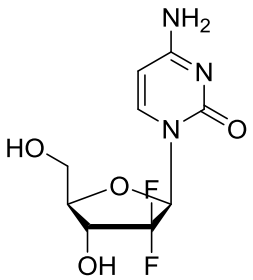

Figure 1. Structure of gemcitabine.

Gemcitabine is a nucleoside analogue which arrests DNA replication through two different mechanisms. The first mechanism occurs by gemcitabine triphosphate replacing the cytidine nucleotide during replication. The addition of this faulty nucleotide allows for chain elongation by only one nucleotide resulting in apoptosis. The second mechanism is through inhibition of ribonucleotide reductase (RNR).[13] In this mechanism, gemcitabine diphosphate binds irreversibly to the RNR active site, inhibiting the production of the deoxyribonucleotides necessary for DNA replication and repair and leading to apoptosis.[14]

1.1.1.2. 5-Fluorouracil

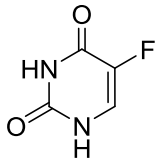

Figure 2. Structure of 5-fluorouracil.

5-Fluorouracil (5-FU) is a pyrimidine analogue inhibitor which principally works through irreversible inhibition of thymidylate synthase. This blocks the synthesis of thymidine, arresting DNA replication and either forcing the cell into apoptosis or causing thymineless death.[15] Although gemcitabine has a superior response rate amongst patients, studies have shown that when used in combination with other drugs (notably cisplatin),[16] 5-FU still has a place in pancreatic cancer treatment.[17]

1.2. Introduction to prostate cancer

Prostate cancer is the fourth most common cancer worldwide and second most common form of cancer among men; with more than 1.1 million new cases in 2012, accounting for 15% of all male cancers.[18] Prostate cancer is largely asymptomatic in its early stages. As the cancer advances it often starts to put pressure on the urethra resulting in symptoms such as difficulty passing urine or having to urinate more frequently and, in rare cases, pain passing urine or blood in the urine.[19]

Prostate cancer initially presents in a hormone, or androgen, responsive state and usually responds well to androgen receptor (AR) antagonists. After 2-3 years of androgen deprivation treatment, the cancer can become unresponsive and enter a castrate resistant stage (CRPC). Current therapies for CRPC increase median survival rate by only 2-4 months and therefore treatment at this stage is largely palliative.[20] Previously considered to be totally hormone independent by this stage, it has now been shown that, although now not

responsive to castration treatment to reduce androgens by chemical or surgical methods, CRPC still has a dependence on hormones for androgen receptor activation.[21] As such, AR is emerging as a key target in CRPC treatment.[22]

Prostate cancer has several associated risk factors. These include race, family history and diet; but it is most closely correlated with age.[23] Prostate cancer is rarely diagnosed in men below the age of 65, with 22% of cases being diagnosed in men over 80. The late onset of the disease is one reason for the apparent lack of symptoms. Late onset also means that many men do not undergo any therapy and often die *with* prostate cancer rather than *of* prostate cancer.

One of the biggest advances in prostate cancer treatment came in 1990 with the introduction of prostate specific antigen (PSA) screening. This is a quick, and comparatively cheap, test for the PSA biomarker; a protein produced by the prostate. Whilst basal levels of PSA do increase slightly with age, an increased level is also associated with prostate problems. Due to the fact that increased PSA levels are not necessarily indicative of prostate cancer, there are conflicting opinions on whether the PSA tests are the reason for decreasing mortality since 1990, or if this is coincidental or related to the fact that disease treatment has improved in general.[23–25] Regardless of whether or not the PSA test itself is the reason for the decreasing mortality rate, it is likely that more cases of prostate cancer are being followed up with more determinative tests due to the ease and low-risk of the test. These can include digital rectal examinations (DRE), biopsy, MRI or CT scans.

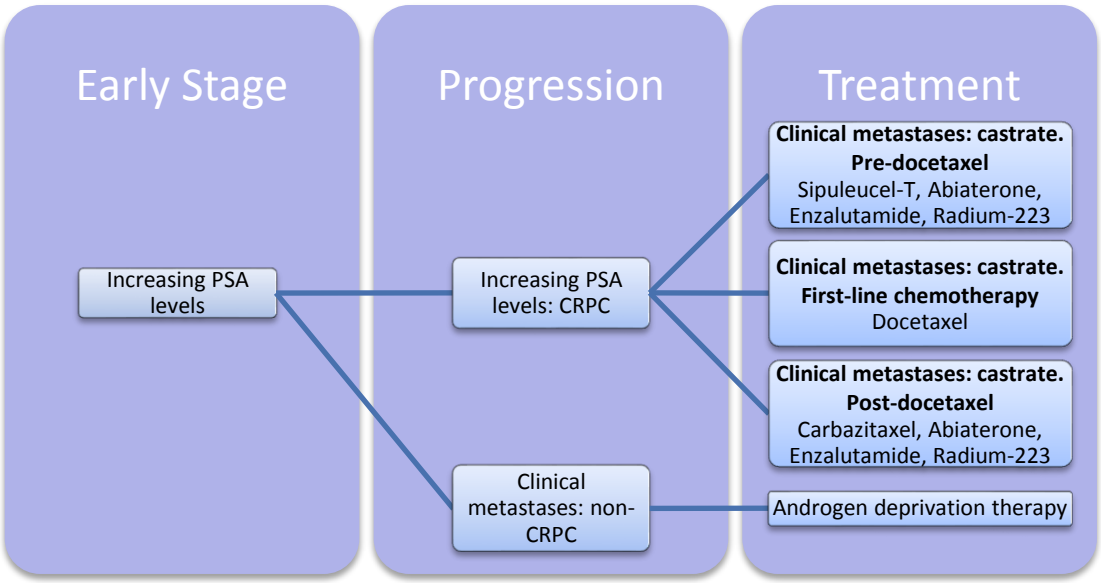

Figure 3. Clinical progression of prostate cancer. Adapted from.[26]

There are multiple treatments available for prostate cancer and these are dependent on the stage of the cancer.[26] For localised prostate cancer, common interventions include radical prostatectomy, radiotherapy, permanent seed brachytherapy, high-intensity focused ultrasound (HIFU) and cryotherapy.[27]

1.2.1. Current chemotherapeutic interventions in prostate cancer

There are several classes of chemotherapeutics currently used in the treatment of prostate cancer. This section will briefly discuss some of the major classes of drugs in current chemotherapy.

1.2.1.1. Gonadotropin-releasing hormone agonists

Gonadotropin-releasing hormone (GnRH) agonists are used during the androgen responsive stage of prostate cancer. This class of chemotherapeutics includes leuprolide, buserelin, histrelin, goserelin, nafarelin, triptorelin and deslorelin. These are all based on a natural decapeptide with specific modifications which enhance pharmacokinetic stability.[28] They act by suppressing testosterone and dihydrotestosterone; both of which are required by the tumour cells to grow.[29]

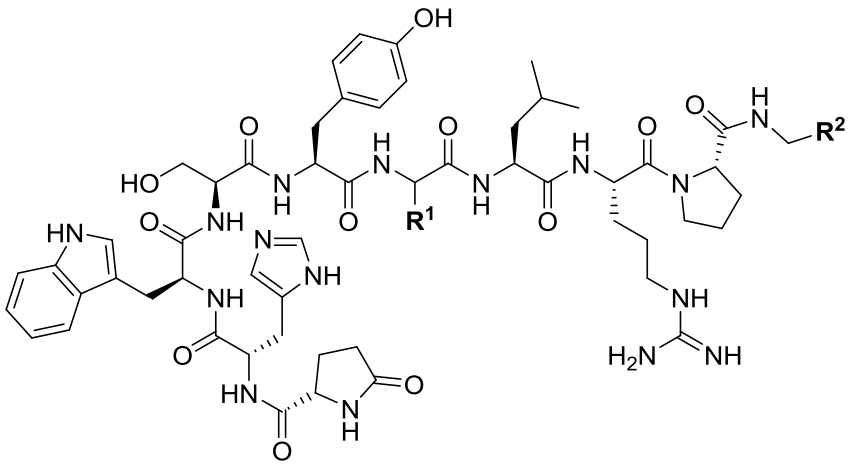

Figure 4. Structure of representative GnRH agonist leuprolide (R^1 = (*R*)-*i*-butyl, R^2 = H) as compared to natural decapeptide ligand ($R^1 = H_2$, $R^2 = C(O)NH_2$).

1.2.1.2. Androgen receptor antagonists

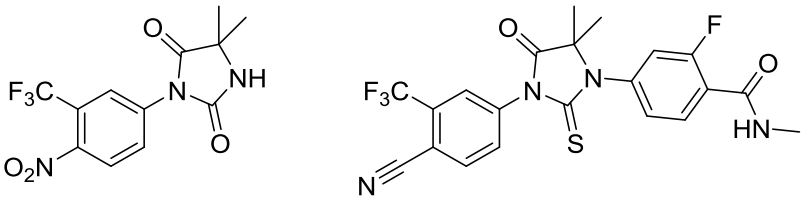

Figure 5. Structures of nilutamide (left) and enzalutamide (right).

Androgen receptor (AR) antagonists are a standard treatment for advanced prostate cancer and are often administered in combination with surgery. Early antagonists such as nilutamide and flutamide have been largely superseded by bicalutimide because of the improved prognosis and improved toxicological profile.[30] In 2012, enzalutamide was approved by the FDA as a treatment for CRPC.[31] Enzalutamide has been shown to convey significant advantages over bicalutimide in randomised trials and in recent years has become the gold standard amongst androgen receptor antagonists.[32] The downside of enzalutamide treatment is its cost compared to bicalutimide; with enzalutamide costing up to 50 times more per tablet, though this may be predominantly due to the production monopoly for enzalutamide.[33]

1.2.1.3. Anti-mitotic agents

There are several classes of drugs within the anti-mitotic family of chemotherapeutics. One of the main classes for use in prostate cancer is the taxane class exemplified by drugs such as paclitaxel and docetaxel. These have been shown to be active in castrate resistant prostate cancer and slightly to improve survival rates relative to anti-mitotic agents in the anthrocycline class such as mitoxantrone.[34,35]

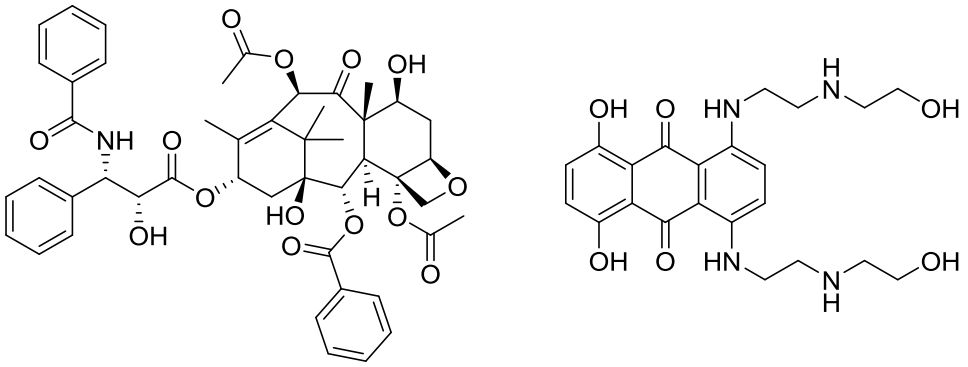

Figure 6. Structures of paclitaxel (left) and mitoxantrone (right).

1.2.1.4. Immune system activators

Cytotoxic T lymphocyte-associated antigen 4 (CTLA-4) binding antibody ipilimumab is an immune system activator currently in clinical trials in the treatment of CRPC.[36,37] CTLA-4 is involved in blocking the activation of T-cells[38] and thus the binding of this glycoprotein stops immunosuppression and, in turn, allows the body to better combat the cancer cells. Programmed Death-1 (PD-1) receptor has also been suggested as a target in CRPC treatment.[39] PD-1 activator nivolumab has been examined in a number of cancer models, including CRPC,[40] and also in combination with ipilimumab as a treatment for advanced melanoma.[41] These studies suggest a manageable safety profile and the combination approach, having shown great promise in melanoma, has been suggested as a tractable approach for CRPC.[26] Progress has been made in immunotherapy but current treatment still requires it to be administered in combination with chemotherapy.

1.3. NF-κB and NIK

Nuclear factor κB (NF-κB) is a transcription factor which is responsible for the transcription of over 180 target genes.[42] Of specific interest to oncology, these genes regulate a host of targets involved in cell survival, angiogenesis, epithelial-mesenchymal transition (leading to migration), proliferation, inflammation, invasion and metastasis.[43] NF-κB is activated in response to a diverse range of stimuli. These include, but are not limited to, inflammatory cytokines, immune-related stress, virus, UV irradiation, environmental triggers and oxidative stress.[42]

1.3.1. NF-κB activation

The mammalian NF-kB family contains five members: NF-kB1 (p105 and p50), NF-kB2 (p100 and p52), RelA (p65), RelB and c-Rel.[44] These subunits form varying combinations of dimers - most commonly p52:RelB and p50:RelA, though also many others - and translocate into the nucleus whereupon they regulate gene transcription.

1.3.1.1. Non-canonical pathway

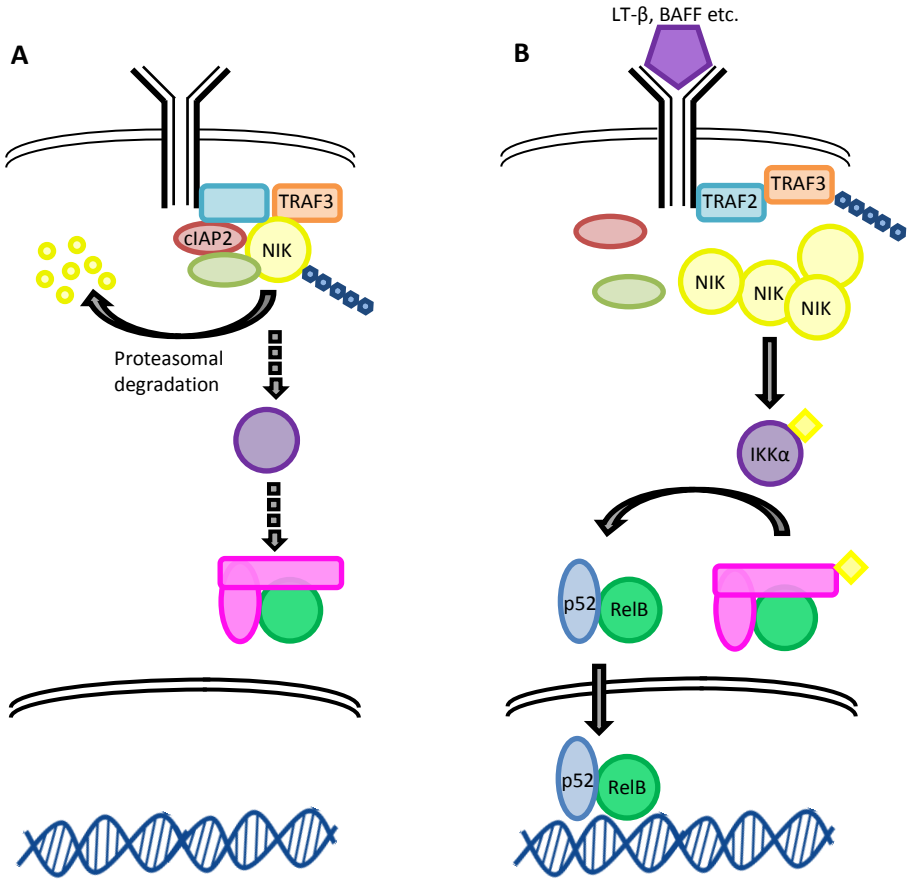

Figure 7. Panel **A** shows the non-canonical NF-κB pathway under basal conditions, with panel **B** showing activated pathway. In the absence of any stimulus NIK is held in a regulatory complex by cIAP1 & 2 and TRAF2 & 3. NIK is ubiquitinated and undergoes proteasomal degradation. As shown in panel **B**, when the pathway is activated, NIK is released from its regulatory complex and phosphorylates IKKα. This, in turn, induces processing of p100 to p52 which then dimerises with RelB. This dimer complex then translocates into the nucleus where it can regulate gene transcription.

Under basal conditions NIK is rapidly ubiquitinated and sent for proteasomal degradation; a process regulated by E3 ligases cellular inhibitors of apoptosis 1 and 2 (cIAP1/2) and TNF receptor associated factors 2 and 3 (TRAF2/3). The non-canonical NF-κB pathway is activated by a range of cytokines including, but not limited to, lymphotoxin beta (LT-β), B-cell activating factor (BAFF), receptor activator for NF-κB (RANK) and CD40.[45] Activation leads to one of two possible processes. The first process involves recruitment of TRAF proteins leading to the disassembling of the degradative complex and the subsequent release of NIK. The alternative process involves the ubiquitination and degradation of the E3 ligases and thus the release of NIK.[46] In either case, NIK is stabilised and stimulates the non-canonical pathway by phosphorylation of IKKα which in turn phosphorylates p100, the processing of which releases the p52-RelB dimer followed by nuclear translocation.[47]

1.3.1.2. Canonical pathway

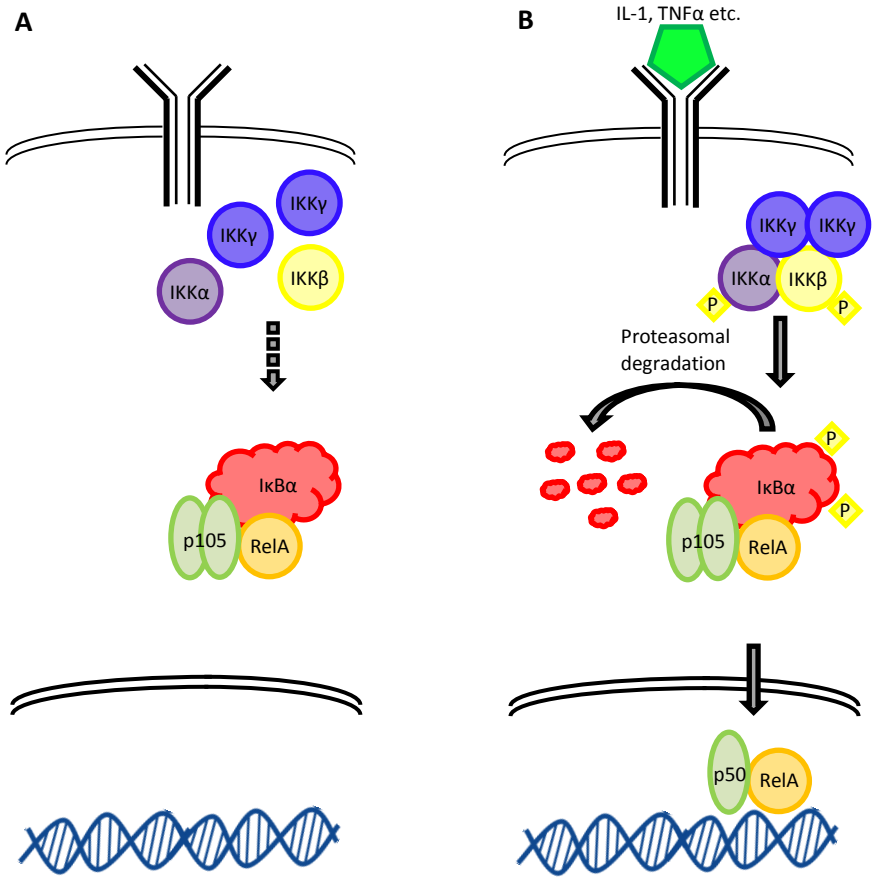

Figure 8. Panel **A** shows the canonical pathway under basal conditions and panel **B** shows pathway upon activation. With no activating influence from the IKK complex, IκBα holds the p105 and RelA subunits in an inactive complex. Upon stimulation, IKKα and IKKβ scaffold with IKKγ to form an activating complex which phosphorylates residues in the IκBα complex leading, ultimately, to its proteasomal degradation. This degradation releases p105, which is then proteolytically cleaved to form p50, and RelA. These subunits dimerise and translocate to the nucleus.

The canonical pathway NF-κB is activated by a stimulation of receptors such as tumour necrosis factor (TNF) receptors (TNFR), toll-like receptors (TLR) or T-cell receptors (TCR). On stimulation of these receptors by either TNFα or interleukin-1 (IL-1), receptor interacting protein (RIP) and TRAF2 or TRAF6 respectively bind to the receptor.[48] RIP and TRAF binding results in assembly and activation of the inhibitory-κB kinase complex (IKK) complex consisting of catalytic proteins IKKα and IKKβ and scaffolding protein NEMO (also known as IKKγ).[49] Upon phosphorylation by the IKK complex, the IκB complex - which acts to hold p65 (RelA) and p105 in an inactive state in the cytoplasm - undergoes proteasomal degradation.[50] This degradation results in the processing of p105 to p50 and subsequent release of the p50-RelA dimer. This, after nuclear translocation, is able to bind to DNA and regulate transcription.

1.3.1.3. Atypical pathway

Aside from these two pathways, NF-κB activation can also occur independently of the IKKs, or at least have atypical mechanisms of activation. There are at least 3 other known pathways and, although these have not been nearly as well described as the canonical and non-canonical pathways, it is important that they are considered nonetheless.[51] The first of these is a genotoxic stress response which involves the translocation of IKKγ to the nucleus followed by dimerisation with the kinase ATM. Upon ubiquitination this complex returns to the cytoplasm where it activates the canonical IKK complex. The other two main atypical pathways result in the translocation of the p50-RelA complex to the nucleus in much the same way as the canonical pathway does. The first route to this is as a result of hypoxia wherein an unknown tyrosine kinase phosphorylates Y42 of the IκBα complex, leading to its degradation and subsequent release of the p50-RelA dimer. The second pathway is in response to UV-induced DNA damage and involves the p38-mediated activation of the kinase CK2 which in turn phosphorylates IκBα, again, resulting in degradation and release p50-RelA.[48]

1.3.2. NIK structure

Mitogen-activated protein kinase kinase kinase 14 (MAP3K14), also known as NIK, is a 44-100 kDa serine/threonine protein kinase which is responsible for phosphorylating IKKα.[52] The full length protein consists of a negative regulatory domain (NRD), which includes a basic region (BR) and a proline-rich repeat region (PRR); the kinase domain and a non-catalytic region (NCR) where it is thought TRAF and IKKα binding occurs.[53]

Figure 9. Linear schematic of NIK structure. Adapted from.[53]

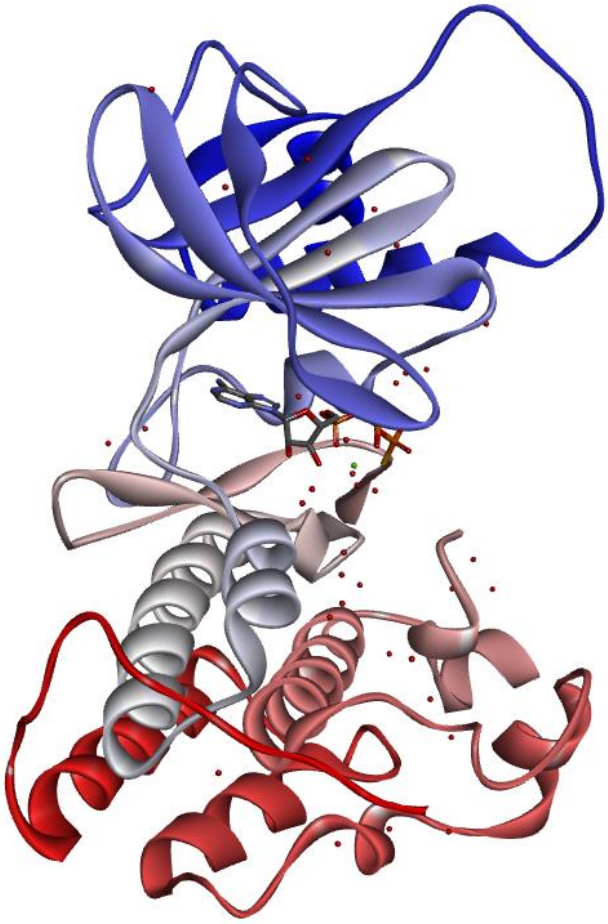

Figure 10. Ribbon structure of NIK with ATP bound in ATP binding site (PDB code 4DN5).[53] Image created using Accelrys Discovery Studio 4.0.[247]

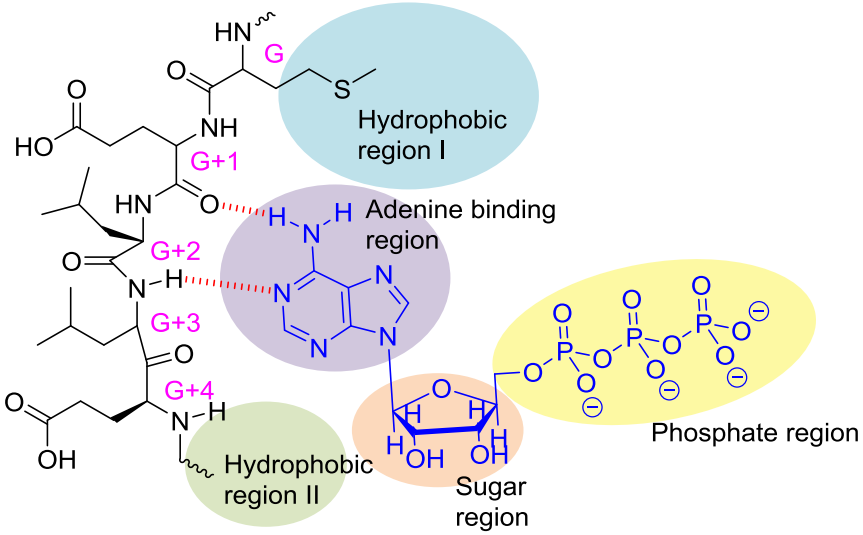

Figure 11. Schematic represeantationof NIK hinge binding region.

Like most protein kinases, the catalytic kinase domain comprises an *N*-terminal lobe and a *C*-terminal lobe joined by a 'hinge' region as shown in **Figure 10**Error! Reference source not ound.. As shown in **Figure 11**, the hinge region of NIK comprises a methionine gatekeeper, gatekeeper + 1 (G+1) glutamic acid and G+2 & 3 leucines, where G+1 and G+3 traditionally form the binding interactions with adenine when ATP is bound. The adenine binding region of NIK is very hydrophobic, comprising leucine and valine moieties.

Whilst being structurally and functionally similar to most other kinases, NIK has a significant dynamic difference to many kinases. In general, there is a perceived "active" and "inactive" state adopted by kinases typified by the so-called "DFG in/out" states respectively.[54] Due to the fact that proteins are dynamic entities, these are extremes of a spectrum of conformations rather than binary modes, but they are nonetheless useful generalisations to describe small molecule binding. The inactive, "DFG out", protein can adopt a range of conformations since the Asp-Phe-Gly motif makes no specific interactions to lock it in place. When the DFG loop moves to the active "in" state, however, far fewer conformations are available to the protein. NIK has so far not been observed to adopt this "out" state. The transition to the active form is generally modulated by phosphorylation of a residue in the activation loop, however available crystal structures show the protein in its active state without evidence of phosphorylation.[53,55] This structural elucidation provides useful insight into appropriate methods of targeting NIK.

1.4. Role of NIK in cancer

NIK mediated NF-κB activation has been shown to be a key driver of oncogenic progression in, among many others, prostate and pancreatic cancer.[56] Non-canonical NF-κB is involved in the transcription of a wide variety of genes, including those which code for cyclooxygenase-2 (COX2), TNF, interleukin1 (IL-1), lymphotoxin β (LT-β), CD40 and B-cell associated factor (BAFF), which have been shown to be involved in tumour promotion, angiogenesis, metastasis and increased cell survival[44,57,58] and also to be upregulated in multiple cancer settings.[42,59] The activation of NF-κB has been linked to increased chemotherapeutic resistance and the overexpression of NF-κB proteins themselves has been linked to the development of cancer, blocking of apoptosis and promotion of cell proliferation.[42]

Tumour cells need oxygen to survive and thus the growth of tumours, particularly solid state tumours, can be limited by a poor blood supply. Angiogenic growth factors such as VEGF and MCP-1, both of which are regulated by NF-κB, are required for effective tumour growth. For metastasis to occur, cancerous cells must be able to pass in and out of the vessel walls so they can be transported to other parts of the body. Only specific molecules are able to mediate the ability of other molecules to cross vessel walls, and these are expressed in response to signals from inflammatory cells and tumour cells. These specific molecules include ICAM-1 (Intercellular Adhesion Molecule-1), ELAM-1 (Endothelial Cell Leukocyte Adhesion Molecule-1) and VCAM-1 (Vascular Cell Adhesion Molecule-1), all of which are thought to be expressed in response to the activation of NF-κB.[60,61]

NIK levels in pancreatic cancer cells have been shown to be upregulated. Experiments by Storz *et al.* showed that, relative to normal human pancreatic ductal epithelial (HPDE) cells, NIK was overexpressed in multiple pancreatic cancer cell lines.[62] In particular, active p-T559 was highly expressed in seven of nine tested cell lines. Gene silencing experiments using shRNA against NIK have shown in pancreatic cancer models that NF-κB induction is almost halved and, as a result, rate of cell proliferation is decreased by the same ratio.

Non-canonical NF-κB signalling has also been shown to be a key player in prostate cancer. Work published by Lessard *et al.* showed a strong correlation between nuclear RelB and prostate cancer patients' Gleason score; a grading system categorising the overall health of prostate cells.[63] Whilst other Rel proteins were also found, RelB was the only one to show a strong correlation, suggesting that although the canonical pathway is involved to an extent in the progression of prostate cancer, the main driver is the non-canonical pathway through dysregulation of NIK.

1.5. Strategies to target the non-canonical pathway

To date, there are no known therapies designed to specifically target the non-canonical NF-κB pathway in any clinical setting. Several interventions have been suggested to target the non-canonical pathway for multiple indications including prostate and pancreatic cancer and some of these will be discussed in this section.

1.5.1. Pancreatic cancer

The first way in which pancreatic cancer could be targeted through the non-canonical pathway is by NIK inhibitors.[64] Whilst in principle this should be an effective method of intervention, past efforts have proved unsuccessful: mainly due to either a lack of specificity or lack of effectiveness *in vivo*.[65] At the outset of this project, a series of NIK inhibitors in the pyrazolo[4,3-c]isoquinoline series had been reported, however these showed no specificity for NIK as the canonical NF-κB pathway was also affected.[66,67] Many more NIK inhibitors have been published since the outset of this work and these will be discussed later in this thesis.

TRAF2, as shown in **Figure 7**, is involved in the regulation of NIK. TRAF2 downregulation has been shown to be closely associated with NIK accumulation in pancreatic ductal adenocarcinoma (PDAC).[62] Stabilisation of the TRAF2, either directly in its complex with TRAF3 and cIAPs or by inhibition of cIAPs to limit receptor sequestration of the complex upon stimulation, has been suggested as an intervention upstream of NIK.[62] The caveat to this is that TRAF2 has a dual role in the canonical versus non-canonical NF-κB pathways,

"whereby in the canonical pathway TRAF2 and IAPs participate in nondegradative ubiquitination reactions necessary for the assembly of the NF-κB-activating complex, while they participate in NIK degradation in the non-canonical pathway. Thus the outcome of IAP inhibition on the balance and dynamics of NF-κB activity is difficult to predict."[64]

This has been demonstrated with the TRAF2 inhibitor P_3-25 which works by disrupting TRAF2-TANK interactions which in turn decreases TRAF2-dependant IKK activity[68] and thus it is difficult to predict the consequences of interfering with TRAF and IAP signalling.

TGF-β–activated kinase 1 (TAK1), in conjunction with its binding partner TGF-β activated kinase binding protein 1 (TAB1) is responsible for, amongst other things, activation of the non-canonical pathway through phosphorylation of NIK.[69] Under basal conditions, formation of the TAK1-TAB1 complex is slow, whereas in KRAS driven PDAC, TAK1-TAB1 complexation is significantly upregulated.[70] Due to this upregulation in PDAC, TAK1 inhibition may represent a feasible strategy for the inhibition of NF-κB activity.[64] TAK1 inhibitor 5Z-7-oxozeaenol, first examined in an inflammatory setting,[71] is commonly used as a chemotherapeutic intervention and has shown involvement in disrupting cell cycle progression but also shows activity against a panel of other kinases. A more recent, type II

inhibitor, of TAK1 shows greater selectivity than 5Z-7-oxozeaenol and, whilst warranting further investigation, still has a greater affinity for MAP4K2 than TAK1 and has only limited cellular data to date.[72]

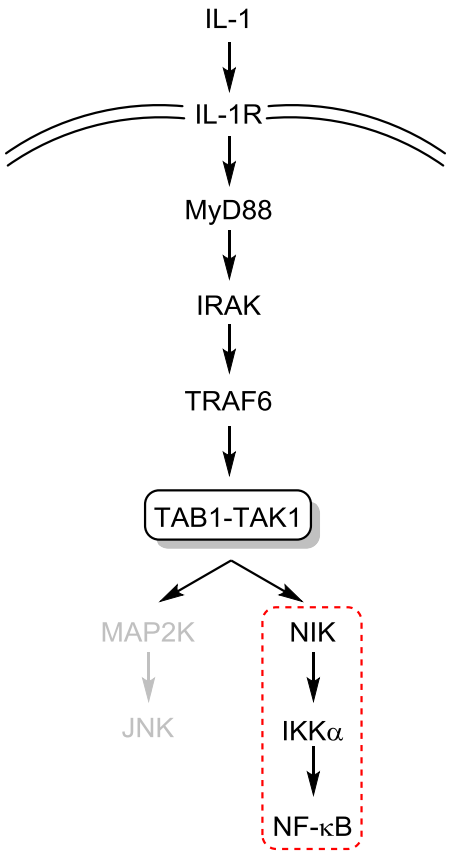

Figure 12. Schematic of TAK1 - NIK - IKK signalling. Adapted from.[69]

GSK3 is a kinase, comprising two isoforms, which plays a key role in cell cycle progression and apoptosis. The GSK3α isoform is involved in promotion of constitutive IKK and NF-κB activity in pancreatic cancer by targeting TAK1 stabilising the interaction of the TAK1-TAB1 complex.[73] It has also been suggested that GSK3 plays a role in the stabilisation of the nuclear RelB/p52 heterodimer as shown in **Figure 13**. The non-specific GSK3 inhibitor AR-A014418 has been shown to reduce tumour growth in pancreatic cancer cell lines and GSK3 has therefore been suggested as another potential therapeutic target.[73]

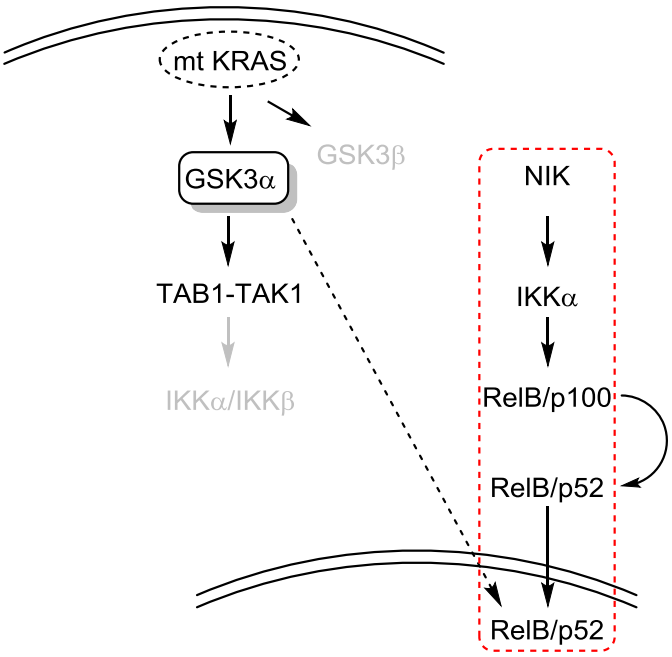

Figure 13. GSK3α activation of non-canonical NF-κB by nuclear p52 stabilisation. Adapted from.[73]

1.5.2. Prostate cancer

As research into the links between NF-κB signalling and cancer has progressed, a significant body of evidence has developed linking the non-canonical NF-κB pathway components NIK and IKKα with prostate cancer. Literature also suggests that these can act either through the activation of the non-canonical pathway, leading to the translocation of RelB/p52 to the nucleus,[74,75] or through NF-κB independent mechanisms.[76,77] IKKα is known to be able to translocate to the nucleus, whereupon it can, amongst other things, phosphorylate histone H3[78] and SMRT.[79] These processes may have particular significance in CRPC because phosphorylation of histone H3 has been implicated in transcription regulation in response to androgen stimulation[80] and one of the targets of SMRT repression is AR (**Figure 14**).[81,82] Lessard *et al* have also shown that targeting IKKα with RNAi leads to an IKKα-dependent nuclear accumulation of non-canonical components p100 and p52 in LNCaP prostate cancer cells,[83] further indicating a relationship between AR and the non-canonical NF-κB pathway in hormone-dependent cancers such as CRPC.

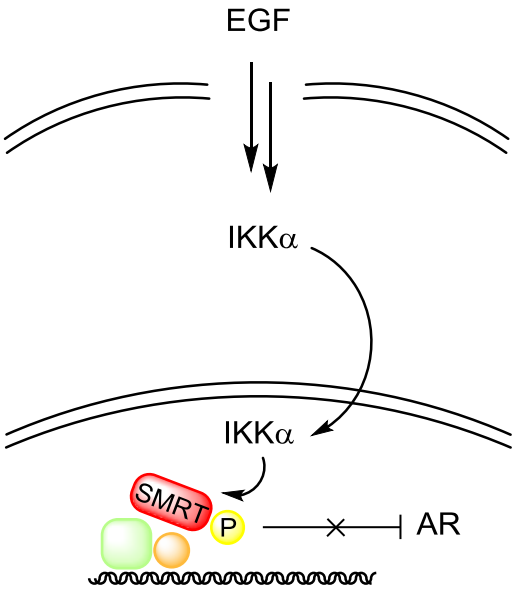

Figure 14. AR derepression through IKKα mediated phosphorylation of SMRT.

The TNF superfamily member cytokine receptor activator of NF-κB ligand (RANKL) had already been established as a driver of oncogenesis in an, at least partial, NF-κB dependent manner in breast cancer.[84–86] Further work by Karin *et al.*, however, suggested that this was not the case in prostate cancer and that RANKL drives translocation of IKKα to the nucleus and is involved in repression of maspin: a suppressor of tumour metastasis.[77,87] IKKα has the ability to phosphorylate histone H3 once in the nucleus and it is thought that this phosphorylation affects gene transcription and may therefore include that of the serpin gene which translates maspin.[88]

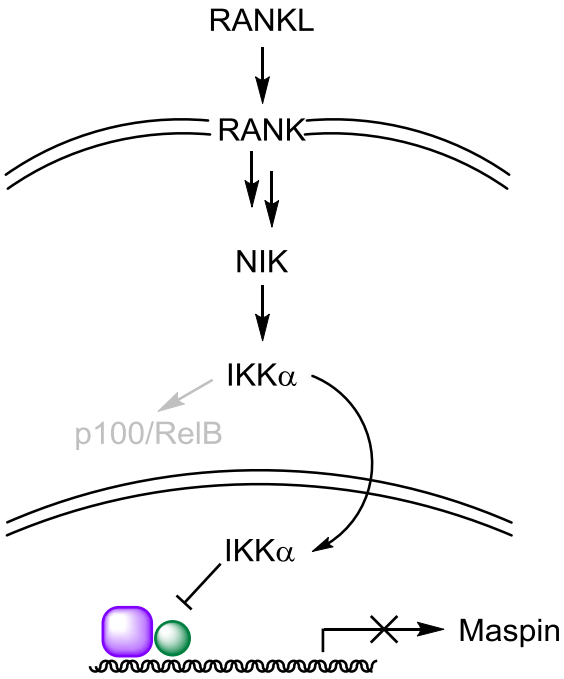

Figure 15. RANKL-mediated IKKa translocation and maspin suppression. Adapted from.[77]

These literature observations open up several possible avenues of therapeutic intervention for prostate cancer around the non-canonical NF-κB pathway. The first option could be to target RANKL itself, as the driver of the maspin repression pathway through IKKα. RANKL inhibitors have been developed and, in 2013, denosumab was approved for clinical use by the FDA in patients with bone cancers.[89] Denosumab has also recently been used in clinical trials to decrease bone metastasis and osteoporosis in CRPC treatment.[90] Results have shown a decrease in bone metastasis and increase in bone density with treatment, making denosumab superior to the currently used zoledronic acid.[91]

NIK represents an alternative therapeutic target for prostate cancer treatment. The current state of clinical NIK inhibitors is discussed in section 1.5.1.

A third intervention is to target the kinase downstream of NIK: IKKα. As discussed, this kinase has been suggested to be of great importance in controlling prostate cancer metastasis through suppression of maspin,[77] and proliferation through SMRT.[81,82,92] A wide array of papers and patents have emerged in the last 20 years detailing IKK inhibitors, though the majority of these are dual IKKα/IKKβ, or IKKβ selective, inhibitors. A full discussion of these is outside the purview of this work, but a review by Llona-Minguez *et al.* provides a broad overview of the IKK inhibitor landscape.[93] Arguably, the most important

published work on IKKα selective inhibitors has come from GlaxoSmithKline. The first of these publications came in 2008 and claimed a series of azaindoles as IKKα selective inhibitors.[94] The same year, a series of 4-phenyl-7-azaindoles were patented by the same group. No inhibitory values were provided but the compounds were claimed to be IKKα selective and to show sub-micromolar potency against both IKKα and IKKβ.[95] Compared to publications on IKKβ inhibitors, there has been a dearth of IKKα inhibitors and, to date, there are no known IKKα-selective inhibitors in any clinical trials.

1.6. Selected alternative strategies

As alluded to at the outset, and as shown in **Figure 16**, cellular regulation of oncogenic processes is extremely complex. This section will cover a few selected pathways currently under investigation within the prostate and pancreatic cancer setting.

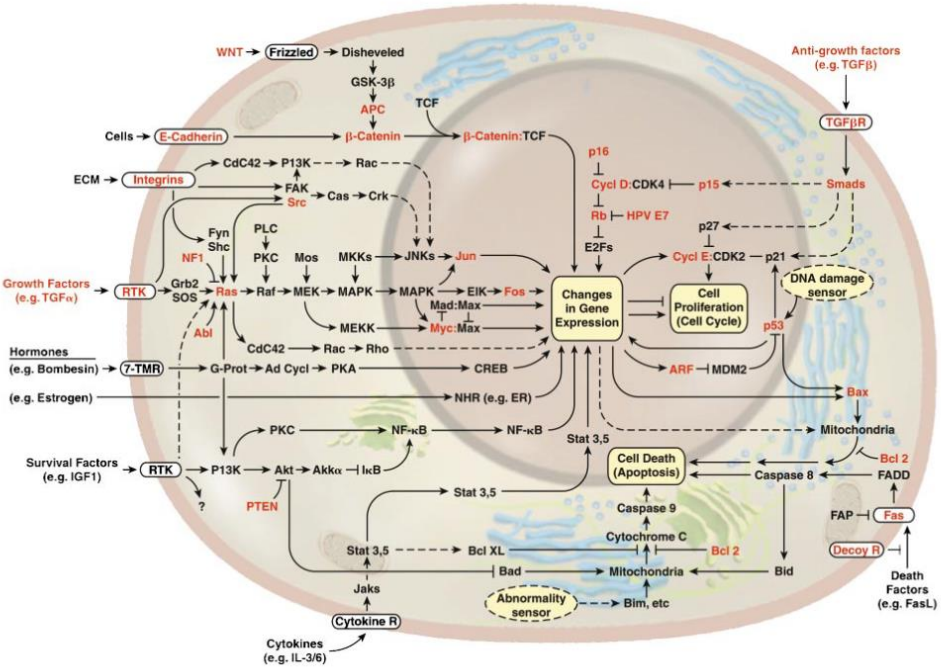

Figure 16. Oncogenic signalling pathways.[3]

1.6.1. Hedgehog

The Hedgehog (Hh) pathway has been shown to have a role in cancer through multiple mechanisms and constitutive activation leading to tumourigenesis has been observed in several cancers, including prostate and pancreatic.[96]

The full signalling pathway is far too complex to examine here; however, because of its therapeutic potential within both prostate and pancreatic cancer, it is worth a brief overview. Within vertebrates, Hh proteins are a set of three homologous extracellular signalling proteins which bind to the *Patched 1* transmembrane protein (PTCH).[96] In the absence of an Hh ligand, PTCH inhibits the activity of another transmembrane protein known as Smoothened (SMO).[97] Under basal conditions, downstream GLI transcription factors are proteolytically processed and are largely repressive with respect to Hh target genes. Upon activation, however, the 7-transmembrane GCPR SMO activates GLI transcription factors leading to expression of Hh target genes.[98]

Several Hh pathway inhibitors have been published which target the SMO protein within the pathway. These include SANT1 - SANT4,[99] CUR61414[100] and IPI-926[101], however two which are of particular interest to pancreatic cancer are sonidegib and vismodegib. These are FDA approved SMO receptor inhibitors for use in treating basal-cell carcinomas[102,103] and are both in clinical trials for use in resectable (i.e. non-metastatic) pancreatic cancer.[104–106]

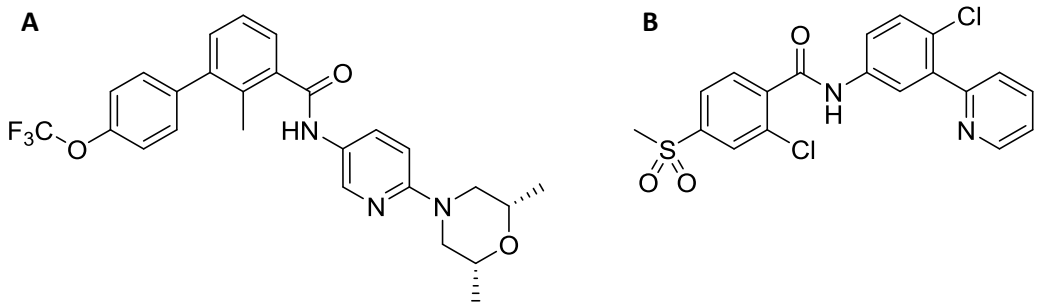

Figure 17. Structure of (**A**) sonidegib and (**B**) vismodegib.

1.6.2. PI3Ks

The phosphoinositide 3‑kinase (PI3K) pathway has generated a lot of interest due to its role in tumour cell biology.[107] PI3K-AKT pathway has been implicated in all of the hallmarks of cancer, described at the outset, through a range of downstream pathways including NF-κB.[108]

PI3K is, in reality, a family of 8 kinases across three classes. The most important of these is the so-called class I enzymes, termed PI3Kα, PI3Kβ, PI3Kγ and PI3Kδ.[107] These are comprised of a 110 kDa catalytic subunit and a regulatory subunit; though there is some debate over whether PI3Kγ should be in a separate "class IB" due to it dimerising with a different regulatory subunit to the other three.[108]

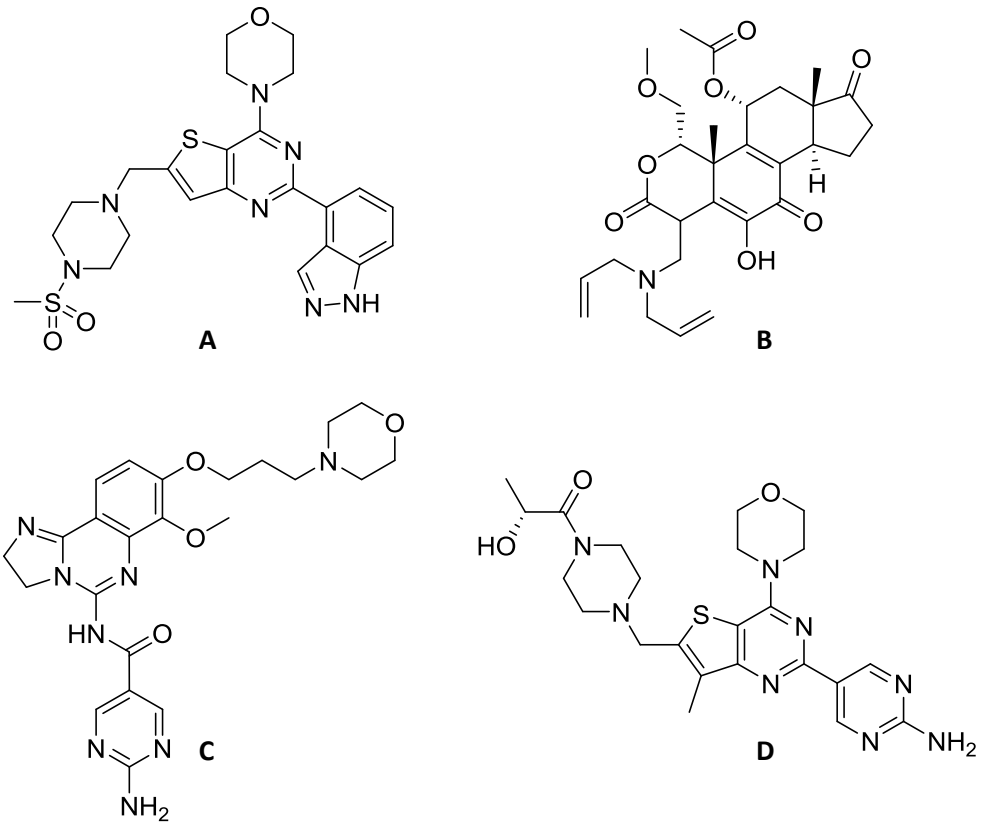

Figure 18. Structures of PI3K inhibitors (**A**) GDC-0941, (**B**) PX-866, (**C**) BAY 80-6946 and (**D**) GDC-0980.

The PI3K pathway is involved in cross-talk with a host of enzymes in other pathways; many of which have also been targeted within a cancer setting. These include MEK, for which trametinib has been approved for BRAF-mutated melanoma;[109] ERK, for which ulixertinib is

in phase I trials;[110] and a range of MNK inhibitors still in pre-clinical development, to name a few.[111]

To date, all PI3K inhibitors have been targeted against one or more isoforms of the class I enzymes with some also targeting mTOR.[112] Two of these are in clinical trials against prostate cancer and two against pancreatic cancer.[112] All four of these inhibitors inhibit PI3Kα and PI3Kβ, but also others in combination, with GDC-0941 in phase IB/II for pancreatic cancer and PX-866 in phase II for prostate cancer also targeting the PI3Kγ and PI3Kδ isoforms; BAY 80-6946 in phase I for pancreatic only targeting PI3Kα and PI3Kβ and GDC-0980 in IB/II for prostate hitting PI3Kγ, PI3Kδ and mTOR.[112]

PI3K is a particularly attractive target in prostate cancer because of interplay with androgen receptor (AR) signalling.[113] In prostate cancer cells which are tumour suppressor *PTEN*-null, inhibition of the PI3K-AKT pathway acts as an upregulatory feedback mechanism for AR signalling and vice-versa,[114] thus maintaining tumour cell survival even in castrate-resistant prostate cancer. It has been shown, however, that pharmacological inhibition of both PI3K and AR signalling led to near complete cancer regression in human xenografts.[113] It is noteworthy that both AKT and ATM (another PI3K family member) have been shown to phosphorylate IKKα and promote its translocation to the nucleus.[92] As already discussed, this has considerable effects on AR signalling and further validates these pathways in prostate cancer treatment.

1.7. Advantages of non-canonical NF-κB inhibition over canonical NF-κB inhibition

Whilst there is no one clear piece of conclusive evidence, there is a collective body of work which, overall, suggests that targeting the canonical NF-κB pathway is less favourable than targeting the non-canonical NF-κB pathway.

In the arguments against canonical NF-κB inhibition, there is evidence that long-term inhibition of IKKβ has the potential for significant cell death and apoptosis in normal epithelial cells and cardiac cells respectively.[115,116] Due to canonical NF-κBs influential role in immune system regulation there is also concern that IKKβ inhibitors would have to be taken with broad spectrum antibiotics for only a short duration to avoid excessive inflammasome activation during bacterial infection.[57] Rel A deficient mice also exhibit embryonic lethality after around 15 days of gestation and it is thought that this is due to liver degeneration by programmed cell death.[117] Whilst this is only observed in knockout mice, a small population

of the Cree people in Canada have been found to carry a mutation which leaves them IKKβ null and severely immunocompromised, leading to death usually within months of birth.[118] These observations have raised the question as to whether "excessive IKKβ inhibition will result in hepatic toxicity and immunosuppression."[119]

There have not been any such reports of toxicity from non-canonical NF-κB inhibitors; though this is likely to be in large part because so few of them have been published, and those which have are very recent and thus lack expansive toxicological data. Whilst in theory this is encouraging, non-canonical NF-κB inhibitors are not without their problems. Two of the most obvious targets directly in the non-canonical pathway are NIK and IKKα. IKKα is known to play a significant role in the canonical pathway[48,120] and is also known, in some settings, to be involved in the phosphorylation of IKKβ.[46] It has also been shown to play roles outwith the NF-κB signalling pathway, such as its role in histone phosphorylation discussed in section 1.5. NIK is able to phosphorylate IKKβ to a much lesser extent than IKKα and has been shown to have far fewer roles outside the non-canonical pathway.[46] From a medicinal chemistry perspective, a NIK inhibitor with no canonical activity is also likely to be more tractable than a specific IKKα inhibitor due to the high level of homology between IKKα and IKKβ. IKKα, however, remains an attractive target, particularly in prostate cancer treatment, due to the interconnected nature of AR and non-canonical NF-κB signalling.

1.8. Protein kinases as drug targets

Over the last 15 years, protein kinases have become the most important drug target class in the field of cancer[121] and now represent the second most targeted drug class after GCPRs.[122] By January 2016, 28 kinase inhibitors had been approved for clinical use by the FDA, generating revenues topping $18 billion in 2014 alone. With only a small proportion of the kinome explored for its therapeutic potential in cancer treatment, it is expected that growth in kinase inhibitor sales will continue to increase until at least 2024.[123]

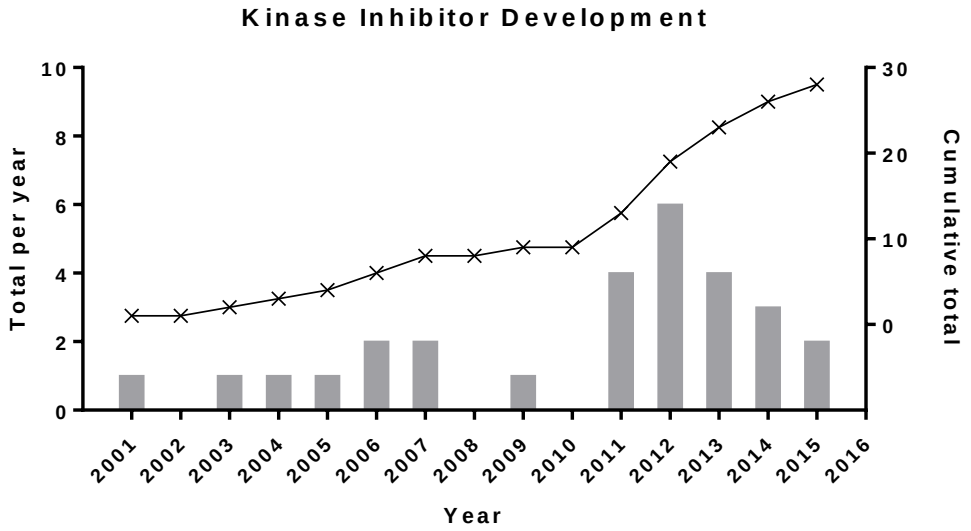

Figure 19. FDA approved kinase inhibitors.

1.8.1. Binding modes of protein kinase inhibitors

There are, broadly, four binding mode categories into which kinase inhibitors are generally classed. Type I inhibitors cover those which are directly ATP competitive and bind to the active form of the kinase in a very similar way to ATP itself. Inhibitors are classed as type II if they bind in a similar region to type I but to the inactive form of the kinase. These are often capable of binding to specific pockets adjacent to the ATP site but not accessible in the active form. Most kinase inhibitors to date fall into one of these first two categories.[124] Type III encompasses inhibitors which bind to an allosteric site adjacent to the active site but without making any direct interactions with it and are not competitive with ATP, whilst type IV inhibitors are those which bind to a remote allosteric site away from the ATP binding site.[125] A schematic of these binding modes is shown in **Figure 20**.

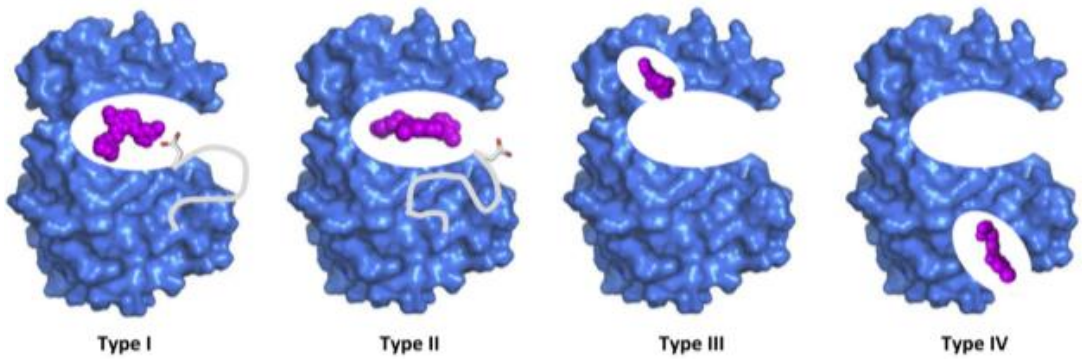

Figure 20. Inhibitor binding modes.[124]

A fifth category of type V inhibitors consisting of bisubstrate and bivalent inhibitors has also been described but, as yet, is sparsely exemplified.[126]

1.8.2. Chemical features of kinase inhibitors

Of the 28 small molecule kinase inhibitors (SMKIs) licenced to date, only 2 of them - trametinib, type III and lenvatinib, type V - do not fit into the type I or type II classes (though lenvatinib does occupy the ATP binding site).[127,128] Because kinase ATP sites are so highly conserved, this section will focus on just ATP competitive SMKIs and the common features which can be explored. The first is that, since these molecules are ATP competitive, they all have some form of adenine analogue which binds to the hinge. Several variations have been made to convey selectivity or potency but all tend to focus around pyri(mi)dines, quin(az)olines and pyrrolopyri(mi)dines.[124] The G+1 and G+3 provide an acceptor-donor-acceptor motif, whilst adenine possesses a donor-acceptor motif. These corresponding partners form hydrogen bonds which anchor ATP to the hinge of the kinase as shown in **Figure 21**. Because SMKIs are built around an adenine scaffold, they also tend to be very planar and have few rotatable bonds; with an average over 3 aromatic rings and fewer than 6 rotatable bonds, whereas marketed drugs in general have a fraction of sp^3 centres of 0.46.[127,129] Whilst this rigidity helps with selectivity and specificity, it is detrimental to solubility and means that many kinase inhibitors, to overcome this, have long-chained water-solubilising groups incorporated.

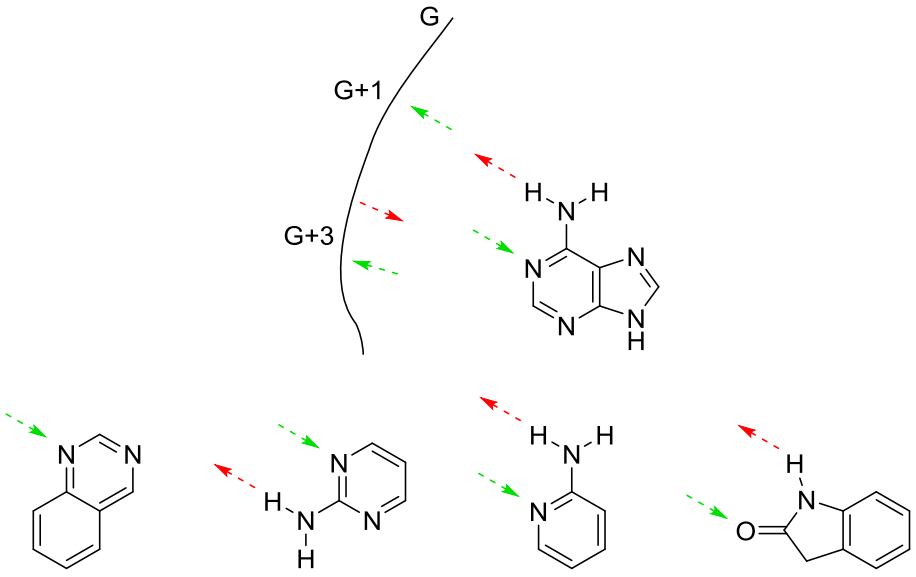

Figure 21. Schematic of adenine hinge binding and common SMKI analogues. Red arrows denote hydrogen bond donors, green arrows denote hydrogen bond acceptors.

Another problem encountered in balancing potency and water solubility is that kinase ATP sites are very hydrophobic. This means that to maximise interaction with the pocket, SMKIs are themselves quite hydrophobic. This is demonstrated by that fact that many fail to adhere to Lipinski's rules regarding logP < 5 and molecular weight < 500; either because they are inherently very hydrophobic, or because, in order to reduce the logP, they have a substantial mass increase from water solubilising groups.[127]

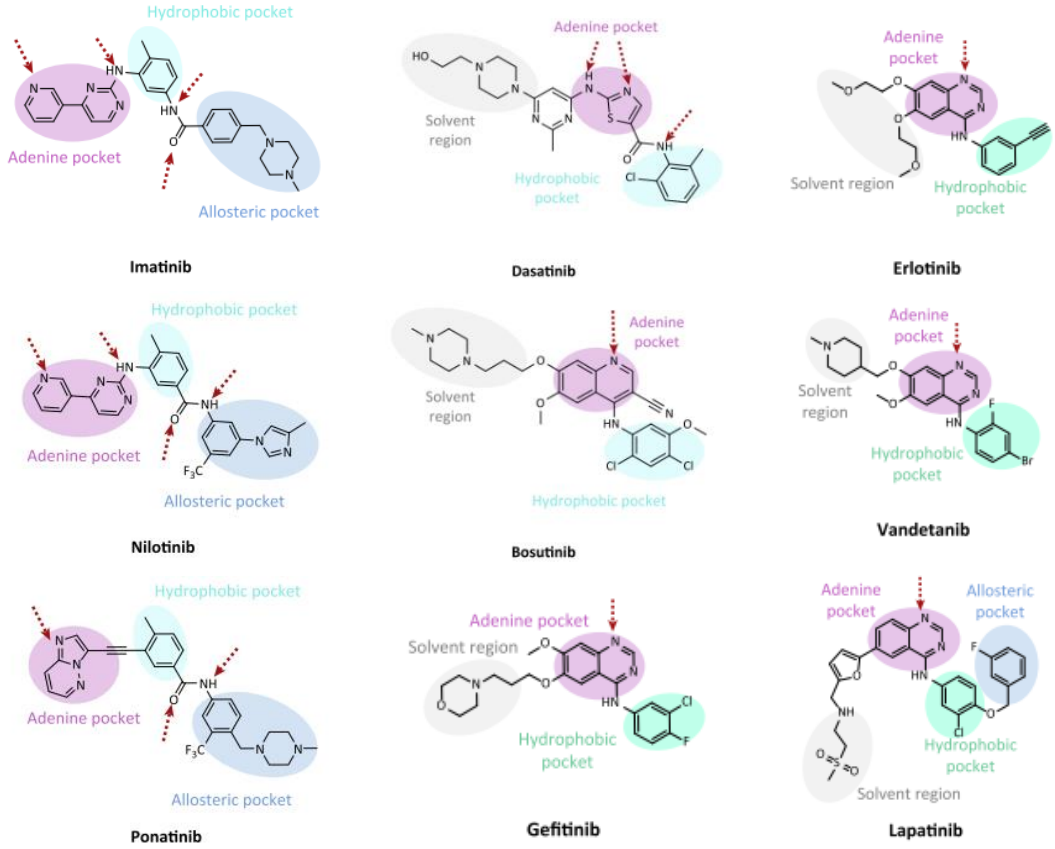

Figure 22. Examples of inhibitors binding in the adenine pocket and adjacent hydrophobic pocket.[124]

Almost all of the earliest approved kinase inhibitors, and many most recent ones, use two pockets, the adenine pocket and the adjacent hydrophobic pocket, to anchor the molecule in the active site, but because of the conserved nature of this site across the kinome, it is often difficult to derive any selectivity from these sites alone. Accessing the hydrophobic region behind the gatekeeper residue can convey some selectivity depending on the nature of the gatekeeper and the size of the hydrophobic pocket. There are 12 licenced inhibitors

which target Bcr-Abl or VEGFR2.[124] Inhibitors of these kinases have relatively easy access to the hydrophobic region due to the gatekeepers being threonine and valine respectively. A number of inhibitors of these kinases, such as imatinib and nilotinib, have been designed to exploit this access and use it to create linkers, through the hydrophobic region, to a remote allosteric pocket which is otherwise difficult to target. Inhibitors of, for example, EGFR, however, encounter a methionine gatekeeper. This, being much larger than threonine or valine, limits access to this pocket and so selectivity has had to be sought elsewhere. NIK and IKKα also possess methionine gatekeepers and thus this allosteric site behind the hydrophobic region is likely to be difficult to target.

Another pocket which type I SMKIs can target is exemplified by the inhibitor palbociclib. The specificity pocket is located around the gatekeeper +4/+5 region. Since these residues are not involved in binding the native ATP, this region has much greater variety than the residues in the adenine binding pocket and, as in this example, has been exploited to allow for greater selectivity for CDK6.

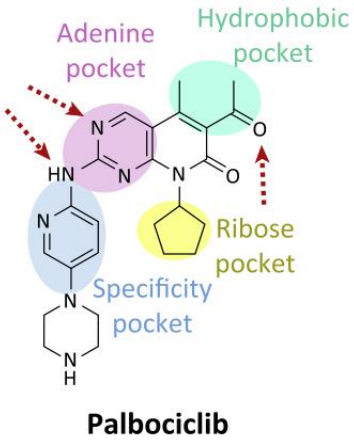

Figure 23. Binding mode of palbociclib.[124]

1.8.3. Issues surrounding targeting protein kinases

The first, and possibly most obvious, issue when targeting protein kinases is that the human kinome is represented by over 500 kinases and, since all of these catalyse the hydrolysis of ATP, all therefore have similar catalytic sites. Given that kinases control so many cellular processes it is important that any potential inhibitors exhibit some level of selectivity. From a therapeutic perspective, "selectively non-selective", or multi-kinase inhibitors (MKIs) may be advantageous. The concept of MKIs is that, to circumvent the problems of developing a truly selective inhibitor, inhibition of multiple kinases which cumulatively give the desired therapeutic outcome are sought, whilst tuning out potency against kinases whose inhibition is detrimental.[122] MKIs are often serendipitously discovered during kinase screens rather than specifically designed but, once a kinase profile is understood, it can be exploited.

MKIs can also combat another problem with kinase inhibitors and that is the problem of emerging resistance. Drug resistance in cancer cells can occur through a multitude of processes such as decreased uptake of drugs requiring active uptake to enter cells, mutations and enhanced metabolism of drugs by cytochrome P450, but the main mechanisms affecting kinase inhibitors are changes in cells that affect the capacity of cytotoxic drugs to kill cells, such as alterations in cell cycle, increased repair of DNA damage and reduced apoptosis; and increased energy-dependent efflux of hydrophobic drugs.[130,131] Analogous multi-target drug discovery (MTDD) strategies have been used for other indications and have proved very successful. For example, since 1996, HIV treatment has involved targeting a combination of targets with a cocktail of drugs.[132] A multi-target single agent example is ertiprotafib, which was developed as a protein tyrosine phosphate 1B (PTP1B) inhibitor to treat type II diabetes, but was later found to also be a potent IKKβ inhibitor. NF-κB has been linked to the reversion of insulin resistance and it may be that the targeting of multiple enzymes accounts for ertiprotafib's observed *in vivo* effect.[133–135]

Imatinib, the first FDA approved kinase inhibitor, is an example of emerging resistance in kinases. Developed as a Bcr-Abl inhibitor, and approved for use in chronic myeloid leukaemia, mutations have been found at more than 20 points in the kinase domain of the Bcr-Abl complex which reduce, or even negate, imatinib's ability to bind.[136] Second generation inhibitors nilotinib and dasatinib are good examples of MTDD in the field of kinases and are both effective in certain instances of imatinib failure.[137] Dasatinib exhibits a

multi-kinase inhibitory profile and is also capable of binding to multiple conformations of the protein, enabling it to overcome mutations which imatinib cannot.[138]

Given these examples, it may be that a similar approach is of value in this project, wherein inhibition of more than one kinase is desirable: possibly another kinase in the pathway such as IKKα, or kinase in a complementary pathway.

1.8.4. Setting up a drug discovery project

Developing a new drug or therapy is a costly and time-consuming business, usually taking upwards of a decade and $1 billion from target and hit identification to clinical candidate.[139] It is important, therefore, to have a logical workflow in place which enables the efficient identification of active compounds, collates important pharmacokinetic (PK) and pharmacodynamic (PD) data and feeds back into the medicinal chemistry process to allow further compound development. Ultimately, the goal of any medicinal chemistry programme is a pre-clinical candidate that shows activity against the disease of interest in an animal model, but there are several stages which must be undertaken first. **Figure 24** outlines the workflow plan which will be adopted for this project.

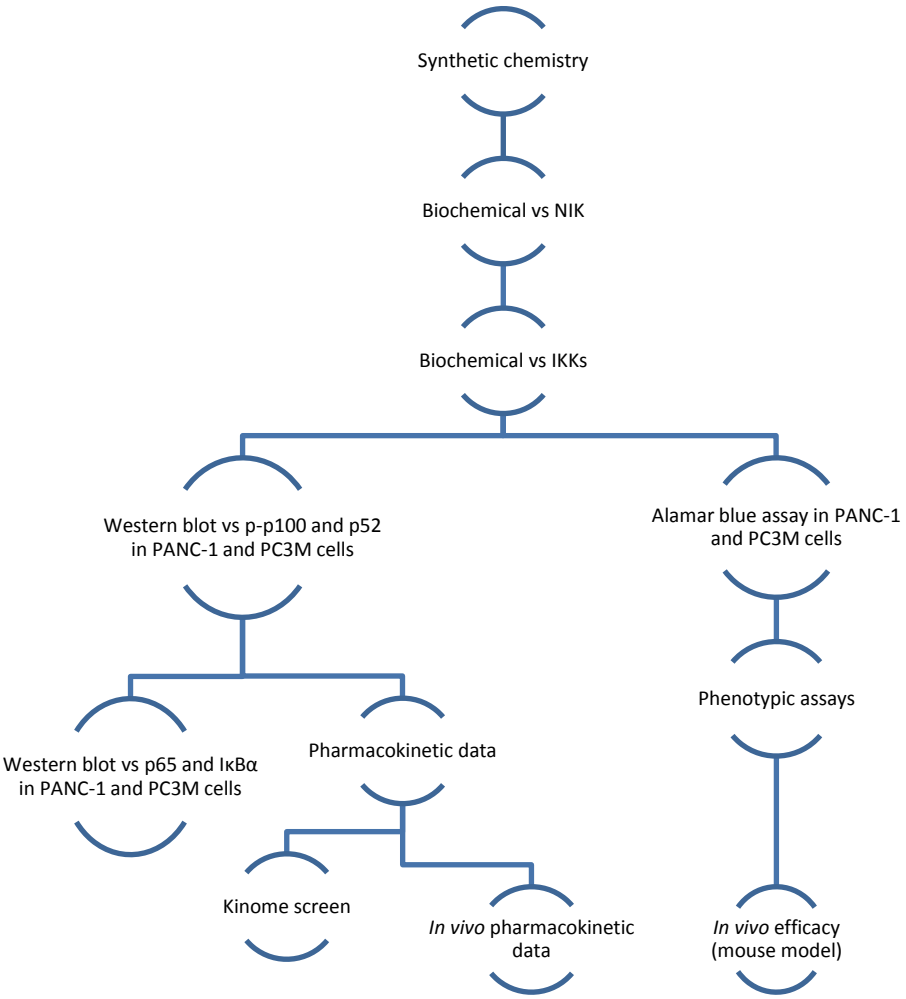

Figure 24. Workflow plan for assessment of synthesised compounds.

Before a project can begin, a target must be validated to assess its applicability to a specific disease. This in itself can be a long and complex process and often has to be carried out alongside an early drug discovery project as, sometimes, the only available way to interrogate a biological pathway may be through small molecule intervention. A 2011 review by Hughes *et al.* gives an excellent description of various target identification and validation techniques.[139]

Once a target has been identified and an initial series of chemical probes have been selected or synthesised, the first assessment in a drug discovery project, where possible, must always be a biochemical assay against the target of interest. The reason for this is that if the compound which has been made does not show activity against the desired target in an isolated setting it is certainly not going to in the much more complex setting of a cell, let

alone an animal. The primary biochemical assay used in this project was developed in-house and will be discussed later in chapter 3.2.1.

The second stage in this project is to test compounds which are active in the NIK biochemical assay against both the IKKα and β isoforms in a second biochemical assay. This is to give an early indication of whether the compound is likely to have an effect on the canonical NF-κB pathway. Compounds which are active against NIK and show little or no activity against IKKβ can then be taken forward for testing in cells.

It is important to show not only target engagement, but also that engaging that target has an effect on the pathway of interest. This is often done by what has become known as proteomics.[140] This involves looking at the expression of a protein downstream of the target with and without therapeutic intervention and one of the simplest ways to do this is by Western blot. **Figure 7** and **Figure 8** show the proteins involved in the NF-κB pathway. Since these are closely related to NIK and its activity, many of these will be used to assess the effect of engaging NIK. Firstly, downregulation of the non-canonical pathway must be established and so phosphorylation of p100 and p52 expression will be observed. If non-canonical engagement is observed, then testing to ensure no effect on the canonical pathway will be carried out by blotting for p-IκBα and p65.

As well as testing for target engagement and an effect on the pathway, it must also be demonstrated that the compound is having a phenotypic effect. In the case of anti-cancer compounds this would hopefully be either a cytotoxic or cytostatic (senescent) effect. The first way to test this is through a cell viability assay: in this case, alamarBlue®. This gives an indication of the overall metabolic activity of the cells but, if a decrease is observed, it does not give any indication as to why that might be. If a decrease is observed, the compound can then be investigated in more specific phenotypic assays such as migration, proliferation or apoptosis assays to elucidate the mechanism.

Alongside these PD investigations, the pharmacokinetics of the compound must also be investigated. PK investigates how a compound survives within the body and is as important as PD when developing a clinical drug since “there is no point in perfecting a compound with superb drug-target interactions if it has no chance of reaching its target”.[141] At a more basic level, this involves developing compounds that are water soluble and avoiding functional groups such as esters which are readily hydrolysed in the blood stream and may

result in an inactive compound. Water solubility is desirable so that compounds can be formulated for oral administration. This helps with issues of patient compliance which may be seen if administration is by IV. As development progresses, however, it is also important to understand, among many other factors, how the compound is metabolised and how quickly this happens (half-life); its ability to pass through tissues (permeability); the rate at which the compound is removed from the body (clearance) and whether the compound stays in cells (efflux). These are all initially investigated *in vitro* but at later stages of development it must also be established whether these hold true in an *in vivo* model.

With any drug discovery programme it is also important to test for unwanted off-target effects. Some of these are quite general such as inhibition of hERG or cytochrome p450 enzymes as these may lead to cardiac arrhythmia and hepatotoxicity respectively. Inhibition of CYP450 enzymes can also result in the body being unable to metabolise certain compounds. This is becoming more important as many anti-viral and anti-cancer therapies now utilise combination therapies.[142] If drug metabolism is inhibited then this can lead to potentially dangerous drug-drug interactions. For a kinase inhibitor project, it is also necessary to investigate the effect of a compound on other kinases. This is primarily because pan-inhibition can lead to unwanted toxicity,[143,144] but also makes it difficult to understand if observed phenotypic effects are through the primary target.

As previously mentioned, the goal during the pre-clinical phase of development is to test a lead compound in an animal model to prove the effects seen *in vitro* can be translated to the *in vivo* setting. If a pharmacologically active compound with acceptable toxicological profile can be shown at this stage then the next stage is clinical trials.[139]

2. Objectives

The main aim of this medicinal chemistry project is to discover and synthesise novel compounds which inhibit the non-canonical NF-κB pathway whilst having minimal impact on the canonical pathway. This will be done by means of library screening and iterative drug design processes, drawing upon information from available literature and molecular modelling.

Structure-activity relationship (SAR) studies will be carried out on any hit compounds by developing analogues and determining their activity against purified IKK, or NIK, enzyme to understand the effect of changes within the chemical series.

Compounds which show good potency against the purified NIK/IKK enzyme will be taken forward for further testing against other kinases in the NF-κB pathway, and potentially a broader kinase panel in order to better understand the off-target effects of the compound. They will also be assessed in prostate and pancreatic cancer cell lines to gain insight into their effect on the NF-κB pathways in a cellular setting and the phenotypic effect of non-canonical inhibition.

These efforts will ultimately culminate in the selection of a novel compound which could be used in an *in vivo* setting to assess the suitability of non-canonical NF-κB inhibition by small molecules in the treatment of prostate and pancreatic cancer. This compound should show low nanomolar potency in a biochemical setting, correlated target engagement in a cellular setting and a good pharmacokinetic profile along with potent cytotoxicity against cancerous cell lines.

3. Results and Discussion

At the outset of this project, research into small molecule inhibitors of NIK was in its infancy. Although a few compounds showing inhibitory activity against, amongst others, NIK had been disclosed, the first crystal structure was released in 2012 and, until recently, there have been problems in the expression of stable recombinant NIK protein.[66] As such, early work focused on developing a series of compounds based on a scaffold being worked on in-house, which had known IKKα and IKKβ activities, whilst an appropriate biochemical assay for NIK was developed. These compounds would aim to improve potency against IKKα and to improve selectivity over IKKβ and thus target the non-canonical NF-κB pathway preferentially over the canonical: the same goal as any future NIK inhibitors. They would cover a range of chemical space to provide a preliminary SAR study.

3.1. IKKα inhibitors

The first series of compounds synthesised was based on a 2-amidopyridine scaffold from a proprietary in-house library, as shown in **Figure 25**.

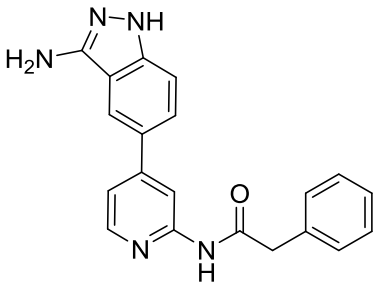

1

Figure 25. Structure of 2-amidopyridine hit.

3.1.1. Homology model

Compound **1** was docked using GOLD suite software (CCDC) in a homology model of IKKα. A crystal structure of *homo sapiens* IKKβ has been published but not IKKα and so the published IKKβ structure has been used to generate this homology model. Docking simulations, particularly on homology models, must be interpreted with caution but nonetheless provide useful information on possible binding modes. These will be discussed later in the chapter.

In order to obtain a more realistic model of IKKα, after "mutating" the IKKβ sequence to match the IKKα sequence, the kinase domain was subjected to an extended molecular dynamics simulation and an average minimised structure produced. This allowed the model to relax any disfavoured interactions and form new, more highly favoured interactions between mutated residues. A more detailed explanation of the MD process, which is outwith my own work, is available in appendix I.

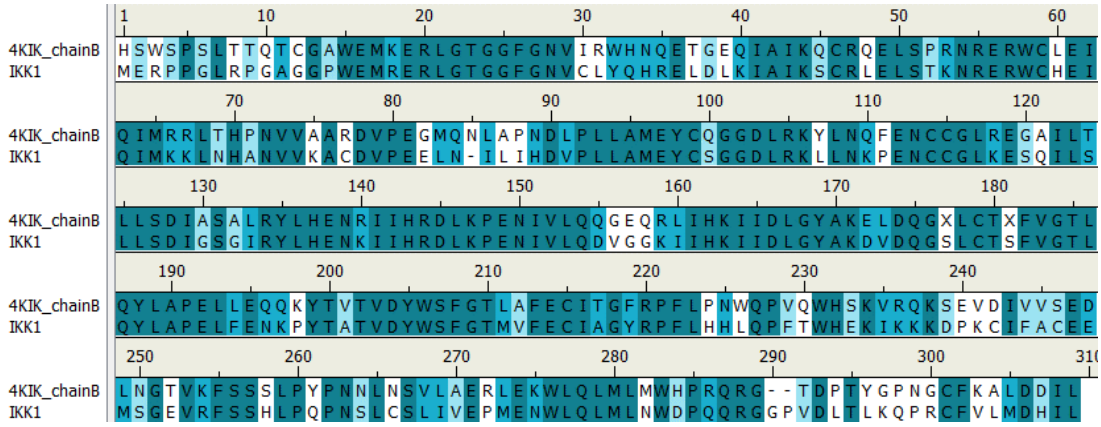

Figure 26. Sequence alignment of IKKα and IKKβ. Darker colours indicate greater similarity.

The molecular dynamics suggested that, particularly in the region around the mouth of the catalytic pocket, the IKKα isoform was significantly more flexible. This has implications for generating isoform selective compounds as it is likely that the IKKα isoform can tolerate much larger functional groups in this region, whereas larger groups may be detrimental to binding in IKKβ. A more detailed discussion on this, in relation to specific compounds, can be found in section 3.1.3.

3.1.2. IKK biochemical assay

As discussed in chapter 1, there is a need for a primary biochemical assay to screen compounds against a specific target is essential for drug discovery. Although a range of assay kits are commercially available to assess a multitude of targets, in this case only an HTScan™ kit for IKKβ was available (Cell Signaling Technology, USA). The downside of these kits for large-scale screening purposes is that they very quickly become very costly and it was therefore decided to adapt this kit to utilise commercially available components and gain the ability to screen against IKKα.

The final assay conditions implemented are detailed as follows: recombinant IKKα (active) 37 nM or recombinant IKKβ (active) 37 nM, (Millipore, Dundee, UK) were incubated with IκBα (Ser32), biotinylated peptide substrate (0.375 µM or 0.18 µM respectively) (New England Biolabs, Hitchin, UK) and ATP (40 µM or 10 µM respectively) in assay buffer (40 mM Tris-HCl (pH 7.5), 20 mM $MgCl_2$, EDTA 1 mM, DTT 2 mM and BSA 0.01 mg/mL) in a V-bottom 96-well plate in the presence and absence of test compound or standard.

The assay plate was then incubated for 1 hour at 30 °C, after which the kinase reaction was quenched by the addition of 50 mM EDTA, pH8. The resulting mixture was transferred to a streptavidin coated 96-well plate (Perkin Elmer, Beaconsfield, UK) and incubated for 1 hour at 30 °C to immobilise the substrate peptide. After three washes with wash buffer (0.01 M PBS, 0.05% Tween-20, pH 7.4), p-IκBα (Ser32/36) mouse mAb (New England Biolabs, Hitchin, UK) (1:1000 dilution with 1% BSA in wash buffer) (40 µL) was added and incubated at 37 °C for 2 hours.

After a further three washes, a secondary europiated antibody (Eu-N1 labelled anti-mouse IgG, (Perkin Elmer, Beaconsfield, UK) diluted 1:500 with 1% BSA in wash buffer) (40 µL) was added and incubated at 30 °C for 30 minutes. After a further five washes, DELFIA enhancement solution (Perkin Elmer, Beaconsfield UK) was added and allowed to incubate for 10 min at room temperature, protected from light. The relative fluorescence units (RFU) signal were measured on a Wallac Victor2 1420 multilabel counter (Perkin Elmer, Beaconsfield, UK), in time-resolved fluorescence mode. The counter was set at an excitation wavelength of 340 nm with a 400 µs delay before detecting emitted light at 615 nm.

The apparent K_i was calculated for each compound using the Cheng-Prusoff Equation.[145]

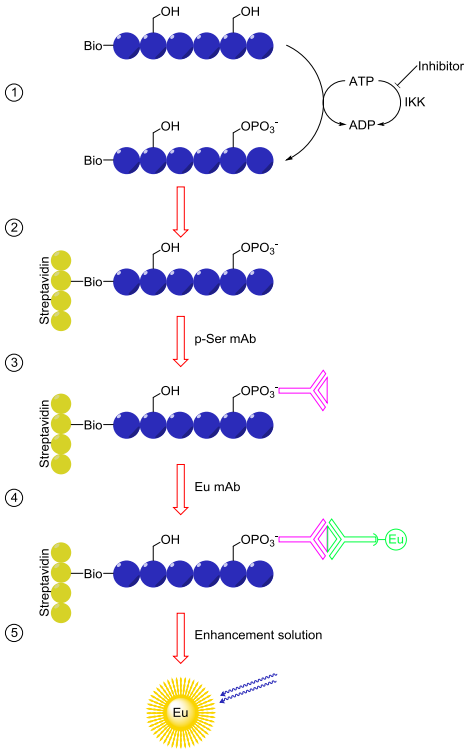

Figure 27. Schematic of DELFIA kinase assay.

Step 1 of the biochemical assay replicates the kinase reaction; wherein IKK catalyses the hydrolysis of ATP to ADP and transfers a molecule of inorganic phosphate to a serine residue of IκBα. The biotinylated hexapeptide used in the assay mimics the phosphorylation site of IκBα and using a phospho-specific antibody, as shown in step 3, enables the amount of ATP hydrolysis to be indirectly quantified by measuring phosphorylation of the substrate. Introducing an inhibitor into the kinase reaction in step 1 slows the rate of ATP hydrolysis, lessening production of inorganic phosphate and thus less peptide phosphorylation. The one to one reaction of phosphorylated peptide with the antibodies means that measured fluorescence is correlated with ATP hydrolysis in a linear relationship.

3.1.3. SAR study

A range of modifications were envisaged to probe the interactions with the binding site as shown in **Figure 28**. The main efforts were focused on substituting the phenyl ring (orange) to probe the influence steric and electronic alterations had on binding affinity. Analogues with a longer alkyl chain (purple) and reducing the amide to an amine (green) were also synthesised. A final series looking at the interactions of the "head group" (red) was synthesised in an attempt to probe which interactions were important for binding and to optimise those interactions where possible. The compounds were then tested in the in-house IKK biochemical assay described above, the results of which are shown in **Table 1**.

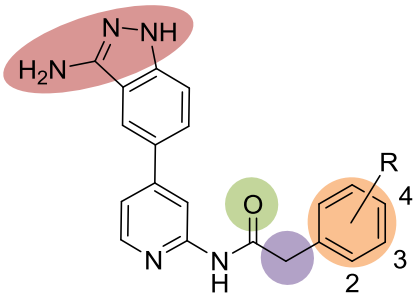

1

Figure 28. Compound **1** modifications.

Compound	R =	K_i IKKα (nM)	K_i IKKβ (nM)	Selectivity (β/α)
1	H*	23	336	15
2	Cyclohexyl*	342	4,190	12
3	2-F	18	407	23
4	3-F*	34	838	25
5	4-F*	14	187	13
6	2-Cl	55	587	11
7	3-Cl	31	461	15
8	4-Cl	45	432	10
9	2-pyridyl	4	109	27
10	3-pyridyl	18	158	9
11	4-pyridyl*	10	67	7
12	2-CF_3	54	>30,000	>556
13	3-CF_3	104	1,676	16
14	4-CF_3	62	>30,000	>484
15	3-NH_2*	8	747	93
16	4-NH_2	48	2,389	50
17	3-NO_2*	14	415	30
18	3-NHBoc	94	1,215	13
19	4-NHBoc	66	1,886	29
20	3-OBz*	78	419	5
21	4-SCH_3	63	2,179	35
22	2-OCH_3	159	3,101	20
23	3-OCH_3	33	4,065	123
24	4-OCH_3	81	1,844	23
25	3-SO_2CH_3	40	335	8
26	4-SO_2CH_3	42	754	18
27	2-CH_3	184	1,173	6
28	3-CH_3	53	990	19
29	4-CH_3	27	1,928	71

Table 1. IKK biochemical assay results for analogues of compound **1**.

* Synthesised by either Dr Judith Huggan or Dr David Breen

One of the best ways of understanding SAR is through crystal structures. This provides a snapshot of the bound ligand in the target of interest and gives a strong indication of how structural analogues may bind. To best assess these results, a crystallisation of compound **1** was sought. It was hoped that a crystal structure with compound **1** in at least one IKK isoform could be obtained. This was, unfortunately, not possible but a crystal structure was obtained with compound **1** bound in CDK2: a kinase closely related to IKKα in structure. Using a BLAST sequence alignment to compare IKKα and CDK2 (uniprot IDs O15111 and P24941), these two kinases have a 31% sequence identity and 48% similarity, with an E-value, denoting significance, of 3×10^{-21}.[146,147] An E-value of less than 1×10^{-4} is considered to be a good match.[148] A sequence alignment of the kinase domains of CDK2 and IKKα is shown in **Figure 29**.

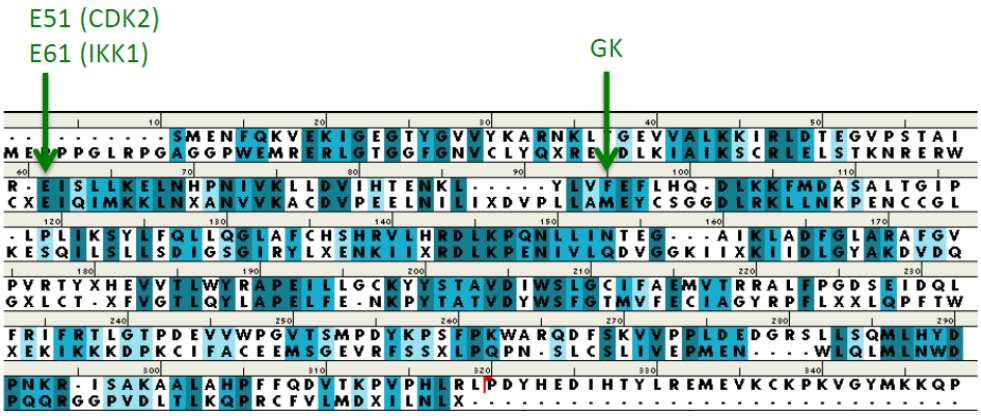

Figure 29. Sequence alignment of CDK2 and IKKα.

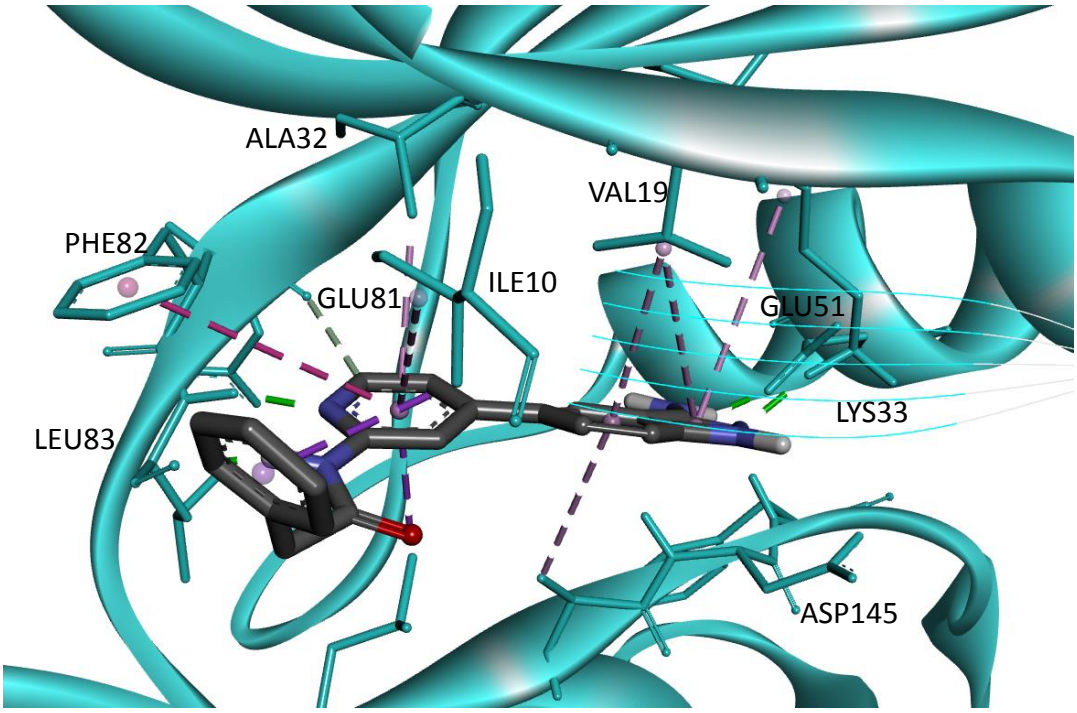

Figure 30. Crystal structure of compound **1** bound to CDK2 and showing important interactions with key residues. Beta sheet displayed as lines for clarity.

The crystal structure showed the amidopyridine bound to the gatekeeper +3 and the aminoindazole in the phosphate binding region with the exocyclic amine interacting with GLU51, the endocyclic nitrogen with catalytic LYS33 and the phenyl at the mouth of the catalytic pocket. The endocyclic NH is also positioned in such a way that an interaction with ASP145 is also possible, though not specifically indicated by Discovery Studio modelling software. The pendant phenyl ring is interacting with hydrophobic residues at the mouth of the catalytic pocket.

Overlaying of the CDK2 crystal structure with the IKKα homology model suggests that many of the interactions proposed from the crystal structure would translate into IKKα. Whilst this is only an assumption, the combination of sequence homology between the two proteins and the structural similarity between the CDK2 crystal structure and IKKα homology model gives some strength to this hypothesis

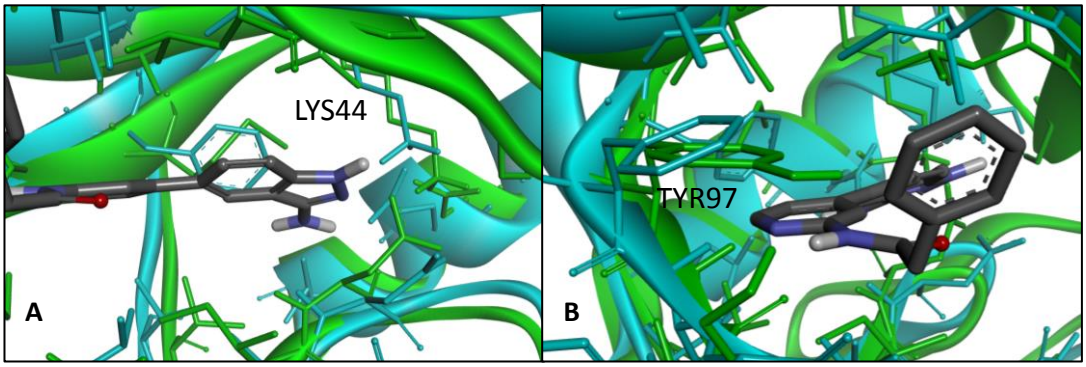

Figure 31. Overlay of CDK2 (cyan) and IKKα (green) with compound **1** bound. Noted residues are those of IKKα amino acids. Panel **A** shows the region of the catalytic site around the catalytic lysine, while panel **B** shows a view from the mouth of the pocket.

Using this superimposition, it is possible to generate a 2 dimensional interaction map showing the key interactions likely to be made between compound **1** and IKKα. These are shown in **Figure 32**.

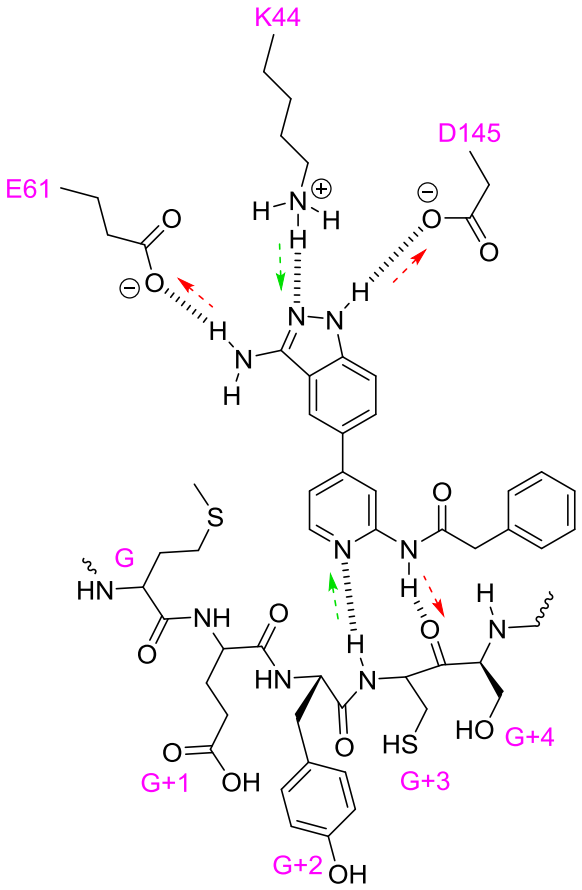

Figure 32. Interaction map of compound **1** with important residues in IKKα.

Docking simulations of compound **1** suggested very similar poses to that seen in the crystal structure. The major difference between the homology model and the crystal structure was that binding of the aminoindazole was flipped; however this can be explained by the donor-acceptor-donor motif of the aminoindazole which has the capacity to bind in two orientations while maintaining strong hydrogen bonding interactions. The schematic shown in **Figure 33** assumes the protein is a rigid structure and the molecule binding is a static event and thus a third hydrogen bond is not shown in the right-hand diagram. In reality, however, neither of these constraints holds true and a third interaction is feasible; though possibly with slightly weakened interaction elsewhere in the molecule.

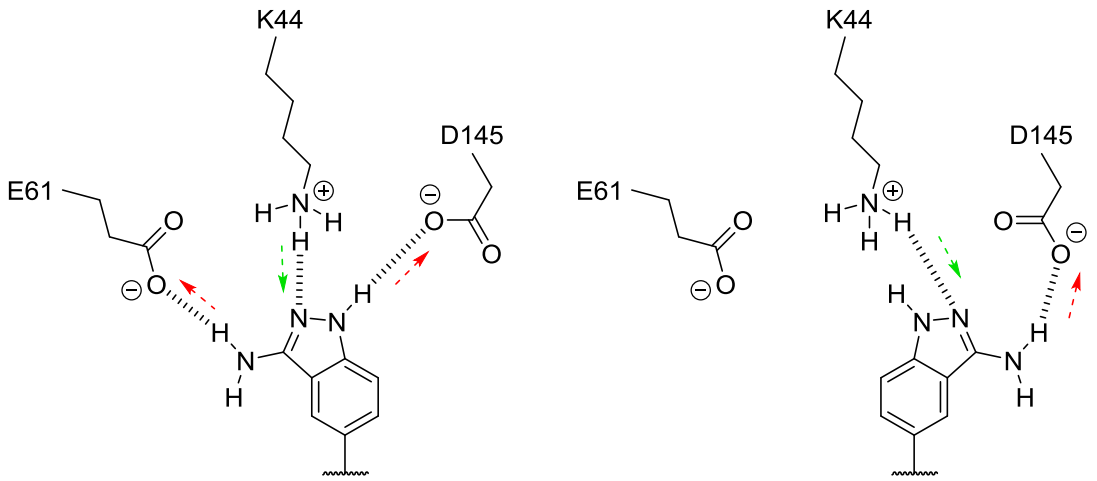

Figure 33. Flipped binding poses of the aminoindazole.

Since the hinge binding amidopyridine scaffold docked analogously to the pose indicated by the crystal structure, it was decided that conclusions could still be drawn from the docking simulation since the modifications of interest would be largely unaffected by the orientation of the aminoindazole.

Several trends are evident within this series of compounds. The first is that pyridyl substituted compounds **9**, **10,** and **11** show excellent potency, particularly against IKKα. This improvement, compared to compound **1** is possibly due to an additional interaction made by the pyridyl nitrogen to the G+4 residue as shown in **Figure 34**.

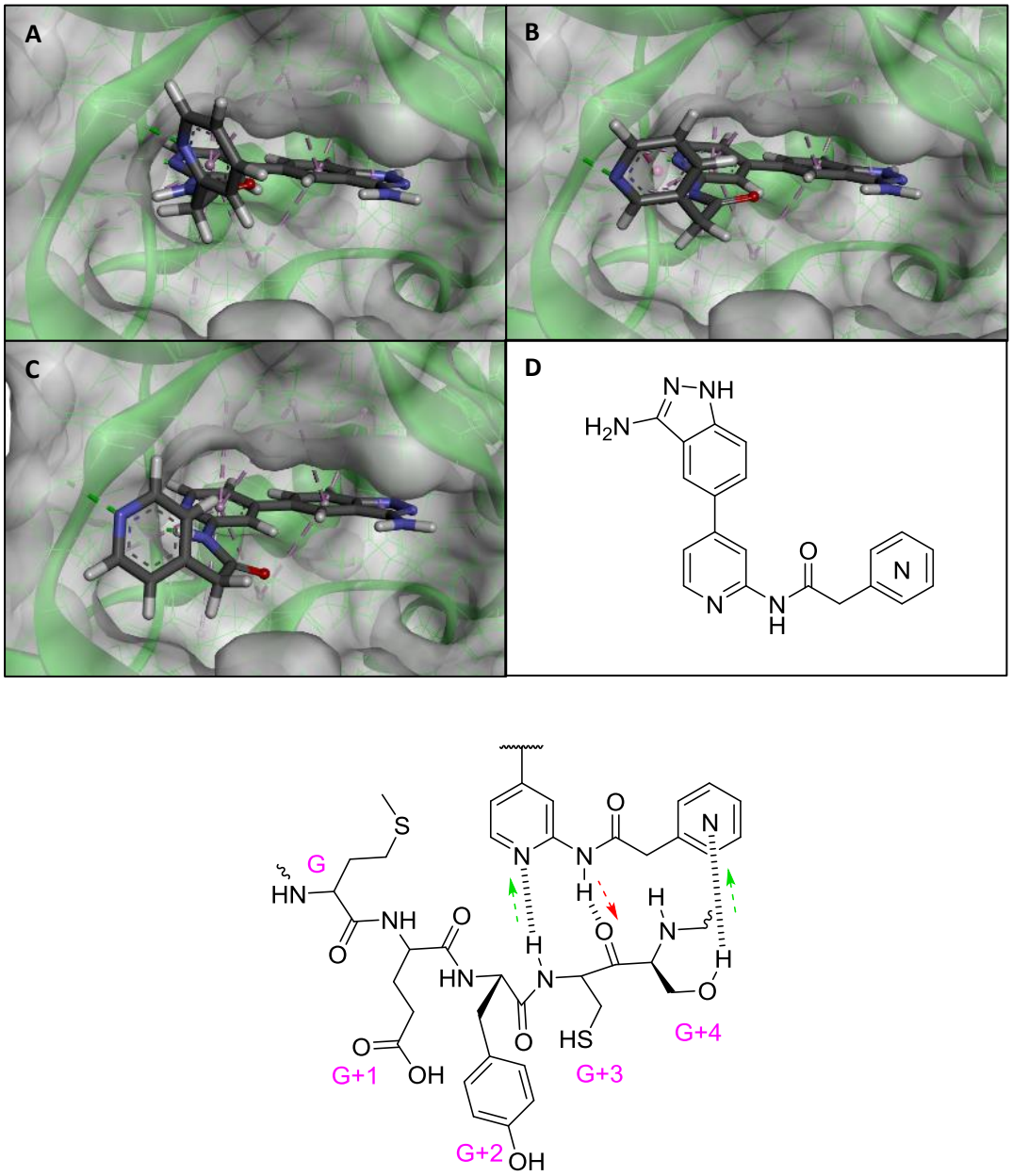

Figure 34. Compounds **9** (panel **A**), **10** (panel **B**), and **11** (panel **C**) docked in IKKα with 2-D representation of key hydrogen bonding interactions. Green dashes represent hydrogen bonds and hydrophobic interactions shown as purple dashes. Parent structure shown in panel **D** for clarity.

The G+4 residue differs between IKKα and IKKβ. As shown above, IKKα has a serine residue whereas in IKKβ it is a glutamine. The comparable increase in IKKβ activity compared to

compound **1** is likely to be because this is also capable of forming a hydrogen bond to the pyridyl nitrogen through the side chain NH_2.

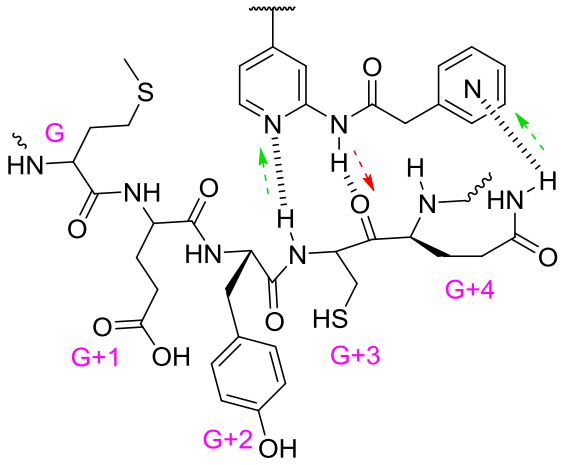

Figure 35. Key interactions of compounds **9, 10** and **11** with IKKβ**.**

The second trend is that trifluoromethyl substituents, exemplified by compounds **12-14**, particularly **12** and **14**, show very high selectivity for IKKα over IKKβ, though less potency than the pyridyl series. Both of these substituents are found in the upper right quadrant of the Craig plot (**Figure 36**) indicating electron density and increased hydrophobicity relative to H, whilst a major difference between them is in hydrogen-bonding capability. The hydrogen-bonding capability accounts for the potency of the pyridyl analogues in both IKK isoforms and the electron deficiency of pyridyl relative to trifluoromethylphenyl is similar

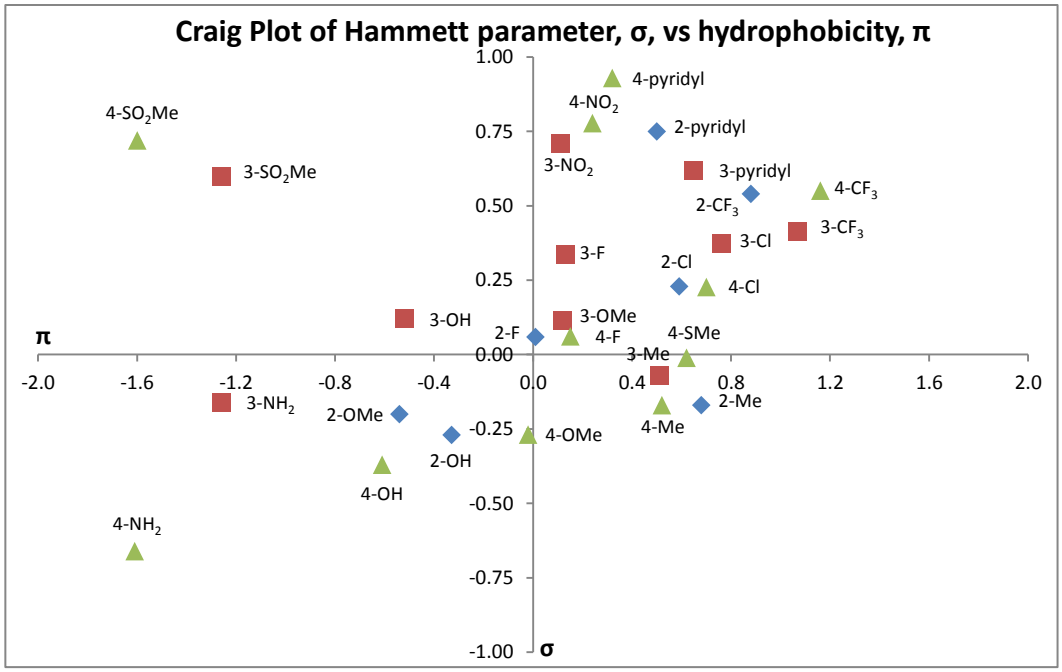

and thus unlikely to account for the selectivity. The Craig plot does however suggest that all three CF_3 analogues are more hydrophobic than the pyridyl analogues.

Figure 36. Craig plot for aromatic substituents of σ vs π. Values obtained from.[149–157]

Using Cresset TorchLite software[158,159] to display projected fields, it can be seen that the trifluoromethyl analogues project a similar, or even larger, hydrophobic field to a tolyl substituent.

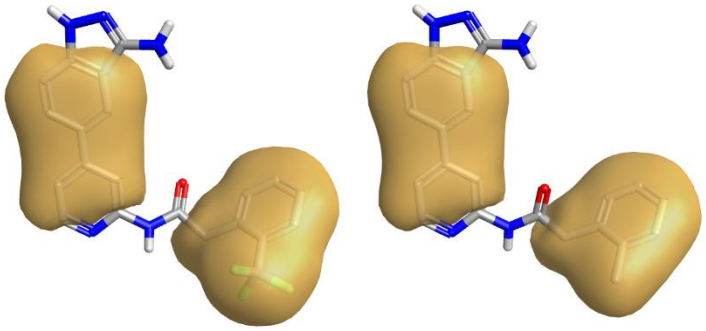

Figure 37. Hydrophobic field projected by compounds **12** and **27.**

Given that the mouth of the catalytic pocket contains several charged and polar residues, presumably from the need to guide the highly charged phosphate tail of ATP into the active site, it could be that larger, hydrophobic, substituents are detrimental to binding as there is no way the molecule can be positioned to avoid interaction with a polar residue. This alone would not account for the selectivity between the two IKK isoforms, as both are very polar in this region. The answer is likely to be the topology of the two kinases at the mouth of the catalytic pocket.

As can be seen in **Figure 38**, and as alluded to in section 3.1.1, the mouth of the catalytic pocket around the hinge is slightly more open and flexible in IKKα, shown in green, than in IKKβ, shown in red. It is therefore likely that the additional space in IKKα allows for the accommodation of this hydrophobicity, albeit with a small penalty relative to compound **1**, whereas there is simply not enough space in IKKβ to comfortably accommodate this hydrophobicity. Since CF_3 is generally considered to be similar to isopropyl and even larger than trimethylsilyl,[160] synthesis of these analogues may indicate whether the hydrophobicity is the most important factor to this selectivity.

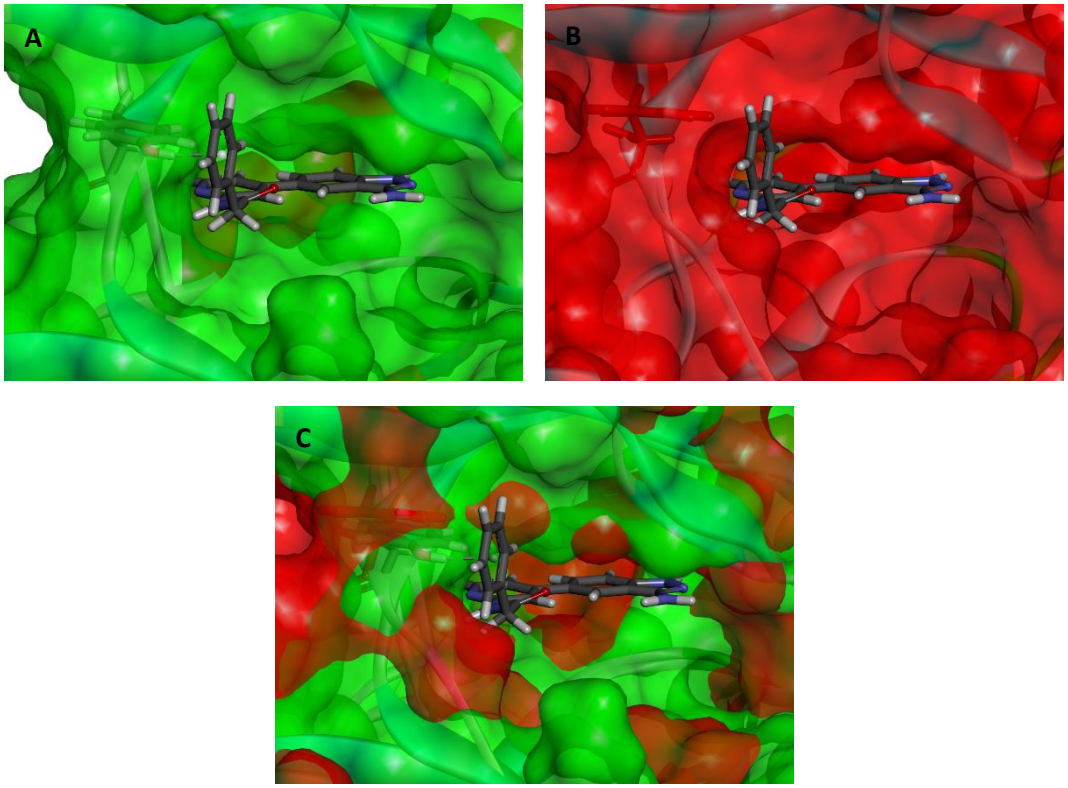

Figure 38. Docked binding poses of compound **1** in IKKα (panel **A**), IKKβ (panel **B**) and overlaid IKKα and IKKβ (panel **C**).Overlay indicates a tighter binding pocket around the mouth the catalytic pocket in IKKβ.

Whilst the large hydrophobic nature of CF_3 relative to a hydrogen atom is not ideal for binding in IKKα, the larger mouth allows for the positioning of the trifluoromethyl group in one of two small hydrophobic pockets above and below the molecule as shown below.

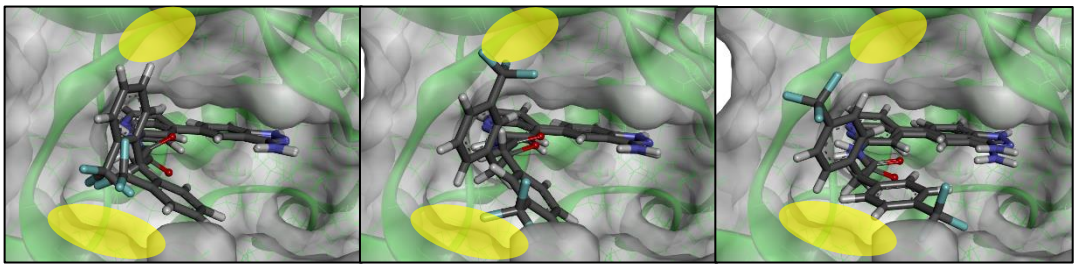

Figure 39. Most likely docking poses of compounds **12**-**14** in IKKα.

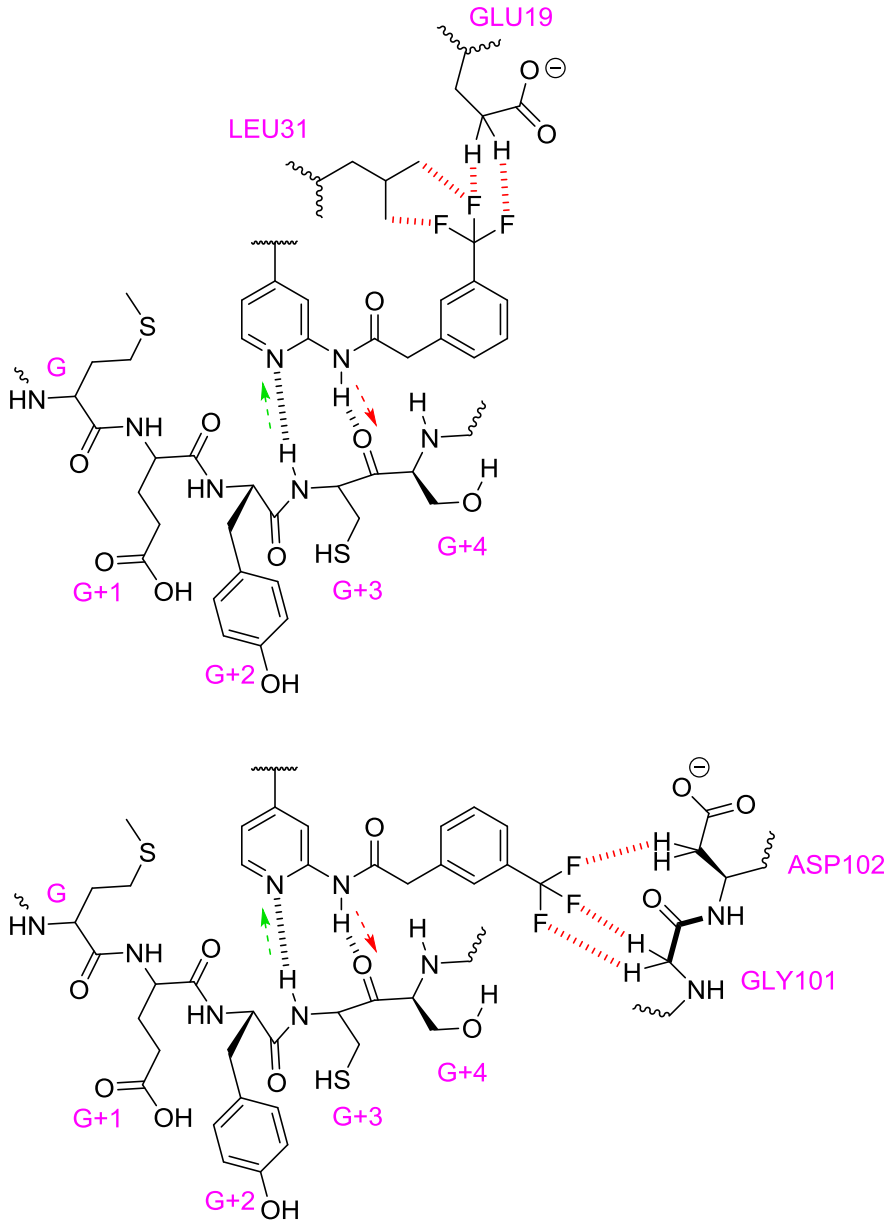

Figure 40. Possible interaction motifs for compound **13** with IKKα. Red dashes denote hydrophobic interactions.

Computational modelling of the 3 CF_3 analogues in IKKβ also only allows for the *meta*-substituted **12** to bind in the same orientation as that shown by the CDK2 crystal structure. This gives an indication of why the decrease of activity against IKKβ, relative to compound **1**, is less marked than for *ortho*- and *para*-substituted analogues, as it may be the only one able to adopt this most favourable pose and position the CF_3 in one of the hydrophobic regions.

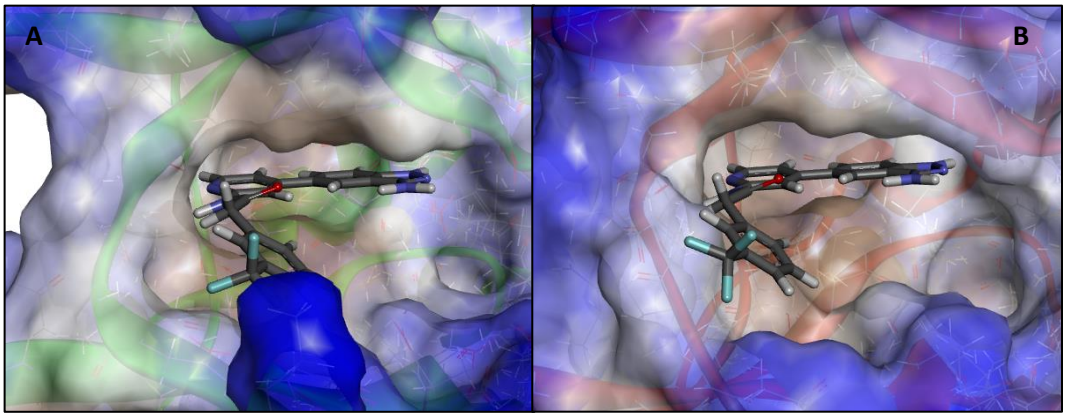

Figure 41. Compound **13** docked in IKKα (panel **A**) and IKKβ (panel **B**).Hydrophobic regions shown in white, hydrophilic regions in blue.

Assuming the same binding pose, **Figure 38** also explains the decrease in IKKβ activity for compound **2**. The change from the planar phenyl ring of compound **1** to the cyclohexyl of compound **2** increases the steric bulk at the mouth of the catalytic pocket and, as previously discussed, this area contains several polar residues - leading to unfavourable interactions in both isoforms - but is also smaller in IKKβ than in IKKα. The greater lipophilicity of compound **2** possibly accounts for the decrease in potency against both isoforms relative to compound **1** but an even greater decrease is seen against IKKβ because of the increased steric hindrance.

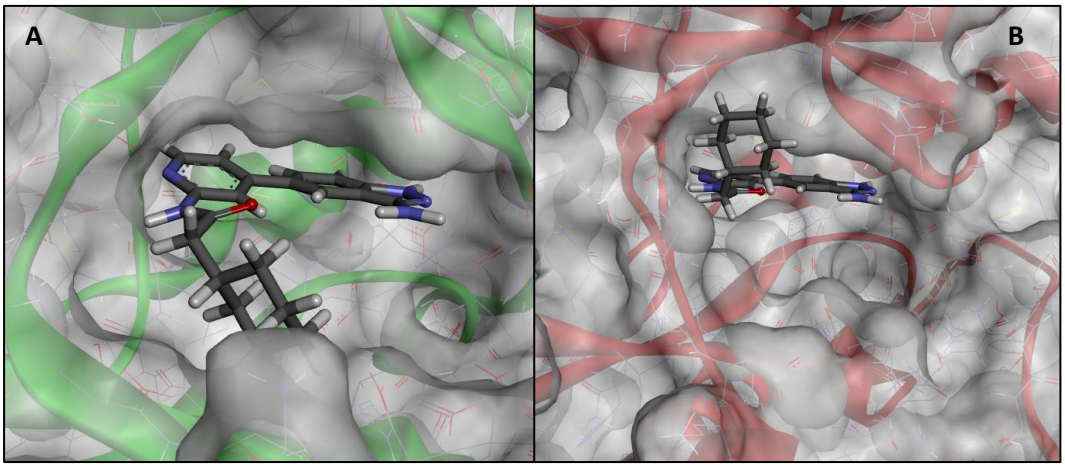

Figure 42. Compound **2** docked in IKKα (panel **A**) and IKKβ (panel **B**).

Another observation to be made about this series is the decrease in activity, against both isoforms, when larger *ortho*-substituents are incorporated, such as those seen in compounds **22** and **27** and to a lesser extent, **6** and **12**. In the case of compound **1**, the lowest energy conformation is with the pendant ring co-planar with the carbonyl, enabling the formation of an intramolecular pseudo-hydrogen bond.

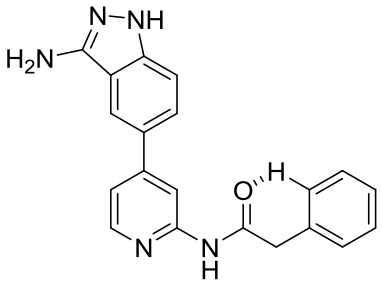

Figure 43. Intramolecular bonding in compound **1.**

Compound **3** remains equipotent because it is able to rotate through 180°and form the same interaction with the other *ortho*-H. F is still a relatively small substituent and can still be tolerated at the hinge

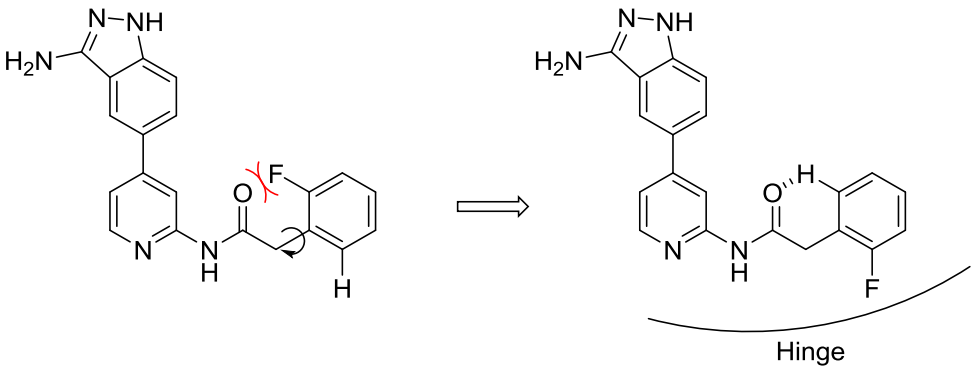

Figure 44. Intramolecular bonding in compound **3.**

With substituents larger than F, as in **6**, **12**, **22** and **27**, the rings now have no choice but to be forced out of alignment as these substituents cannot be tolerated at the hinge and will be repelled by the amide carbonyl. This results in the rings being orthogonal to each other which is less well tolerated due to the size of the binding site.

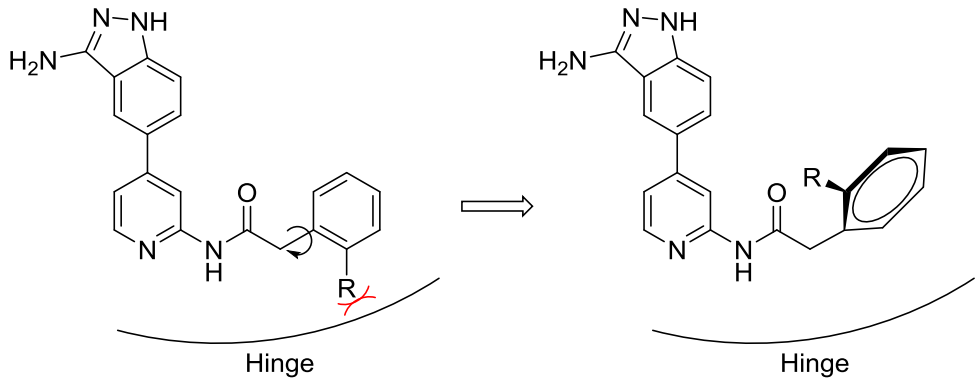

Figure 45. Position of *ortho*-substituted analogues of compound **1**.

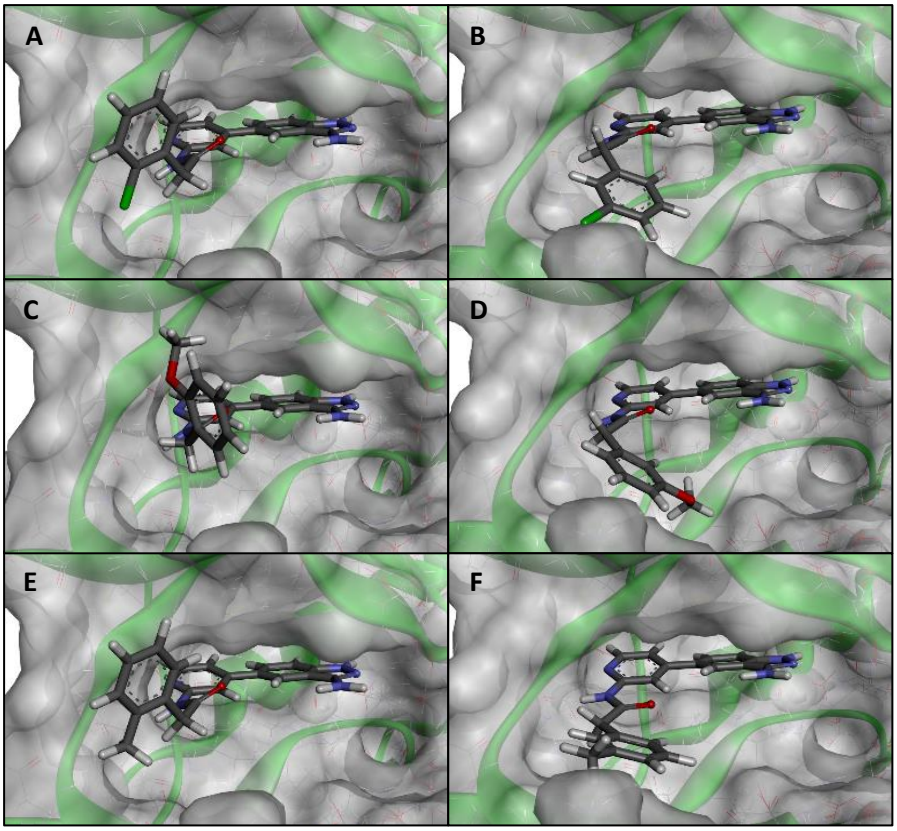

Figure 46. Docked poses in IKKα showing compounds **6, 22** and **27** (panels **A**, **C** and **E**) with orthogonal pendant phenyl ring compared with compounds **7, 23** and **28** (panels **B**, **D** and **F**) with close to co-planar phenyl.

Having investigated a range of phenyl ring substituents, other structural features of compound **1** were investigated to assess their effect on potency and isoform selectivity.

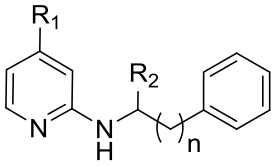

Compound	R_1 =	R_2 =	n =	K_i IKKα (nM)	K_i IKKβ (nM)	Selectivity (β/α)
30	3-C(O)NH_2Ph	=O	1	>30,000	>30,000	n/a
31	4-C(O)NH_2Ph	=O	1	>30,000	>30,000	n/a
32	1*H*-Benzimidazole-5-yl	=O	1	1,636	>30,000	>18
33	4-$CH_2N(CH_3)_2$ Ph	=O	1	>30,000	>30,000	n/a
34	3-Aminoindazole-5-yl	H(H)	1	19	587	31
35	3-Aminoindazole-5-yl	=O	2	157	838	5

Table 2. Further results of IKK biochemical assessment of compound **1** derivatives.

With the exception of compound **32**, all changes to the aminoindazole at R_1 resulted in an inactive compound. Benzimidazole **32** showed moderate activity against IKKα and, since no activity against IKKβ was detected, could form a second series of IKKα selective compounds: however, other changes would have to be made that would result in a big increase in potency against IKKα given the 70-fold decrease in activity relative to compound **1**.

The most obvious reason for the decrease in potency from compound **1** to other head group analogues **30**-**33** is the loss of hydrogen bonding capability in all cases. The crystal structure of **1** with CDK2 shows the aminoindazole making three hydrogen bonds to residues in the phosphate binding region. These residues translate into K44, E61 and D145 in IKKα. As the schematic representations in **Figure 47** show, modelling suggests that **30** and **31** make two hydrogen bonds in this region and **32** and **33** make only one. Since none of these make interactions with both acidic residues, it is likely that at least one of these has a significant influence on binding.

As already stated, benzimidazole **32** maintained moderate activity against IKKα. Modelling suggests that the bicyclic ring system of the benzimidazole forms sigma-pi interactions with V29 which is directly above it in the roof of the catalytic pocket. This interaction is analogous to a possible interaction with the aminoindazole and this residue. Since **32**, **31** and **33** are all incapable of making this interaction, it suggests that this capability is extremely important for the binding of these compounds.

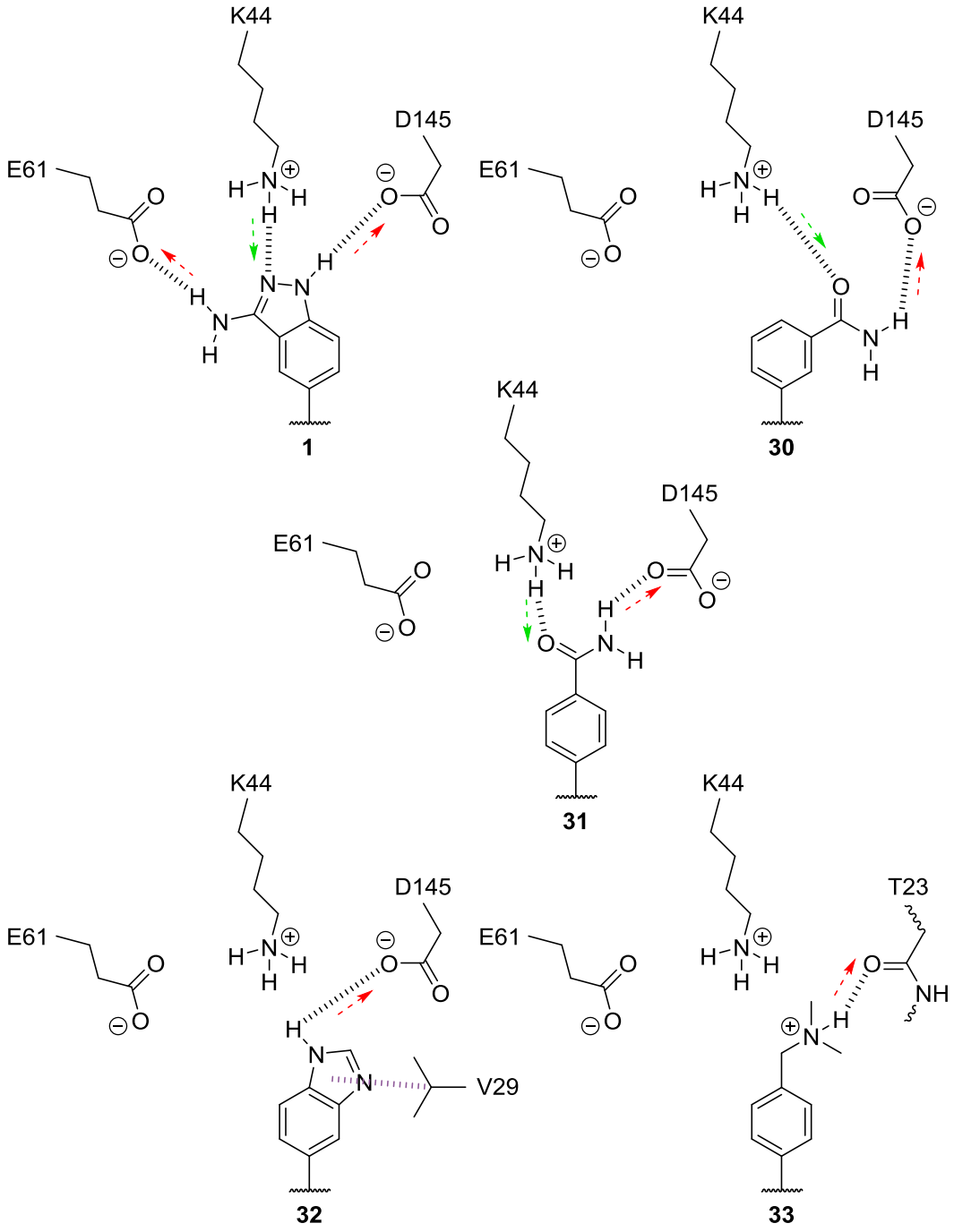

Figure 47. Schematic of binding poses of compounds **30-33** as suggested by modelling. Purple dashes denote pi-interactions.

Compound **34** suggested that the amide linker could be reduced to an amine and still retain activity and selectivity. Docking in IKKα suggests a very similar binding pose to compound **1** which agrees with the results of the biochemical assay.

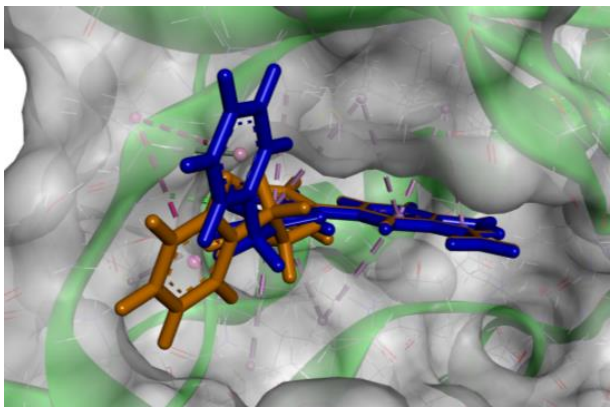

Figure 48. Docking of compounds **1** (blue) and **34** (orange) in IKKα.

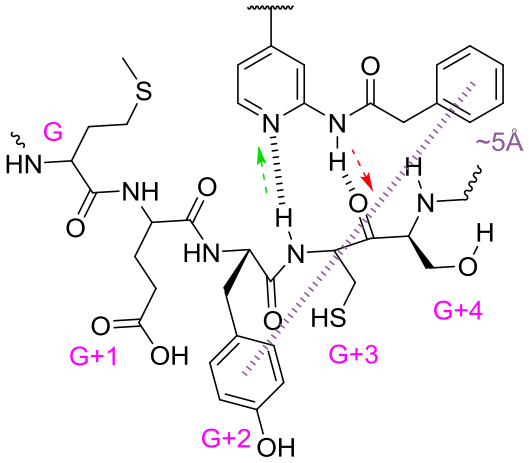

Figure 49. Interaction map showing selected interactions of compound **1** with IKKα.

The pi-pi interaction between the phenyl ring of **34** and the G+2 tyrosine is less available according to the model of the same compound in IKKβ. It suggests that, because of the tighter pocket in IKKβ, the chain flips down to form a pi-sigma interaction with VAL152. Assuming this binding mode, the moderate increase in selectivity could be due to this interaction not being as strong as the pi-pi interaction in IKKα

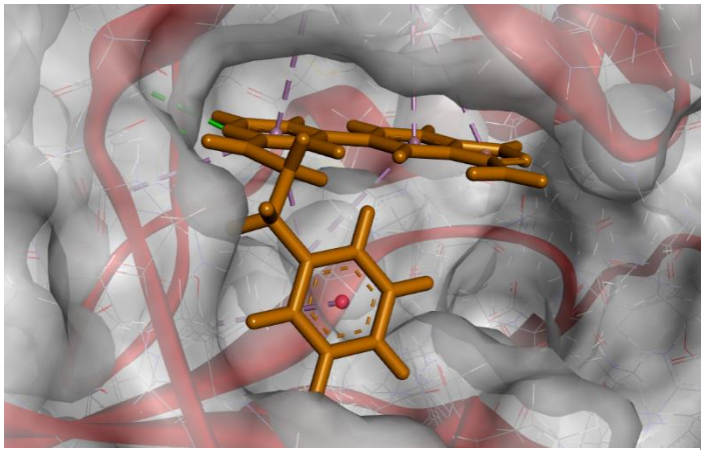

Figure 50. Compound **34** docked in IKKβ.

The reduction of the amide to the amine could be an advantage in terms of both TPSA and ligand efficiency, however this must be counter-balanced against the increased flexibility this results in, which may make the compound more promiscuous and increase off-target effects.

Lengthening the linker in compound **35** led to a decrease in both potency and selectivity relative to **1**. The loss in potency against IKKα is likely to be because lengthening the chain removes the ability of the pendent phenyl to make the pi-pi interaction with the G+2 tyrosine discussed above. This effect seems to be somewhat ameliorated by the long range sigma-pi interaction with LEU21.

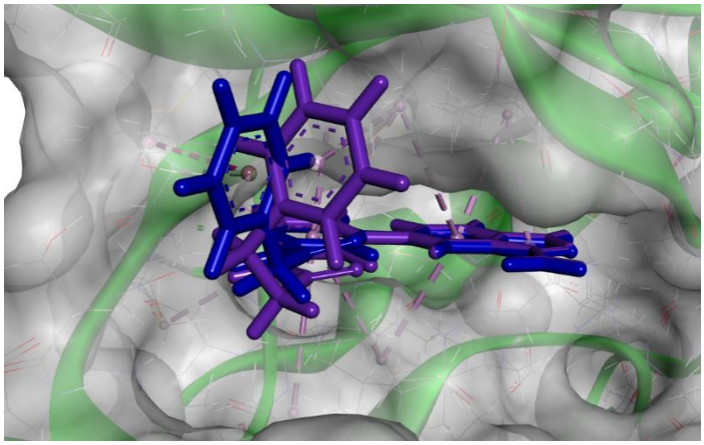

Figure 51. Docking of compounds **1** (blue) and **35** (purple) in IKKα.

Docking the same compound in IKKβ, as shown in **Figure 52** suggests that the pendant phenyl ring does not make any specific interactions with the protein which would account for the drop in activity.

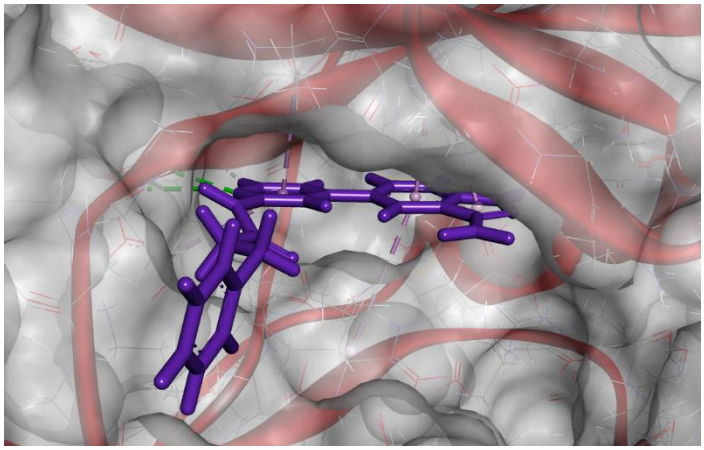

Figure 52. Compound **35** docked in IKKβ.

3.1.4. Chemistry

3.1.4.1. Amide coupling

The amide motif is a very common feature in a wide variety of drugs and drug-like compounds.[161] The most direct way of forming amide bonds is a condensation between a carboxylic acid and an amine. This is, however, a very crude reaction and will only occur at high temperatures, usually well above a temperature at which both reactants are stable.[162] By far the most common way of overcoming this problem is by activating the carboxylic acid in some way. To this end, there has been a plethora of reactions developed to facilitate this reaction.[161]

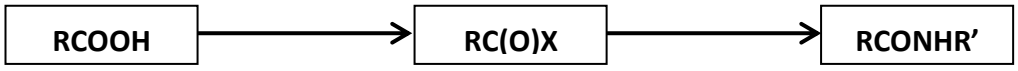

The form of the activating agent can vary hugely, although the majority can be broadly grouped into about 10 sets of similar reactions.[161,163] These include the use of acyl chlorides and phosphate activating groups.

Intermediate 4-chloro-2-amidopyridines were synthesised by reacting 2-amino-4-chloropyridine with either the appropriately substituted phenylacetyl chloride or phenylacetic acid with T3P as a coupling agent.

The red arrows in **Scheme 1** show the probable mechanism of amide formation using acyl chlorides. The reaction likely proceeds through attack of the amine nucleophile into the electrophilic sp^2 carbonyl centre, through a tetrahedral intermediate and elimination of chloride. The protonated amide is quickly neutralised by the presence of an organic base.

As shown by the blue arrows in **Scheme 1**, the phenylacetic acid substrate is pre-activated by an organic base, such as triethylamine, deprotonating the acid and subsequent attack by the carboxylate at one of the T3P phosphorus atoms, ring opening the cyclic anhydride. The ring opened T3P is then substituted by the amine through an analogous mechanism before deprotonation to yield the final product.

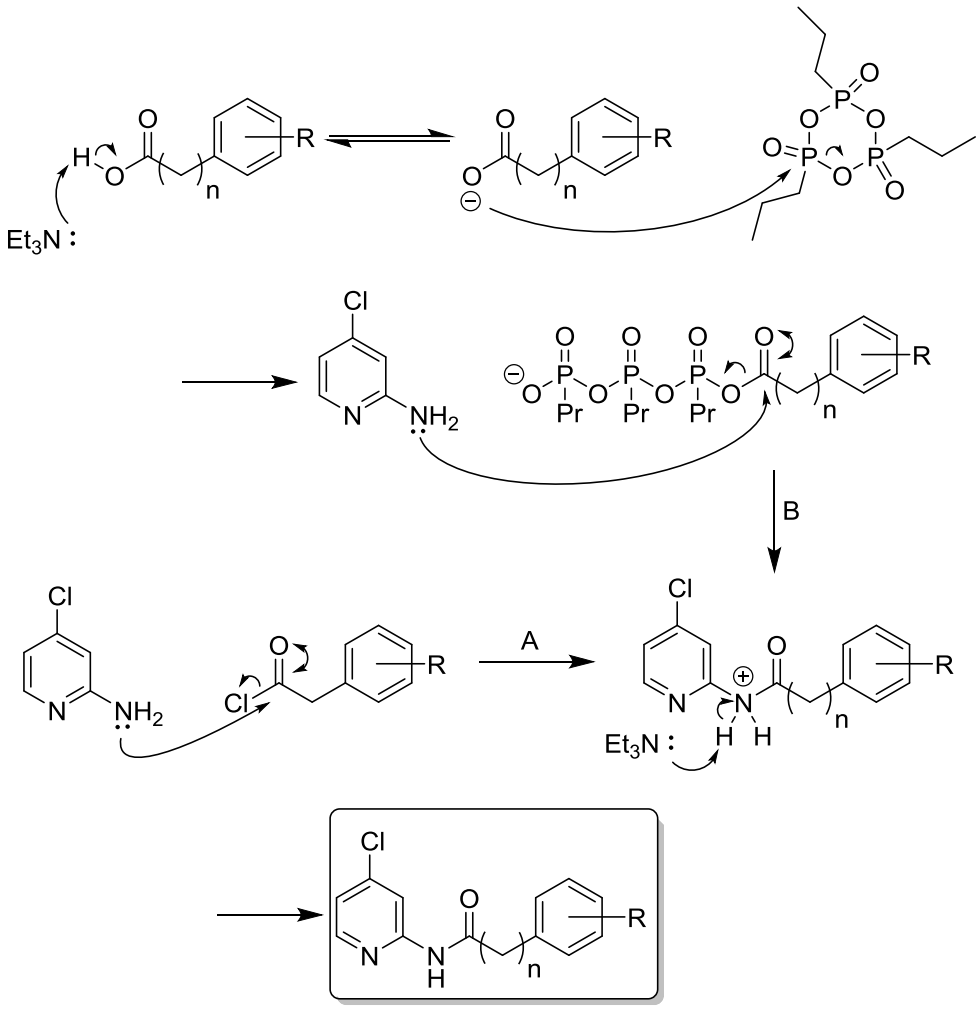

Scheme 1. Mechanisms of amide coupling using acyl chloride or activated carboxylic acid substrates. As shown by arrows A and B, both routes lead to a proposed common intermediate.

^{1}H NMR of the reaction products showed a characteristic amide -NH peak at around 11 ppm suggesting formation of the desired compounds. Acyl chloride starting materials showed no peaks in this region of the spectrum and carboxylic acid peaks were found around 12.5 ppm. A small, but significant, shift of less than 10 ppm was also observed by ^{13}C NMR for the carbonyl carbon providing further evidence of conversion.

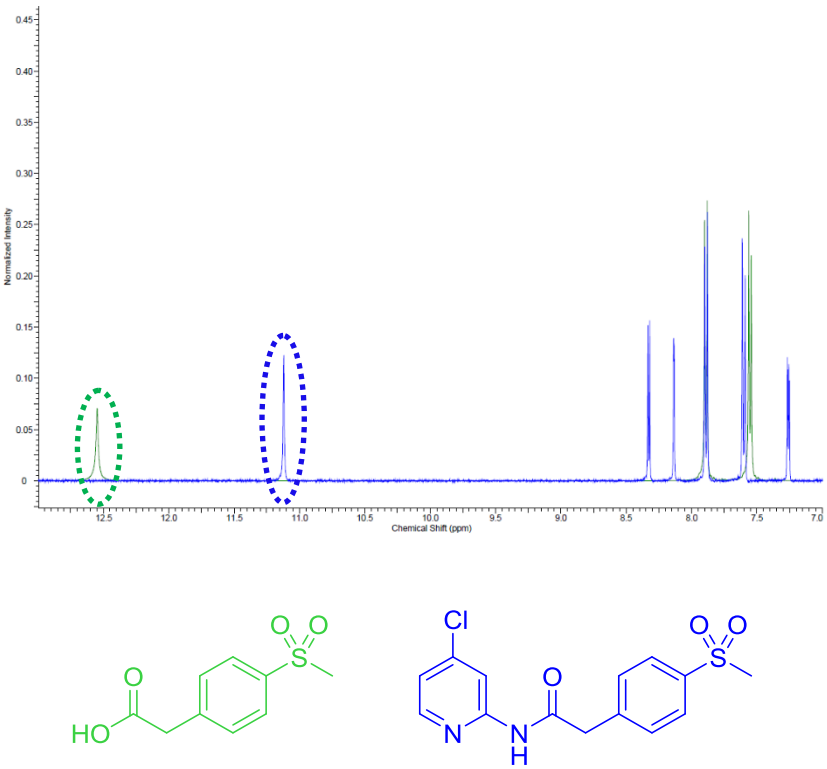

Figure 53. ^{1}H NMR showing carboxylic acid (green) overlaid with amide product (blue) for pre-compound **26**. ^{1}H NMR in d_6-DMSO at 400 MHz.

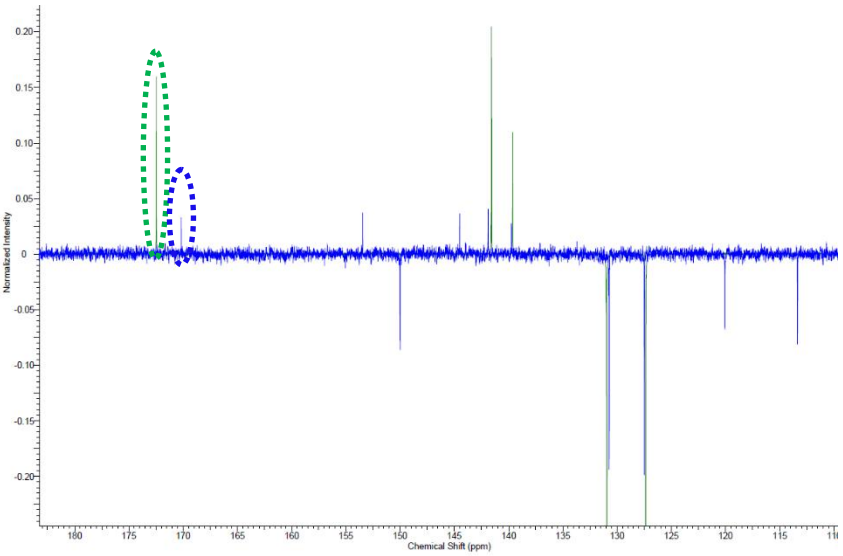

Figure 54. DEPTQ spectra comparing acid (green) and amide (blue). DEPTQ in d_6-DMSO at 100 MHz.

3.1.4.2. Aminoindazole synthesis

3-Aminoindazole-5-boronic acid pinacol ester was synthesised from a 2-fluorobenzonitrile starting material and hydrazine hydrate. The reaction is thought to proceed via a S_NAr reaction, with hydrazine acting as the nucleophile to substitute the fluorine. After this displacement the other nitrogen of the hydrazine performs a 5-exo-dig intramolecular cyclisation which, after proton transfer, yields the desired boronic ester.

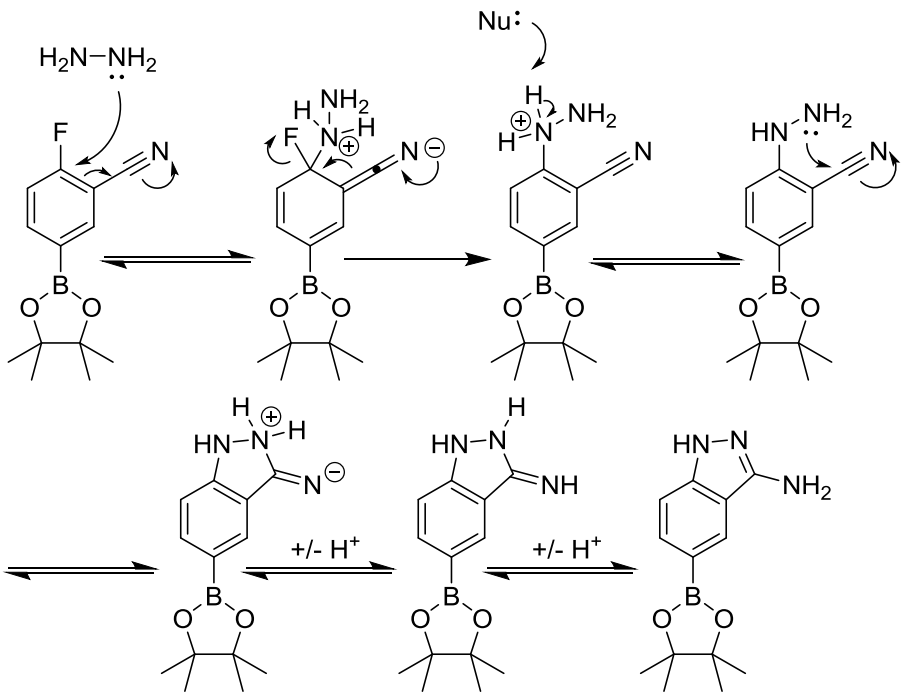

Scheme 2. Synthesis of 3-aminoindazole-5-boronic acid pinacol ester.

The cyclisation proceeded in moderately good yields and work up proved facile, with filtration and aqueous wash proving adequate to obtain the product in high purity. This reaction was also amenable to scale-up and could be carried out on a multi-gram scale and, provided it was largely protected from oxidative conditions, could be stored for long periods of time; allowing for batches to be made in advance of the final coupling.

Appearance of endocyclic -NH peak at 11.5 ppm and exocyclic -NH_2 at 5.5 ppm in ^{1}H NMR was indicative of successful cyclisation.

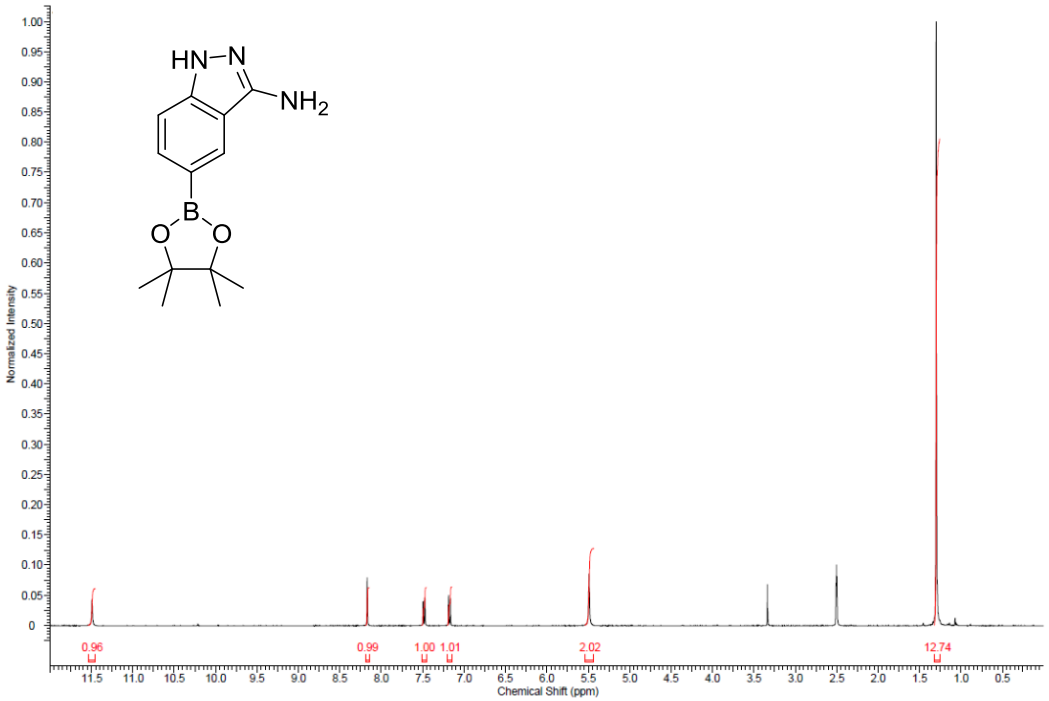

Figure 55. ^{1}H NMR spectrum of 3-aminoindazole-5-boronic acid pinacol ester. ^{1}H NMR in d_6-DMSO at 400 MHz.

3.1.4.3. Suzuki reaction

Today, the formation of biaryl systems through palladium cross-catalysis is so well exemplified and so widely used that the two have become almost synonymous.[164] Possibly the best known palladium-catalysed aryl-aryl bond formation is the Suzuki reaction, the proposed catalytic cycle for which is shown in **Scheme 3**.

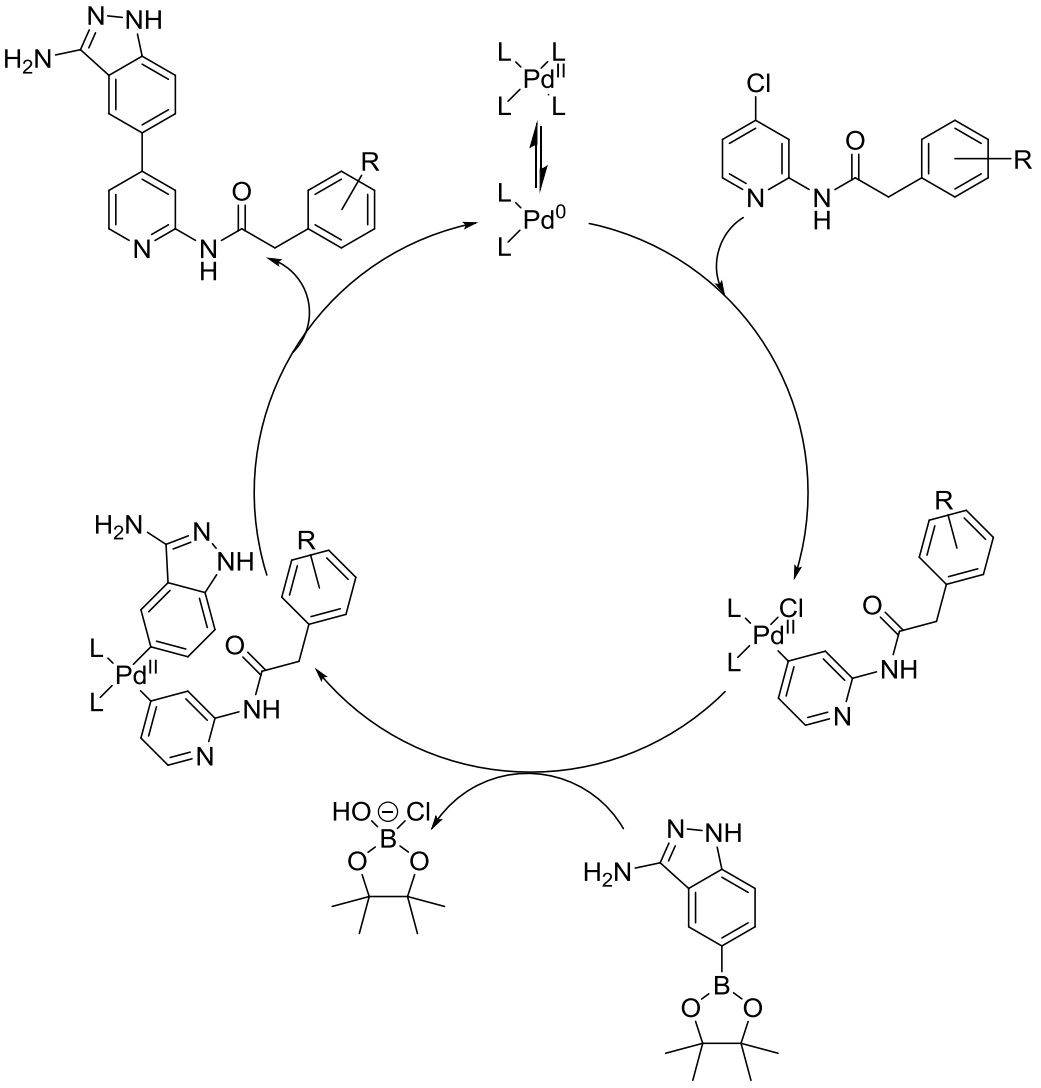

Scheme 3. Proposed catalytic cycle for the synthesis of compound **1** and related analogues.

This first step involves the reduction of palladium II to palladium 0, which is the active form of the catalyst. Over the years, the choice of catalysts has widened substantially. The first catalysts used in palladium cross-coupling employed simple, monodentate ligands such as chloride[165], acetate[166] or triphenylphosphine[167]. As more complex reactions were

developed, however, the need for more active catalysts grew. This led to the development of a range of alternative ligands: both more complex monodentate ligands[168–172] and multidentate ligands.[173] This increase in catalyst choice has also made the coupling of less active aryl substrates, such as chlorides, possible.[174,175] This has proved invaluable as 4-bromo- or 4-iodo-2-aminopyridine are considerably more expensive than the chloro analogue and so more active catalysts have been employed to avoid the need for high temperatures or long reaction times. Use of a di-*tert*-butylphosphinoferracene bidentate ligand allowed the reaction to proceed in good yields at 70 °C overnight. This was particularly useful in avoiding hydrolysis of the amide bond, which had been observed with some examples when higher temperatures had been used.

Following catalyst reduction and activation, the halide reactant oxidatively adds across the catalyst. The halide is then substituted by a more active ligand which comes from the base used in the reaction. This is often an alkoxide[171] or phosphate.[170] A second ligand substitution is then thought to occur. This can also be described as a transmetallation because the second coupling partner is transferred from the boron "ate" species to the palladium complex, substituting the base. The final step is a reductive elimination in which the final coupling occurs to yield the product and the palladium returns to oxidation state 0 making it available to start another cycle.

The rate of the reaction is determined by many things and the rate determining step is thought to be governed by the relative reactivity of the leaving group during the oxidative addition step. For example, in mechanistic studies carried out by Smith *et al.*, it was shown that, if the halide coupling partner was an aryl iodide, the rate limiting step was transmetallation. If, however, an aryl bromide was used, then oxidative addition is the rate determining step.[176] This is consistent with the general order of reactivity of leaving groups that $I^- > {}^-OTf > Br^- >> Cl^- >>> F^-$.[177] Choice of base is also important because the rate of halide substitution can alter the rate of the reaction depending on the relative rate of this step compared to the others. Work in 1987 by Uenishi *et al.* showed that changing the nature of a hydroxide base can alter the relative rate by up to 60 times.[178] This was, again, important as previous work within the group had shown tribasic phosphate to be a suitable base for the reaction. The suitability of the base allowed the reaction to proceed with <1.4 equivalents which limited the amide hydrolysis seen with >2 equivalents.

The relative rates of the reductive elimination step can also vary based on the nature of the product. These broadly follow the series aryl-aryl > aryl-alkyl > *n*-propyl- *n*-propyl > ethyl-ethyl > methyl-methyl,[177] though there is some variance from this depending on other steric and electronic factors.

3.1.4.4. Boc deprotection

Compounds **15** and **16** were obtained by Boc deprotection of **18** and **19**. Phenyl amines were protected during the amide coupling step to avoid polymerisation as shown in **Scheme 4**.

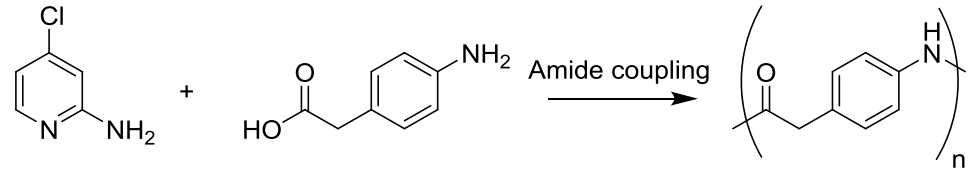

Scheme 4. Polymerisation of 4-aminophenylacetic acid under amide coupling conditions.

The Boc deprotection was achieved by stirring in 2:1 dichloromethane:trifluoroacetic acid. The mechanism involves protonation of the ether oxygen of the carbamate and loss of *tert*-butyl cation (as *iso*-butane gas) and decarboxylation of the unstable carbamic acid.

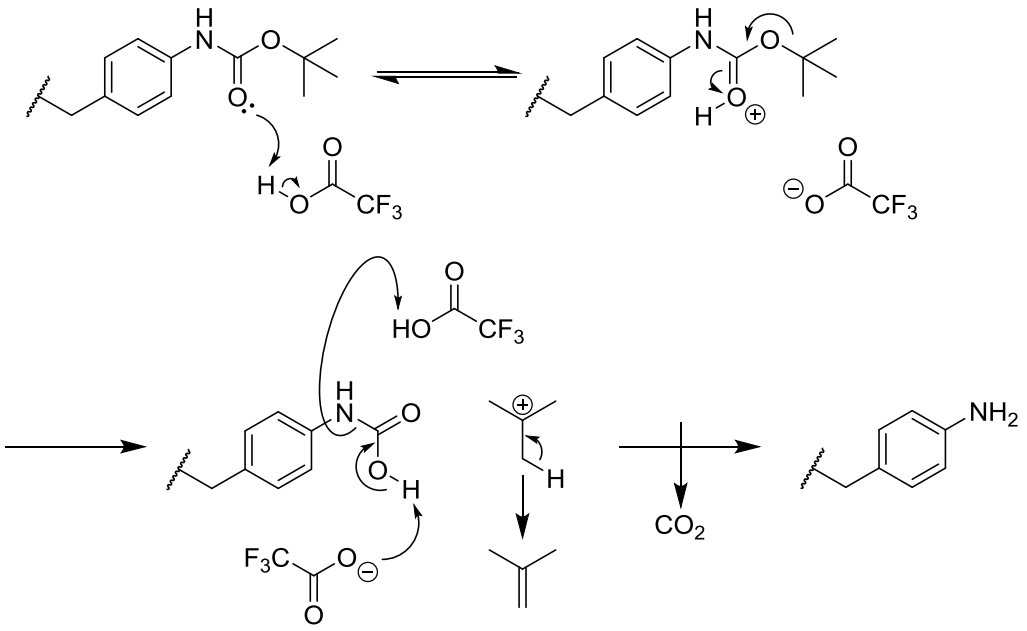

Scheme 5. Proposed mechanism of Boc deprotection.

3.1.5. Conclusions and synthetic schemes

Work described in this chapter has generated a series of compounds which show low nanomolar potency against IKKα and up to 550-fold selectivity over the IKKβ isoform. These compounds represent excellent tools for investigations into the role of IKKα within the NF-κB signalling pathway. The compounds have been synthesised in two steps, beginning with either an amide coupling reaction or a nucleophilic aromatic substitution followed by a Suzuki coupling to provide compounds with high levels of purity after chromatographic purification.

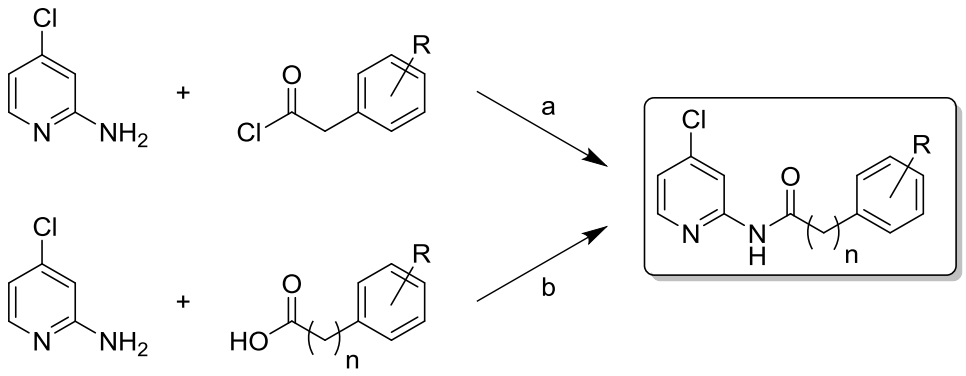

a) NEt_3 (2.5 equiv.), CH_2Cl_2, 0 °C, 30 mins - reflux, 16 h; b) NEt_3 (4 equiv.), T3P (2 equiv.), THF, r.t., 16 h, n = 1 or 2.

Scheme 6. Synthesis of 2-amido-4-chloropyridines.

Compounds **6**-**8** contain a chloro-substituted phenyl ring. To avoid unwanted side-reactions, the precursors were made using a 4-bromo-2-aminopyridine starting material. Whilst the amidopyridine ring is likely to be more electron deficient than the pendant phenyl ring, and therefore the halogen substituent more reactive towards the oxidative addition step, the difference in reactivity is likely to be quite small. The use of bromo-substituted starting material avoided this issue, with no chloro-coupling seen in the final Suzuki step and the boronic ester substituting preferentially at the bromine.

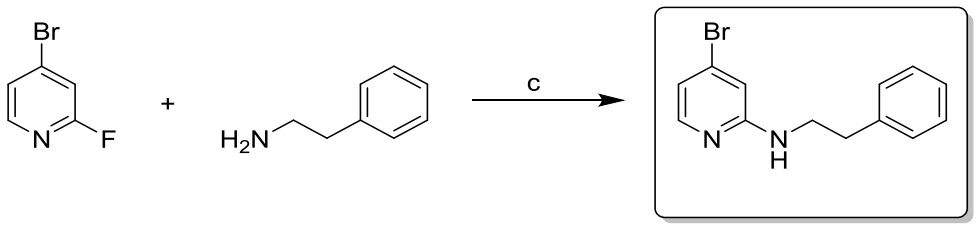

Scheme 7. Synthesis of compound **6-8** precursors.

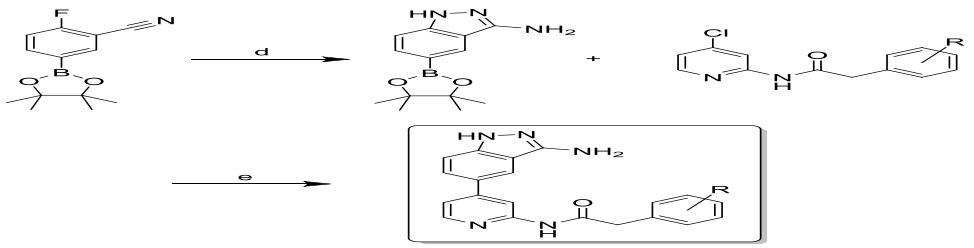

b) NEt_3 (4 equiv.), T3P (2 equiv.), THF, r.t., 16 h; c) 1,4-Dioxane, µwave, 180 °C, 1 h.

Scheme 8. Synthesis of 4-bromo-*N*-phenethylpyridin-2-amine.

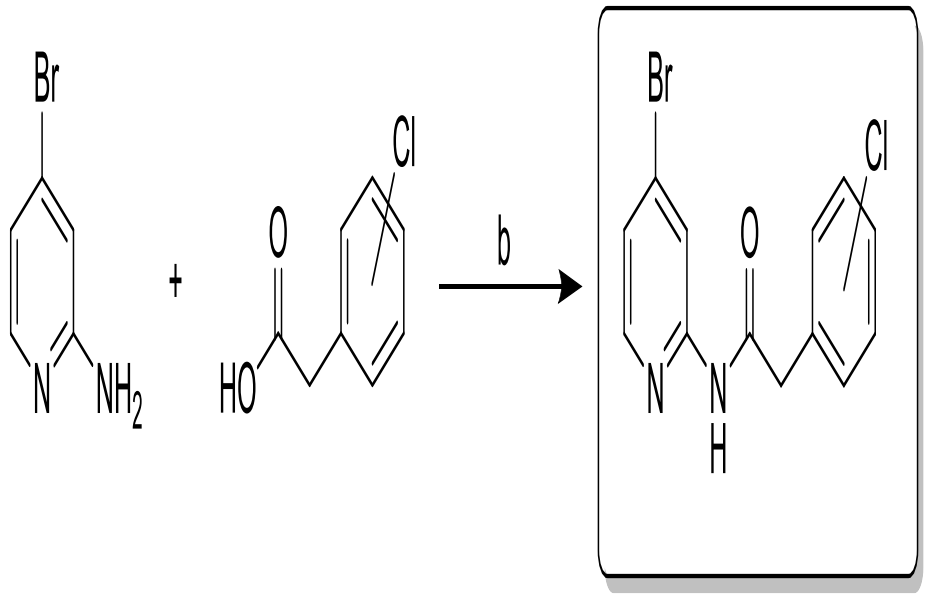

d) $N_2H_4 \cdot H_2O$ (5 equiv.), EtOH, reflux, 30 h.; e) $Pd(dtbpf)Cl_2$ (0.1 equiv.), EtOH, $K_3PO_{4\,(aq)}$, 70 °C, 16-24 h.

Scheme 9. Synthesis of 4-(3-aminoindazol-5-yl)-2-amidopyridines.

3.2. NIK Inhibitors

3.2.1. NIK biochemical assay

Due to the lack of a low-cost, high-throughput assay, it was decided to develop a new primary assay which was based on a Promega ADP-Glo® protocol.[179] The methodology decided upon utilised Promega's, cheaper, Kinase-Glo® in a 96-well half-area plate format in order to keep enzyme use to a minimum.

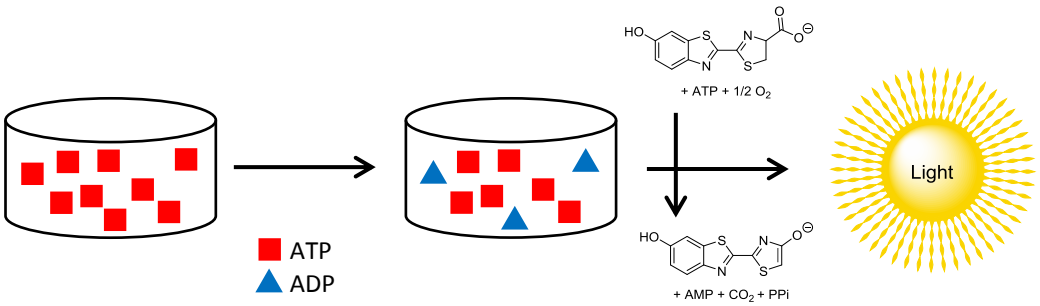

Figure 56. Schematic of kinase glo assay.

Similarly to the IKK biochemical assay, the initial kinase assay mimics the biological reaction of ATP hydrolysis to ADP and subsequent phosphorylation of a substrate. Unlike the IKK assay, however, where detection relies upon trapping and tagging of phosphorylated substrate, the residual amount of ATP is measured directly. This is done by adding Kinase-Glo® reagent which contains luciferase: an enzyme which converts ATP to AMP resulting in the generation of light.

In the NF-κB signalling pathway, the downstream kinase phosphorylated by NIK is IKKα. This would be the ideal protein substrate to use in this assay; however it is well documented that IKKα possesses significant autophosphorylation capabilities.[180] Since the Kinase-Glo® method is a measure of residual ATP after the kinase reaction, IKKα could not be an appropriate substrate as there would be no way to determine whether observed changes in ATP concentration were due to NIK or IKKα activity. It was therefore decided that myelin basic protein (MBP) would be used as the substrate. MBP is a protein known to be phosphorylated at multiple sites by a wide range of serine/threonine and tyrosine kinases.[181–184] As such, MBP has become a commonly used substrate for kinase activity assays.[185] A Kinase-Glo® methodology for investigation of NIK has been briefly reported before but did not use any substrate.[186] Parallel reactions run in-house incorporating and

excluding substrate using a focused compound library showed that the use of a protein substrate for NIK was critical to obtaining consistent results.

Throughout the development process, two steps were identified which had significant bearing on the reliability of the assay. The first of these was using freshly prepared buffer solution. Assays using buffer solution prepared more than approximately 3 hours before addition did not give consistent results. This was thought to be due to the degradation of dithiothreitol (DTT) which was used to stabilise the enzyme in solution. In addition, the pH of the buffer solution was assessed at 30 °C so as to ensure a pH of 7.5 during incubation.

The second detail was the equilibration period after incubation. After incubation at 30 °C, it was critical that the plate be allowed to return to room temperature (21 °C) before addition of the Kinase-Glo® reagent. This equilibration took 10-15 minutes and failure to adhere to an equilibration period of at least 10 minutes led to unusable results.

The initial assay optimisation involved a calculation of K_m and V_{max} for the ATP substrate. K_m apparent was determined to be 33.0 ± 3.4 μM (**Figure 56**) and titration of NIK found 5nM to be a sufficient concentration for the assay. Due to the limitations of the plate reader, saturation kinetics were not able to be obtained for the MBP. A concentration of 0.1 mg/mL was used based on Promega's ADP-Glo® methodology.

A commonly used indicator of the stability of a high throughput screening assay is the Z' factor,[187] which is calculated using the following equation:

$$Z' = 1- (3(\sigma_{+ve} + \sigma_{-ve})/(\mu_{+ve} - \mu_{-ve}))$$

where σ is the standard deviation and μ is the mean.

After optimisation, the assay was calculated to have a Z' factor of 0.64 ± 0.11 (n = 4) indicating a stable and robust assay and demonstrating that the assay is suitable for high throughput screening. An example assay is shown in **Figure 58**.

The kinase pan-inhibitor staurosporine was used as a control compound for the assay and was evaluated over a range of 100 pM to 30 μM. IC_{50} was calculated to be 67 nM (n = 3) which is comparable to previously published data[179]. This compound was subsequently added as a standard compound to every assay plate to ensure consistency of results.

The optimised assay conditions were as follows: recombinant human NIK (active) 5 nM (Promega, USA) was added to MBP 0.1 mg/mL (Promega, USA) and 5 µM ATP in assay buffer (40 mM Tris-HCl (pH 7.5 ± 0.05), 20 mM $MgCl_2$, BSA 0.1 mg/mL and DTT (50 µM) in a white half well 96-well plate (Greiner Bio One GmbH, Germany), in the presence and absence of test compound, to a total volume of 20 µL. Plate was covered with a lid, wrapped in cling film and placed in a foil bag (previously stored streptavidin coated plate (Perkin Elmer, UK)) and shaken on a Stuart microplate shaker (Bibby Scientific Ltd, UK) at 850 rpm for 1 minute before incubating at 30 °C for 1 hour. Plate was removed from foil bag and allowed to equilibrate to 21 °C for 15 minutes before addition of Kinase-Glo® reagent (Promega, USA) (20 µL). Mixture was incubated in the dark for 10 minutes and luminescence was detected on a Wallac Victor^2 1420 multilabel counter (Perkin Elmer, UK). IC_{50} values were converted to K_i values using the Cheng-Prusoff Equation.[145]

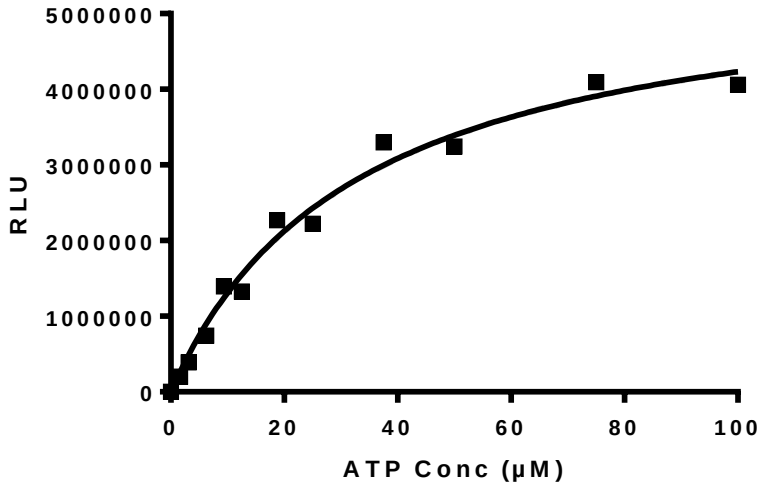

Figure 57. Michaelis-Menten plot for determining Km of ATP using Kinase-Glo method. Data points show average of duplicated data. Calculated Km = 33.0 ± 3.4 µM.

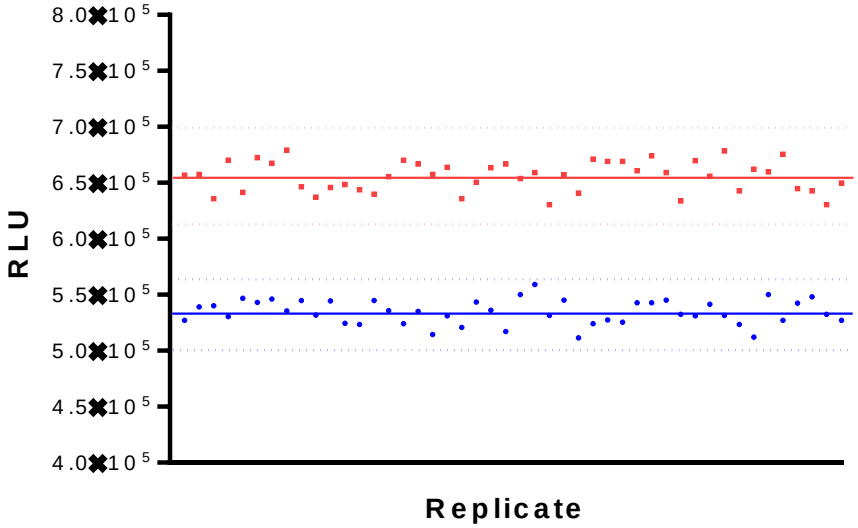

Figure 58. Exemplar Z' assay with means indicated by solid lines and 3 standard deviations shown as dotted lines. Red indicates assay in the presence of ATP but excluding enzyme, blue indicates assay in the presence of ATP and enzyme.

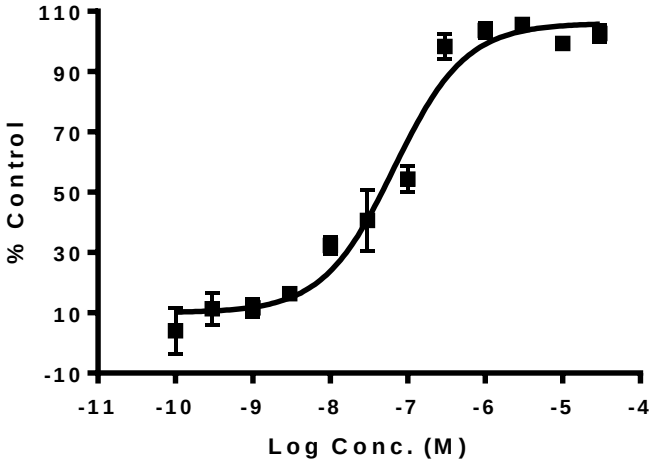

Figure 59. Dose-response curve of staurosporine vs NIK. Data points show mean (± standard error mean) from three separate experiments. The IC_{50} ± SEM value was 67 ± 1.24 nM. R^2 = 0.942. K_i = 57 nM.

3.2.2. Compound screen

Compounds **1**-**35** were screened for activity against NIK at 30 and 10 µM, single point concentration in triplicate. The results are shown in **Figure** below:

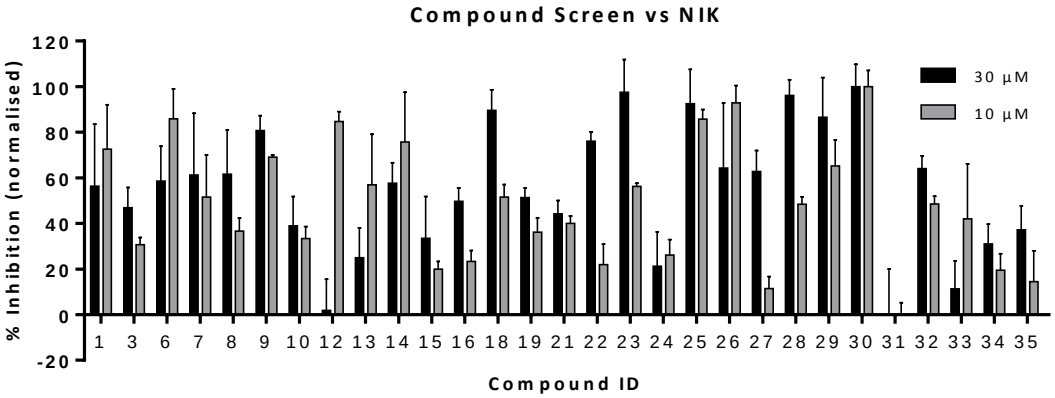

Compound	R =	Compound	R =
1	H	**18**	3-NHBoc
3	2-F	**19**	4-NHBoc
6	2-Cl	**21**	4-SCH_3
7	3-Cl	**22**	2-OCH_3
8	4-Cl	**23**	3-OCH_3
9	2-pyridyl	**24**	4-OCH_3
10	3-pyridyl	**25**	3-SO_2CH_3
12	2-CF_3	**26**	4-SO_2CH_3
13	3-CF_3	**27**	2-CH_3
14	4-CF_3	**28**	3-CH_3
15	3-NH_2*	**29**	4-CH_3
16	4-NH_2		

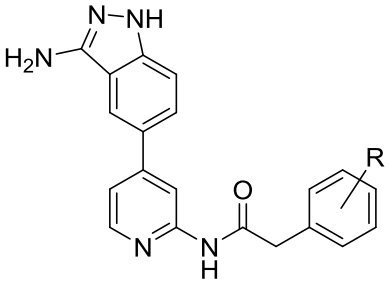

Figure 60. Results of compound screen vs NIK and tables of structures.

Compound	R_1 =	R_2 =	n =
30	3-C(O)NH_2Ph	=O	1
31	4-C(O)NH_2Ph	=O	1
32	6-Benzimidazole	=O	1
33	4-$CH_2N(CH_3)_2$ Ph	=O	1
34	3-Aminoindazole	H(H)	1
35	3-Aminoindazole	=O	2

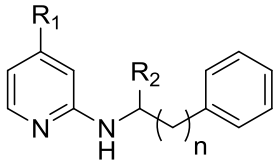

Figure 60 (cont.). Results of compound screen vs NIK and tables of structures.

As will be discussed later, screening small molecules at high concentrations can lead to a not insignificantly high rate of error. Examples of this can be seen in compounds **12**-**14**, where inhibition seems to increase with decreasing concentration. These compounds are all isomers of a trifluoromethylphenyl series and it is thought that the erroneous results could be due to solubility problems in this assay at 30 μM. This seems to be a reasonable assumption as the series has the highest calculated logP, at 3.83, of any compound in this screen and such a marked inverse concentration-activity relationship is not seen with any other compound.

The reason for carrying out this assay at two concentrations was to reduce the rate of false positive hits. Had these compounds only been tested at 30 μM, compounds such as **18**, **23** and **28** would have looked quite promising, and given that all are 3-substituted, there could have been a rational explanation for consistent results. However, on assessing at 10 μM, it becomes clear that this activity is not borne out at lower concentration, with the inhibitory profile quickly dropping off.

Of the compounds assessed in this screen only three showed consistently good inhibition at both 30 and 10 μM. Compounds **25** and **26** are both methylsulfonate analogues of compound **1** and so further analysis of substituents located in the upper left quadrant of the Craig plot could prove interesting. From the perspective of canonical inhibition, however, both compounds exhibit sub-micromolar activity against IKKβ and this would therefore need to be significantly ameliorated with compound development. Conversely compound **30**, which showed similar activity to both **25** and **26**, was shown to have no activity against either IKK isoform assessed biochemically. This is likely to be due to the

replacement of the aminoindazole head group, which seems to convey potency in both IKKα and IKKβ, albeit with some slight bias towards IKKα. The *m*-phenylcarboxamide and 3-aminoindazole possess many similar binding capabilities; with both having similarly placed hydrogen bond donating NH_2 groups and analogous O or N hydrogen bond acceptors, and both having a central benzene ring capable of forming either hydrophobic interactions or pi-bonding to residues in the pocket. The fact that the 3-aminoindazole shows only moderate potency against NIK but good potency against IKKα and IKKβ, whilst the *m*-phenylcarboxamide is inactive in both IKK isoforms but shows activity against NIK suggests that the precise orientation of the analogous groups is important or that the endocyclic NH in the aminoindazole is important in differentiating between the different enzymes.

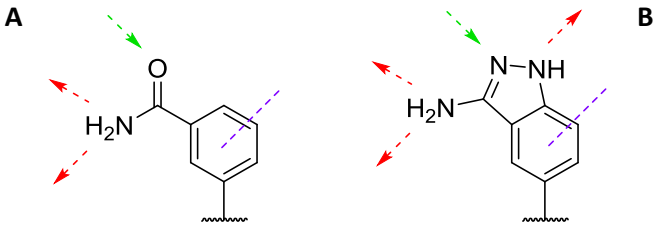

Figure 61. Binding capabilities of *m*-carboxamide (**A**) and aminoindazole (**B**). Hydrogen bond donor capabilities are shown in red, hydrogen bond acceptors in green and hydrophobic or pi-stacking in purple.

As a result of this screen, compound **30** was used as a template for compound development. Titration of compound **30** against NIK revealed an apparent K_i of 4.4 µM, as shown in **Figure 62**.

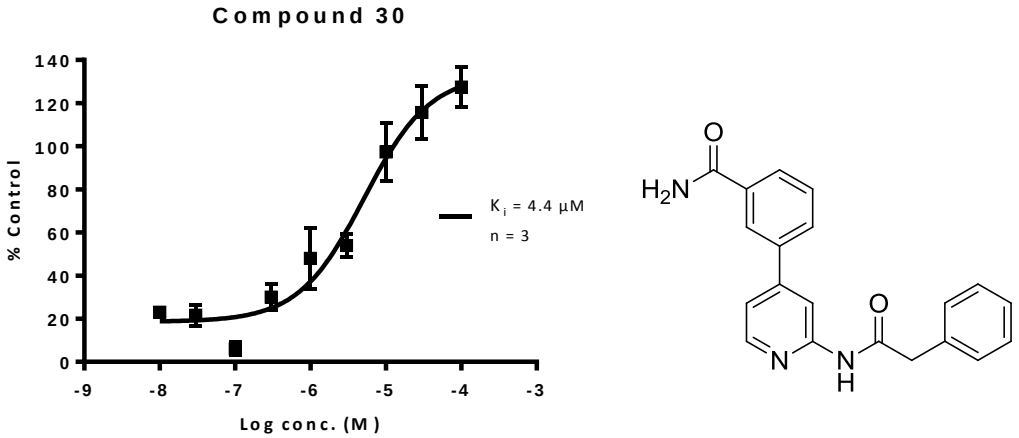

Figure 62. Inhibition curve of **30** against NIK with structure of **30** shown alongside.

The initial compound library had explored the pendent phenyl ring without conveying any great improvement in potency. Since the replacement of the aminoindazole with the *m*-phenylcarboxamide provided a noticeable increase in potency, a library was synthesised for a small fragment-based screen which retained this motif but searched for an alternative scaffold core to replace the amidopyridine to provide alternative vectors which could be used to exploit the catalytic pocket.

3.2.3. Fragment-based approaches in drug discovery

Fragment based drug discovery is a form of medicinal chemistry wherein initial hits are found by screening libraries of small molecules, which broadly comply with the so-called 'rule of three': molecular weight < 300; hydrogen bond donors ≤ 3; hydrogen bond acceptors ≤ 3 and logP ≤ 3.[188] There are a range of methodologies for finding fragment hits; each with their pros and cons and each leading to a slightly different optimisation technique.[189] Probably the two most contrasting methods are functional screening and X-ray crystallography. Functional screening involves testing each fragment at high concentration against the target of interest. This has the advantage of often being high-throughput compatible and uses comparatively small amounts of protein. On the other hand, it gives little, or no, indication of binding mode and can often lead to false positives.[189] Crystallography, by contrast, gives very clear information on mode of binding and no functional assay need be developed in order to screen. This does, however, require large amounts of protein - on top of the appropriate conditions to crystallise it - and is very low-throughput compared to functional assay testing.[189]

Although a hit compound had already been discovered and therefore some rational design is involved, the methods employed here fall within the description of fragment-based functional screening, in that the molecules adhere to the rule of three and are screened at high concentration to discover hits.

3.2.4. SAR

Compound	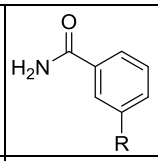	K_i vs NIK (μM)
36	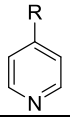	28
37	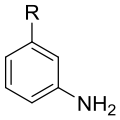	>100
38	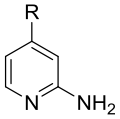	25
39	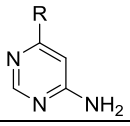	37
40	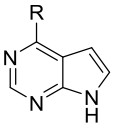	1.2
41	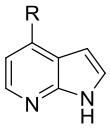	1.7
42	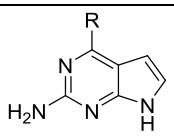	1.7
43	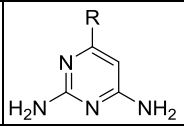	4.9

Table 3. Results of changing proposed hinge binding motif.

Screening compounds **36**-**43** showed vast differences in activity between monocylic and bicyclic systems. Inferring from the crystal structure of compound **1,** from docking simulations and from common hinge binding motifs of published kinase inhibitors, it is assumed that this is the hinge binding portion of the molecule. The lower affinities of compounds **36** and **37** are assumed to be because only 1 hydrogen bond is being made with the hinge. Compounds **38** and **39** have the capacity to make two hydrogen bonds with the hinge in one of two orientations: either with the G+1 acceptor-donor motif, or with the G+1 donor and G+3 acceptor. It was thought that this additional interaction and ability for the molecule to choose a more favourable conformation would improve potency compared to compounds **36** and **37** but little, if any, improvement was observed. Compounds **40**-**42** were all observed to be equipotent. Docking simulations suggest that the improvement in activity compared to the monocyclic compounds is due to an increase in the number of hydrophobic interactions made with the pocket. The change in electronics and the angle of the NH donor may also be factors.

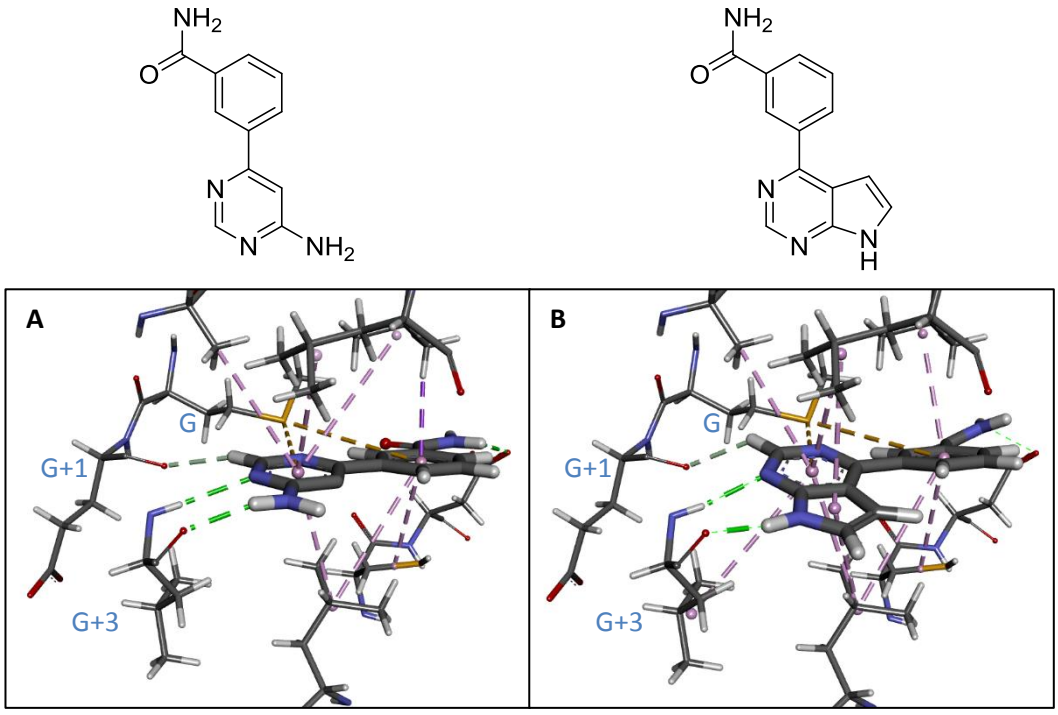

Figure 63. Docked poses of (**A**) compound **39** interactions and (**B**) compound **40** interactions. Green dashes show hydrogen bonds, purple shows hydrophobic interactions.

Compound **40** conveys a number of advantages as a hit compound over compound **30** as shown in **Table 4**.

	30	**40**
Calculated TPSA (Å^2)	96.9	79.8
Calculated logP	2.57	1.39
K_i (μM)	4.4	1.2
Molecular weight (Da)	332	238
Ligand efficiency	0.30	0.45

Table 4. Properties of **30** vs **40**.

Whilst the TPSA of both compounds is within the generally accepted limit for permeating cell membranes,[190] compound **30** is getting towards the upper limit of around 120-130 Å^2. Similarly with logP, compound **40** shows greater promise for development since lower logP conveys greater water solubility. The fact that this is slightly more potent and has a lower molecular weight also means that it is a much more efficient ligand than **30**.

Ligand efficiency is a relatively recent addition to the pharmaceutical world. In 1999, Kuntz and co-workers put forward a paper suggesting ligand efficiency as an alternative to simply relying on affinity, and suggested comparing the Gibbs free energy (ΔG) with the number of non-hydrogen atoms in the molecule (N), with ΔG defined as -RTlnK_i.[191] This leads to the following equation to calculate ligand efficiency:

$$LE = 1.4 \, {}^{\Delta G}/_{N}$$

Due to their similarity to adenine, pyrrolopyrimidine scaffolds are very common in kinase inhibitors. Of the 28 licensed SMKIs, 2 have pyrrolopyrimidine hinge binding motifs, with a further two containing pyrrolopyrimidine-like pyrrolopyridine or purine scaffolds.[124] In 2008, Aronov *et al.* postulated that

"A compound is likely to have kinase activity if (i) it contains two or more heteroaromatic nitrogens (N_{aro}), (ii) it contains one or more heteroaromatic NH groups (NH_{aro}), (iii) it contains one or more anilines (Ar-NH), and (iv) it contains one or more nitriles (R-CN)."[192]

A combination of these factors led to further research being concentrated on pyrrolopyridine and pyrrolopyrimidine scaffolds.

To assess whether further improvements in activity could be made with an alternative to the amide moiety, a series of structural changes were made designed to probe the interactions made by this group.

Compound	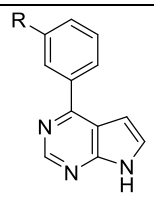	K_i vs NIK (μM)
40	$C(O)NH_2$	1.2
44	H	5.2
45	CH_3	5
46	NH_2	1.6
47	OH	2.5
48	CH_2OH	3.8
49	CN	1.6
50	COOH	3.2
51	$NHC(O)NH_2$	1.7
52	SO_2NH_2*	2.6
53	$C(O)NH(CH_2)_3N(CH_3)_2$	3.5
54	$C(O)NH(CH_2)_3OCH_3$	7.6
55	$C(O)NH(CH_2)_2CH(CH_3)_2$	7.9

Table 5. Results of 3-phenyl substituents. *Uses pyrrolo[2,3-*d*]pyridine scaffold.

The decrease in activity from **40** to **44** and **45** suggests that the functional group has a positive role in binding (as suggested by docking studies) but no significant difference was found through iterations of hydrogen bond donors, hydrogen bond acceptors, acidic and basic groups or secondary amides.

Secondary amines **53**-**55** were synthesised to try and investigate ways of targeting the hydrophobic pocket behind the methionine gatekeeper. The published NIK crystal structure (PDB code 4DN5) with ATP bound in the catalytic site suggested a narrow opening which, with the right vector, could possibly provide access to this region. Docking compound **40** indicated that the substituted amide may provide this vector, assuming a flipped geometry compared to the docked pose, and that an alkyl chain may interact with this hydrophobic region whilst **53** and **54** were synthesised to explore any potential hydrogen bonding interactions. Unfortunately, although docking studies suggested that this was a valid hypothesis, biochemical assessment of these compounds showed, at best, no improvement in activity against NIK.

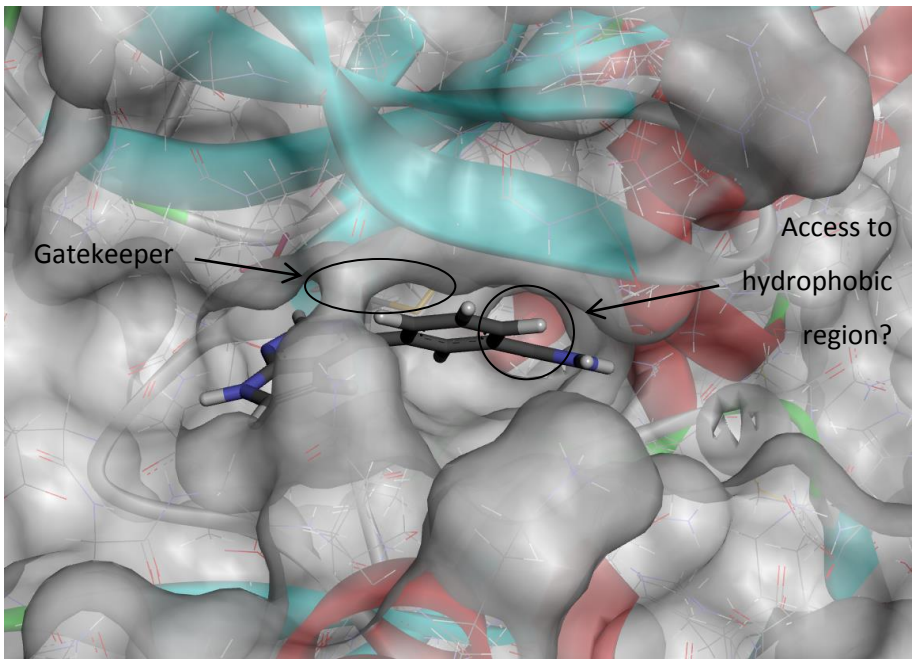

Figure 64. Compound **40** docked in NIK with gatekeeper and potential access to hydrophobic region shown.

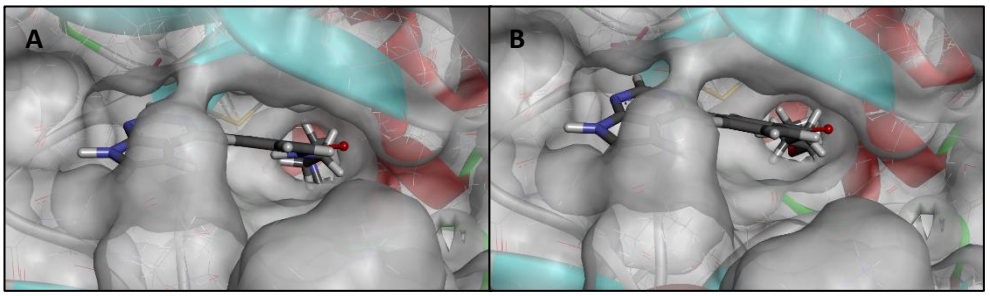

Figure 65. Docked poses of **53** (panel **A**) and **54** (panel **B**) in NIK.

A further hypothesis examined in this series was substitution of the 3-position as a means of introducing an additional hydrogen bonding group. This was intended to form an interaction with Q479 which sits close to the mouth the catalytic pocket and, from the crystal structure, looked to be a useful residue to target from the 3-position using a small functional group. The hydrogen bond donor/acceptor capabilities of the glutamine amide also made it an attractive target.

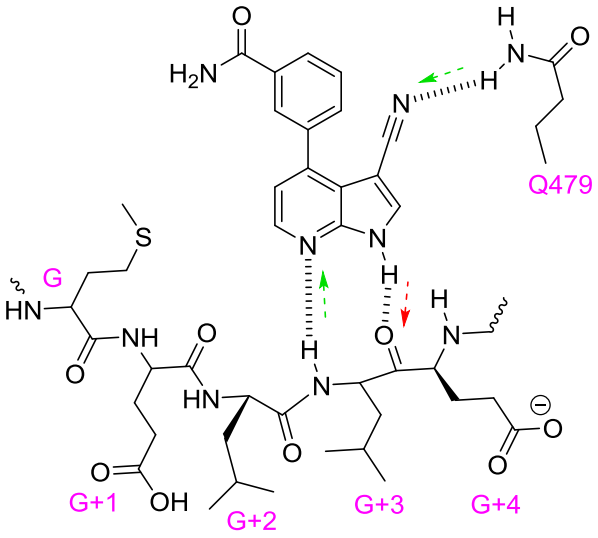

Figure 66. Proposed interaction motif for 3-substituted pyrrolopyridines.

Substitution of the pyrrolopyridine at the 3-position decreased potency with increasing hybridisation, such that sp > sp^2 >> sp^3.

Compound	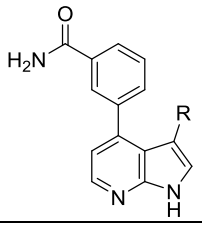	K_i vs NIK (μM)
56	CN	1.8
57	CHO	5.1
58	CH_2OH	>30

Table 6. Results of 3-substituted pyrrolopyridines.

This decrease in activity is thought to be due to steric hindrance forcing the two ring systems out of plane with each other as the hybridisation gains more p-orbital character. This theory is somewhat backed-up by running a very crude energy minimisation using Discovery Studio's Dreiding-like force field minimisation.[193] This simulation shows that, in the lowest energy conformation, the torsion angle between the two rings increases and the relative energies also increase.

Compound	Torsion angle (°)	Energy (arbitrary units)
56	23.64	33.9
57	27.85	37.2
58	29.25	49.9

Table 7. Results of energy minimisation for compounds **56**-**58**.

Whilst this is by no means conclusive proof that the relative geometry is the reason for the decrease in activity, it is certainly a reasonable assumption that reducing the number of available conformations is likely to be unfavourable for the ligand to adopt an optimal binding pose. Since the energy results provided by Discovery Studio are only relative, it is also unclear whether this difference is significant or not in terms of how difficult the energy barrier is to overcome and whether the act of binding to a receptor may be enough to outweigh that.

As will be discussed in the related chemistry section, 3-substitution of the pyrrolopyridine scaffold proved much more facile than 3-substitution of the pyrrolopyrimidine scaffold and, as such, only 3-substituted pyrrolopyridines were investigated at this stage.

3.3. 2-amino-5-carbonitrile series

3.3.1. Library screen and hit compounds

Since compounds **53**-**55** had suggested that the vector provided by compound **40** had failed to target the hydrophobic region as desired, a screen of a proprietary in-house library was carried out in an attempt to identify other scaffolds which may provide this vector while still showing some level of NIK activity. Two compounds of particular interest from this library showed promise, with activity values comparable with analogous to compound **40** Alterative vectors to these analogues were provided through the amine linker in the case of **59** and the 5,6-ring system of **60**

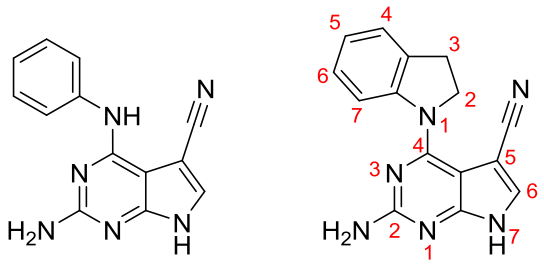

60

Figure 67. Structures of in-house hits with numbering system for clarity.

Compounds **59** and **60** were assessed biochemically and found to have K_is of 3.0 and 2.8 µM respectively. As 3-carbonitrile **56** had shown no improvement over pyrrolopyridine **41** and pyrrolopyrimidine **40** was slightly more potent than 2-amino-pyrrolopyrimidine **42**, a series of 4-indolyl- and 4-indolinyl-pyrrolopyrimidines were synthesised to investigate the effect of a 6-substituent on the indole, or indoline, ring.

3.3.2. 4-indoline series

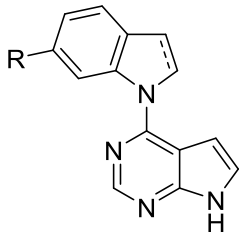

Compound	4-substituent	R =	K_i (μM)
61	Indoline	H	2.8
62	Indoline	Br	6.6
63	Indoline	C≡C-CH_2OH	5.3
64	Indoline	C≡C-$(CH_2)_2OH$	3.0
65	Indoline	C≡C-$C(CH_3)_2OH$	0.930
66	Indole	H	5.1
67	Indole	Br	1.1
68	Indole	C≡C-CH_2OH	4.6
69	Indole	C≡C-$(CH_2)_2OH$	2.5
70	Indole	C≡C-$C(CH_3)_2OH$	0.574

Table 8. Results of 6-substitution of indole and indoline ring systems.

Very little difference was seen between these two series, though the general trend seemed to be that the indole analogues were slightly more potent. Modelling suggests that there is little qualitative difference in binding so an alternative explanation is the geometry of the indole ring compared to the indoline. Indole C-2 and C-3 atoms are sp^2 as opposed to the indolines sp^3 centres, which slightly lessen steric interactions with the proton at C-5 of the pyrrolopyrimidine, thus allowing the indole greater flexibility to adopt a more favourable binding conformation.

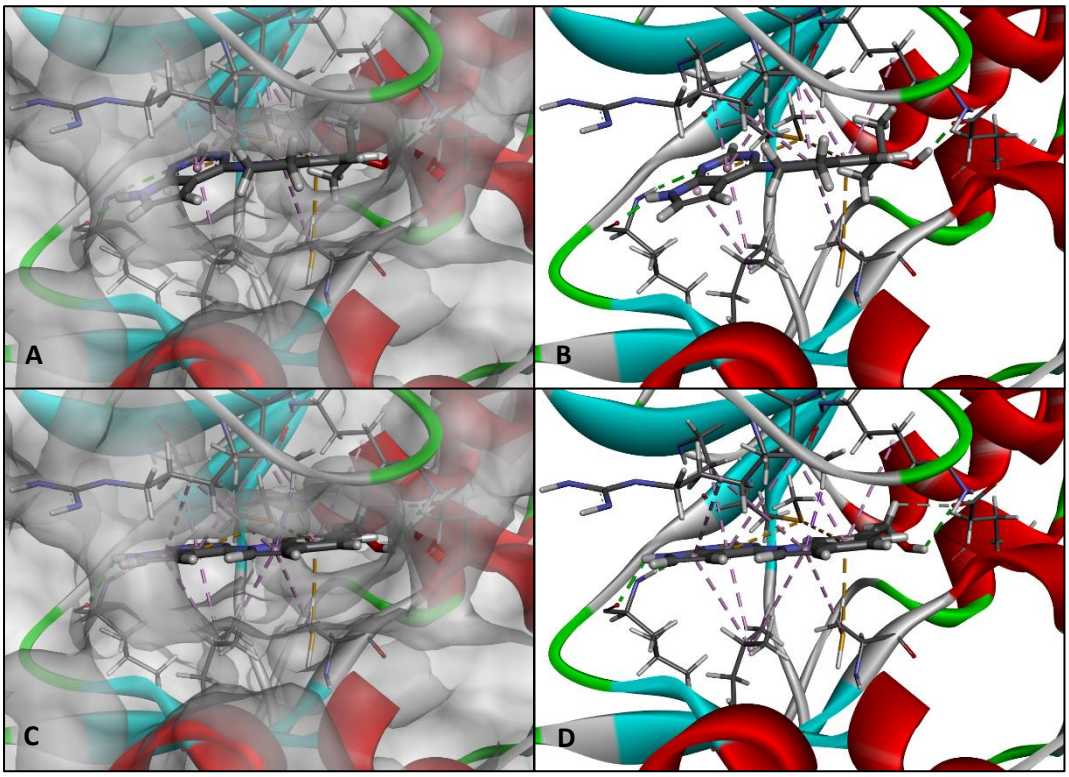

Figure 68. A and **B** Compound **65** showing receptor interactions with and without protein surface**; C** and **D** Compound **70** showing receptor interactions with and without protein surface.

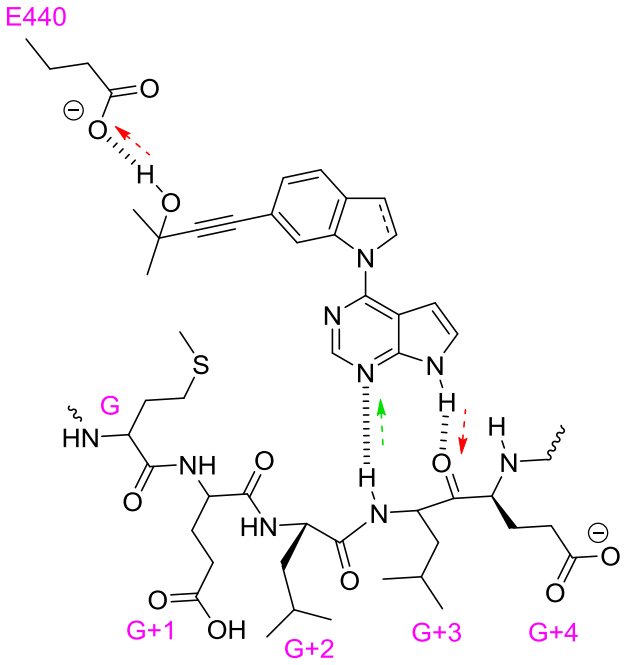

Figure 69. Interaction map of **65**/**70** showing proposed hydrogen bonds to NIK.

The potency afforded by the *gem*-dimethylhydroxyalkynyl analogues, as exemplified by compounds **65** and **70** led to the examination of the orientation of this group within its proposed binding site. Two further series of compounds were synthesised in order to investigate this. The first series looked to affect the binding orientation of the whole molecule by substituting the pyrrolopyrimidine for other proposed hinge binding motifs. This would allow for different combinations of G+1 and G+3 binding patterns and, also change the electronic properties of the ring, providing slight differences in the strength of the hydrogen bonds formed to the hinge and thus the binding orientation. Substituting the pyrrolopyrimidine would also have the secondary effect of altering the planarity of the two rings and thus the elevation of the alkyne substituent in the hydrophobic pocket. The second series investigated the effect of "untethering" the phenylalkyne portion of the molecule by substituting the indoline for aniline. This retained the nitrogen linker and the phenyl but changed the relative angle of the alkyne.

Compound	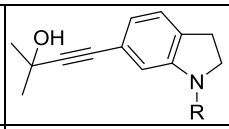	**K_i vs NIK (μM)**
71	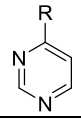	0.569
72	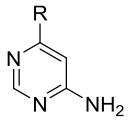	2.47
73	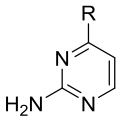	0.015
74	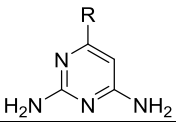	0.506
75	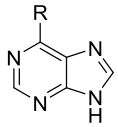	0.531
76	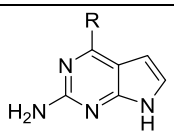	0.558
65	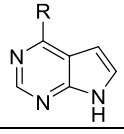	0.930

Table 9. Results of hinge binding motif alterations.

Replacement of the pyrrolopyrimidine with alternative hinge binders provided unexpected results. Compounds **71** and **74**-**76** all appeared equipotent in the biochemical assay and the reasoning for this is unclear. **71** is only capable of forming one hydrogen bond to the hinge, while **75** can make two, and **74** & **76** can make three. Whilst the arrangement of the DAD motif of **74** and **76** may not be ideal for making all three hydrogen bonds, both should still be capable of two hydrogen bonds and thus, along with **75**, show a greater potency than that exhibited by **71**. An alternative binding pose to the one proposed cannot be ruled out, though the molecules do not possess another traditional hinge binding motif and so, if this were the case, they are unlikely to bind as classical type I SMKIs. This could be established, either by increasing the concentration of ATP in the assay, the effect of which would indicate whether the molecules were ATP competitive, or with a crystal structure.

3.3.3. Existing NIK inhibitors

Subsequent to the synthesis of compounds **71**-**76**, two papers were found detailing structures of NIK inhibitors based around an aminopyrimidine hinge binding motif, substituted at the 4- position with a variety of [3.4.0]-bicyclic ring systems.[186,194]

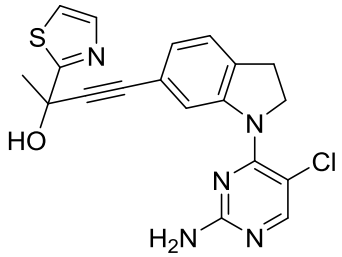

77

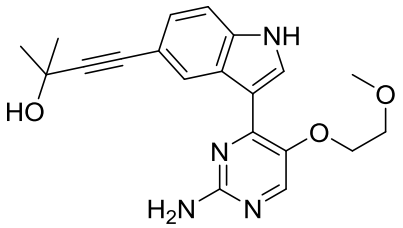

78

Figure 70. Example NIK inhibitors from de Leon Boenig *et al*. (**77**) and Li *et al*. (**78**).

These papers included crystal structures and, given the structural similarity of **77** and **78** to compounds **71**-**76**, these could be used to guide further compound development and validate conclusions from SAR.

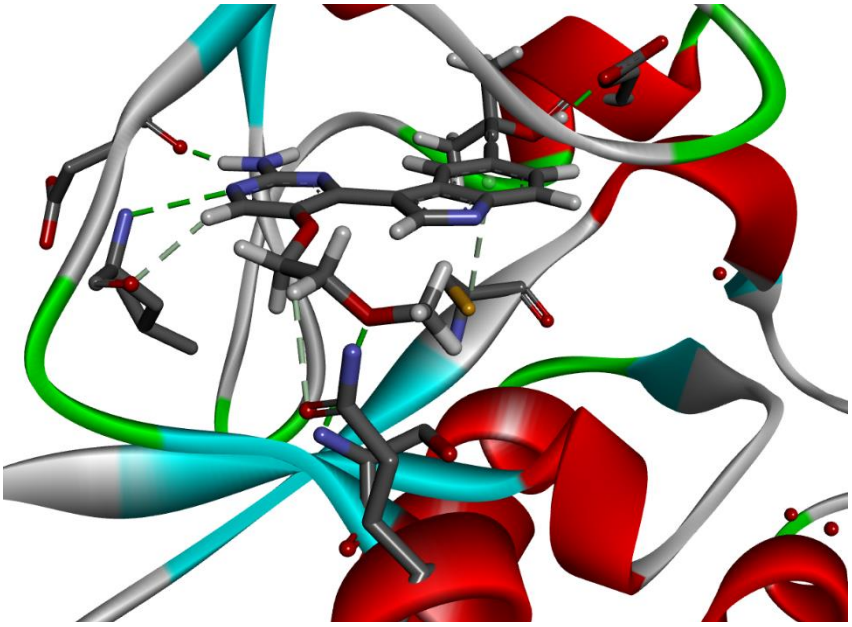

Figure 71. Crystal structure of compound **78** in NIK. (PDB code 4IDV).[194]

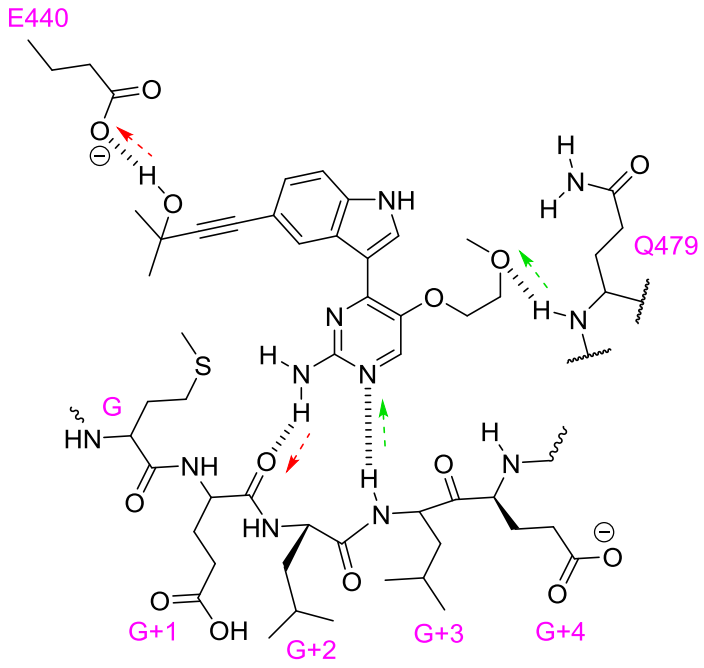

Figure 72. Interaction map of compound **78** in NIK.

The crystal structure (**Figure 71**) validates the binding mode of the alkynyl alcohol proposed by the docking study as shown in **Figure 69**; wherein the alcohol forms a hydrogen bond with E440. It also shows a G+1 and G+3 binding motif for the aminopyrimidine. This may be the preferred orientation or this may be due to the polyether chain at the 5-position of the pyrimidine ring. The crystal structure suggests that there is no space for this to flip to a

solely G+3 binding mode because the polyether would be in too close proximity to the methionine gatekeeper. Unfortunately, there is no crystal structure of an analogue of **78** bound in NIK which does not have a substituent at the 5-position. The incorporation of a polyether also validates the hypothesis that the glutamine residue Q479 can be targeted from the catalytic pocket but that the molecular arrangement of compounds **56**-**58** is not optimal to make this interaction.

From an SAR perspective, possibly the most interesting observation is the difference in activity between **72** and **73**. Compound **73** is a known compound which has been described in the literature as an inhibitor of NIK; albeit with very little detail.[195] Subsequent work by Li *et al.* provided a crystal structure of a very similar compounds which helps to draw some conclusions.[194]

The crystal structure shows the aminopyrimidine bound to the G+1 and G+3 residues of the hinge, with the alkynyl alcohol pointing back into the hydrophobic back pocket as modelling of compounds **65** and **70** suggested it would. If the same binding mode is assumed for compounds **72** and **73**, the only difference between them is the positioning of the pyrimidine nitrogen (panels **A** and **D** of **Figure 73**). The alternative for **72** to analogously position the pyrimidine nitrogen is a G+3 only binding pose (panels **B** and **C**).

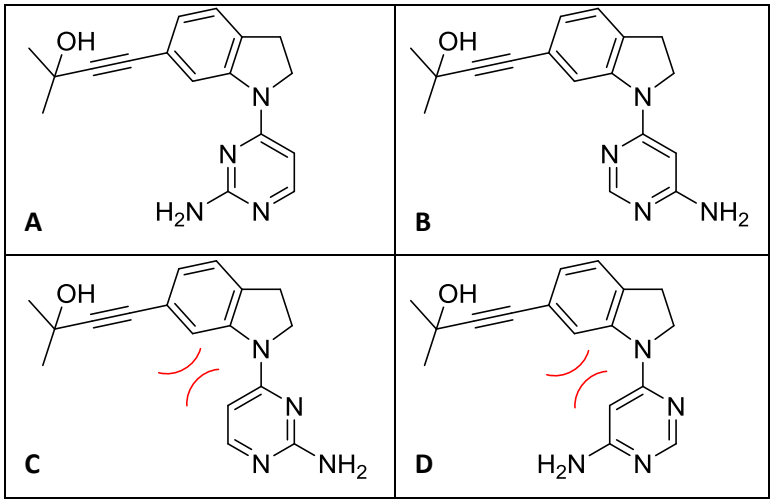

Figure 73. Possible effects of intramolecular interactions on binding orientation. The rotation about the pyrimidine C4 - indoline N1 bond can result in a steric clash between protons on the two ring systems (panels **C** and **D**) leading to distortion between the ring systems which will likely adversely affect binding.

Whether or not the binding mode changes between the two compounds is unclear, however one contributing factor, if it does, which may help to explain the difference in potency, is shown in panels **C** and **D** of **Figure 73**. Molecular mechanics using a simple Dreiding-like force field[193] indicate that the interactions shown in panels **C** and **D** do lead to a distortion of the molecule as shown in **Table 10**.

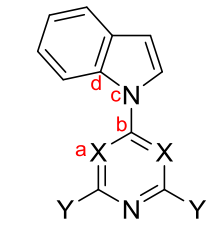

X = N/CH, Y = H/NH_2

Figure 73 Panel	Torsion angle (°)	Bond angle (abc) (°)	Bond angle (bcd) (°)
A	7.74	119.82	126.39
B	7.76	119.90	126.54
C	12.22	123.69	130.54
D	11.74	123.76	130.66

Table 10. Selected torsion and bond angles of compounds **72** and **73**.

With the pyrimidine nitrogen to the right of the molecule, as drawn, there is a steric interaction between the pyrimidine C-H and the 7-position C-H of the indoline. If both **72** and **73** adopt the G+1, G+3 binding mode (panels A and D), this steric interaction is only present in **72**. This interaction may result in a sub-optimal binding pose for **72**, or it may even necessitate the alternative binding pose shown in panel B.

As discussed, modelling and crystal structures of aminopyrimidines in NIK suggest that binding occurs preferentially with the amino group interacting with the G+1 residue (as shown in **Figure 71**). In the case of the 6-aminopyridine, however, this results in not only a steric clash with the indoline 7-position C-H, but also the positioning of the pyrimidine nitrogen in the centre of a very hydrophobic pocket. It is not known whether this contributes to the detrimental effect on binding seen between the 6-amino and the 2-aminopyrimidine. In an attempt to understand this, efforts were made to synthesise the 2-aminopyridine analogue as shown in **Figure 74**. Unfortunately, despite several attempted routes, synthesis proved unsuccessful.

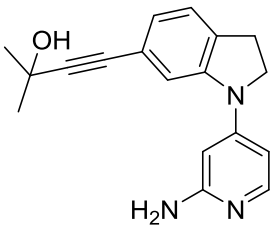

Figure 74. Structure of desired 2-aminopyridine analogue.

Despite it being an already disclosed compound, the potency of compound **73** made it an attractive tool compound to investigate one of the aims of this project: to synthesise a representative known NIK inhibitor and use it to interrogate the non-canonical NF-κB pathway. Reported NIK inhibitors, to this point, have been decidedly promiscuous[65,196,197] and compound **73** is no exception to this.

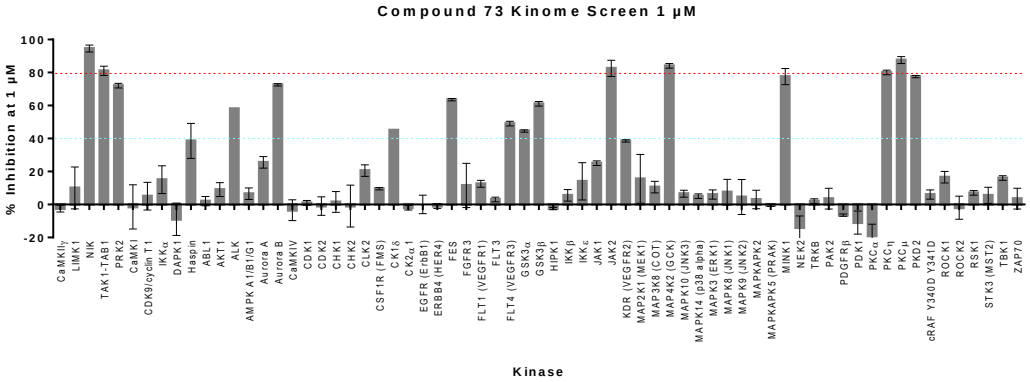

Figure 75. Kinome screening results for compound **73**.

As shown in **Figure 75**, compound **73** shows greater than 80% inhibition of 7 kinases, excluding NIK, out of the 67 assessed. Since the full kinome is represented by over 500 kinases this figure could well extrapolate to around 60 kinases. This level of off-target activity is likely to result in unwanted toxicity and thus, from a drug discovery perspective, it does not make a good prospective lead compound and, therefore, further investigation was required to search for ways of improving selectivity across the kinome. The potent NIK activity of compound **73** did, however, represent an excellent opportunity to further understand the non-canonical NF-κB pathway in a cancer setting. This work is discussed further in chapter 4.

3.3.4. Development of novel scaffolds

To begin investigating potential future scaffolds which may improve kinome selectivity over compound **73**, a series of three carbazole analogues of compound **73** were synthesised.

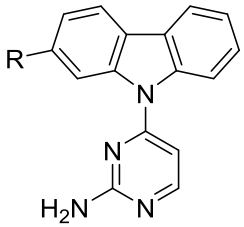

	R =	K_i vs NIK (μM)
79	H	4
80	Br	1.1
81	$C{\equiv}C(CH_3)_2OH$	0.350

Table 11. Results for carbazole structures.

Introduction of this additional phenyl ring could provide a greater level of selectivity and also provide a scaffold for a range of substitution patterns to probe additional or alternative interactions around the catalytic pocket. Introduction of first 6-bromo and then alkynyl alcohol moiety showed the same trend of increasing potency as observed in the indoline series. The bromine is thought to have a favourable entropic effect on binding by displacement of water, whilst modelling suggests the alkynyl alcohol makes a hydrogen bond to ASP440. The reason for the decrease in activity compared to compound **73** is thought to be because of the molecular distortion as shown in **Table 10**. Because of the symmetry of the carbazole, there will always be an intramolecular interaction between the two ring systems as they approach co-planarity. Modelling suggests the optimal pose is with the rings co-planar, which is a pose unlikely to be adopted. This means that the receptor-ligand interactions will be sub-optimal providing a rationale for the decreased potency.

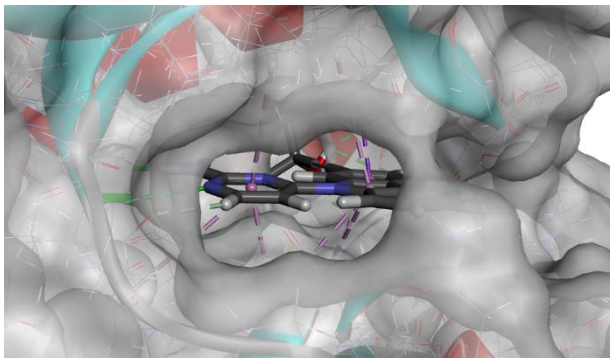

Figure 76. Compound **81** docked in NIK.

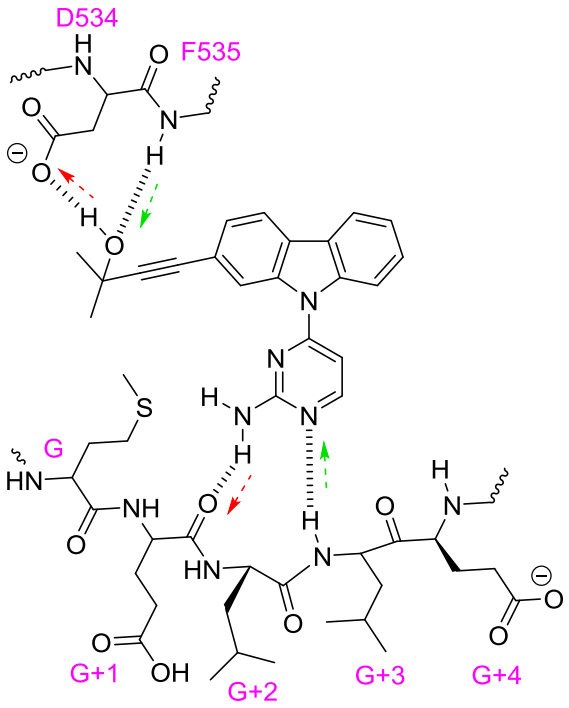

Figure 77. Interaction map of compound **81** in NIK.

Substitution of indoline with aniline caused a considerable drop in activity. 2-Aminopyrimidine **84** still showed much greater potency than the 6-aminopyrimidine but as the most potent in this series, and still less potent than **67**, it was decided that this was not a tractable series.

Compound	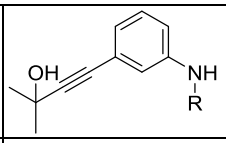	K_i vs NIK (μM)
82	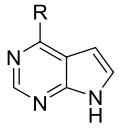	9.8
83	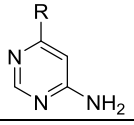	>30
84	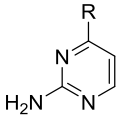	1.22
85	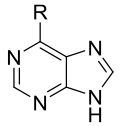	14

Table 12. Results for alkynylaniline compounds.

These results suggest that the angle of the alkyne is very important for binding. Whilst the positioning of the residues shown in **Figure 77** and **Figure 78** is not accurate, it can be seen that the alkynyl alcohol moiety of **84** (**Figure 78**) is binding to an amino acid earlier in the sequence than that of the analogous group in **81** (**Figure 77**) and therefore likely to interact with the methionine gatekeeper disfavourably. This is not surprising considering the vector created by the *meta*-substituted anilines compared to the 6-substituted indolines but it is a trend seen across the aniline series **82**-**85**.

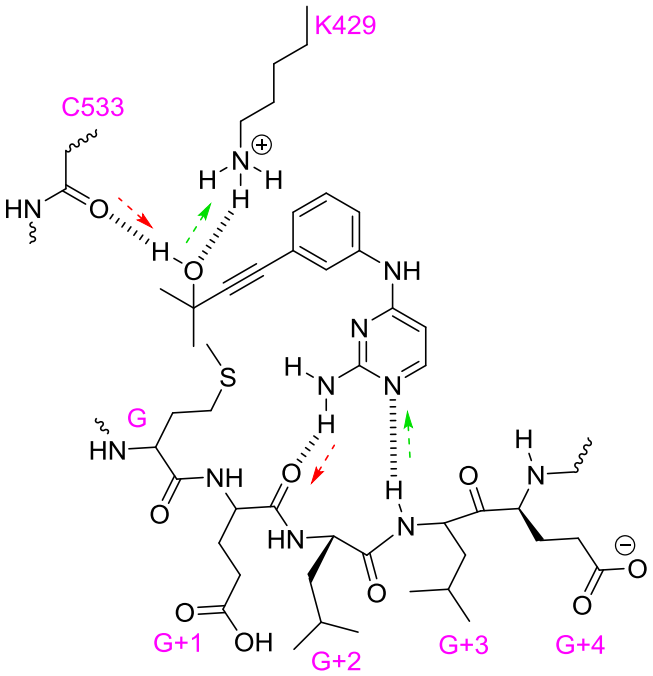

Figure 78. Interaction map of compound **84** in NIK.

Since compounds **59** and **60** had shown comparable activities to **61**, SAR was carried out to investigate the effects of the 2-amino and 5-cyano groups on activity.

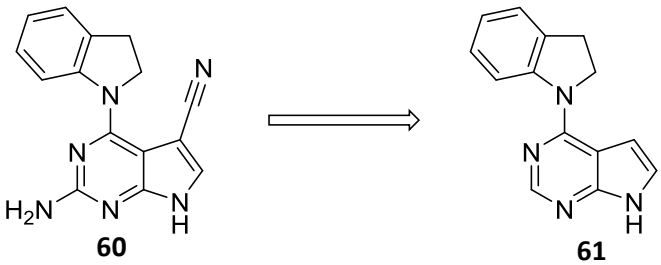

60
(2.8 µM)

61
(2.8 µM)

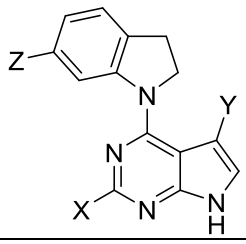

Compound	Substituent	K_i (μM)
61	X=H, Y=H, Z=H	2.8
65	X=H, Y=H, Z=-CC≡C-C$(CH_3)_2$OH	0.930
76	X=NH_2, Y=H, Z=-CC≡C-C$(CH_3)_2$OH	0.558
60	X=NH_2, Y=CN, Z=H	2.8
86	X=H, Y=CN, Z=-CC≡C-C$(CH_3)_2$OH	0.789
87	X=NH_2, Y=CN, Z=-CC≡C-C$(CH_3)_2$OH	0.080
88	X=H, Y=-CC≡C-CH$(CH_2)_2$, Z=-CC≡C-C$(CH_3)_2$OH	26

Table 13. Effects of 2- and 5-position substitutions on compound potency against NIK.

Despite the substitutions on compound **60** not seeming to confer any increase in potency over compound **61**, these same substitutions do show an improvement for compound **87** over **65**. Docking suggests that the alkynylindoline binds in the same orientation as compound **67**, with the 2-amino group making an additional interaction to G+1 and the 5-cyano group making hydrogen bond to Q479: analogous to the interaction made by the polyether of compound **78**. As neither the 2-amino or 5-cyano substituent, by themselves, appear to account for a large improvement in potency, it is assumed that it is the combination of substituents that orientates the molecule in such a way as to maximise its binding potential.

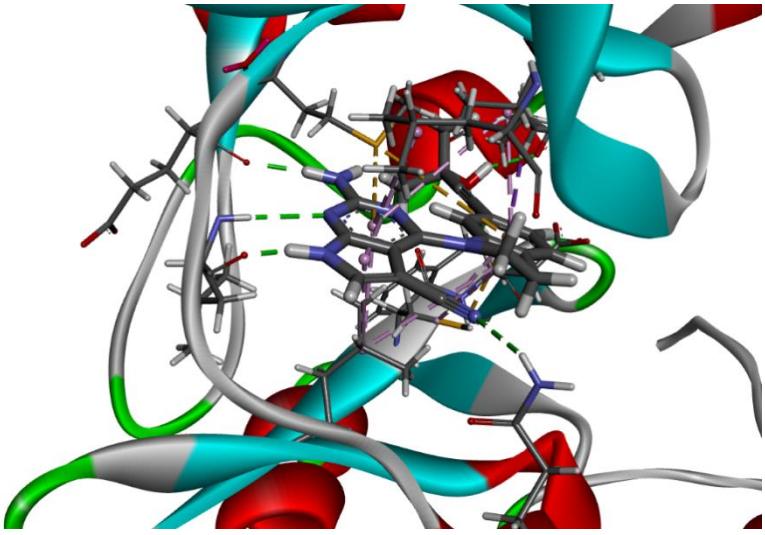

Figure 79. Docked binding pose for compound **87** in NIK.

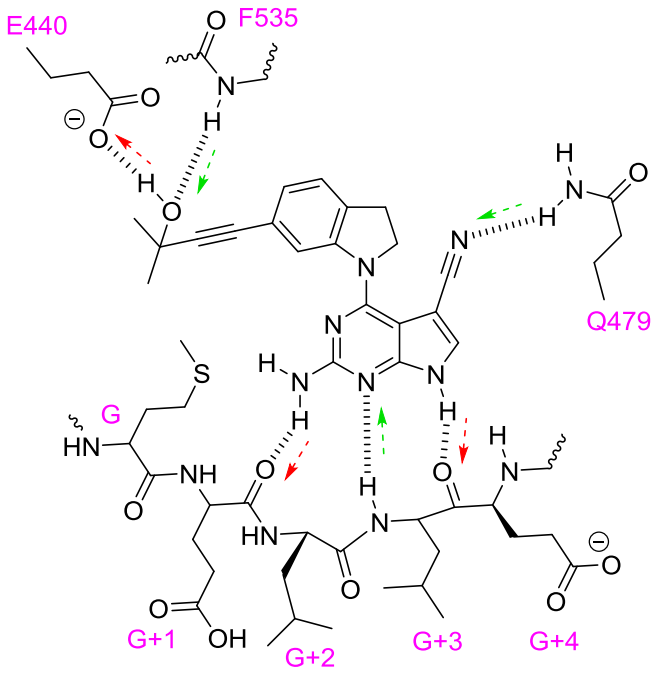

Figure 80. Interaction map for compound **87** in NIK.

Compound **88** provided an interesting twist to the SAR. This showed a considerable drop in potency (K_i = 26 µM) compared to **86** but, with the terminal alkyne direct analogue not being available for comparison it is not possible to draw accurate conclusions as to why this is: since there is a change in sterics (C≡N compared to C-CH(CH_2)$_2$); in hydrogen bonding capability (H-bond acceptor vs no interactions); in hydrophobicity and in polarity. Nevertheless, the reason for such a marked decrease in potency remains unclear using the existing binding model. Docking suggests that the compound adopts a similar binding pose to **87**, and adding a rendering indicating hydrophobicity to the protein suggests that the cyclopropyl occupies a relatively large hydrophobic cleft.

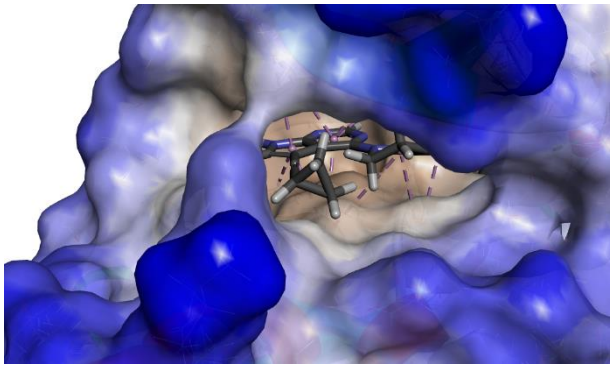

Figure 81. Docked pose of **88** in NIK. Blue regions are hydrophilic and brown regions are hydrophobic.

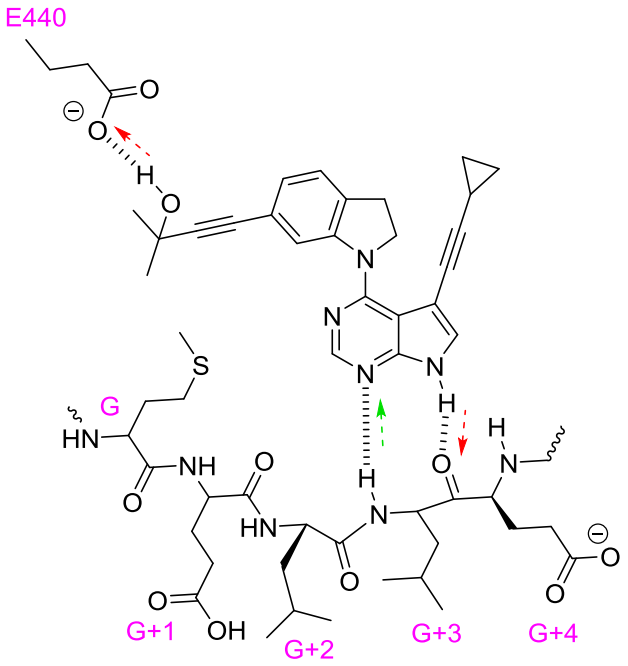

Figure 82. Interaction map of **88** in NIK.

If this is the case, the assumption would be for the compound to exhibit a potency similar to that of **65**: with the pyrrolopyrimidine and the alkynyl alcohol forming the main interactions. This is not the case, however, and further analogues would need to be synthesised to investigate this. Whilst several analogues were planned, synthesis of these proved non-trivial and only the cyclopropyl could be obtained.

3.3.5. Chemistry

3.3.5.1. 3-Phenylcarboxamides and analogues

Compounds **36**-**43** were synthesised in one step from 3-aminocarbonylphenylboronic acid and the corresponding aryl chloride or bromide.

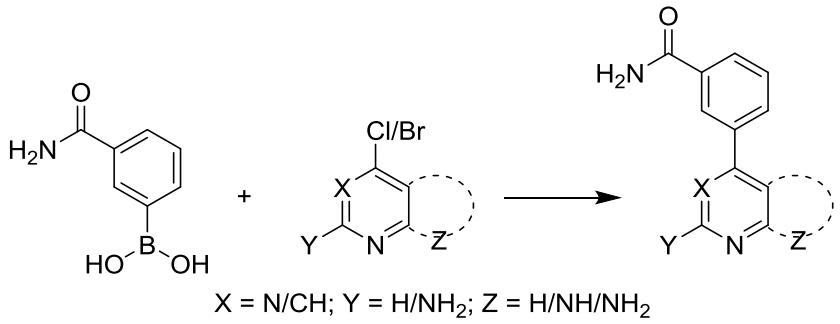

X = N/CH; Y = H/NH_2; Z = H/NH/NH_2

Scheme 10. Suzuki coupling of 3-phenylcarboxamide to aryl chloride.

Products were obtained in good to excellent yields with the exception of **38** and **39** which were poorly yielding. The reasons for this are unclear but since bidentate nitrogen containing ligands are well known[198–201] it is possible that the electronic properties and geometry of these examples enable them to chelate to the palladium catalyst and thus slow the turnover rate, though the fact that there is such a large discrepancy between the yields of these two examples and the rest suggest several factors may be at play.

Many of the boronic acid starting materials for the analogues of compound **40** were commercially available and were synthesised as shown in **Scheme 10**. Secondary amides **53**-**55** were synthesised via an amide coupling reaction from compound **50** and appropriate amines in moderate yields utilising the T3P coupling shown in **Scheme 1**.

Urea **51** was synthesised from amine **46** by a nucleophilic addition reaction with potassium cyanate as shown in **Scheme 11**. The mechanism is thought to proceed through nucleophilic addition into the nitrile carbon under acidic conditions before proton transfer to yield urea **51**.

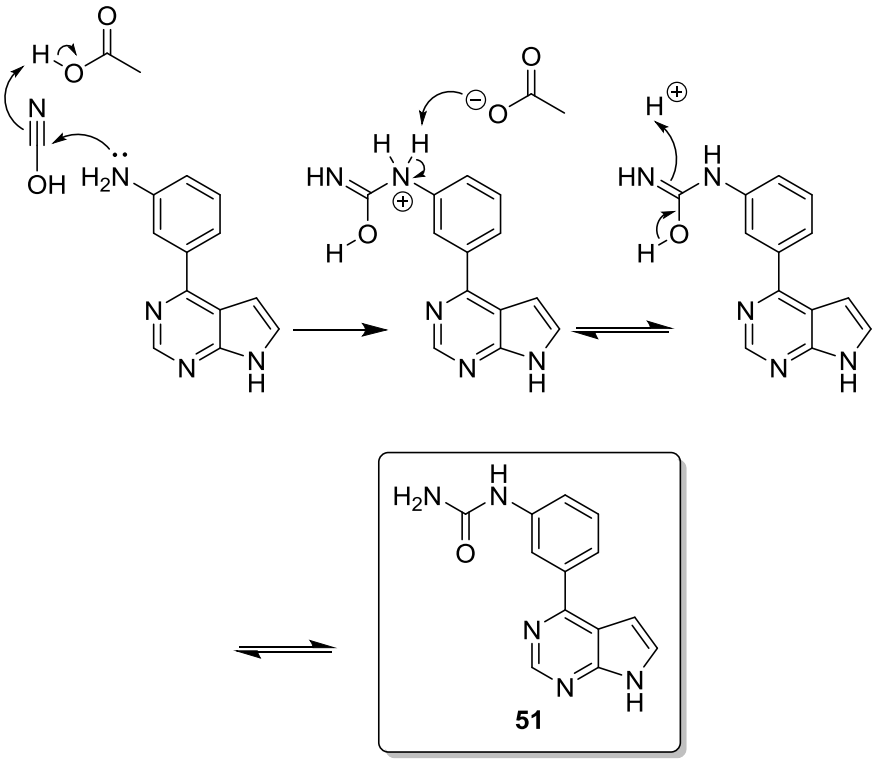

Scheme 11. Nucleophilic addition of cyanate to aromatic aniline **46**.

Compound **47** was synthesised on the pyrrolopyridine core scaffold rather than the pyrrolopyrimidine. Reaction using 4-chloropyrrolopyrimidine was attempted but mass spectrometry suggested the formation of compound **89** and no formation of desired product. This was thought to be due to the labile nature of the aryl chloride, whereas the problem was not observed with the more electron rich pyrrolopyridine.

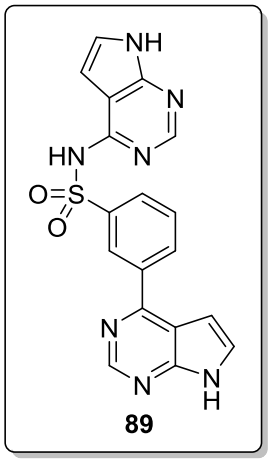

3.3.5.2. 3-Substituted pyrrolopyridines

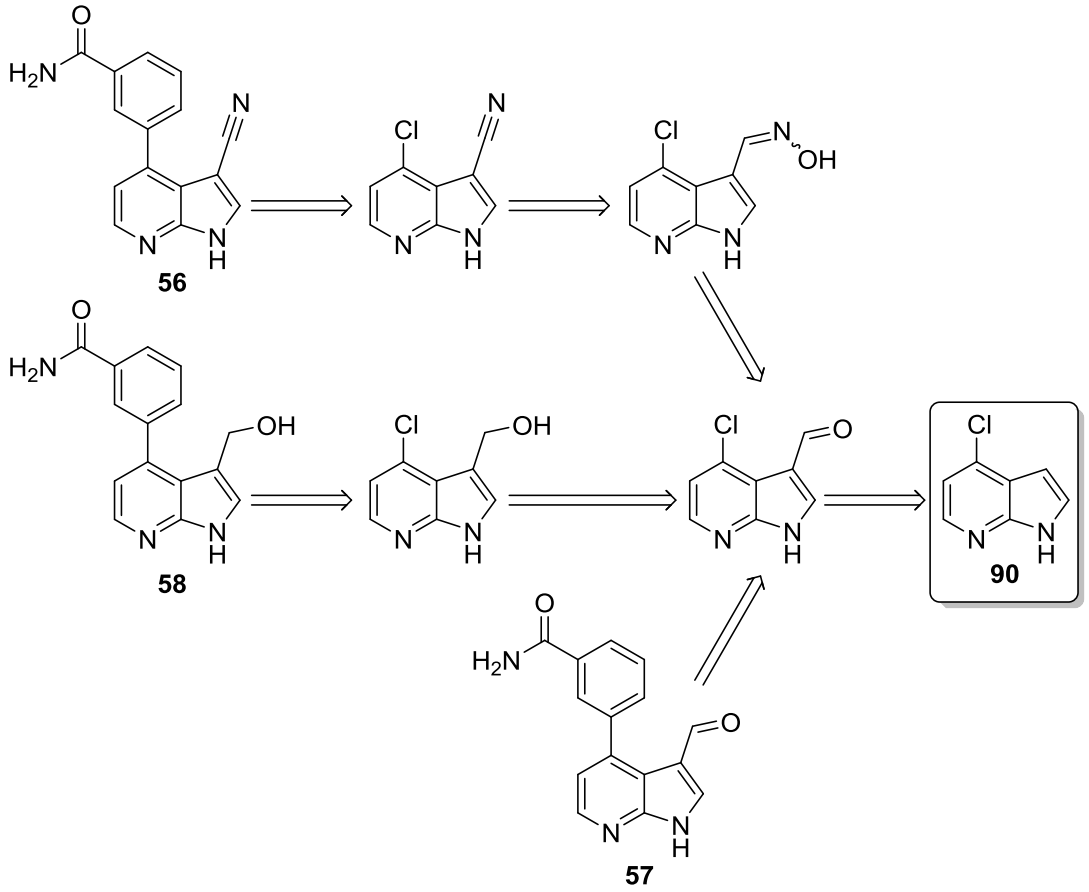

Scheme 12. Retrosynthetic analysis of 3-substituted pyrrolopyridines.

Compounds **56**-**58** were all synthesised from starting material **90** through common aldehyde intermediate as shown in **Scheme 12**. Aldehyde intermediate was synthesised using the Duff reaction in which the aldehyde is formed through introduction of an imine derived from hexamethylenetetramine under acidic conditions as shown in **Scheme 13**.[202,203] Hexamethylenetetramine spontaneously ring opens under acidic conditions before attack of the nucleophilic C-3 position of the pyrrolopyridine into the newly formed iminium. Subsequent protonation and intramolecular proton transfer followed by hydrolysis furnished aldehyde **91** in moderate yields.[202]

Attempts were made to synthesise the pyrrolopyrimidine analogue of **91** since this scaffold had shown slightly better activity, however Vilsmeier-Haack formylation, organolithium followed by quenching with DMF and Duff reaction on this scaffold all proved unsuccessful. Since compound **36** could still be used to assess the effect of 3-substitution, however, it was decided to investigate these effects using the pyrrolopyridine series.

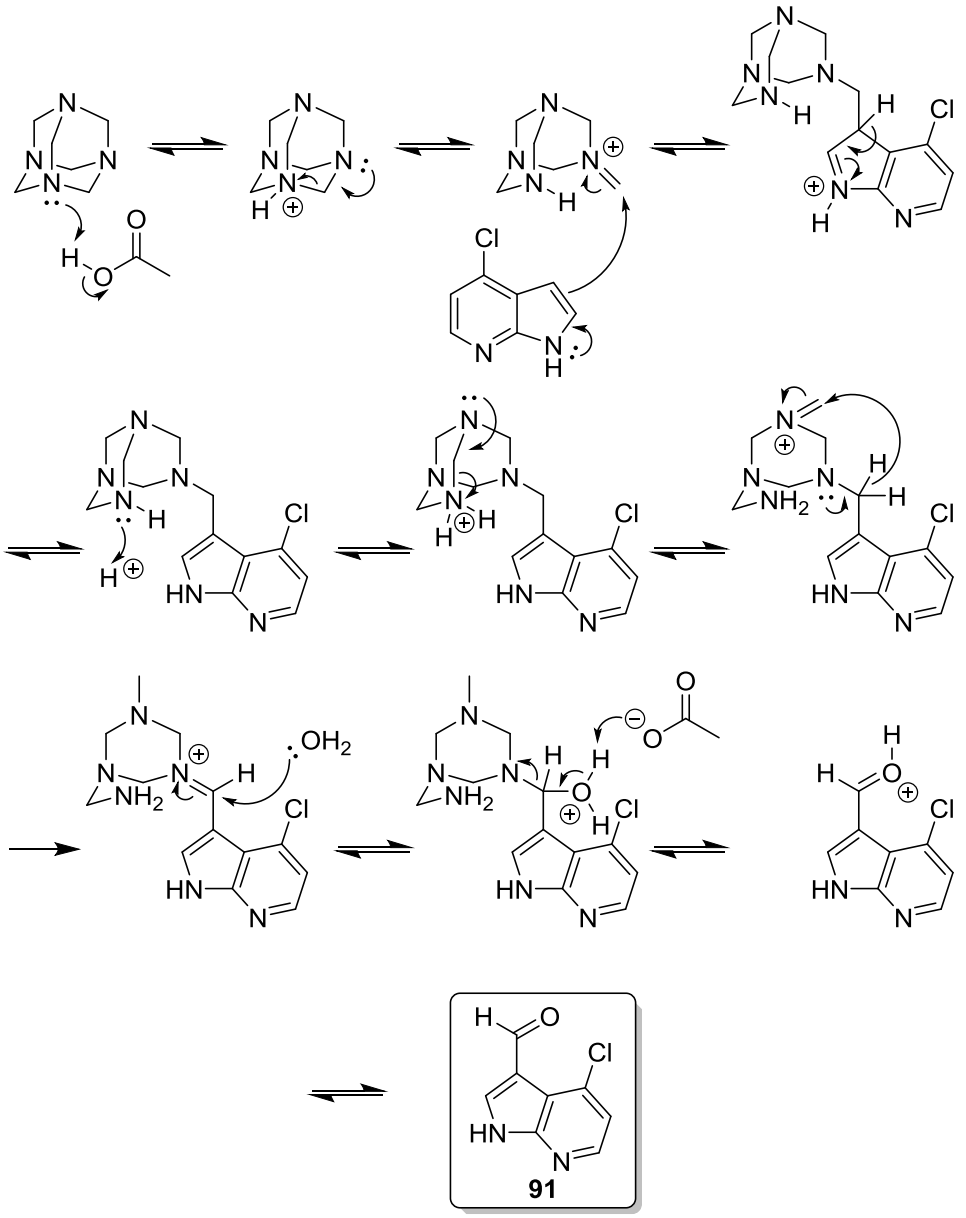

Scheme 13. Proposed mechanism of Duff reaction.

Compound **57** was synthesised by Suzuki reaction of **91** with 3-aminocarbonylphenylboronic acid under microwave conditions in moderate yields. Reaction under thermal heating conditions returned only starting material **91** after overnight reaction, whereas 50% yield was obtained under microwave conditions at 120 °C after 1 hour.

Compound **91** was further reacted under reductive conditions[204] (**Scheme 14**) and amination conditions[205] (**Scheme 15**) to furnish alcohol and oxime intermediates in good yields.

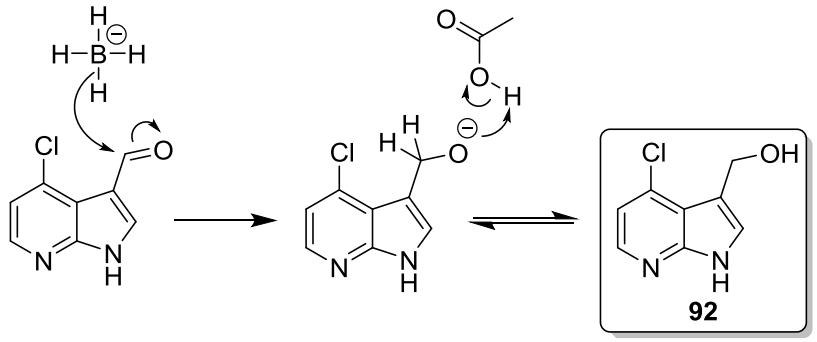

Scheme 14. Borohydride reduction of aldehyde **91**.

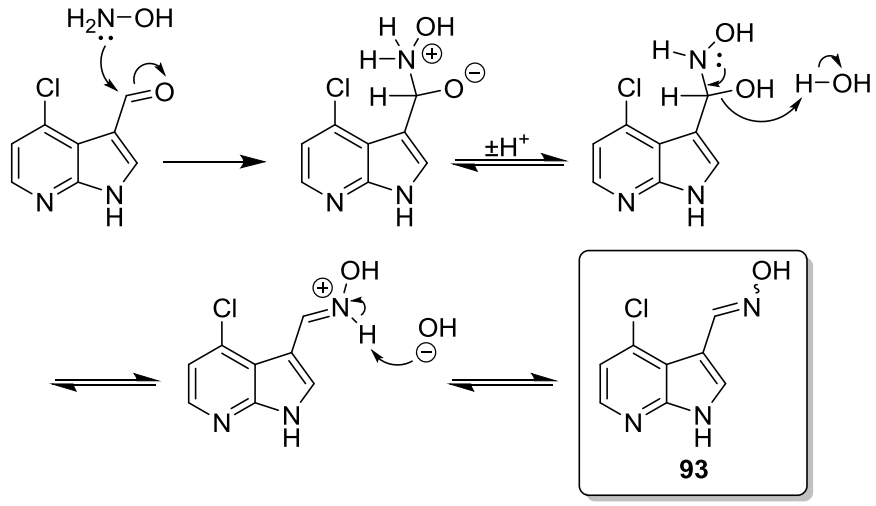

Scheme 15. Reaction of hydroxylamine with aldehyde **91**.

Alcohol **92** was further reacted under Suzuki conditions as shown in **Scheme 9** to yield compound **58** in moderate yield. Nucleophilic attack of hydroxylamine into aldehyde **91** and subsequent dehydration led to oxime **93** in excellent yield.

The final functional group interconversion of oxime **93** to nitrile **94** was achieved by treating with thionyl chloride as shown in **Scheme 16** to provide product in good yield.[206] Oximes are classically thought to undergo Beckmann rearrangement under dehydrating conditions.[207] This reaction involves a rearrangement as shown in red in **Scheme 16**. However, it is also known that hydrogen migration is rare in the conventional Beckmann rearrangement[208] and a second mechanism, such as E2 elimination, is also plausible.

Nitrile **94** was reacted similarly to alcohol **92** using thermal heating conditions to yield compound **56** near-quantitatively.

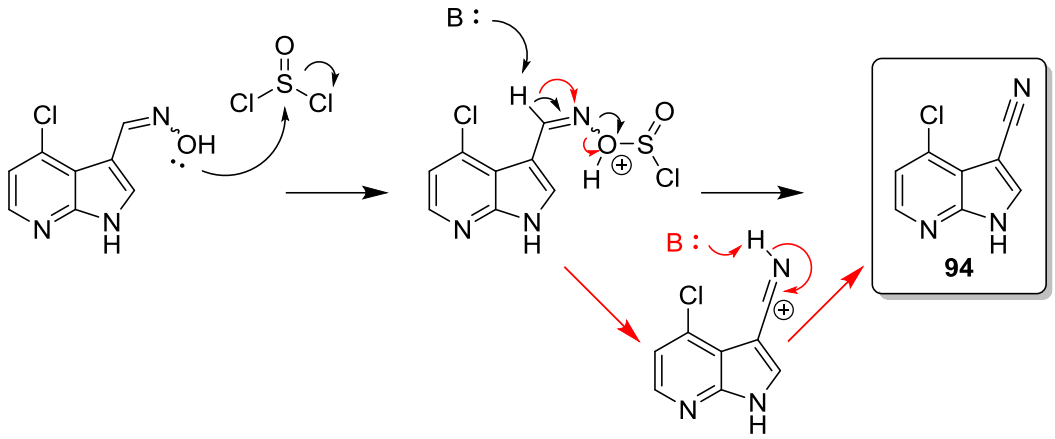

Scheme 16. Possible mechanisms of dehydration of oxime by thionyl chloride.

3.3.5.3. S_NAr reactions

Formation of the pyrrolopyrimidine C-4 to indoline N-1 bond was completed through a S_NAr nucleophilic aromatic substitution (NAS) reaction. NAS reactions can proceed via several different mechanisms including S_N1,[209] benzynes[209] and metal-catalysed substitution:[210,211] most widely exemplified by the Buchwald-Hartwig coupling. One of the most commonly used methods, however, is the addition-elimination reaction, known as the S_NAr reaction. In this reaction, a nucleophile is added to a substituted aromatic carbon to form a Meisenheimer, or σ-, complex before departure of the leaving group.[212,213]

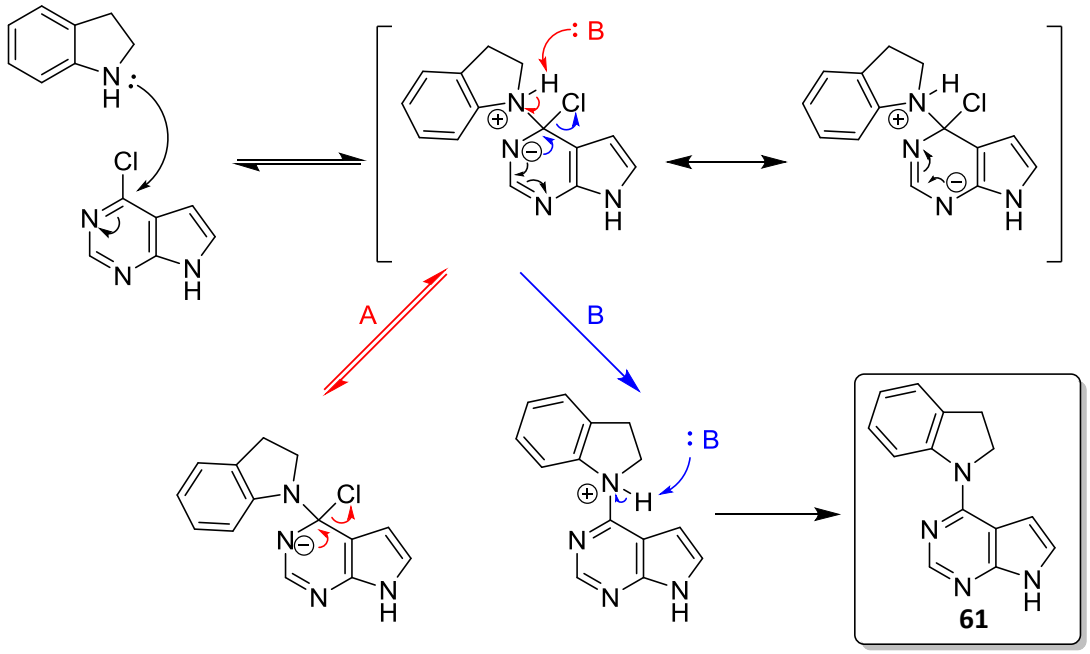

Scheme 17. S_NAr reaction proceeding through Meisenheimer complex.

S_NAr reaction was carried out by reacting aryl chlorides under microwave conditions in a 2:1 *iso*-propanol-dioxane mixture with 1 equivalent of desired indoline. Similar reactions have been reported by Caldwell *et al.*[214,215] but it was decided to attempt the reactions excluding base. Base is normally added to facilitate proton transfer, often the rate-limiting step, from the zwitterionic Meisenheimer complex and so push the equilibrium towards the anionic complex as shown in route A.[212] Studies looking at this, however, have used aliphatic nitrogen nucleophiles, and it was thought that, since the product extended conjugation relative to the starting materials, this driving force, combined with indoline or the generated chloride acting as the base, would be enough to push the equilibrium towards the product, opening a second plausible mechanism in route B.

Reactions were monitored by TLC and consumption of the starting material was seen after 2 hours of reaction at 130 °C. **61**, or the 6-bromoindoline derivative of **62**, were obtained by precipitating from water and LCMS suggested near quantitative conversion, and so this method, with variations in temperature and reaction time, depending on substrate reactivity, was used for many further examples.

S_NAr did not prove a viable method of directly introducing indole derivatives. This is likely to be due to indole being less amenable to protonation which will result in a loss of aromaticity; as opposed to indoline, where the nitrogen does not play a part in its aromatic system. Since S_NAr with the indoline had proved successful, the solution was to oxidise the indoline to the indole after substitution. A method using 2,3-dichloro-5,6-dicyano-1,4-benzoquinone (DDQ) was utilised,[216] affording oxidised product in moderate yields.

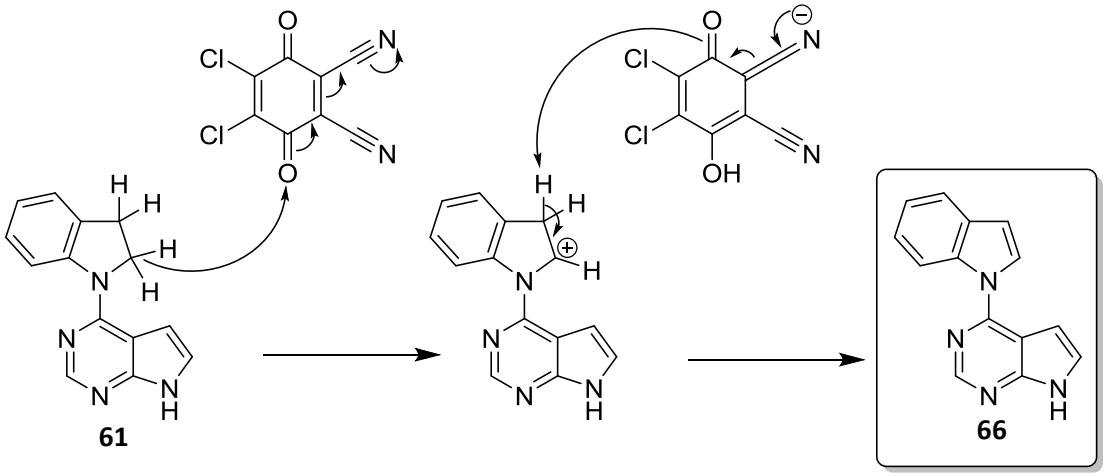

Scheme 18. DDQ oxidation of indoline **61** to indole **66**.

This oxidation was, unfortunately, not universally applicable to the compounds synthesised. Compounds with exocyclic NH_2 groups were not amenable to DDQ oxidation. One way around this would be to protect the NH before carrying out the oxidation but this would not have provided a solution the second problem, which was the issue of substituting the carbazole through S_NAr. Like the indole, the NH is part of the aromatic make up of carbazole and, again like the indole, does not protonate as readily as the indoline. To overcome this, a method was developed whereby the indole, or carbazole, was stirred in sodium hydride prior to addition of the chloro- electrophile. This preformed an anionic nucleophile which reacted much more readily with the electrophile.

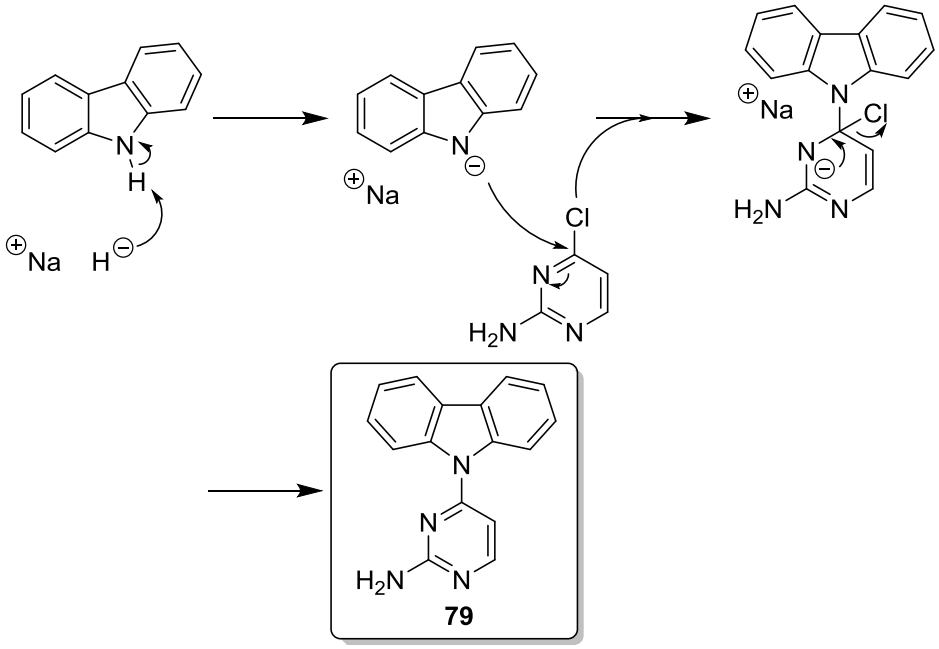

Scheme 19. S_NAr reaction with preformed anionic nucleophile.

3.3.5.4. Sonogashira reaction

The Sonogashira reaction is a relatively new addition to the field of palladium cross-coupling reactions. Copper-mediated alkyne-coupling reactions have been known since the mid-19th century,[217] while early variants of what is now called the Sonogashira reaction were published in 1975.[218–220] It wasn't until the 2000s, however, that significant volumes of work began to be published detailing the use of Sonogashira reactions.[173]With the work that has gone into developing catalyst systems and understanding the role bases and solvents play with regard to specific substrate systems, the Sonogashira reaction is now a highly versatile method for introducing alkyne substituents into molecules without the need for stoichiometric quantities of metal.[173,221]

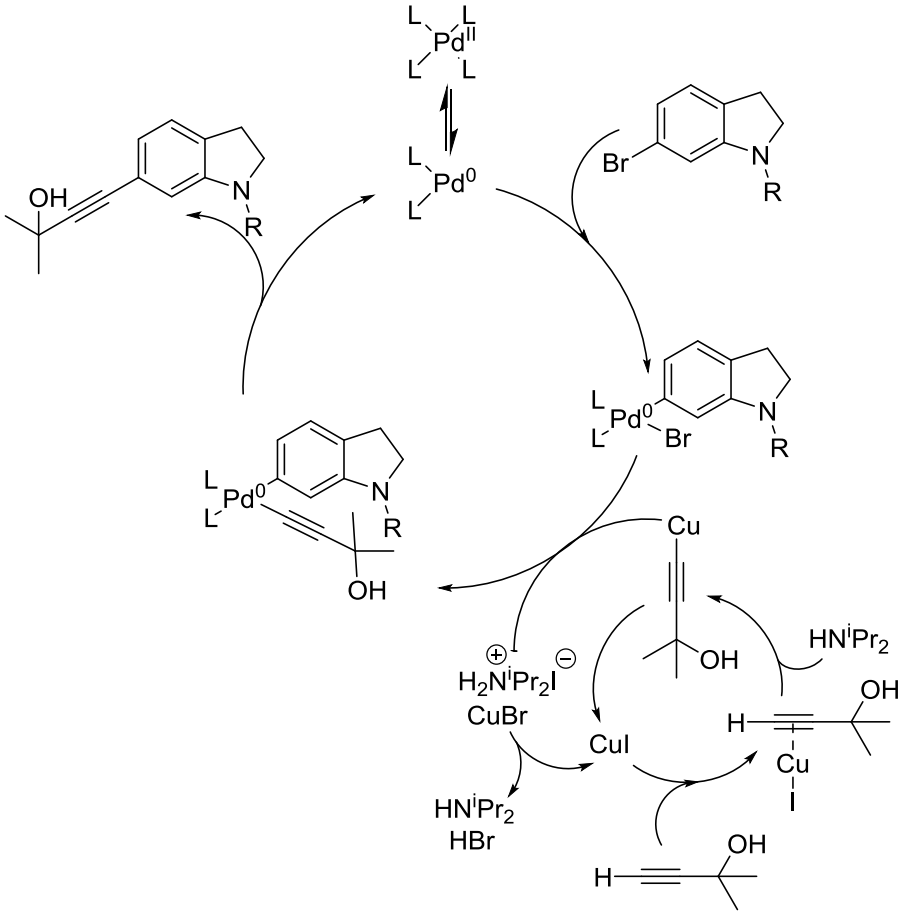

Scheme 20. Proposed catalytic cycle for Sonogashira reaction. Adapted from.[221,222]

The Sonogashira reaction is thought to follow the same general pathway as the Suzuki reaction: namely oxidative addition - transmetallation - reductive elimination.[216] The Sonogashira differs in that the substrate for transmetallation is formed *in situ* from a second catalytic cycle. The copper iodide complexing with the alkyne acts to decrease the pKa of the terminal proton. The decrease in pKa allows for deprotonation by an organic base such as diisopropylamine or triethylamine and generate a copper acetylide.[222] The reactivity of aryl iodides often allow the oxidative addition step, often considered to be the rate limiting step in the Sonogashira process,[222] to take place at room temperature. Aryl bromides are somewhat less reactive and therefore often require elevated temperatures or more specialised catalysts to undergo this process.[174]

With easy access to 6-bromoindoline, and a method established for coupling this in high yields to the pyrrolopyrimidine scaffold, a series of Sonogashira reactions were completed to probe the hydrophobic pocket protected by the gatekeeper. TLC analysis showed consumption of starting material and, seemingly, conversion to a single product. This was further strengthened by LCMS analysis of the crude reaction mixtures after reacting overnight which showed greater than 90% conversion in all cases in the UV trace (example trace in **Figure 83**.

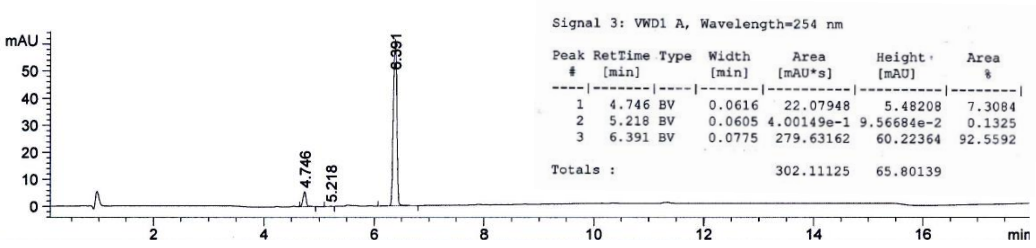

Figure 83. HPLC UV trace of crude reaction mixture for compound **63**.

Problems with purification were a common theme for final compounds bearing alkynyl alcohol substituents. As seen from TLC analysis and the above LCMS trace, reactions seemed to proceed near-quantitatively, however final yields after purification were very low. Flash column chromatography proved insufficient for purification and so HPLC purification was used to obtain final compounds. This afforded products with acceptable purities but often in <10% yields. It is thought that the multiple ring systems and conjugated nature of the molecules result in a planar stacking arrangement. This, in turn, leads to difficulty re-solubilising compounds once out of solution.

3.3.5.5. Anilines

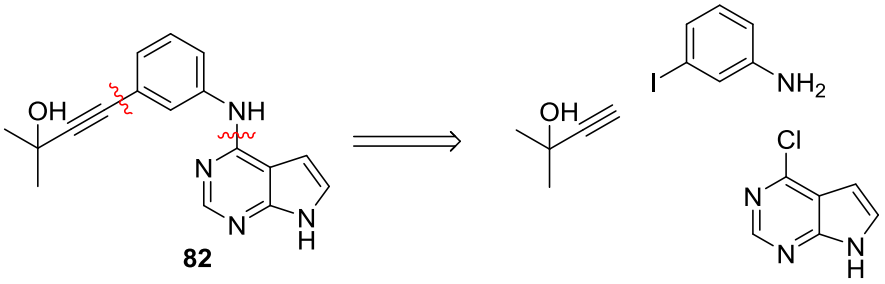

Scheme 21. Synthetic disconnections of alkynylanilines.

Anilines **82**-**85** were synthesised analogously to indoline series through S_NAr reaction and subsequent Sonogashira. Yields were improved slightly relative to indoline series, with yields of up to 27%. The aniline series was marginally more water soluble than the indoline series - with the anilines having slightly lower calculated LogP values - and the improved solubility in polar solvent possibly accounts for improved recovery from reverse phase purification.

3.3.5.6. 2-Amino-5-carbonitriles

Compound **57** was synthesised previously in-house using reported ring-building synthesis reactions for 2-amino-pyrrolopyrimidine-5-carbonitriles.[223–226]

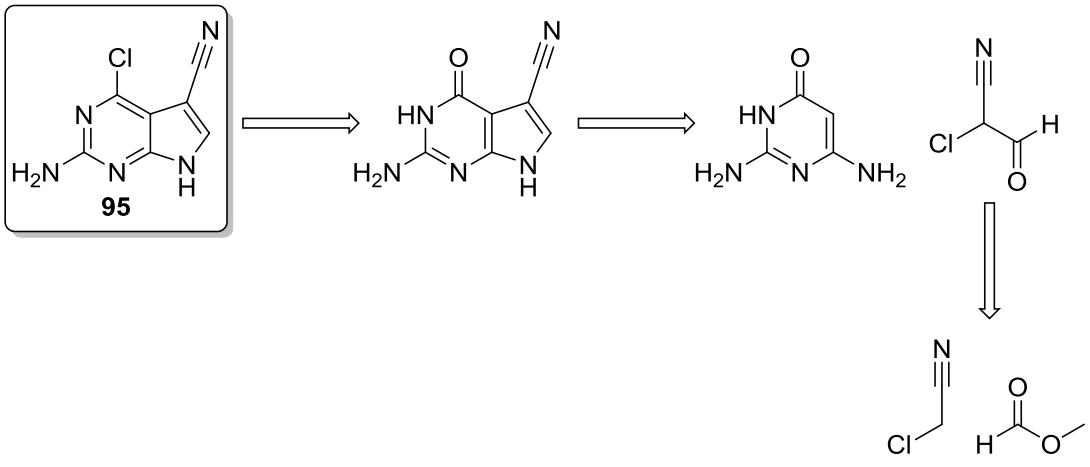

Scheme 22. Retrosynthetic analysis of 2-amino-4-chloro-pyrrolopyrimidine-5-carbonitrile.

Final reaction conditions reported by Minguez and Mackay[227] begin with deprotonation of the chloracetonitrile α-position by methoxide before nucleophilic attack of the resulting anion into the carbonyl of methyl formate to yield 2-chloro-3-oxopropanenitrile.

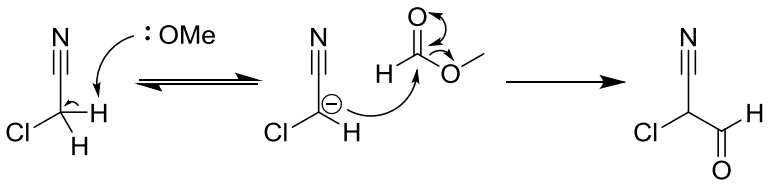

Scheme 23. Suggested mechanism for preparation of 2-chloro-3-oxopropanenitrile**.**

Condensation of intermediate chloroaldehyde with diaminopyrimidone **96** yielded the 4-oxo-pyrrolopyrimidine known as *pre-Q_0* shown in **Scheme 24**.[227]

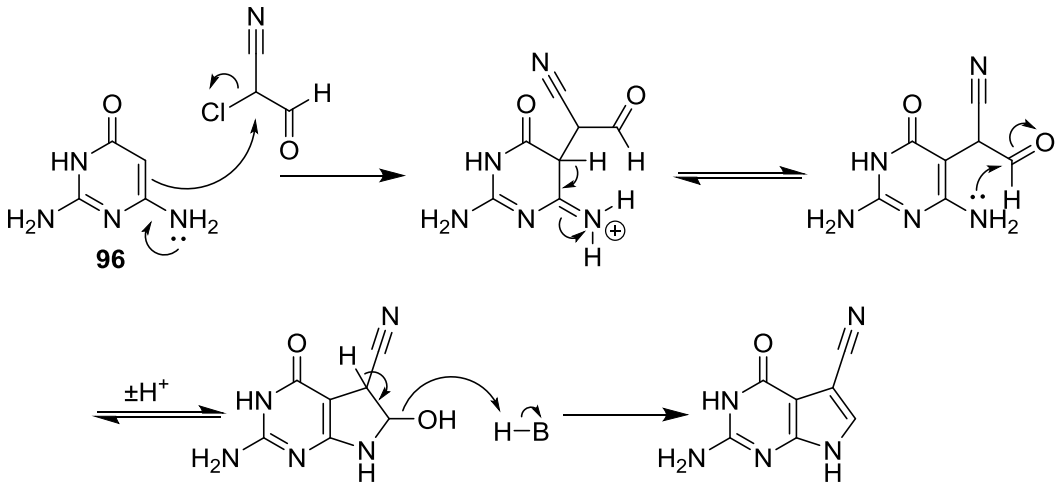

Scheme 24. Proposed mechanism for formation of *Pre-Q_0*.

Chloro-intermediate **95** was obtained by reaction of *pre-Q_0* with $POCl_3$.

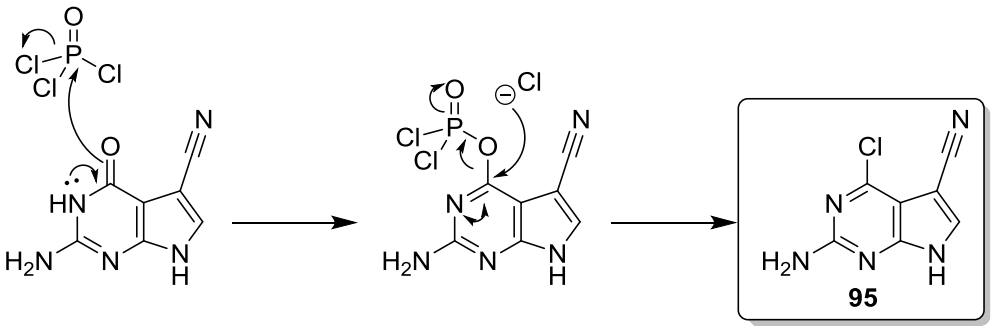

Scheme 25. Chlorination mechanism of *pre-Q_0* by $POCl_3$.

62 and **87** were obtained via S_NAr of indoline and 6-bromoindoline respectively with **95**. Reaction with 6-bromoindoline required more forceful reaction conditions than those required for initial indoline series such as compound **63**: with temperatures of 175 °C furnishing **87** in 82% yield as opposed to the 130 °C necessary for compound **63**.

Compound **86** was not obtainable through the same route as the electronics of the 6-amino-pyrimidin-4-one do not allow for the same ring building synthesis and therefore a different route was required. As such, the retrosynthesis shown in **Scheme 26** was proposed.

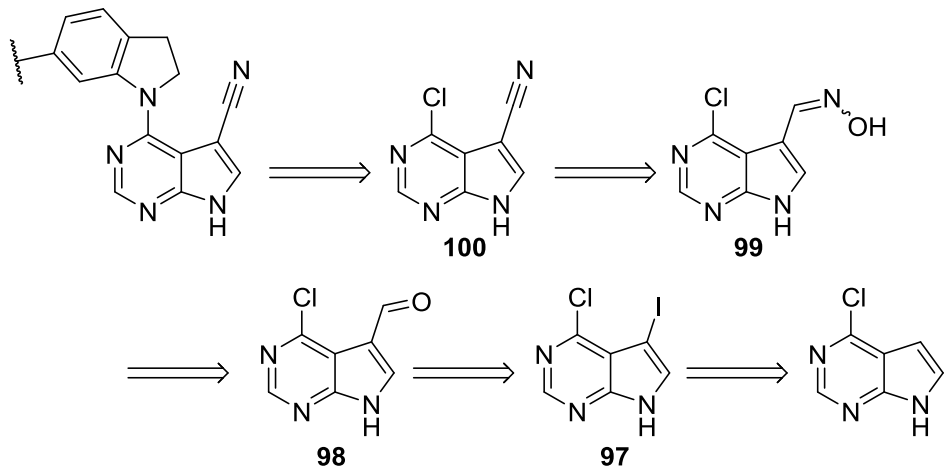

Scheme 26. Retrosynthetic analysis for 4-indolyl-5-carbonitriles.

Synthesis began with the iodination of commercially available 4-chloropyrrolopyrimidine using NIS as an electrophilic source of iodine according to a literature procedure.[228] The introduction of, specifically, iodine as the halogen had several key advantages over chlorine or bromine. First, it is the most reactive halogen to metal-halogen exchange which would prove beneficial for the introduction of the formyl group.[209] Related to this is the fact that the iodine would react preferentially over the 4-chloro substituent in the metal-halogen exchange reaction due to the difference in reactivity.[209] Finally, it was hoped that the iodine could be used as a synthetic handle to investigate the effect of introducing alkyne substituents, as isosteres to the nitrile, through Sonogashira reactions. Iodine is also the most reactive halogen in palladium cross-coupling and should therefore prove the easiest of the halogens to displace.[177]

Completion of the iodination reaction was supported by loss of 5-H in the ^{1}H NMR spectrum and loss of coupling at the 6-H proton.

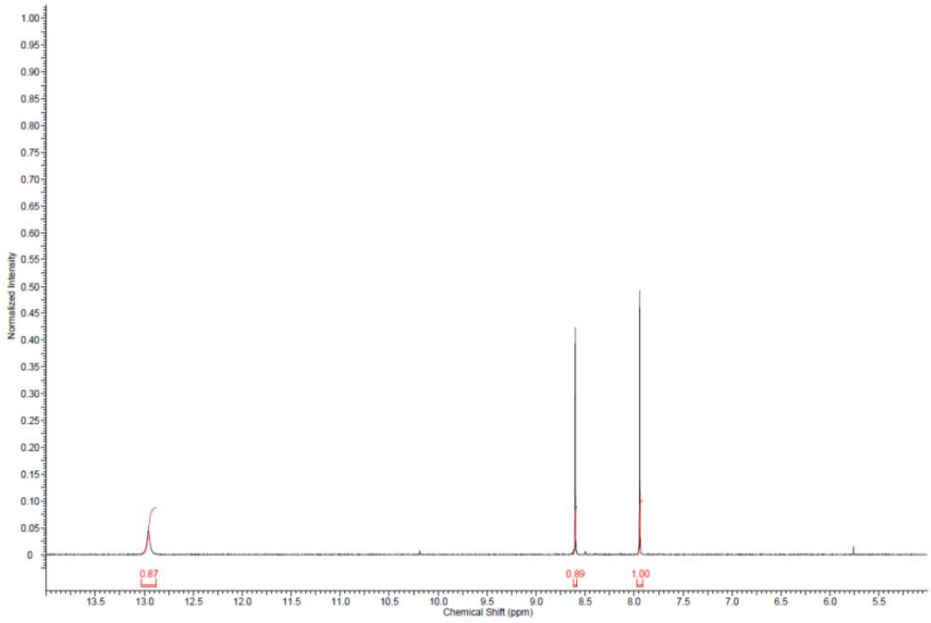

Figure 84. ^{1}H NMR spectrum of **97**. ^{1}H NMR in d_6-DMSO at 500 MHz.

This was further supported by ^{13}C NMR which showed the upfield shift of C-5 of the product to 52.1 ppm.

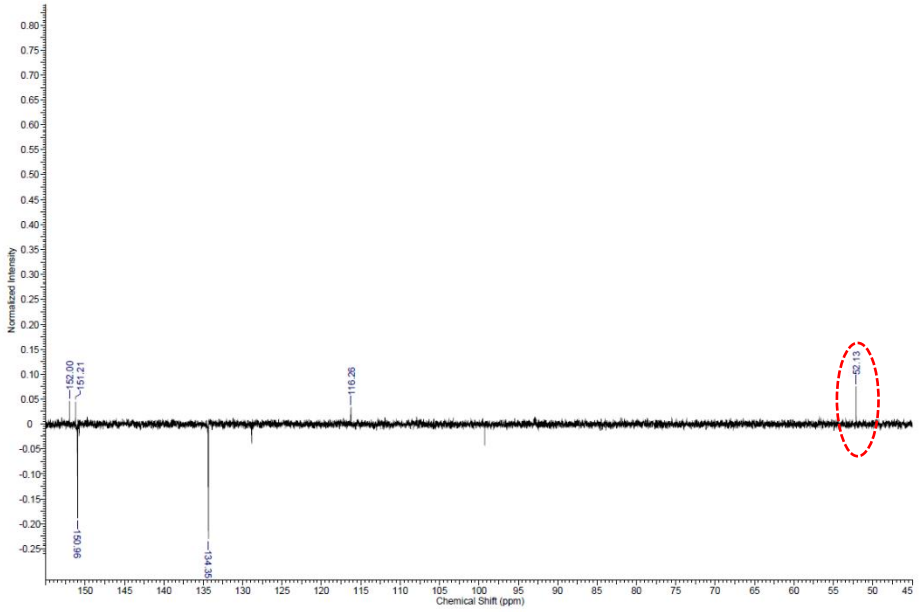

Figure 85. DEPTQ spectrum of **97**. DEPTQ in d_6-DMSO at 125 MHz.

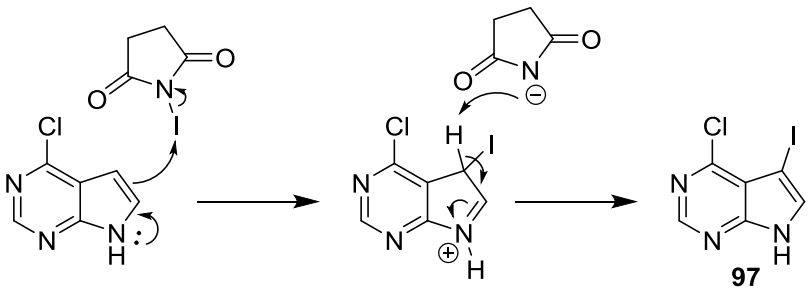

Scheme 27. Proposed mechanism of iodination by NIS.

As discussed earlier in this chapter, formylation of the 5-position of the pyrrolopyrimidine scaffold had proved problematic. Reasons for this are unclear since the transformation using a bromo-substituent has been previously reported in good yields.[229–231] Conversions of no more than 25% by ^{1}H NMR of **97** to **98** could be obtained and, due to both **97** and **98** having very similar R_f values, crude material was used for the next step.

A small portion of material was purified for analysis and formyl product was suggested by the appearance of a new peak in the ^{1}H NMR at 10.25 ppm indicative of the introduction of the aldehyde.

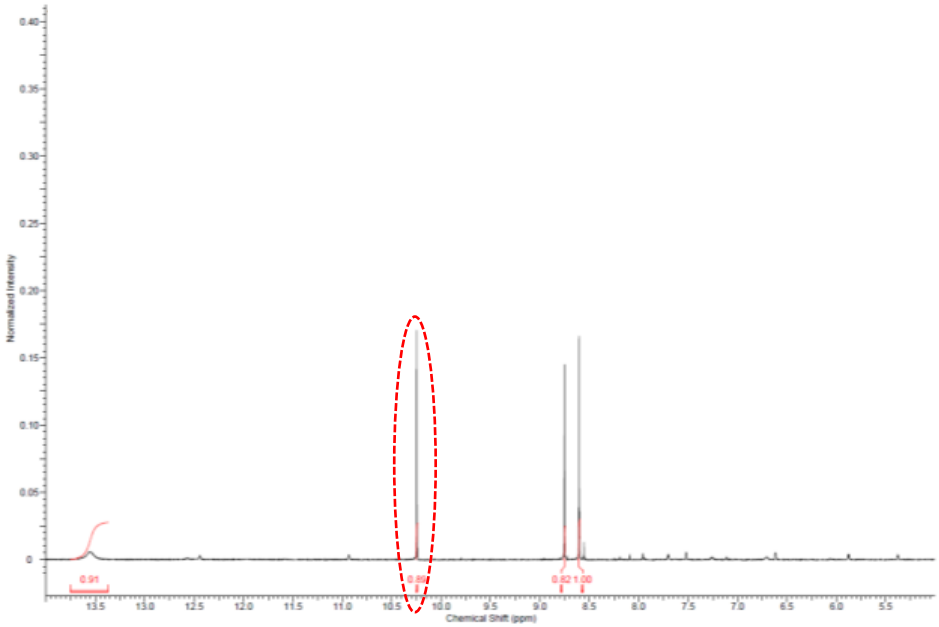

Figure 86. ^{1}H NMR spectrum of **98**. ^{1}H NMR in d_6-DMSO at 500 MHz.

^{13}C also showed the appearance of a new peak at 184.4 ppm corresponding to the carbonyl carbon and loss of the **C**-I quaternary carbon: though quaternary carbons were not easily observable in DEPTQ and so this was not relied upon.

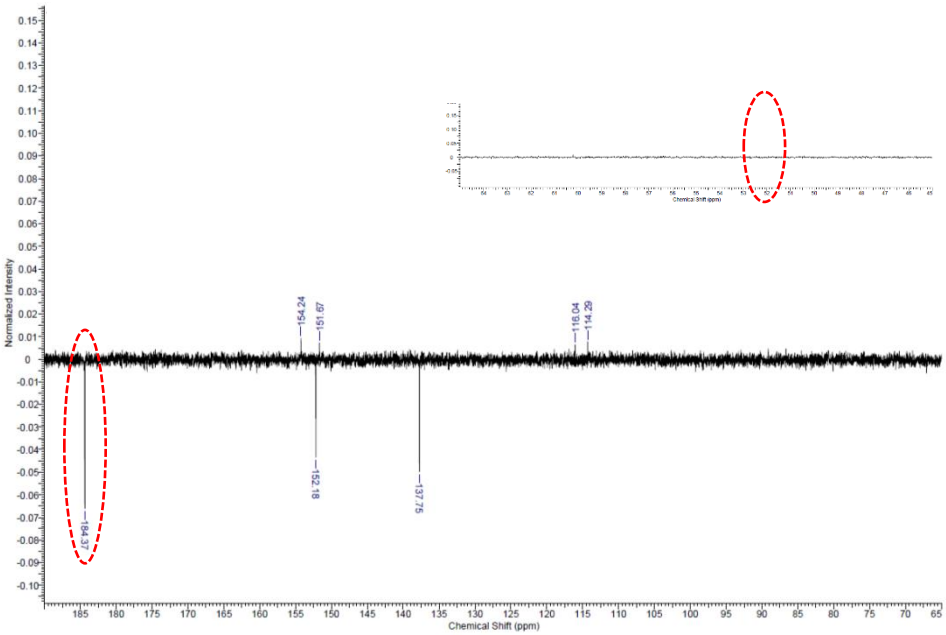

Figure 87. DEPTQ spectrum of **98**. DEPTQ in d_6-DMSO at 125 MHz.

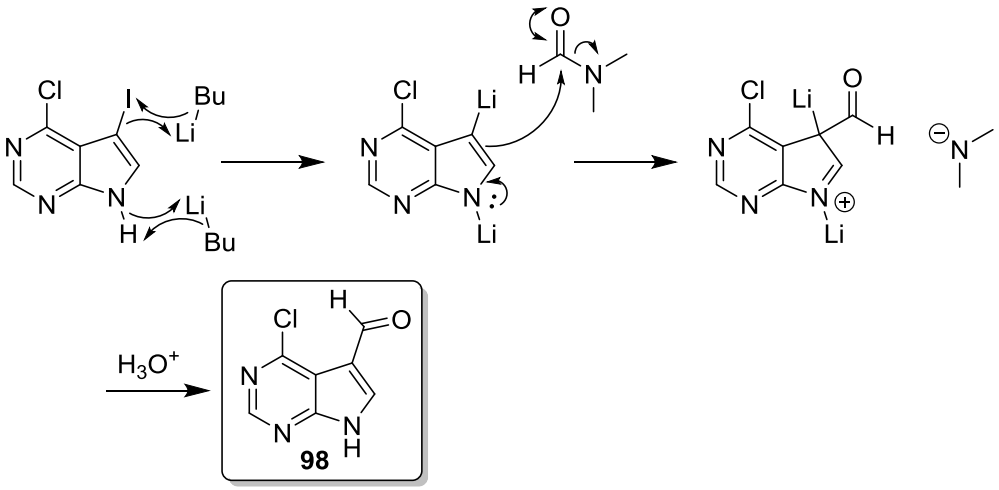

Scheme 28. Formation of compound **98** by proposed covalent lithium-halogen exchange mechanism.

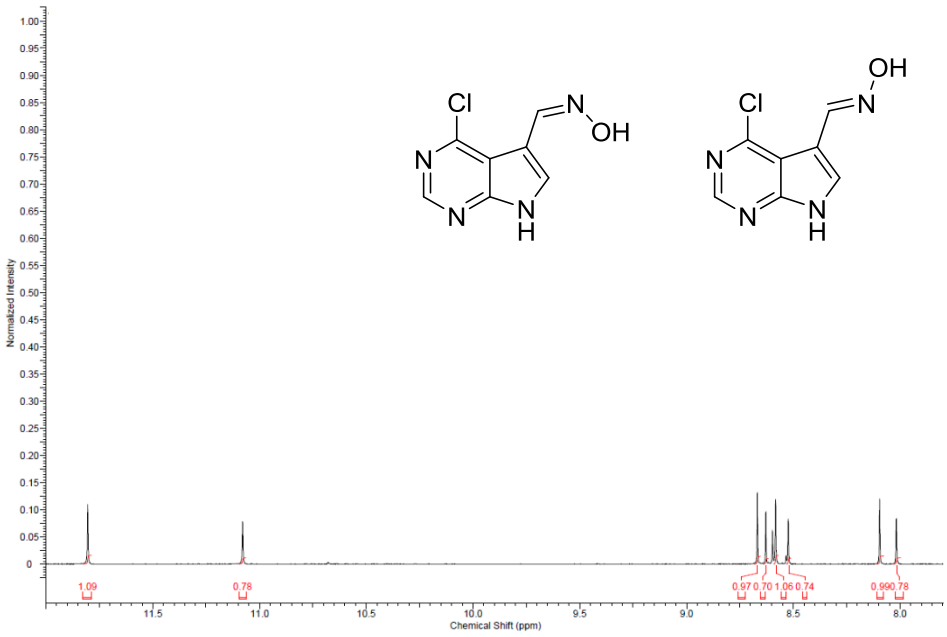

Figure 88. ^{1}H NMR of **99** showing 1:1.4 mixture of *cis* and *trans* isomers. ^{1}H NMR in d_6-DMSO at 500 MHz.

Nitrile moiety in compound **99** was furnished by use of the same reactions as shown in **Schemes 15** and **16**. Both of these proceeded in moderately good yields and provided material to be used in the previously described S_NAr and Sonogashira reactions, yielding compound **86** in 0.3% yield across 6 steps. Introduction of the nitrile was supported by FTIR which showed a distinctive band at 2239 cm^{-1} usually associated with sp geometry triple bonds.[232]

3.3.5.7. 5-Alkynyl derivatives

As discussed earlier in this section, the 5-iodo moiety was introduced with the hope that it could be used for the introduction of alkyne analogues of **86**. This was unfortunately not as successful as hoped; with only cyclopropylalkyne analogue **88** being accessed.

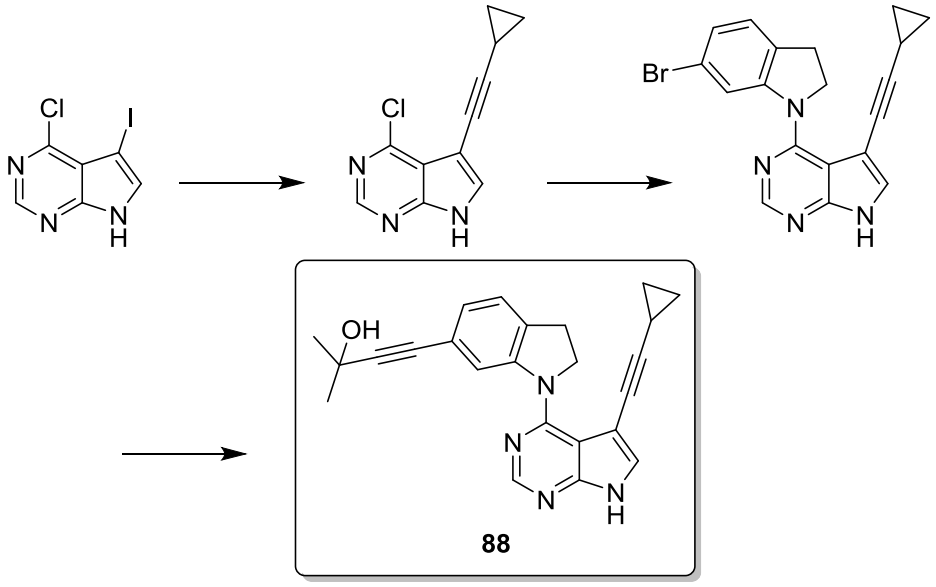

Scheme 29. Synthetic route to cyclopropylalkyne **88**.

The initial plan had been to synthesise the terminal alkyne by introducing the silyl protected alkyne which would be deprotected in the last step to yield terminal alkyne **101** which could be subsequently diversified.

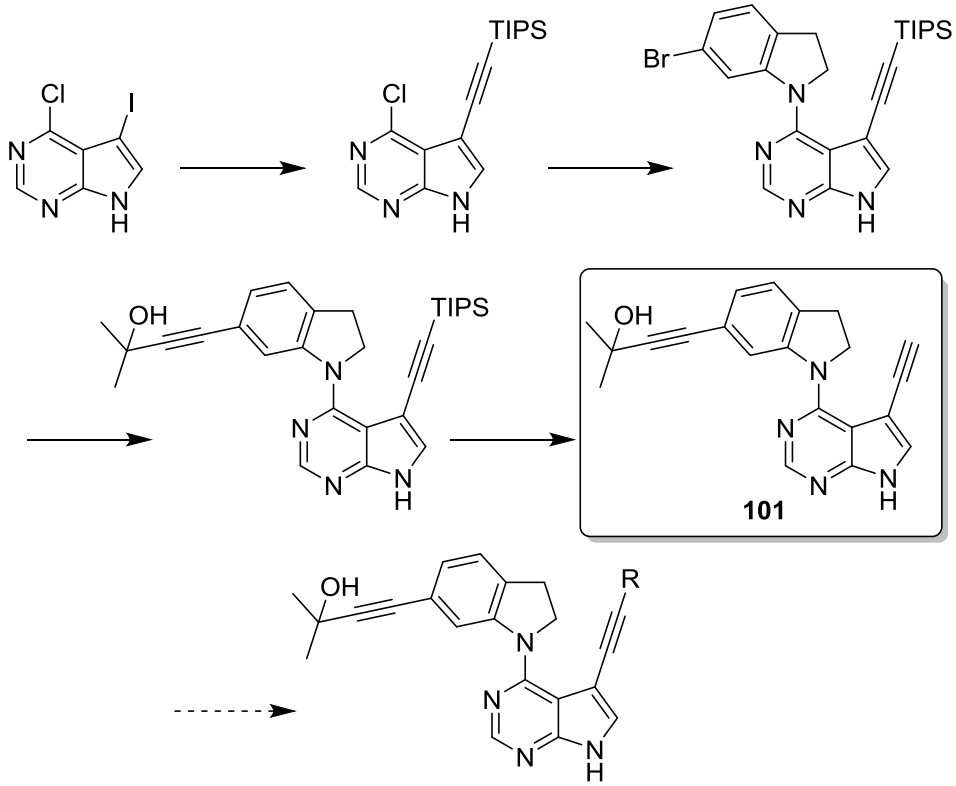

Scheme 30. Planned synthetic route to 3-alkynyl pyrrolopyrimidines.

Sonogashira reaction between tosyl protected **97** and triisopropylsilylacetylene proceeded in excellent yield at room temperature using $Pd(PPh_3)_2Cl_2$ as a catalyst. Subsequent S_NAr reaction with 6-bromoindoline was, however, unsuccessful. It is thought that the size of the triisopropylsilyl group was too large for the Meisenheimer complex to form. Using the smaller trimethylsilylacetylene also failed to allow the S_NAr reaction to proceed and so an alternative strategy was devised, wherein a smaller, terminal alkyne would be introduced. Whilst it was unknown whether a terminal alkyne would be reactive under the S_NAr conditions, being isosteric with the nitrile it was at least known that it would not be too large, thus blocking the reaction site.

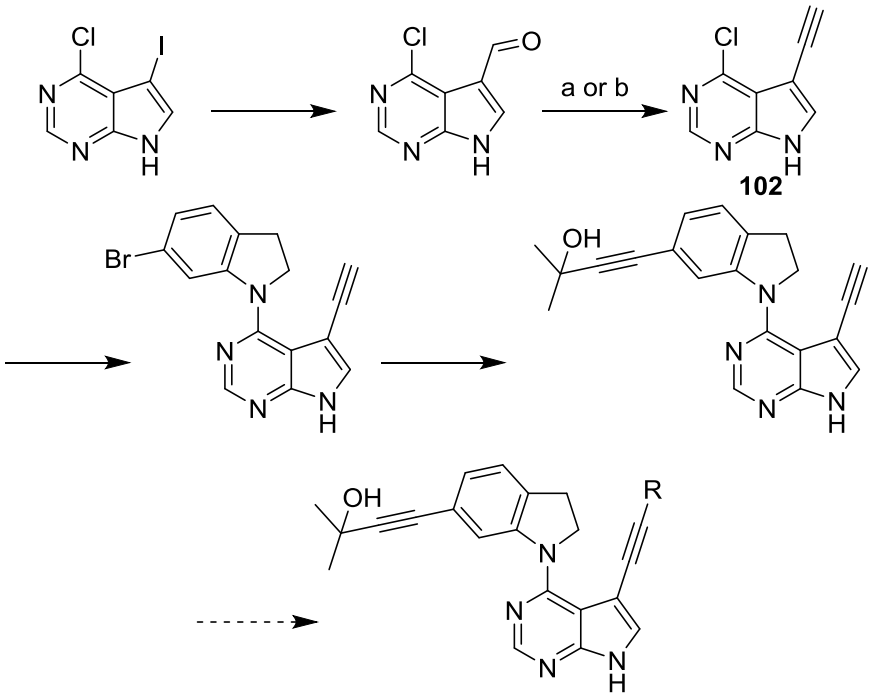

Scheme 31. Alternative synthetic route to 3-alkynyl pyrrolopyrimidines.
a) Ohira-Bestmann reaction; b) Corey-Fuchs reaction.

Following preparation of aldehyde **98**, and protection of the indole NH, alkyne substitution was attempted via Ohira-Bestmann or Corey-Fuchs reaction, according to literature preparations.[233,234] No reaction was observed using the Ohira-Bestmann reagent, with only starting material recovered. Corey-Fuchs conditions led to initial success in synthesising the dibromovinyl intermediate. Upon treatment with butyllithium, however, no reaction was observed and only starting material recovered. A variation of the Corey-Fuchs reagent

((bromomethyl)triphenylphosphonium bromide) yield the monobromovinyl intermediate, but this too proved unreactive with butyllithium.

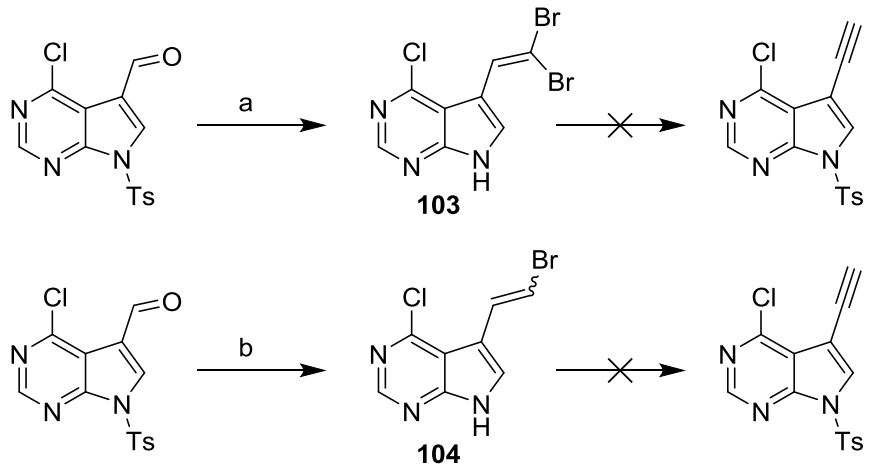

a) CBr_4, PPh_3, CH_2Cl_2; b) $P^+Ph_3Br{\cdot}Br^-$, KO^tBu, THF, -78 °C

Scheme 32. Attempted Corey-Fuchs reactions

As shown in scheme **32**, the tosyl protecting group was removed during the conversion of the aldehyde to the alkene. This deprotection may be the reason the subsequent reaction with butyllithium was unsuccessful. Treating intermediate **103** or **104** with BuLi would first deprotonate the NH. The resultant anion is in conjugation with the alkene as shown in **Scheme 33**

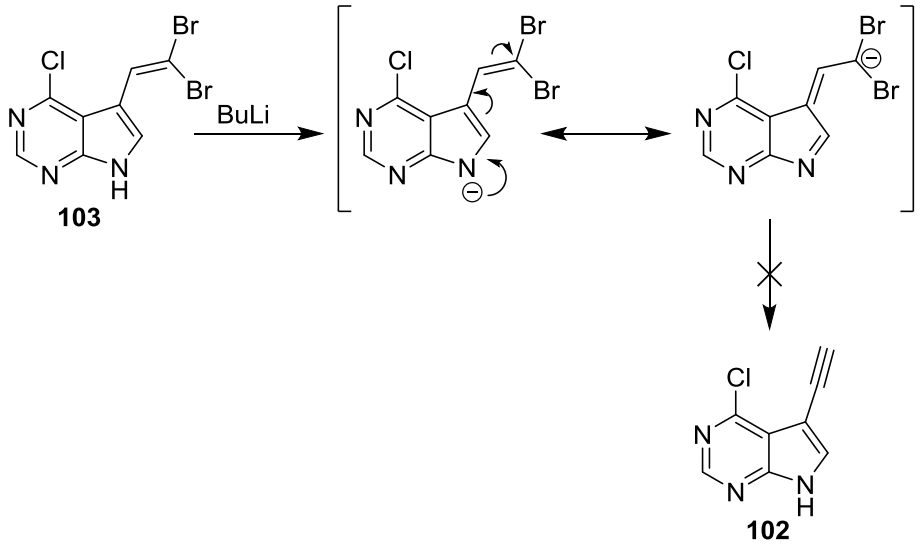

Scheme 33. Possible mechanistic explanation for failed conversion of intermediate **103**.

Replacement of the tosyl protecting group with one stable to basic conditions, such as Boc, would likely rectify this and allow preparation of intermediate **102**.

Since the Sonogashira reaction between silyl protected acetylenes and 3-iodo compound **97** had proved successful, a less efficient strategy using an early stage diversification was possible using commercially available alkynes: as was used for the preparation of **88** (**Scheme 29**). Intermediate hydroxymethyl and methyl alkynes **105** and **106** were successfully introduced, with the latter being introduced using the Kumada reaction, where the alkyne is introduced as a Grignard reagent.

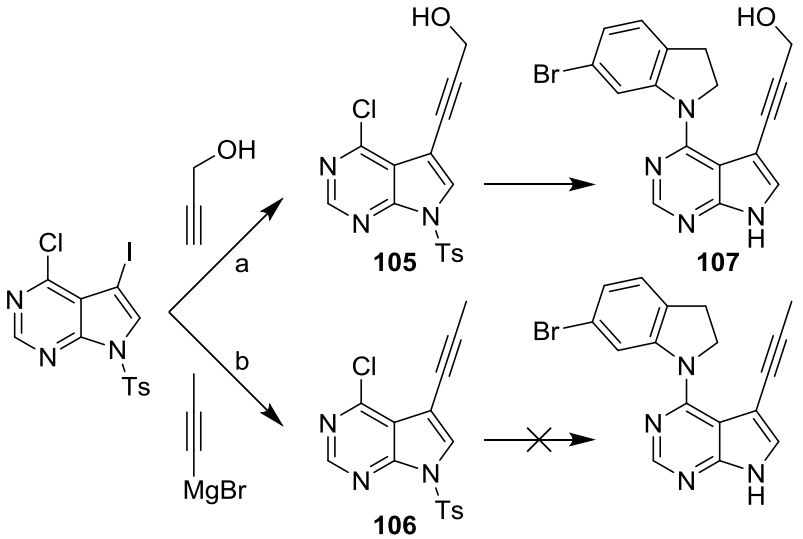

a) $Pd(PPh_3)_2Cl_2$, CuI, DIPA, DMF, 35 °C, 16 h; b) $ZnBr_2$, $Pd(PPh_3)_4$, THF, 0 °C then 50 °C, 72 h.

Scheme 34. Preparation of **105** and **106** by Sonogashira and Kumada coupling.

Mass spectrometry suggested the successful substitution of chloro- intermediate **105** with 6-bromoindoline, with loss of the tosyl protecting group, however, only starting material was recovered for the analogous reaction with **106**. Subsequent Sonogashira reaction between **107** and 2-methylbut-3-yn-2-ol resulted in an inseparable mixture, with mass spectrometry of the crude material indicating no starting material or desired product.

The successful S_NAr reactions of 6-bromoindoline with hydroxymethyl **106** and the cyclopropyl analogue indicate that routes analogous to that shown in **Scheme 29** to 4-indolinyl-5-alkynylpyrrolopyrimidines are viable, but that more development work is required to understand steric and electronic parameters within which the S_NAr reaction is able to proceed.

4. Case study: compound 73 development

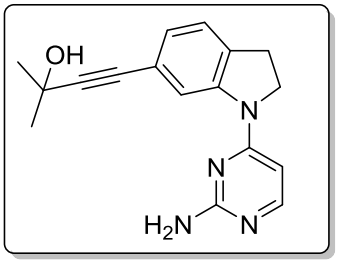

As discussed in chapter 3, **73** is a known compound which has previously been disclosed as a NIK inhibitor.[195] Existing biological or pharmacological data relating to this compound are, however, scarce: with the published data merely stating that it showed a biochemical potency <1 μM.[195] In-house assessment provided a K_i of 15 nM and so it was decided to use compound **73** as a tool compound to, firstly, investigate the biological and phenotypic effects of NIK inhibition and, secondly, to obtain PK and off-target data as a benchmark for potential improvement.

Biochemical assessment against IKKα and IKKβ showed no activity of the compound up to 30 μM and so a pancreatic and a prostate cancer cell line (PANC-1 and PC3M respectively) were selected to observe effects on protein levels with treatment and to study the phenotypic effects of treatment with compound **73**.

The canonical and non-canonical NF-κB pathways are shown in **Figure 89** for reference. Under basal conditions, the canonical marker IκBα exists as a stable complex, incorporating the inactive p65 (RelA) subunit and p105. Upon stimulation, IκBα is phosphorylated by the IKKα/β/NEMO complex and degrades, resulting in the release of the phosphoprotein p65 and proteolysis of p105 to p50. When canonical inhibition occurs, the expected observation is a reversal of IκBα degradation accompanied by increasing pp65 and decreasing p105 levels.

In the non-canonical pathway, basal conditions involve the rapid proteolysis of NIK and thus minimal phosphorylation of IKKα and, consequently, low pp100 levels correlated with low p52 levels. Activation of the pathway leads to phosphorylation of IKKα, subsequent phosphorylation of p100 and release of p52. By inhibiting this pathway, this process is expected to be reversed, with pp100 and p52 levels decreasing in a dose-dependent manner.

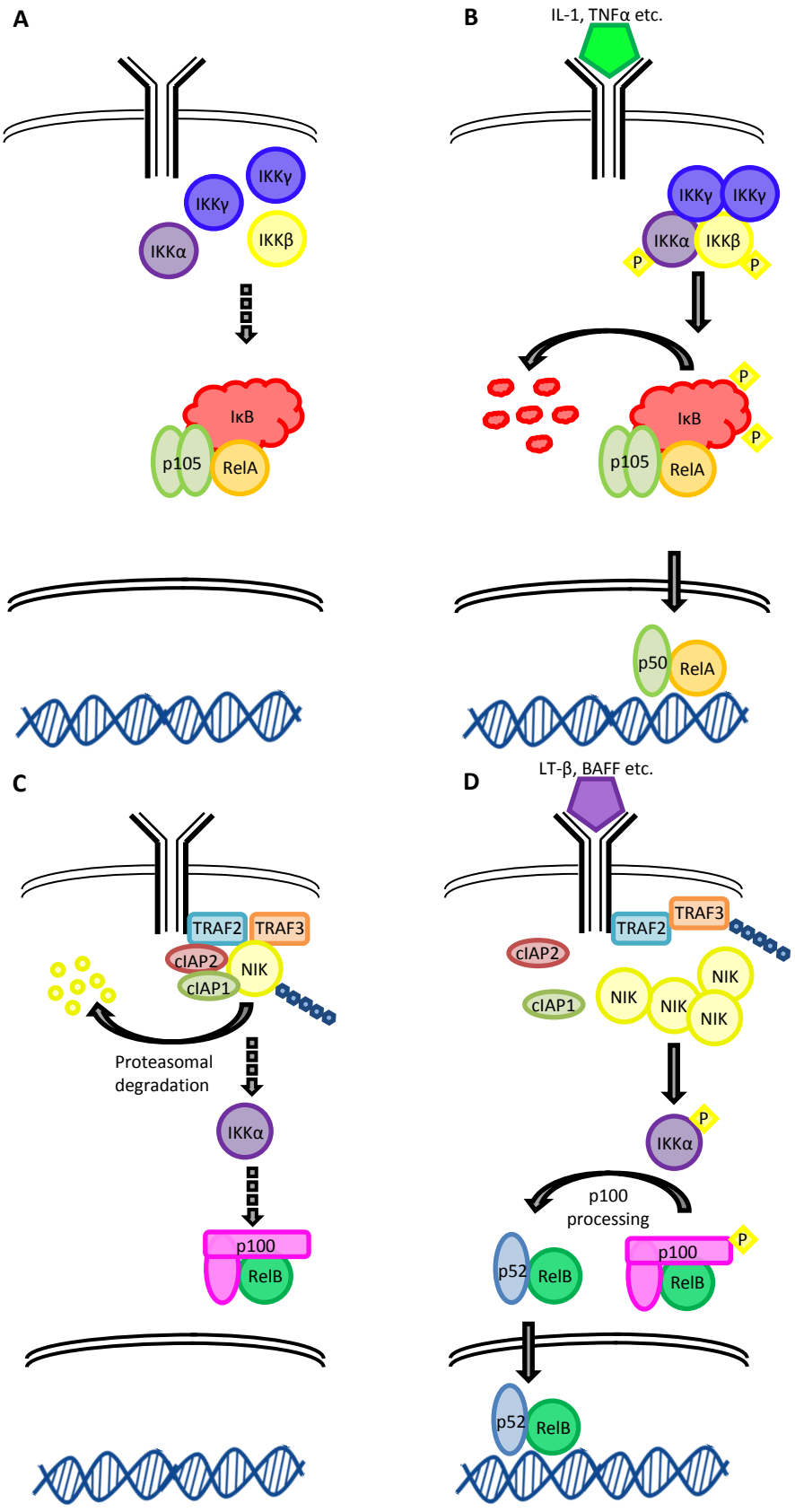

Figure 89. Canonical (panels **A** and **B**) and non-canonical (panels **C** and **D**) NF-κB pathways.

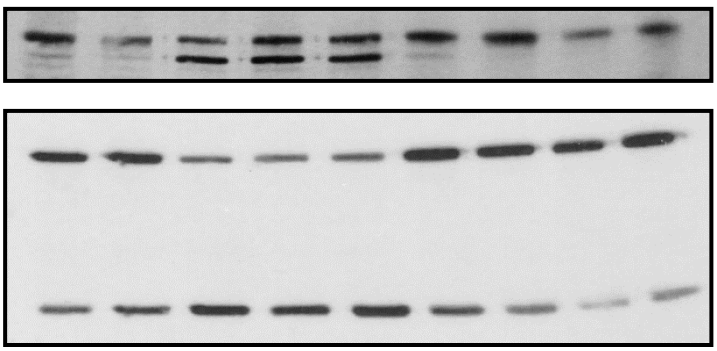

-	-	+	+	+	+	+	+	+	LTα1β2 (15ng/ml)
-	-	-	+	-	-	-	-	-	DMSO (30 μM)
-	10	-	-	0.1	0.3	1	3	10	**73** (μM)

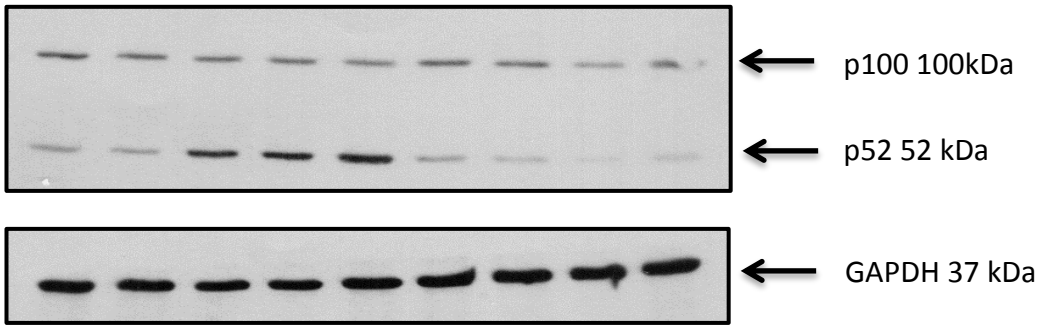

-	-	+	+	+	+	+	+	+	LTα1β2 (15ng/ml)
-	-	-	+	-	-	-	-	-	DMSO (30 μM)
-	10	-	-	0.1	0.3	1	3	10	**73** (μM)

Figure 90. Western blot analysis of compound **73** against NF-κB markers in PANC-1 cells.

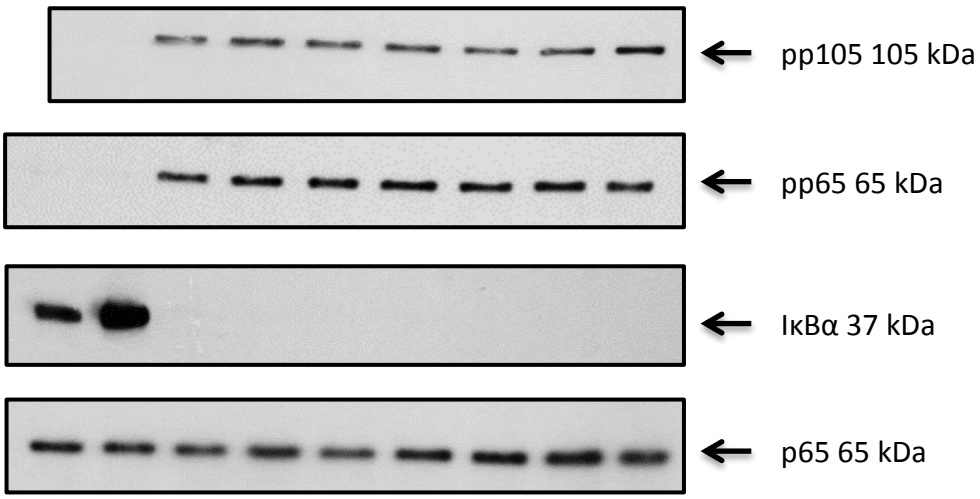

-	-	+	+	+	+	+	+	+	TNFα (10ng/ml)
-	-	-	+	-	-	-	-	-	DMSO (30 μM)
-	10	-	-	0.1	0.3	1	3	10	**73** (μM)

Figure 90 (cont). Western blot analysis of compound **73** against NF-κB markers in PANC-1 cells.

Western blot analysis, completed by Ka Ho Ho and Ahlam Al-Obaidi, determined the cellular IC_{50} for phosphorylation of p100 to be 149 nM in PANC-1 cells. No effect on canonical markers pp105, pp65 or IκBα was observed up to 10 μM, suggesting no engagement of the canonical NF-κB pathway. A similar trend was also observed against non-canonical pp100 and p52 markers and canonical marker pp65 in PC3M cells, with IC_{50} for both p52 and pp100 less than 1 μM.

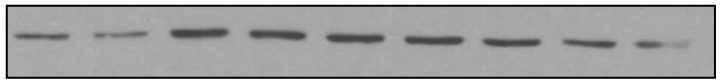

pp65 (65kDa)

---	---	+	+	+	+	+	+	+	TNFa (10ng/ml)
---	---	---	+	---	---	---	---	---	DMSO (30 µM)
---	30	---	---	0.1	0.3	1	3	10	**73** (µM)

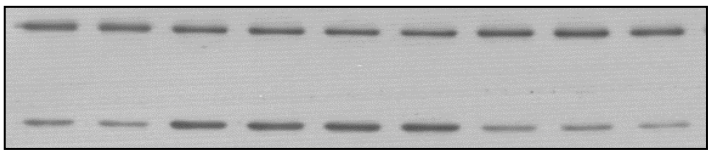

p100 (100kDa)

p52 (52kDa)

---	---	+	+	+	+	+	+	+	LTXα1β2 (30ng/ml)
---	---	---	+	---	---	---	---	---	DMSO (10 µM)
---	10	---	---	0.1	0.3	1	3	10	**73** (µM)

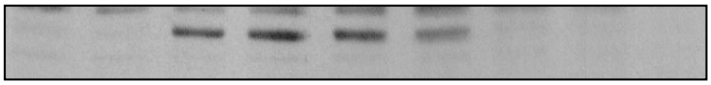

pp100 (100kDa)

---	---	+	+	+	+	+	+	+	LTXα1β2 (15ng/ml)
---	---	---	+	---	---	---	---	---	DMSO (10 µM)
---	10	---	---	0.1	0.3	1	3	10	**73** (µM)

Figure 91. Western blot analysis of compound 73 against NF-κB markers in PC3M cells.

Since the selectivity profile against the two main NF-κB pathways observed in the biochemical assay was largely translated into the cellular setting, an alamarBlue® cytotoxicity assay was carried out to investigate to what phenotypic response the observed target engagement led. Cell viability IC_{50} in PANC-1 was shown to be 490 nM.

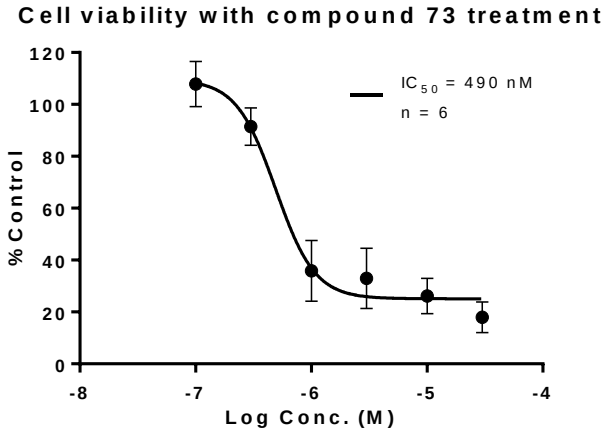

Figure 92. PANC-1 viability after 48 hours as determined by alamarBlue®**.**

AlamarBlue® does not give any indication of mechanism of cell death; only viability compared to a control group as determined by metabolic activity. The key component is resazurin; a blue dye which is efficiently reduced in mitochondria to the pink coloured resorufin.

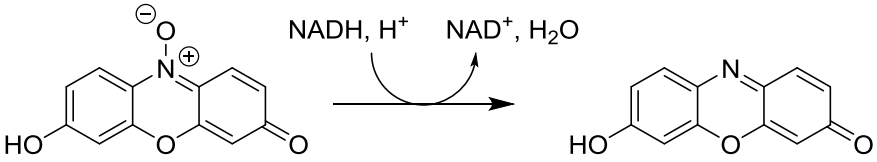

Scheme 35. Reduction of resazurin to resorufin.

Alongside the phenotypic assay, *in vitro* PK data was obtained from Cyprotex (Macclesfield, UK). The results are shown in **Table 14**.

Compound 73	
Caco-2 permeability	29.6 x 10^{-6} cms^{-1}
Efflux ratio	1.14
Clearance	3.08 µL min^{-1} mg^{-1}
Half-life	225 mins

Table 14. PK data for compound **73**.

Compound **73** showed good permeability in the Caco-2 setting. Data generated by Cyprotex and Zhao *et al.* suggest that compounds with Caco-2 permeability between 10^{-6} and 10^{-5} cms^{-1} are likely to show 70-90% human intestinal absorption.[142,235] The cell permeability experiment also suggested that the compound was not effluxed from cells. This means that the compound is able to remain within the cell and is therefore able to exert its pharmacological effect. A clearance, based on the mouse S9 microsomal fraction, of 3.08 µL $min^{-1}mg^{-1}$ is considered low which suggests that the compound is metabolised for excretion quite slowly, giving it more time to exert its effect on the target.[236] A mouse microsomal half-life of 225 minutes is difficult to interpret as an isolated figure; however this is compared to a midazolam (anaesthesia) standard with a half-life of less than 32 minutes.

These results suggest that this kind of scaffold could be amenable to further development for *in vivo* investigation. A screen against a representative panel of kinases, performed by Life Technologies (Paisley, UK), however, indicated that compound **73** is active against a selection of other kinases.

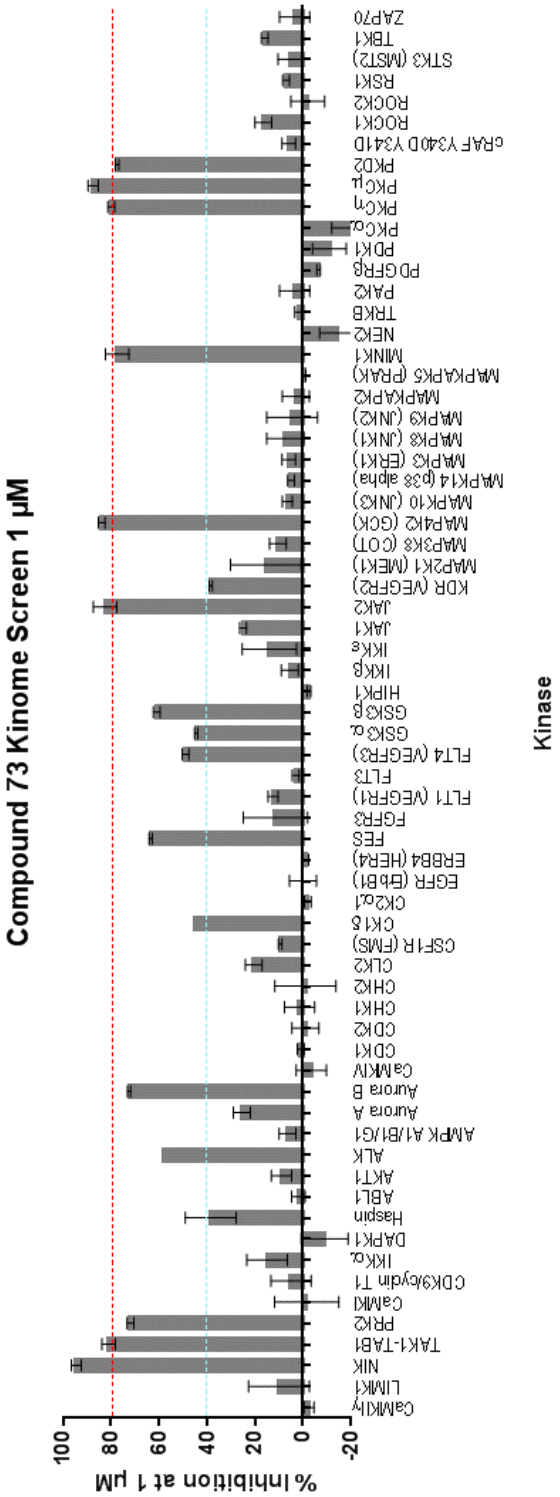

Figure 93. Kinome screen of compound **73** at 1 µM.

As discussed in the introductory section, a multi-kinase inhibitor may, clinically, be very desirable; particularly when some of the kinases inhibited by compound **73**, such as TAB1-TAK1 and the GSKs have themselves been suggested as targets for cancer treatment.[70,73] Promiscuity can also be detrimental, however, as multi-kinase inhibition may result in unwanted toxicity.[144] Multi-kinase inhibition is also not desirable for tool compounds designed to interrogate signalling pathways, as it is often difficult to determine which observed phenotypic effects are a consequence of the inhibition of each target. It was therefore important that compounds with differing kinome profiles be developed. Firstly, as useful tool compounds to investigate the effects of targeting different kinases along with NIK, and secondly to provide different scaffolds which may confer selectivity for different kinases and, consequently, affect different cell lines in different ways. Compounds **81** and **87** were assessed for activity against the same panel of 67 kinases as compound **73**.

Both compounds **81** and **87** showed an improved selectivity profile when compared to compound **73**: with 3 and 0 other kinases showing greater than 80% inhibition at 1 μM respectively compared with 7 for compound **73**. It should be noted that, due to the significantly reduced potency of compound **81** versus **73** (K_i = 350 nM vs 15 nM), NIK inhibition was determined to be 62% at 1 μM. Taking this into account, however, only 2 other kinases tested exhibited greater than 40% inhibition at 1 μM. Unfortunately, no crystal structures exist in the PDB for many of the kinases which exhibit stark differences in their inhibitory profile such as MINK1, MAP4K2 (GCK) and PKCη and thus it is difficult to explain this disparity.

The potency of compound **81** against JAK2 is very interesting. Biochemically, almost no activity is observed at 1 μM, however, modelling this compound in a published crystal structure of JAK2 (PDB code 5L3A) suggests an almost identical interaction map as that observed for NIK. The reason for such a marked decrease in potency is therefore unclear and a crystal structure is likely to be the only way to fully understand the reasons for it.

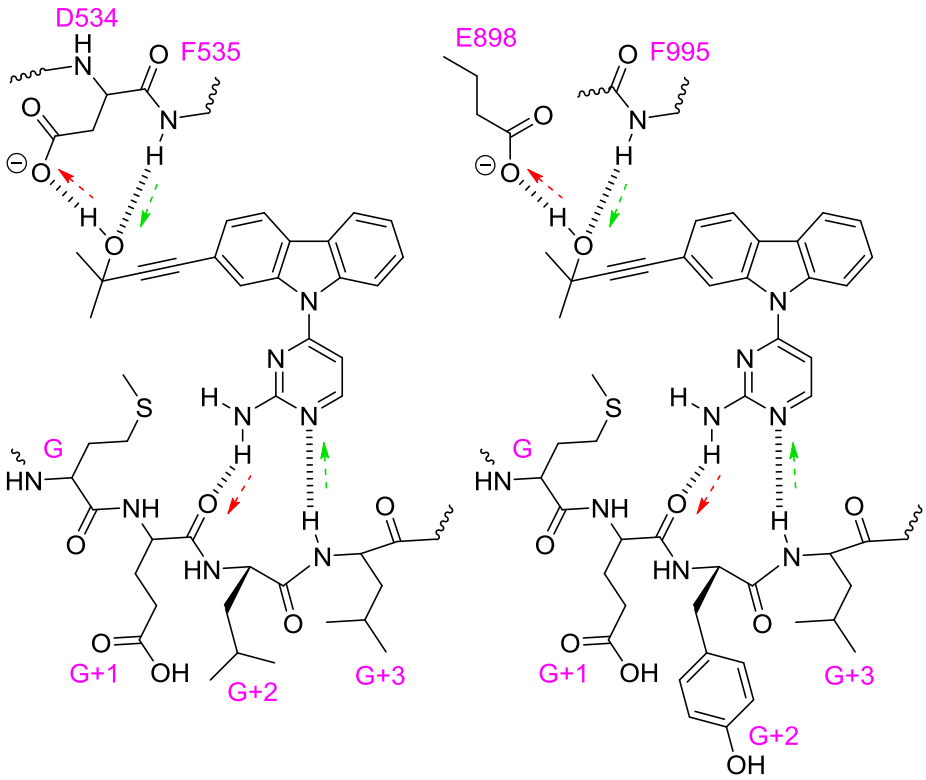

Figure 94. Interaction map suggested from computational modelling showing key interactions of compound **81** with NIK (left) and JAK2 (right).

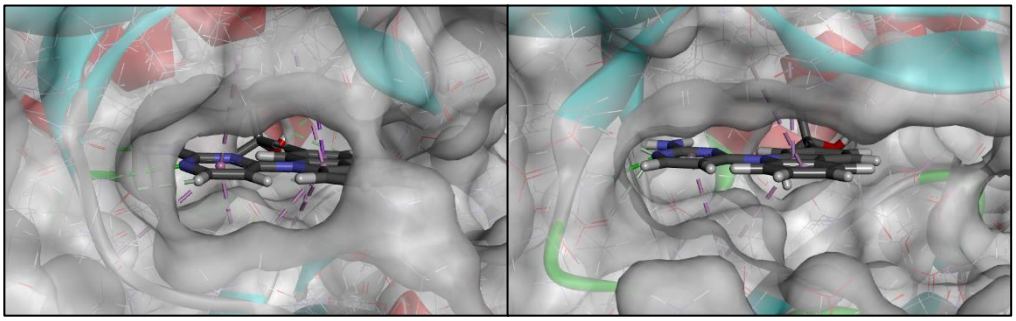

Figure 95. Docked pose of compound **81** in NIK (left) and JAK2 (right).

The smaller decrease in JAK2 activity from **73** to **87** is more easily understood, assuming the binding pose is consistent between the two kinases. The analogous residue to Q479 in JAK2 is D939. This is not capable of forming a hydrogen bond to the nitrile in its ionised state and thus, with one fewer hydrogen bond, the interaction with **87** and JAK2 is weaker than between **87** and NIK.

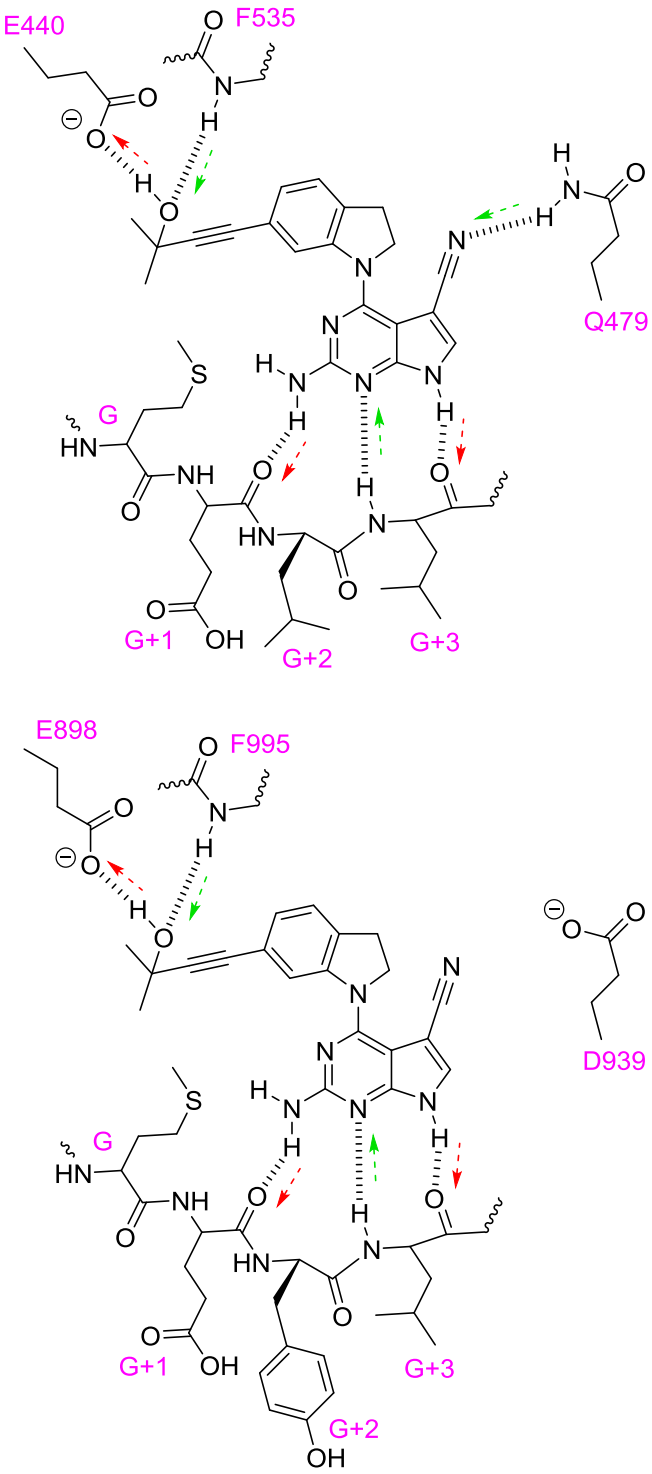

Figure 96. Comparison of proposed binding modes of **87** in NIK (top) and JAK2 (bottom).

The only remarkable increase in inhibitory activity against any kinase in the panel was the effect of **87** against CLK2. One distinct difference between NIK and CLK is, again, the gatekeeper residue, which is also a phenylalanine in CLK2. Whilst this does not account for the marked change in activity between the two kinases, it is thought that the change in gatekeeper allows for alternative binding poses for the pyrrolopyrimidine scaffold in CLK2 which are either not available to, or less favourable for, the aminopyrimidine scaffolds of **73** and **81**. Docking studies using a published CLK2 structure (PDB code 3NR9) suggest that the proposed biding mode of **73** and **81** in NIK is not transferable to CLK2 and the biochemical activity suggests that there is no favourable binding pose. The addition of the nitrile in **87**, however, provides an extra hydrogen bond acceptor and thus more possible poses, such as the one suggested by modelling in **Figure 97**.

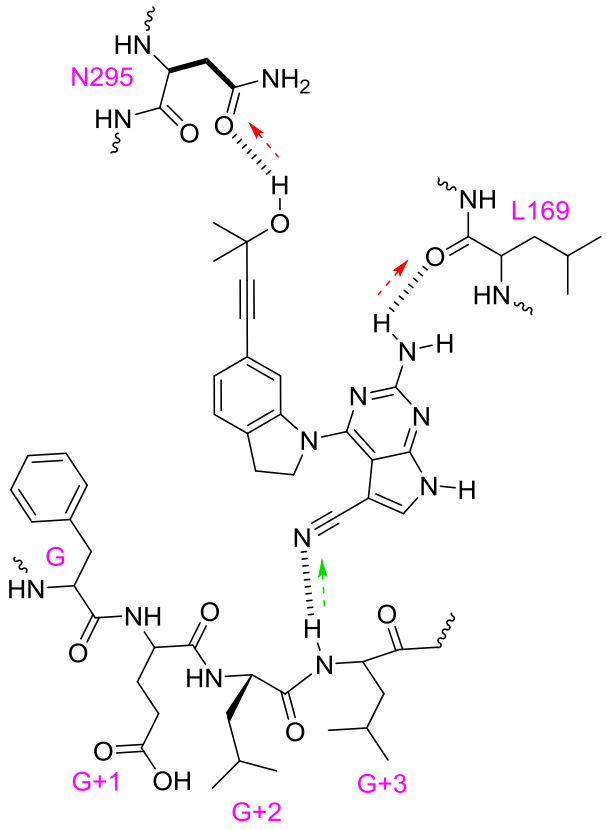

Figure 97. Interaction map of possible binding pose of **87** in CLK2.

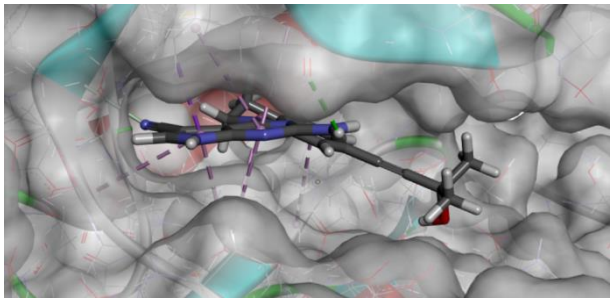

Figure 98. Possible binding pose suggested by modelling of **87** in CLK2.

Along with NIK, all three compounds assessed also show inhibition of TAK1: particularly **73** and **81**. The reason for this is likely to be that all the residues with which the molecules are proposed to interact are conserved and thus there is little difference in the potency of the molecules against each kinase.

Alongside improving the selectivity profile, maintaining good pharmacokinetic properties is an important consideration. Compound **87** was shown to be less stable, and cleared faster, than **73**, however, with a half-life using the liver S9 fraction still greater than 1 hour, and the clearance rate considered not far outside "low",[236] it is still a viable candidate for further development. Compound **81** was shown to be extremely stable in the S9 setting, with no metabolism observed during the experiment. Whilst this is a very encouraging result, there is still the possibility that it is metabolised in a non-cytosolic process. There is also the danger, in an *in vivo* setting, that no metabolism could lead to long-term toxicity as the compound may prove difficult to excrete.

Both **81** and **87** show similar cell permeability profiles to **73**, with both exhibiting permeability in the 10^{-6} cms^{-1} range. This is likely to translate to around 80% absorption in a human intestinal setting.[142] In addition, compound **81** does not seem to undergo efflux, though **87** shows an efflux ratio of 5.47, suggesting that it undergoes moderate efflux from the cell. The drug transporters P-gp and BCRP are both active in Caco-2 cells and so it is likely that one of these is responsible for the observed efflux of **87**. It has been reported that the drug dipyridamole is a substrate for BCRP.[237] This molecule has a similar core scaffold to compound **87** which suggests BCRP is likely more heavily involved in the efflux of **87**.

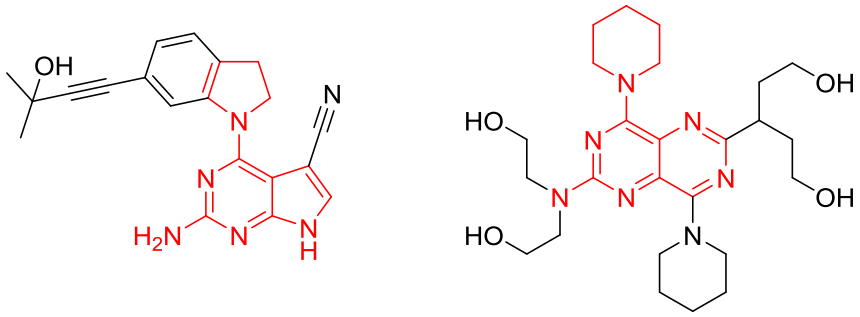

Figure 99. Structures of 87 and dipyridamole highlighting similar scaffolds.

One way of investigating this hypothesis would be to treat the Caco-2 cells with either a P-gp or BRCP inhibitor prior to treatment with compound **87**. If no efflux is observed then whichever transporter has been inhibited is likely to be causing the efflux.

	73	**81**	**87**
Caco-2 permeability (cms^{-1})	29.6 x 10^{-6}	22.8 x 10^{-6}	9.0 x 10^{-6}
Efflux ratio	1.14	0.53	5.47
Clearance ($\mu L\ min^{-1}\ mg^{-1}$)	3.08	Immeasurable	10.8
Half-life (minutes)	225	Stable at 45 mins	64.1

Table 15. Comparison of PK data for **73**, **81** and **87**.

Preliminary testing of **87** against PC3M cells shows no activity against markers of the canonical pathway and a significant drop in cellular potency against non-canonical NF-κB marker pp100 relative to compound **73**. It is likely, however, that this is only a partial picture given that PK data suggests efflux from the cell. Kinome screening suggests very little activity against IKKβ and thus canonical markers are unlikely to be affected, however treatment with an efflux inhibitor may show **87** to be even more potent against non-canonical NF-κB markers.

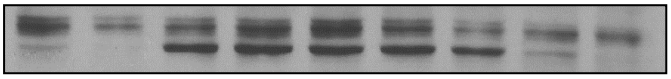

---	---	+	+	+	+	+	+	+	LTXα1β2 (15ng/ml)
---	---	---	+	---	---	---	---	---	DMSO (10 μM)
---	10	---	---	0.1	0.3	1	3	10	**87** (μM)

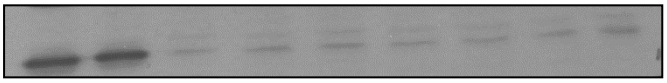

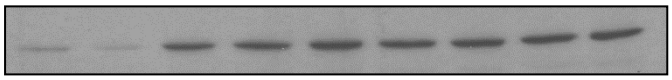

---	---	+	+	+	+	+	+	+	TNFα (10ng/ml)
---	---	---	+	---	---	---	---	---	DMSO (10 μM)
---	10	---	---	0.1	0.3	1	3	10	**87** (μM)

Figure 100. Western blot analysis of compound **87** against NF-κB markers in PC3M cells.

Both compounds **81** and **87** have retained, overall, good pharmacokinetic properties relative to **73**, though moderate efflux is observed in **87**. Both also have improved kinome profiles when compared to **73** and could both, therefore, be useful hit compounds in further developing NIK inhibitors. Cytotoxicity assessment of **87** against both PC3M and PANC-1 cells showed significantly reduced activity relative to **73**, with IC_{50} values around 10 μM, though again, if used in combination with an efflux inhibitor, this may improve. An alternative explanation may be that the cytotoxicity observed with **73** is due to inhibition of kinases not inhibited by **87** which may indicate the benefit of a multi-kinase inhibitor.

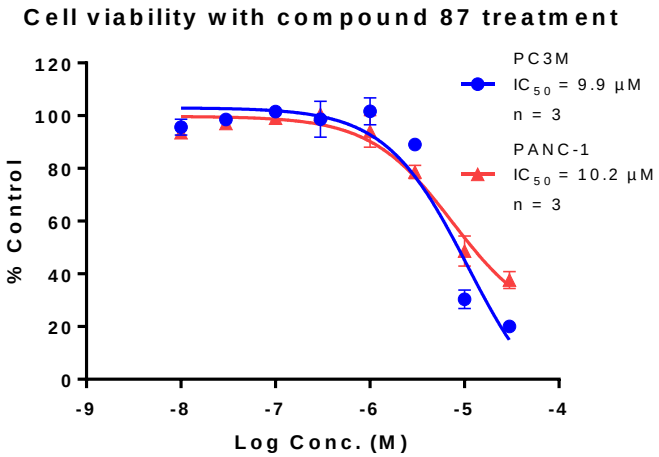

Figure 101. Cell viability after 48 hours as determined by alamarBlue®.

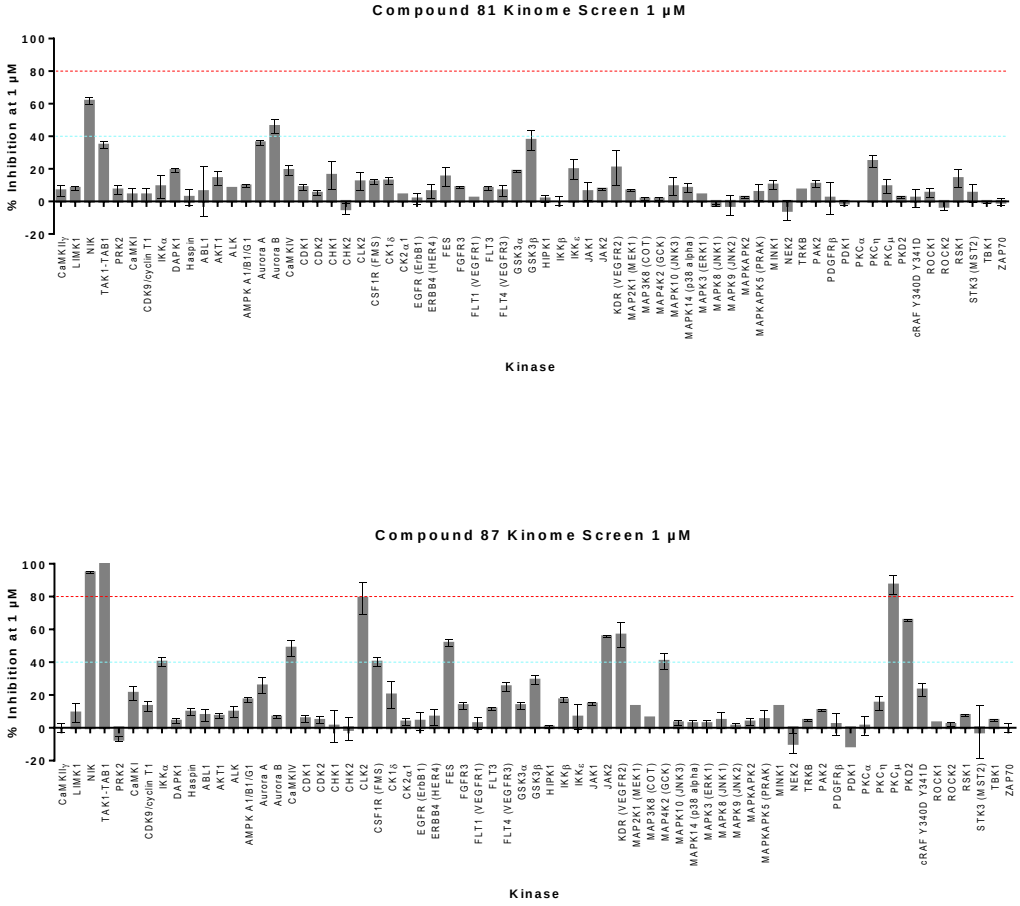

Figure 102. Results of kinome screen for compounds **81** and **87**.

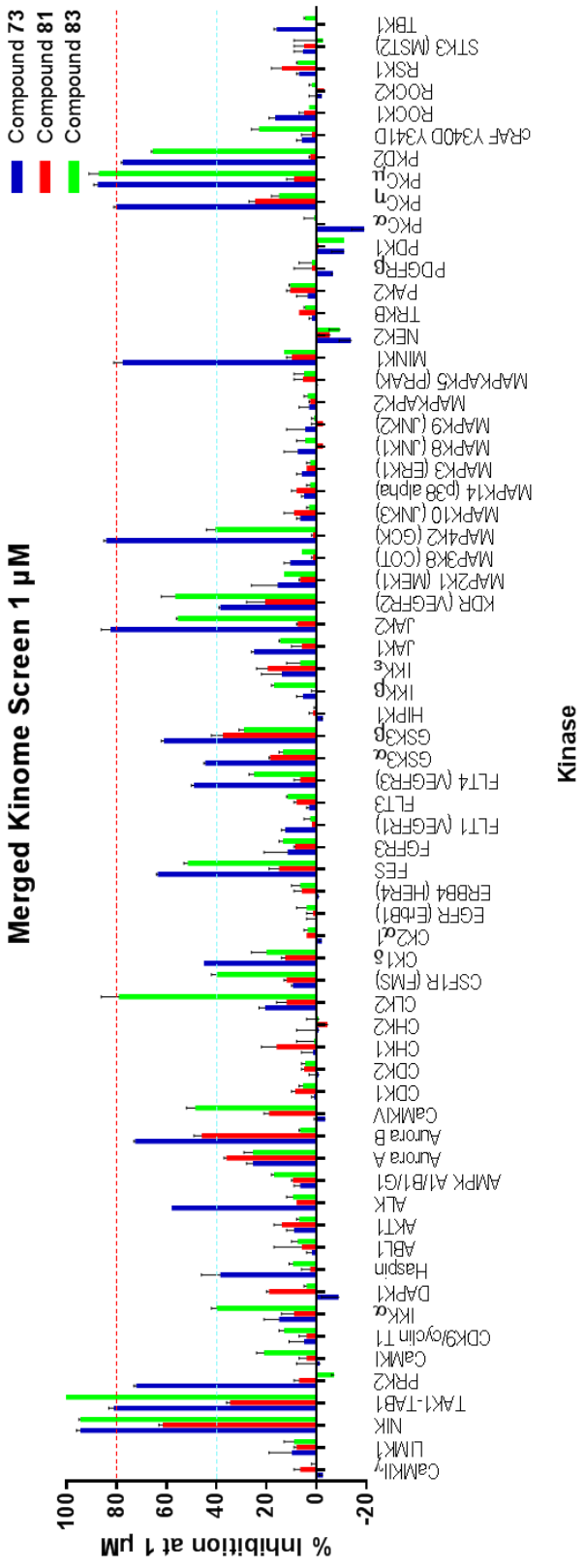

Figure 103. Comparison of kinome screen results for compounds **73**, **81** and **87**.

5. Concluding Remarks and Future Work

The work presented in this thesis has led to a range of interesting chemical tools for investigating the non-canonical NF-κB pathway and some compounds that have the potential to be useful in the treatment of cancers dependent on non-canonical NF-κB signalling. Compounds **9** and **15** represent very potent IKKα inhibitors whilst compounds **12** and **14** show by far the best IKKα selectivity of any published IKK inhibitor.[238]

Promising results have been shown too from both published and novel NIK inhibitors. Compound **73**, a known compound, has been shown to be potent against NIK in biochemical assessment but also shows nanomolar potency in a cellular setting against immortalised cancer cells. 48 hour treatment of pancreatic cancer cells also shows 50% reduction in viability at a sub-micromolar level along with favourable pharmacokinetic properties. Novel NIK inhibitors developed during this project have also shown promise, with compound **87** standing out: showing nanomolar potency in a cell-free assay.

Investigations into the 2-amidopyridine series as IKKα selective inhibitors have shown that the 3-aminoindazole head group is essential for binding and modifications at this position prove detrimental to potency. Amine linked example **34** suggests that the amide carbonyl is not essential for bonding. Further investigation into this series may prove valuable as **34** has a lower TPSA, possibly improving permeability, and more rotatable bonds, possibly improving solubility; though with the caveat that greater flexibility can sometimes lead to greater promiscuity.[239] If the planarity or flexibility of the linker was shown to be important, an alternative to the amide could be an alkene linker. This would also allow for a range of different substituents to be inserted into the linker.

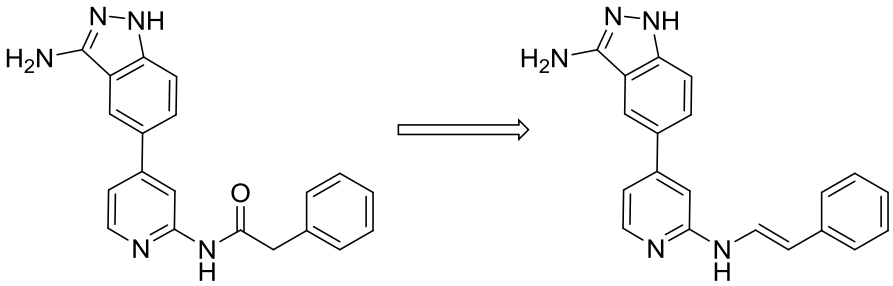

Figure 104. Possible amide isostere.

Given the potency of the compounds exemplified in the upper right quadrant of the Craig plot, further investigation into substituents with similar characteristics such as replacing the pyridyl with diazabenzenes or 5-membered heterocycles,[160] or replacing the trifluoromethyls with trifluromethylsulfonate, trifluoromethoxy or pentafluorosulfanyl groups may be beneficial.[240]

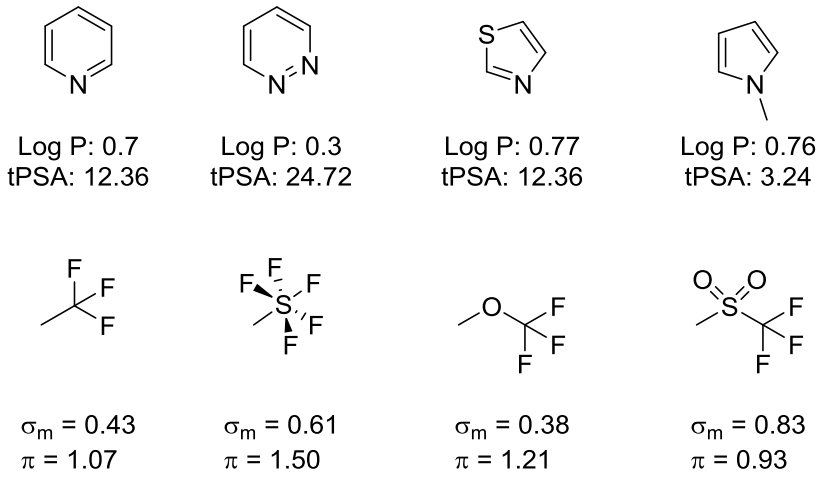

Figure 105. Selected properties of alternative groups.
LogP and TPSA calculated by ChemDraw. σ_m and π parameters from.[150,155]

Work on the NIK inhibitors has shown two main scaffolds that could be useful for generating potent compounds. The first is the published 2-aminopyrimidine scaffold as exemplified by compound **73**. Comparison of compounds **72** and **73** indicate that the positioning of nitrogens in the ring is exceptionally important, with a greater than 160-fold decrease in activity seen between the 6-amino and 2-aminopyrimidines. The angle provided by the 5,6-ring system for the alkyne substitution has been shown to be important. Use of an aniline linker, and thus a reduced angle between the hinge binding motif and the alkyne, leads to a reduction in potency of 1-2 orders of magnitude as demonstrated by compounds **65** and **73** when compared to **84** and **82**. This loss of potency may also be explained by the change from a tertiary to a secondary amine linker. One way to investigate this could be an additional methyl or cyclopropyl group to mimic the lost hydrophobicity and to retain the tertiary amine linker.

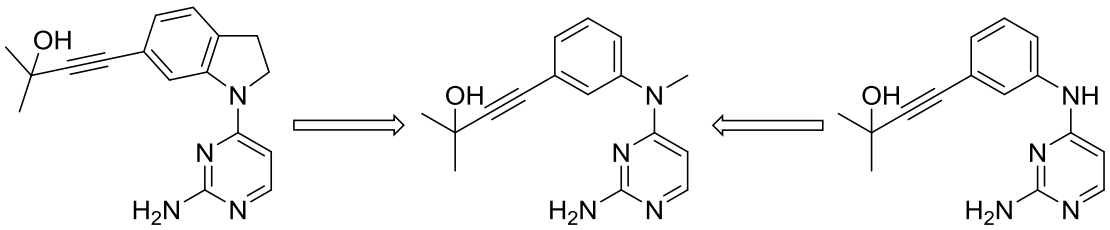

Figure 106. Possible tertiary amine linked analogue.

The alkyne substituents have also proved important. The potency of compounds **65** and **70** relative to **63** and **68** suggest the need for hydrophobicity. This may be due to specific hydrophobic interactions with the back pocket, an entropic effect of displacing water or a use in shielding part of the pocket from the polar alcohol. In any of these cases, a range of hydrophobic substituents of increasing size may prove beneficial.

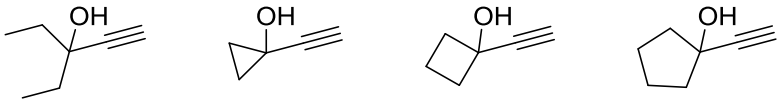

Figure 107. Alternative hydrophobic substituents for alkynyl alcohols.

The substitution pattern of the alkyne has been widely studied in the literature regarding effect on NIK inhibition[195,241] but this could still prove to be of value for use in conjunction with other scaffolds.

One alternative scaffold briefly investigated in this work which has been extensively used in kinase inhibiting compounds,[242,243] though with very different binding motifs, is that of the carbazole and its related analogues, as exemplified by compounds **79**-**81**. Carbazole **81** shows a biochemical potency of 350 nM against NIK, and this could prove to be a useful hit compound in a future NIK inhibitor project. Carbazoles have many isosteres which could retain the 5,6 ring system shown to be important for potency (**Figure 108**, blue), whilst providing a path to novel compounds.

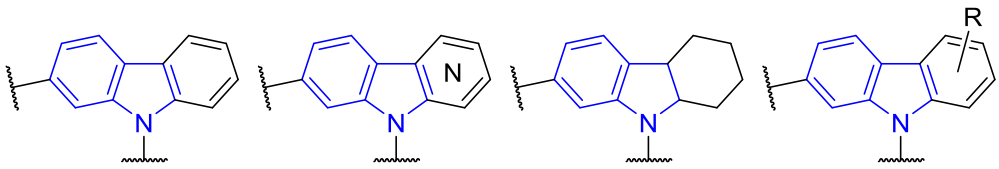

Figure 108. Carbazole analogues: carbolines; tetrahydrocarbazole; substituted carbazoles.

One of the most interesting observations has been the effect of the 2-amino and 5-carbonitrile moieties. As already discussed, individually, these substitutions do not have a significant impact on potency, but a combination of the 2-amino-5-carbonitrile with the *gem*-dimethylalkynyl alcohol in the 6-position of the indoline ring leads to a novel, potent, NIK inhibitor. These results certainly warrant further investigation, with nitrile isosteres possibly being of value.

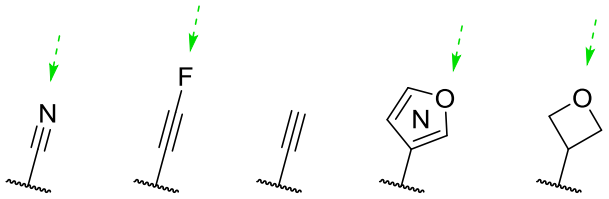

Figure 109. Possible nitrile isosteres.

Whilst the change in potency between compounds **56**-**58** suggests that increasing p-character orbitals at the 5-position decreases activity, the biggest change is from HBA groups to HBD groups, and thus it may be that, although some of the analogues shown in **Figure 109** are sp^2 or sp^3 hybridised, the fact that they are not HBD groups may prove to be more important than the hybridisation. The terminal alkyne may also indicate whether the effect of the nitrile is predominantly a steric one, as it has the same geometry and very similar Van der Waals radius. The 1-fluoroalkyne, accessible from the reaction of perhalostyrenes with organolithium reagents,[244] represents another isostere, mimicking the highly electron withdrawing nature of the nitrile whilst retaining the geometry.

6. Experimental Procedures

a. Reagents

b. Analysis

c. Synthesis and analytical data

d. Biochemical assays

e. Computational methods

a. Reagents

Reagent grade solvents were obtained from Fisher Scientific, anhydrous solvents from either Sigma-Aldrich or Acros and deuterated solvents from Sigma-Aldrich. Chemicals were purchased at >95% purity from Acros, Alfa Aesar, Apollo Scientific, Boron Molecular, Combi-Blocks, Fluorochem, Johnson-Matthey or Sigma-Aldrich and used without further purification.

Air- or moisture-sensitive reactions were carried out under an inert atmosphere of nitrogen or argon.

Microwave reactions were carried out using a Biotage Initiator^{+} system.

b. Analysis

TLC monitoring was performed on Merck-Millipore 60F254 TLC plates and spots visualised using UV light (254/280 nm) and, if necessary, stained with $KMnO_4$, ninhydrin, phosphomolybdic acid or iodine. Column chromatography was performed on a Biotage SP4 using silica stationary phase (60 Å, 35-70 micron, Fisher Scientific).

HPLC purification was completed using a Shimadzu Prominance HPLC. Separation was achieved with a Phenomenex Luna C18(2) 5 µm 21.2 x 50 mm column at 40 °C; flow rate: 6 mL/min; Detection: 254 nm; mobile phase: acetonitrile/0.1% TFA.

FTIR was completed using a Shimadzu IRAffinity-1. Samples were measured neat and vibrational frequency reported in cm^{-1}.

NMR data was collected at 298 K on either a Bruker Avance 3/DPX400 (400 MHz), Bruker AV400 (400 MHz), Bruker DRX500 (500 MHz) Bruker AV500HD (500 MHz) or Bruker AV600 (600 MHz) and analysed using Bruker Topspin or ACD Labs NMR Processor software. Chemical shifts (δ) are reported in parts per million (ppm) and coupling constants (*J*) in Hertz (Hz). All shifts are reported relative to tetramethylsilane (δ = 0 ppm). Abbreviations used to describe multiplicity are as follows: s = singlet, br. s = broad singlet, d = doublet, t = triplet, q = quadruplet, m = multiplet.

LC-MS purity was determined using an Agilent Technologies 1220 series LC system with Agilent 6100 series single quadrupole mass spectrometer in ESI/APCI mode. Separation was achieved with an Agilent Eclipse C18 4.6 x 50 mm column; flow rate: 1 mL/min; Detection: 254 nm; sample volume: 10 µL; mobile phase: acetonitrile/5mM ammonium acetate:water/5mM ammonium acetate; 5%, 1.48 mins; 5-100%, 8 mins; 100%, 13.5 mins; 100-5%, 16.5 mins; 5%, 18 mins. LRMS carried out using a ThermoQuest Finnigan LCQ Duo in ESI mode by direct injection. HRMS was conducted on either a Thermo Scientific Exactive or Thermo Scientific LTQ Orbitrap.

c. Synthesis and analytical data

6.1. *N*-(4-chloropyridin-2-yl)-2-phenylacetamide

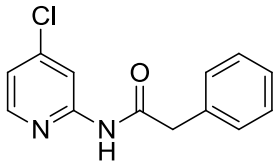

2-Amino-4-chloropyridine (500 mg, 3.9 mmol) and phenylacetyl chloride (773 mg, 660 µL, 5 mmol) were dissolved in DCM (25 mL, anhydrous) to which triethylamine (1.01 g, 1.45 mL, 10 mmol) was added. Reaction was stirred at reflux for 24 hours. Reaction was quenched with water (50 mL) and organics extracted into ethyl acetate (250 mL). These were dried over magnesium sulphate, filtered and adsorbed onto silica under reduced pressure. Chromatographic purification (Biotage SP4, 50 g cartridge, solvent system: hexane/ethyl acetate, 30% 3CV; 30-50% 3CV; 50% 3CV) yielded title product as a yellow oil (780 mg, 81%). (LC-MS purity = 89.8%); ^{1}H (DMSO-d_6, 400 MHz) δ 3.73 (s, 2H), 7.25 (dd, *J* = 5.7 & 1.8 Hz, 2H), 7.33 (m, 4H), 8.15 (d, *J* = 1.8 Hz, 1H), 8.32 (d, *J* = 5.3 Hz, 1H), 11.03 (s, 1H); ^{13}C (DMSO-d_6, 100 MHz) 43.35, 113.31, 119.91, 127.12, 128.80 (2C), 129.67 (2C), 135.94, 144.45, 149.92, 153.59, 171.02.

6.2. *N*-(4-chloropyridin-2-yl)-2-(2-fluorophenyl)acetamide

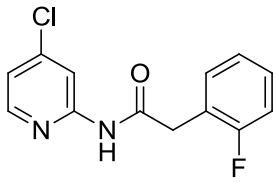

2-Amino-4-chloropyridine (500 mg, 3.9 mmol) was dissolved in dichloromethane (25 mL) to which triethylamine (1.45 mL, 10 mmol) was added at 0 °C with stirring. After 30 mins, 2-fluorophenylacetyl chloride (0.68 mL, 5 mmol) was added and the reaction mixture stirred at reflux for 24 hours. Reaction was quenched with water (40 mL) and organics resuspended in ethyl acetate (100 mL). Organics were washed with saturated $NaHCO_3$ (2 x 50 mL) and 1 M HCl (2 x 50 mL), dried over magnesium sulphate and filtered before concentrating under reduced pressure to yield title compound as a pale brown solid (845 mg, 82%). (LC-MS purity = 93.4%); ^{1}H (DMSO-d_6, 400 MHz) δ 3.85 (s, 2H), 7.18 (m, 2H), 7.25 (dd, *J* = 5.3 & 2 Hz, 1H), 7.33 (m, 1H), 7.39 (td, *J* = 7.7 & 1.5 Hz, 1H), 8.14 (d, *J* = 1.8 Hz, 1H), 8.33 (d, *J* = 5.3 Hz, 1H), 11.02 (s, 1H) ^{13}C (DMSO-d_6, 100 MHz) δ 36.63 (d, *J* = 2.2 Hz), 113.33, 115.49 (d, *J* = 21 Hz), 119.92, 122.92 (d, *J* = 16.1 Hz), 124.71 (d, *J* = 4 Hz), 129.39 (d, *J* = 9 Hz), 132.53 (d, *J* = 4 Hz), 144.47, 149.95, 153.52, 161.17 (d, *J* = 242 Hz), 169.98.

6.3. *N*-(4-bromopyridin-2-yl)-2-(2-chlorophenyl)acetamide

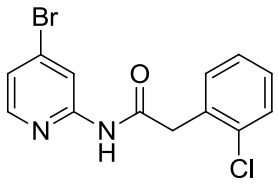

2-Amino-4-bromopyridine (600.4 mg, 3.5 mmol) and 2-chlorophenylacetic acid (511.8 mg, 3 mmol) were dissolved in THF (15 mL, anhydrous) to which triethylamine (1.62 mL, 12 mmol) was added. Stirring continued for 15 mins before addition of T3P (50% w/w in DMF, 3.48 mL, 6 mmol). Reaction mixture was stirred at room temperature for 24 hours. Reaction was quenched with water (100 mL) and the resulting solid was filtered to yield title compound as an off-white solid (948 mg, 97%). (LC-MS purity = 98.8%); ^{1}H (DMSO-d_6, 500 MHz) δ 3.95 (s, 2H), 7.31 (m, 2H), 7.37 (dd, *J* = 5.3 & 1.8 Hz, 1H), 7.43 (m, 2H), 8.25 (d, *J* = 5.3 Hz, 1H), 8.30 (d, *J* = 1.0 Hz, 1H), 11.01 (s, 1H); ^{13}C (DMSO-d_6, 125 MHz) δ 41.09, 116.34, 122.78, 127.55, 129.18, 129.47, 132.76, 133.58, 133.96, 134.20, 149.81, 153.37, 169.86.

6.4. *N*-(4-bromopyridin-2-yl)-2-(3-chlorophenyl)acetamide

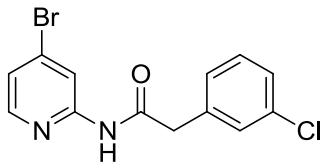

2-Amino-4-bromopyridine (600.4 mg, 3.5 mmol) and 3-chlorophenylacetic acid (511.8 mg, 3 mmol) were dissolved in THF (15 mL, anhydrous) to which triethylamine (1.62 mL, 12 mmol) was added. Stirring continued for 15 mins before addition of T3P (50% w/w in DMF, 3.48 mL, 6 mmol). Reaction mixture was stirred at room temperature for 24 hours. Reaction was quenched with water (100 mL), sonicated for 2 hours and the resulting solid was filtered to yield title compound as an off-white solid (900 mg, 92%). (LC-MS purity = 97.3%); ^{1}H (DMSO-d_6, 500 MHz) δ 3.77 (s, 2H), 7.34 (m, 4H), 7.42 (s, 1H), 8.23 (d, *J* = 5.3 Hz, 1H), 8.30 (d, *J* = 1.3 Hz, 1H), 10.98 (s, 1H); ^{13}C (DMSO-d_6, 125 MHz) δ 42.75, 116.39, 122.91, 127.15, 128.47, 129.62, 130.61, 133.31, 133.59, 138.27, 149.78, 153.27, 170.43.

6.5. *N*-(4-bromopyridin-2-yl)-2-(4-chlorophenyl)acetamide

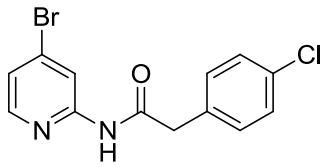

2-Amino-4-bromopyridine (600.4 mg, 3.5 mmol) and 4-chlorophenylacetic acid (511.8 mg, 3 mmol) were dissolved in THF (15 mL, anhydrous) to which triethylamine (1.62 mL, 12 mmol) was added. Stirring continued for 15 mins before addition of T3P (50% w/w in DMF, 3.48 mL, 6 mmol). Reaction mixture was stirred at room temperature for 24 hours. Reaction was quenched with water (100 mL), sonicated for 3 hours and the resulting solid was filtered to yield title compound as an off-white solid (866 mg, 88%). (LC-MS purity = 98.3%); ^{1}H (DMSO-d_6, 500 MHz) δ 3.75 (s, 2H), 7.37 (m, 5H), 8.23 (d, *J* = 5.3 Hz, 1H), 8.30 (d, *J* = 1.5 Hz, 1H), 10.98 (s, 1H); ^{13}C (DMSO-d_6, 125 MHz) δ 42.52, 116.36, 122.86, 128.72 (2C), 131.58 (2C), 131.91, 133.57, 134.91, 149.78, 153.33, 170.62.

6.6. *N*-(4-chloropyridin-2-yl)-2-(2-pyridyl)acetamide

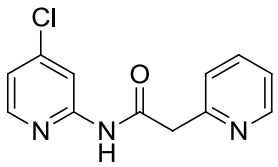

2-Amino-4-chloropyridine (310 mg, 2.4 mmol) and 2-pyridylacetic acid monohydrochloride (347 mg, 2 mmol) were dissolved in THF (5 mL, anhydrous) to which triethylamine (1 mL, 7.4 mmol) was added. Solution was stirred for 15 mins before addition of T3P (50% w/w in DMF, 2.32 mL, 4 mmol). Reaction mixture was stirred at room temperature for 42 hours. Sodium carbonate (1 M, 100 mL) was added and solution cooled to 4 °C before filtering to yield title compound as a pale yellow solid (665 mg, 65%). (LC-MS purity = 99.1%); ^{1}H (DMSO-d_6, 400 MHz) δ 3.96 (s, 2H), 7.27 (m, 2H), 7.39 (d, *J* = 7.9 Hz, 1H), 7.76 (td, *J* = 7.6 & 1.5 Hz, 1H), 8.16 (d, *J* = 1.3 Hz, 1H), 8.33 (d, *J* = 5.7 Hz, 1H), 8.50 (d, *J* = 4.4 Hz, 1H), 8.52 (s, 1H), 11.05 (s, 1H); ^{13}C (DMSO-d_6, 100 MHz) δ 45.80, 113.33, 119.93, 122.46, 124.59, 137.10, 144.45, 149.48, 149.96, 153.48 156.05, 170.04.

6.7. *N*-(4-chloropyridin-2-yl)-2-(3-pyridyl)acetamide

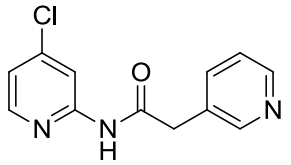

2-Amino-4-chloropyridine (310 mg, 2.4 mmol) and 3-pyridylacetic acid monohydrochloride (347 mg, 2 mmol) were dissolved in THF (5 mL, anhydrous) to which triethylamine (1 mL, 7.4 mmol) was added. Solution was stirred for 15 mins before addition of T3P (50% w/w in DMF, 2.32 mL, 4 mmol). Reaction mixture was stirred at room temperature for 42 hours. Sodium carbonate (1 M, 50 mL) was added and solution cooled to 4 °C before filtering to yield title compound as an off-white solid (832 mg, 82%). (LC-MS purity = 97.1%); ^{1}H (DMSO-d_6, 400 MHz) δ 3.80 (s, 2H), 7.25 (dd, *J* = 5.3 & 1.8 Hz, 1H), 7.36 (dd, *J* = 7.5 & 4.8 Hz, 1H), 7.74 (d, *J* = 7.9 Hz, 1H), 8.14 (d, *J* = 1.3 Hz, 1H), 8.33 (d, *J* = 5.3 Hz, 1H), 8.46 (dd, *J* = 4.8 & 1.3 Hz, 1H), 8.52 (s, 1H), 11.10 (s, 1H); ^{13}C (DMSO-d_6, 100 MHz) δ 40.31 (2C), 113.39, 120.00, 123.88, 131.58, 137.31, 144.48, 148.39, 149.95, 150.72 153.48, 170.47.

6.8. *N*-(4-chloropyridin-2-yl)-2-(2-(trifluoromethyl)phenyl)acetamide

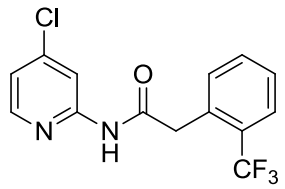

2-Amino-4-chloropyridine (310 mg, 2.4 mmol) and 2-(trifluoromethyl)phenylacetic acid (408 mg, 2 mmol) were dissolved in THF (5 mL, anhydrous) to which triethylamine (1 mL, 7.4 mmol) was added. Stirring continued for 15 mins before addition of T3P (50% w/w in DMF, 2.32 mL, 4 mmol). Reaction mixture was stirred at room temperature for 24 hours. Reaction was quenched with water (50 mL) and the resulting solid was filtered to yield title compound as a pale yellow solid (629 mg, >99%). (LC-MS purity = 98.7%); ^{1}H (DMSO-d_6, 400 MHz) δ 4.03 (s, 2H), 7.25 (dd, *J* = 5.5 & 1.5 Hz, 1H), 7.50 (m, 2H), 7.65 (t, *J* = 7.5 Hz, 1H), 7.71 (d, *J* = 7.9 Hz, 1H), 8.10, (s, 1H), 8.33 (d, *J* = 5.3 Hz, 1H), 11.07 (s, 1H); ^{13}C (DMSO-d_6, 100 MHz) δ **C**H$_2$ peak missing- possibly under DMSO 113.28, 119.88, 124.92 (d, *J* = 274.4 Hz), 126.10, 126.28, 127.92, 128.42 (*J* = 30.8 Hz), 132.73, 133.84, 134.03, 144.47, 149.97, 153.53, 170.04.

6.9. *N*-(4-chloropyridin-2-yl)-2-(3-(trifluoromethyl)phenyl)acetamide

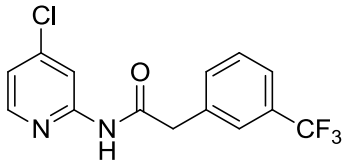

2-Amino-4-chloropyridine (310 mg, 2.4 mmol) and 3-(trifluoromethyl)phenylacetic acid (408 mg, 2 mmol) were dissolved in THF (5 mL, anhydrous) to which triethylamine (1 mL, 7.4 mmol) was added. Stirring continued for 15 mins before addition of T3P (50% w/w in DMF, 2.32 mL, 4 mmol). Reaction mixture was stirred at room temperature for 24 hours. Reaction was quenched with water (50 mL) and the resulting solid was filtered to yield title compound as a pale yellow solid (562 mg, 89%). (LC-MS purity = 94.9%); ^{1}H (DMSO-d_6, 400 MHz) δ 3.88 (s, 2H), 7.25 (dd, *J* = 5.3 & 1.8 Hz, 1H), 7.57 (m, 1H), 7.63 (m, 2H), 7.71 (s, 1H), 8.13, (s, 1H), 8.32 (d, *J* = 5.3 Hz, 1H), 11.08 (s, 1H); ^{13}C (DMSO-d_6, 100 MHz) δ 42.76, 113.39, 120.02, 123.92, 124.47 (d, *J* = 272.7 Hz) 126.42, 129.45 (d, *J* = 31.5 Hz) 129.81, 133.99, 137.24, 144.49, 149.95, 153.47, 170.43.

6.10. *N*-(4-chloropyridin-2-yl)-2-(4-(trifluoromethyl)phenyl)acetamide

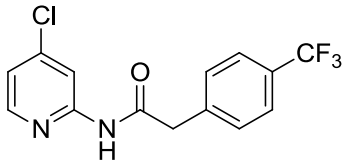

2-Amino-4-chloropyridine (310 mg, 2.4 mmol) and 4-(trifluoromethyl)phenylacetic acid (408 mg, 2 mmol) were dissolved in THF (5 mL, anhydrous) to which triethylamine (1 mL, 7.4 mmol) was added. Stirring continued for 15 mins before addition of T3P (50% w/w in DMF, 2.32 mL, 4 mmol). Reaction mixture was stirred at room temperature for 24 hours. Reaction was quenched with water (50 mL) and the resulting solid was filtered to yield title compound as a pale yellow solid (591 mg, 94%). (LC-MS purity = 97.4%); ^{1}H (DMSO-d_6, 400 MHz) δ 3.87 (s, 2H), 7.25 (dd, *J* = 5.5 & 2 Hz, 1H), 7.56 (d, *J* = 7.9 Hz, 2H), 7.70 (d, *J* = 7.9 Hz, 2H), 8.13, (s, 1H), 8.32 (d, *J* = 5.7 Hz, 1H), 11.10 (s, 1H); ^{13}C (DMSO-d_6, 100 MHz) δ 42.97, 113.38, 120.03, 124.83 (d, *J* = 272.2 Hz), 125.60 (q, *J* = 3.7 Hz, 2C), 127.91 (d, *J* = 31.2 Hz), 130.62 (2C), 140.72, 144.48, 149.95, 153.47, 170.30.

6.11. *N*-(4-chloropyridin-2-yl)-2-(3-Boc-aminophenyl)acetamide

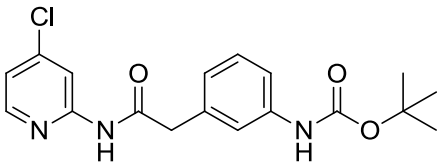

2-Amino-4-chloropyridine (384 mg, 3 mmol) and 3-Boc-aminophenylacetic acid (627 mg, 2.5 mmol) were dissolved in THF (5 mL, anhydrous) to which triethylamine (1.45 mL, 10 mmol) was added. Stirring continued for 15 mins before addition of T3P (50% w/w in DMF, 2.95 mL, 5 mmol). Reaction mixture was stirred at room temperature for 24 hours. Reaction was quenched with Na_2CO_3 (0.5 M, 50 mL), the resulting solid was filtered and washed with water to yield title compound as a pale brown solid (832 mg, 92%). (LC-MS purity = 93.3%); ^{1}H (DMSO-d_6, 400 MHz) δ 1.46 (s, 9H), 3.67 (s, 2H), 6.93 (d, *J* = 7.5 Hz, 1H), 7.18 (t, *J* = 7.9 Hz, 1H), 7.25 (m, 2H), 7.51 (s, 1H), 8.15 (d, *J* = 1.8 Hz, 1H), 8.31 (d, *J* = 5.7 Hz, 1H), 9.34 (s, 1H), 11.02 (s, 1H). ^{13}C (DMSO-d_6, 100 MHz) δ 28.60 (3C), 43.47, 113.31, 117.14, 119.35, 119.90, 123.48, 128.97, 136.37, 140.01, 144.44, 149.92, 153.23, 153.60, 170.96.

6.12. *N*-(4-chloropyridin-2-yl)-2-(4-Boc-aminophenyl)acetamide

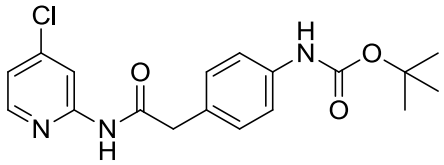

2-Amino-4-chloropyridine (167 mg, 1.3 mmol) and 4-Boc-aminophenylacetic acid (251 mg, 1 mmol) were dissolved in THF (5 mL, anhydrous) to which triethylamine (0.54 mL, 4 mmol) was added. Stirring continued for 15 mins before addition of T3P (50% w/w in DMF, 1.16 mL, 2 mmol). Reaction mixture was stirred at room temperature for 24 hours. Reaction was quenched with water (50 mL) and the resulting solid was filtered to yield title compound as a pale yellow solid (262 mg, 72%). (LC-MS purity = 98.0%); ^{1}H (DMSO-d_6, 400 MHz) δ 1.46 (s, 9H), 3.64 (s, 2H), 7.20 (d, *J* = 8.3 Hz, 2H), 7.24 (dd, *J* = 5.5 & 2 Hz, 1H), 7.38 (d, *J* = 8.3 Hz, 2H), 8.14 (d, *J* = 1.3 Hz, 1H), 8.31 (d, *J* = 5.3 Hz, 1H), 9.30 (s, 1H), 10.94 (s, 1H); ^{13}C (DMSO-d_6, 100 MHz) δ 28.60 (3C), 42.69, 113.25, 118.61, 119.87, 129.39, 129.85 (2C), 138.63, 144.42, 149.86, 149.93 (2C), 153.24, 153.62, 171.26.

6.13. *N*-(4-chloropyridin-2-yl)-2-(4-(methylthio)phenyl)acetamide

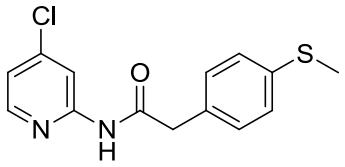

2-Amino-4-chloropyridine (310 mg, 2.4 mmol) and 4-(methylthio)phenylacetic acid (364 mg, 2 mmol) were dissolved in THF (5 mL, anhydrous) to which triethylamine (1 mL, 7.4 mmol) was added. Stirring continued for 15 mins before addition of T3P (50% w/w in DMF, 2.32 mL, 4 mmol). Reaction mixture was stirred at room temperature for 24 hours. Reaction was quenched with water (50 mL) and the resulting solid was filtered to yield title compound as a pale yellow solid (568 mg, 97%). (LC-MS purity = 97.9%); ^{1}H (DMSO-d_6, 400 MHz) δ 2.45 (s, 3H), 3.69 (s, 2H), 7.25 (m, 5H), 8.14 (d, *J* = 1.8 Hz, 1H), 8.31 (d, *J* = 5.7 Hz, 1H), 11.00 (s, 1H); ^{13}C (DMSO-d_6, 100 MHz) δ 15.38, 42.76, 113.29, 119.91, 126.63 (2C), 130.26 (2C), 132.60, 136.76, 144.45, 149.92, 153.58, 170.99.

6.14. *N*-(4-chloropyridin-2-yl)-2-(2-methoxyphenyl)acetamide

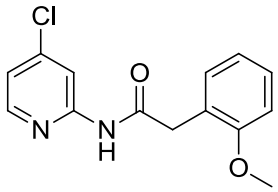

2-Amino-4-chloropyridine (500 mg, 3.9 mmol) and 2-methoxyphenylacetic acid (540 mg, 3.25 mmol) were dissolved in THF (5 mL, anhydrous) to which triethylamine (1.7 mL, 12 mmol) was added at 0 °C. Stirring continued for 15 mins before addition of T3P (50% w/w in DMF, 3.8 mL, 6.5 mmol). Reaction mixture was stirred at room temperature for 24 hours. Resultant solution was diluted with ethyl acetate (100 mL) and washed with 1 M Na_2CO_3 (2 x 50 mL), 1 M HCl (2 x 50 mL) and brine (50 mL) before drying over magnesium sulphate and filtering. Product was concentrated under reduced pressure and recrystallized from THF to yield title compound as a pale brown solid (786 mg, 87%). (LC-MS purity = 99.4%); ^{1}H (DMSO-d_6, 400 MHz) δ 3.72 (s, 2H), 3.74 (s, 3H), 6.90 (t, *J* = 7.5 Hz, 1H), 6.98 (d, *J* = 8.3 Hz, 1H), 7.23 (m, 3H), 8.14 (s, 1H), 8.31 (d, *J* = 5.3 Hz, 1H, 10.83 (s, 1H); ^{13}C (DMSO-d_6, 100 MHz) δ 38.09, 55.88, 111.15, 113.18, 119.71, 120.63, 124.15, 128.68, 131.49, 144.40, 149.94, 153.68, 157.73, 171.06.

6.15. *N*-(4-chloropyridin-2-yl)-2-(3-methoxyphenyl)acetamide

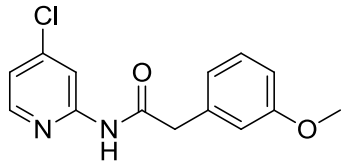

2-Amino-4-chloropyridine (500 mg, 3.9 mmol) was dissolved in anhydrous dichloromethane (25 mL) to which triethylamine (1.01 g, 1.45 mL, 10 mmol) was added at 0 °C and stirred for 30 minutes. 3-methoxyphenylacetyl chloride (0.92 g, 0.78 mL, 5 mmol) was added and the solution stirred at reflux for 24 hours. Resultant solution was washed with saturated $NaHCO_3$ (40 mL), 1 M HCl (2 x 20 mL) and brine (40 mL). Organic layer was washed with further saturated sodium hydrogen carbonate (150 mL) and 1 M HCl (150 mL), dried over magnesium sulphate, filtered and isolated *in vacuo* to yield title product as a pale brown solid (726 mg, 81%). (LC-MS purity = 94.4%); ^{1}H (DMSO-d_6, 400 MHz) δ 3.70 (s, 2H), 3.74 (s, 3H), 6.82 (dd, *J* = 8.3, 1.8 Hz, 1H), 6.90 (m, 2H), 7.24 (m, 2H), 8.15 (s, 1H), 8.31 (d, *J* = 5.7 Hz, 1H), 11.00 (s, 1H); ^{13}C (DMSO-d_6, 100 MHz) δ 42.29, 54.93, 112.03, 112.80, 114.97, 119.40, 121.36, 129.29, 136.81, 143.94, 149.39, 153.06, 159.17, 170.36.

6.16. *N*-(4-chloropyridin-2-yl)-2-(4-methoxyphenyl)acetamide

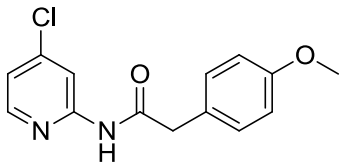

2-Amino-4-chloropyridine (384 mg, 3 mmol) was dissolved in dichloromethane (15 mL) and THF (5 mL) to which pyridine (0.36 mL, 4.5 mmol) was added with stirring. After 15 mins, 4-methoxyphenylacetyl chloride (0.61 mL, 4 mmol) was added and the reaction mixture stirred at room temperature for 24 hours, then at reflux for 6 hours. Solution was diluted in ethyl acetate (100 mL), washed with water (50 mL) and brine (50 mL), organics dried over magnesium sulphate and filtered before adsorbing onto silica under reduced pressure. Chromatographic purification (Biotage SP4, 50 g cartridge, solvent system: hexane/ethyl acetate, gradient: 0-50% 3CV; 50% 3CV; 50-100% 3CV) yielded title product as an off-white solid (432 mg, 52%). (LC-MS purity = 81.9%); ^{1}H (DMSO-d_6, 400 MHz) δ 3.65 (s, 2H), 3.72 (s, 3H), 6.88 (d, *J* = 8.3 Hz, 2H), 7.25 (m, 3H), 8.14 (d, *J* = 1.8 Hz, 1H), 8.31 (d, *J* = 5.3 Hz, 1H), 10.94 (s, 1H); ^{13}C (DMSO-d_6, 100 MHz) δ 42.49, 55.49, 113.27, 114.24 (2C), 119.84, 127.83, 130.68 (2C), 114.43, 149.89, 153.65, 158.59, 171.39.

6.17. *N*-(4-chloropyridin-2-yl)-2-(3-(methylsulfonyl)phenyl)acetamide

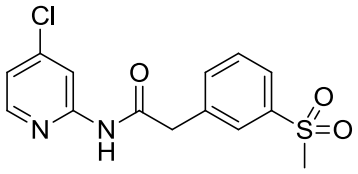

2-Amino-4-chloropyridine (167 mg, 1.3 mmol) and 3-(methylsulfonyl)phenylacetic acid (214 mg, 1 mmol) were dissolved in THF (5 mL, anhydrous) to which triethylamine (0.54 mL, 4 mmol) was added. Stirring continued for 15 mins before addition of T3P (50% w/w in DMF, 1.16 mL, 2 mmol). Reaction mixture was stirred at room temperature for 24 hours. Reaction was quenched with water (50 mL) and the resulting solid was filtered to yield title compound as a pale yellow solid (270 mg, 83%). (LC-MS purity = 98.8%); ^{1}H (DMSO-d_6, 400 MHz) δ 3.22 (s, 3H), 3.90 (s, 2H), 7.26 (dd, *J* = 5.5 & 2 Hz, 1H), 7.62 (t, *J* = 7.9 Hz, 1H), 7.69 (d, *J* = 7.9 Hz, 1H), 7.84 (d, *J* = 7.9 Hz, 1H), 7.92 (s, 1H), 8.15 (d, *J* = 1.3 Hz, 1H), 8.33 (d, *J* = 5.7 Hz, 1H), 11.12 (s, 1H); ^{13}C (DMSO-d_6, 100 MHz) δ 42.77, 43.99, 113.37, 120.05, 125.86, 128.01, 129.92, 135.04, 137.37, 141.32, 144.50, 149.99, 153.47, 170.34.

6.18. *N*-(4-chloropyridin-2-yl)-2-(4-(methylsulfonyl)phenyl)acetamide

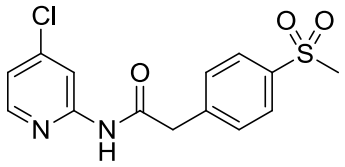

2-Amino-4-chloropyridine (167 mg, 1.3 mmol) and 4-(methylsulfonyl)phenylacetic acid (214 mg, 1 mmol) were dissolved in THF (5 mL, anhydrous) to which triethylamine (0.54 mL, 4 mmol) was added. Stirring continued for 15 mins before addition of T3P (50% w/w in DMF, 1.16 mL, 2 mmol). Reaction mixture was stirred at room temperature for 24 hours. Reaction was quenched with water (50 mL) and the resulting solid was filtered to yield title compound as a pale yellow solid (285 mg, 88%). (LC-MS purity = >99.9%); ^{1}H (DMSO-d_6, 400 MHz) δ 3.20 (s, 3H), 3.89 (s, 2H), 7.26 (dd, *J* = 5.5 & 2 Hz, 1H), 7.60 (d, *J* = 8.3 Hz, 2H), 7.89 (d, *J* = 8.3 Hz, 2H), 8.13 (d, *J* = 1.8 Hz, 1H), 8.33 (d, *J* = 5.3 Hz, 1H), 11.12 (s, 1H); ^{13}C (DMSO-d_6, 100 MHz) δ 43.02, 44.03, 113.36, 120.06, 127.49 (2C), 130.73 (2C), 139.74, 141.89, 144.50, 149.99, 153.44, 170.17.

6.19. *N*-(4-chloropyridin-2-yl)-2-(2-tolyl)acetamide

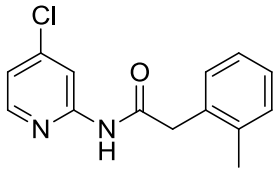

2-Amino-4-chloropyridine (500 mg, 3.9 mmol) and 2-tolylacetic acid (488 mg, 3.25 mmol) were dissolved in THF (5 mL, anhydrous) to which triethylamine (1.7 mL, 12 mmol) was added at 0 °C. Stirring continued for 15 mins before addition of T3P (50% w/w in DMF, 3.8 mL, 6.5 mmol). Reaction mixture was stirred at room temperature for 24 hours. Resultant solution was diluted with ethyl acetate (100 mL) and washed with 1 M Na_2CO_3 (2 x 50 mL), 1 M HCl (2 x 50 mL) and brine (50 mL) before drying over magnesium sulphate and filtering. Product was concentrated under reduced pressure and recrystallized from THF to yield title compound as a pale brown solid (741 mg, 88%). (LC-MS purity = 99.1%); ^{1}H (DMSO-d_6, 400 MHz) δ 2.28 (s, 3H), 3.79 (s, 2H), 7.15 (m, 3H), 7.24, (m, 2H), 8.16 (d, *J* = 1.5 Hz, 1H), 8.32 (d, *J* = 5.3 Hz, 1H), 10.95 (br s, 1H); ^{13}C (DMSO-d_6, 100 MHz) δ 19.28, 40.57, 112.80, 119.34, 125.72, 126.76, 129.85, 130.03, 134.09, 136.67, 143.93, 149.40, 153.08, 170.43.

6.20. *N*-(4-chloropyridin-2-yl)-2-(3-tolyl)acetamide

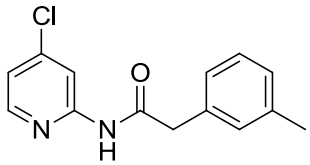

2-Amino-4-chloropyridine (500 mg, 3.9 mmol) and 3-tolylacetic acid (488 mg, 3.25 mmol) were dissolved in THF (5 mL, anhydrous) to which triethylamine (1.7 mL, 12 mmol) was added at 0 °C. Stirring continued for 15 mins before addition of T3P (50% w/w in DMF, 3.8 mL, 6.5 mmol). Reaction mixture was stirred at room temperature for 24 hours. Resultant solution was diluted with ethyl acetate (100 mL) and washed with 1 M Na_2CO_3 (2 x 50 mL), 1 M HCl (2 x 50 mL) and brine (50 mL) before drying over magnesium sulphate and filtering. Product was concentrated under reduced pressure and recrystallized from THF to yield title compound as a pale brown solid (632 mg, 75%). (LC-MS purity = 99.4%); ^{1}H (DMSO-d_6, 400 MHz) δ 2.29 (s, 3H), 3.70 (s, 2H), 7.06 (d, *J* = 7.5 Hz, 1H), 7.14 (m, 2H), 7.21 (t, *J* = 7.3 Hz, 1H), 7.24 (dd, *J* = 5.3 & 3.5 Hz, 1H), 8.16 (d, *J* = 1.8 Hz, 1H), 8.32 (d, *J* = 5.5 Hz, 1H), 10.95 (s, 1H); ^{13}C (DMSO-d_6, 100 MHz) δ 20.92, 42.79, 112.79, 119.38, 126.21, 127.24, 128.18, 129.75, 135.29, 137.32, 142.82, 143.92, 149.39, 153.08, 170.54.

6.21. *N*-(4-chloropyridin-2-yl)-2-(4-tolyl)acetamide

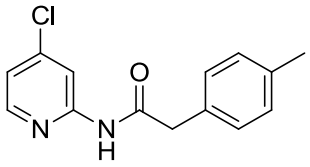

2-Amino-4-chloropyridine (500 mg, 3.9 mmol) and 4-tolylacetic acid (488 mg, 3.25 mmol) were dissolved in THF (5 mL, anhydrous) to which triethylamine (1.7 mL, 12 mmol) was added at 0 °C. Stirring continued for 15 mins before addition of T3P (50% w/w in DMF, 3.8 mL, 6.5 mmol). Reaction mixture was stirred at room temperature for 24 hours. Resultant solution was diluted with ethyl acetate (100 mL) and washed with 1 M Na_2CO_3 (2 x 50 mL), 1 M HCl (2 x 50 mL) and brine (50 mL) before drying over magnesium sulphate and filtering. Product was concentrated under reduced pressure and recrystallized from THF to yield title compound as a pale brown solid (689 mg, 81%). (LC-MS purity = 99.4%); ^{1}H (DMSO-d_6, 400 MHz) δ 2.28 (s, 3H), 3.68 (s, 2H), 7.13 (d, *J* = 7.8 Hz, 2H), 7.23 (m, 3H), 8.15 (d, *J* = 1.8 Hz, 1H), 8.31 (d, *J* = 5 Hz, 1H), 10.93 (s, 1H); ^{13}C (DMSO-d_6, 100 MHz) δ 20.58, 42.44, 112.74, 119.34, 124.26, 128.83 (2C), 128.98 (2C), 132.32, 135.63, 143.90, 149.38, 153.09, 170.66.

6.22. 5-(4,4,5,5-tetramethyl-1,3,2-dioxaborolan-2-yl)-1H-indazol-3-amine

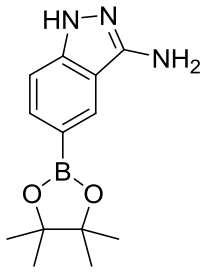

To a solution of 2-fluoro-5-(4,4,5,5-tetramethyl-1,3,2-dioxaborolan-2-yl)benzonitrile (1.98 g, 8 mmol) in ethanol (100 mL) was added hydrazine hydrate (50-60% solution in water, 2.4 mL, 2.47 g, 39 mmol) and the solution refluxed for 30 h. Solvent was removed *in vacuo* and resultant solid suspended in water (100 mL) before filtering to yield title compound as an off-white solid (1.217 g, 59%). ^{1}H (DMSO-d_6, 400 MHz) δ 1.30 (s, 12H), 5.49 (s, 2H), 7.18 (d, *J* = 7.9 Hz, 1H), 7.48 (dd, *J* = 8.3 & 0.9 Hz, 1H), 8.17 (s, 1H), 11.49 (s, 1H); ^{13}C (DMSO-d_6, 100 MHz) δ 25.23 (4C), 83.65 (2C), 109.11, 114.57, 129.29, 131.92, 143.26, 150.27.

6.23. *N*-(4-(3-amino-1H-indazol-5-yl)pyridin-2-yl)-2-phenylacetamide 1

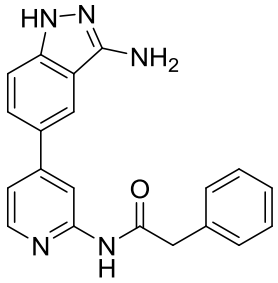

5-(4,4,5,5-Tetramethyl-1,3,2-dioxaborolan-2-yl)-1*H*-indazol-3-amine (100 mg, 0.38 mmol), *N*-(4-chloropyridin-2-yl)-2-phenylacetamide (78 mg, 0.32 mmol) in ethanol (O_2-free, 0.8 mL) and Pd(dtbpf)Cl_2 (21 mg, 0.032 mmol) were placed in a 2-5 mL microwave vial which was sealed and purged with nitrogen for 5 mins. The suspension stirred at 50 °C under nitrogen for a further 10 mins. K_3PO_4 (1 M, 0.4 mL) was added and the solution stirred at 70 °C for 24 hours. Reaction was quenched with water (5 mL) to yield a brown solid which was extracted into ethyl acetate and adsorbed onto silica under reduced pressure. Chromatographic purification (Biotage SP4, 50 g cartridge, solvent system: ethyl acetate/methanol, 0% 2CV; 0-5% 3CV; 5% 4CV) yielded title product as a grey/brown solid (65 mg, 57%). (LC-MS purity = 99.7%); ^{1}H (DMSO-d_6, 400 MHz) δ 3.77 (s, 2H), 5.53 (s, 2H), 7.26 (m, 1H), 7.34 (m, 3H), 7.39 (m, 3H), 7.59 (dd, *J* = 8.8 & 1.8 Hz, 1H), 8.15 (d, *J* = 1 Hz, 1H), 8.35 (d, *J* = 5.3 Hz, 1H), 8.44 (s, 1H), 10.74 (s, 1H), 11.58 (br s, 1H); ^{13}C (DMSO-d_6, 100 MHz) δ 43.51, 110.58, 115.14, 117.34, 119.66, 125.50, 127.05, 127.38, 128.76 (2C), 129.74 (2C), 136.29, 142.00, 148.81, 150.45, 150.59, 153.27, 170.61; HRMS (ESI +ve): For $C_{20}H_{17}N_5O$ requires 344.1506 found 344.1503.

6.24. *N*-(4-(3-amino-1*H*-indazol-5-yl)pyridin-2-yl)-2-(2-fluorophenyl)acetamide 3

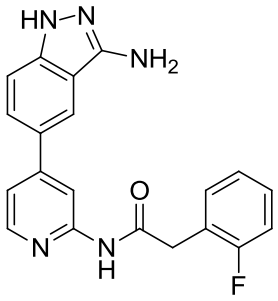

5-(4,4,5,5-Tetramethyl-1,3,2-dioxaborolan-2-yl)-1*H*-indazol-3-amine (85 mg, 0.325 mmol), *N*-(4-chloropyridin-2-yl)-2-(2-tolyl)acetamide (66 mg, 0.25 mmol) and Pd(dtbpf)Cl_2 (9 mg, 0.0125 mmol) were placed in a 2-5 mL microwave vial which was sealed and purged with nitrogen for 5 mins. Ethanol (O_2-free, 1 mL) was added and the suspension stirred at 50 °C under nitrogen for a further 5 mins. K_3PO_4 (1 M, 0.5 mL) was added and the solution stirred at 100 °C for 24 hours. Reaction was quenched with water (8 mL) to yield a brown solid which was filtered and further washed with water (15 x 10 mL) and hexane (8 x 10 mL). Solid was resuspended in 50% ethyl acetate/ methanol (20 mL), filtered and adsorbed onto silica. Chromatographic purification (Biotage SP4, 50 g cartridge, solvent system: 1% NEt_3 in ethyl acetate/methanol, gradient: 0% 3CV; 0-5% 2CV; 5% 4CV) yielded title product as a pale brown solid (7 mg, 8%). (LC-MS purity = 97.5%); ^{1}H (DMSO-d_6, 400 MHz) δ 3.86 (s, 2H), 5.55 (br s, 2H), 7.18 (m, 2H), 7.32 (d, *J* = 8.8 Hz, 2H), 7.40 (m, 2H), 7.59 (d, *J* = 8.3 Hz, 1H), 8.15 (s, 1H), 8.35 (m, 1H), 8.43 (s, 1H), 10.81 (s, 1H), 11.57 (s, 1H); ^{13}C (DMSO-d_6, 150 MHz) δ 36.71, 110.56, 110.59, 115.14, 115.48 (d, *J* = 21 Hz), 117.32, 119.63, 123.26 (d, *J* = 16.1 Hz), 124.68 (d, *J* = 3.4 Hz), 125.50, 127.35, 129.31 (d, *J* = 8 Hz), 132.61 (d, *J* = 4.6 Hz), 142.01, 148.84, 150.47, 150.58, 153.22, 161.23 (d, *J* = 244.5 Hz), 169.58; HRMS: For $C_{20}H_{17}FN_5O$ requires 362.1412 found 362.14.

6.25. *N*-(4-(3-amino-1*H*-indazol-5-yl)pyridin-2-yl)-2-(2-chlorophenyl)acetamide 6

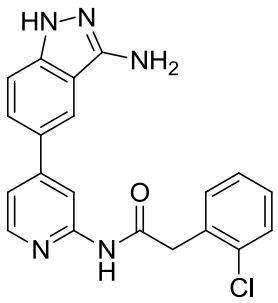

5-(4,4,5,5-Tetramethyl-1,3,2-dioxaborolan-2-yl)-1*H*-indazol-3-amine (165 mg, 0.6 mmol), *N*-(4-bromopyridin-2-yl)-2-(2-chlorophenyl)acetamide (162.4 mg, 0.5 mmol) and $Pd(dtbpf)Cl_2$ (16.2 mg, 0.025 mmol) were placed in a 2-5 mL microwave vial which was sealed and purged with nitrogen for 5 mins. Ethanol (O_2-free, 1.3 mL) was added and the suspension stirred at 40 °C under nitrogen for a further 10 mins. K_3PO_4 (1 M, 0.65 mL) was added and the solution stirred at 70 °C for 24 hours. Reaction was quenched with water (5 mL) to yield a yellowish solid. Organics were extracted into ethyl acetate (50 mL) and adsorbed onto silica under reduced pressure. . Chromatographic purification (Biotage SP4, 50 g cartridge, solvent system: ethyl acetate/methanol, gradient: 0% 2CV; 0-2% 2CV; 2% 4CV) yielded title product as a greenish solid (98 mg, 52%) (LC-MS purity = 99.5%); ^{1}H (DMSO-d_6, 500 MHz) δ 3.97 (s, 2H), 5.52 (s, 2H), 7.31, (m, 3H), 7.39 (dd, *J* = 5.3 & 1.6 Hz, 1H), 7.44 (m, 2H), 7.58 (dd, *J* = 8.6 & 1.7 Hz, 1H), 8.14 (d, *J* = 1.3 Hz, 1H), 8.34 (d, *J* = 5.3 Hz, 1H), 8.43 (s, 1H), 10.78 (s, 1H), 11.55 (br s, 1H); ^{13}C (DMSO-d_6, 125 MHz) δ 41.15, 110.52, 110.56, 115.14, 117.25, 119.60, 124.48, 127.33, 127.51, 129.10, 129.46, 132.83, 134.25, 134.30, 142.01, 148.84, 150.46, 150.55, 153.26, 169.46. HRMS: $C_{20}H_{17}ClN_5O$ requires 378.1116 found 378.1114 (100%) and 380.1086 (31%).

6.26. *N*-(4-(3-amino-1*H*-indazol-5-yl)pyridin-2-yl)-2-(3-chlorophenyl)acetamide 7

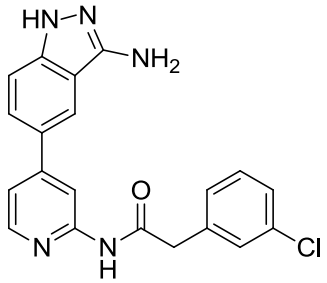

5-(4,4,5,5-Tetramethyl-1,3,2-dioxaborolan-2-yl)-1*H*-indazol-3-amine (165 mg, 0.6 mmol), *N*-(4-bromopyridin-2-yl)-2-(3-chlorophenyl)acetamide (162.4 mg, 0.5 mmol) and Pd(dtbpf)Cl_2 (16.2 mg, 0.025 mmol) were placed in a 2-5 mL microwave vial which was sealed and purged with nitrogen for 5 mins. Ethanol (O_2-free, 1.3 mL) was added and the suspension stirred at 40 °C under nitrogen for a further 10 mins. K_3PO_4 (1 M, 0.65 mL) was added and the solution stirred at 70 °C for 24 hours. Reaction was quenched with water (5 mL) to yield a yellowish solid. Organics were extracted into ethyl acetate (50 mL) and adsorbed onto silica under reduced pressure. . Chromatographic purification (Biotage SP4, 50 g cartridge, solvent system: ethyl acetate/methanol, gradient: 0% 2CV; 0-2% 2CV; 2% 4CV) yielded title product as a brown/green powder (95 mg, 50%) (LC-MS purity = 97.2%); ^{1}H (DMSO-d_6, 500 MHz) δ 3.79 (s, 2H), 5.52 (s, 2H), 7.32, (m, 3H), 7.36 (m, 1H) 7.39 (dd, *J* = 5.3 & 1.9 Hz, 1H), 7.45 (t, *J* = 1.7 Hz, 1H), 7.58 (dd, *J* = 8.8 & 1.6 Hz, 1H), 8.14 (d, *J* = 0.9 Hz, 1H), 8.34 (d, *J* = 5.3 Hz, 1H), 8.41 (s, 1H), 10.77 (s, 1H), 11.56 (s, 1H); ^{13}C (DMSO-d_6, 125 MHz) δ 42.90, 110.58 (2C), 115.14, 117.41, 119.66, 125.49, 127.07, 127.33, 128.54, 129.69, 130.60, 133.29, 138.67, 142.00, 148.84, 150.46, 150.62, 153.18, 170.04. HRMS: $C_{20}H_{17}ClN_5O$ requires 378.1116 found 378.1114 (100%) and 380.1086 (32%).

6.27. *N*-(4-(3-amino-1*H*-indazol-5-yl)pyridin-2-yl)-2-(3-chlorophenyl)acetamide 7

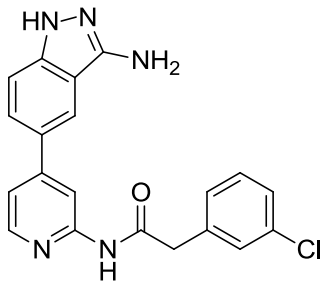

5-(4,4,5,5-Tetramethyl-1,3,2-dioxaborolan-2-yl)-1*H*-indazol-3-amine (165 mg, 0.6 mmol), *N*-(4-bromopyridin-2-yl)-2-(3-chlorophenyl)acetamide (162.4 mg, 0.5 mmol) and Pd(dtbpf)Cl_2 (16.2 mg, 0.025 mmol) were placed in a 2-5 mL microwave vial which was sealed and purged with nitrogen for 5 mins. Ethanol (O_2-free, 1.3 mL) was added and the suspension stirred at 40 °C under nitrogen for a further 10 mins. K_3PO_4 (1 M, 0.65 mL) was added and the solution stirred at 70 °C for 24 hours. Reaction was quenched with water (5 mL) to yield a yellowish solid. Organics were extracted into ethyl acetate (50 mL) and adsorbed onto silica under reduced pressure. . Chromatographic purification (Biotage SP4, 50 g cartridge, solvent system: ethyl acetate/methanol, gradient: 0% 2CV; 0-2% 2CV; 2% 4CV) yielded title product as a brown/green powder (95 mg, 50%) (LC-MS purity = 97.2%); ^{1}H (DMSO-d_6, 500 MHz) δ 3.79 (s, 2H), 5.52 (s, 2H), 7.32, (m, 3H), 7.36 (m, 1H) 7.39 (dd, *J* = 5.3 & 1.9 Hz, 1H), 7.45 (t, *J* = 1.7 Hz, 1H), 7.58 (dd, *J* = 8.8 & 1.6 Hz, 1H), 8.14 (d, *J* = 0.9 Hz, 1H), 8.34 (d, *J* = 5.3 Hz, 1H), 8.41 (s, 1H), 10.77 (s, 1H), 11.56 (s, 1H); ^{13}C (DMSO-d_6, 125 MHz) δ 42.90, 110.58 (2C), 115.14, 117.41, 119.66, 125.49, 127.07, 127.33, 128.54, 129.69, 130.60, 133.29, 138.67, 142.00, 148.84, 150.46, 150.62, 153.18, 170.04. HRMS: $C_{20}H_{17}ClN_5O$ requires 378.1116 found 378.1114 (100%) and 380.1086 (32%).

6.28. *N*-(4-(3-amino-1*H*-indazol-5-yl)pyridin-2-yl)-2-(4-chlorophenyl)acetamide 8

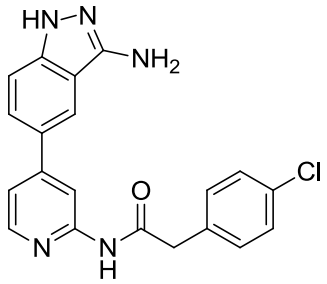

5-(4,4,5,5-Tetramethyl-1,3,2-dioxaborolan-2-yl)-1*H*-indazol-3-amine (165 mg, 0.6 mmol), *N*-(4-bromopyridin-2-yl)-2-(4-chlorophenyl)acetamide (162.4 mg, 0.5 mmol) and $Pd(dtbpf)Cl_2$ (16.2 mg, 0.025 mmol) were placed in a 2-5 mL microwave vial which was sealed and purged with nitrogen for 5 mins. Ethanol (O_2-free, 1.3 mL) was added and the suspension stirred at 40 °C under nitrogen for a further 10 mins. K_3PO_4 (1 M, 0.65 mL) was added and the solution stirred at 70 °C for 24 hours. Reaction was quenched with water (5 mL) to yield a yellowish solid. Organics were extracted into ethyl acetate (50 mL) and adsorbed onto silica under reduced pressure. . Chromatographic purification (Biotage SP4, 50 g cartridge, solvent system: ethyl acetate/methanol, gradient: 0% 2CV; 0-2% 2CV; 2% 4CV) yielded title product as a pale green powder (93 mg, 49%) (LC-MS purity = 100.0%); ^{1}H (DMSO-d_6, 500 MHz) δ 3.76 (s, 2H), 5.51 (s, 2H), 7.32 (d, *J* = 8.5 Hz, 1H), 7.38 (m, 5H), 7.58 (dd, *J* = 8.6 & 1.6 Hz, 1H), 8.13 (d, *J* = 0.9 Hz, 1H), 8.34 (d, *J* = 5.3 Hz, 1H), 8.40 (s, 1H), 10.75 (s, 1H), 11.55 (br s, 1H); ^{13}C (DMSO-d_6, 125 MHz) δ 42.66, 110.58 (2C), 115.15, 117.38, 119.65, 125.48, 127.34, 128.70 (2C), 131.64 (2C), 131.82, 135.27, 141.98, 148.83, 150.46, 150.61, 153.20, 170.24. HRMS: $C_{20}H_{17}ClN_5O$ requires 378.1116 found 378.1114 (100%) and 380.1086 (32%).

6.29. *N*-(4-(3-amino-1*H*-indazol-5-yl)pyridin-2-yl)-2-(2-pyridyl)acetamide 9

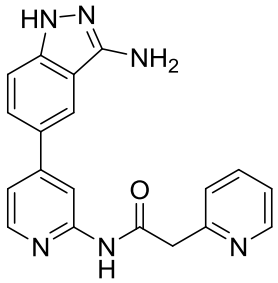

N-(4-chloropyridin-2-yl)-2-(2-pyridyl)acetamide (100 mg, 0.4 mmol), 5-(4,4,5,5-Tetramethyl-1,3,2-dioxaborolan-2-yl)-1*H*-indazol-3-amine (118 mg, 0.45 mmol), and Pd(dtbpf)Cl_2 (26 mg, 0.04 mmol) were placed in a 2-5 mL microwave vial which was sealed and purged with nitrogen for 5 mins. Ethanol (O_2-free, 1.12 mL) was added and the suspension stirred under nitrogen for a further 10 mins. K_3PO_4 (O_2-free, 1 M, 0.56 mL) was added and the solution stirred at 70 °C for 24 hours. Organics were extracted into ethyl acetate/methanol 9:1 (50 mL), washed with water and dried over magnesium sulphate, then adsorbed onto silica under reduced pressure. Chromatographic purification (Biotage SP4, 50 g cartridge, solvent system: ethyl acetate/methanol/1% Net_3, gradient: 0% 5CV; 0-2% 2CV; 2% 4CV) followed by HPLC purification yielded title compound as a bright yellow solid (as TFA salt) (42 mg, 23%) (LC-MS purity = 92.8%); ^{1}H (DMSO-d_6, 400 MHz) δ 4.23 (2, 2H), 7.47 (m, 2H), 7.68 (m, 1H), 7.78 (m, 2H), 8.22 (t, *J* = 7.8 Hz, 1H), 8.29 (s, 1H), 8.41 (m, 2H), 8.76 (d, *J* = 5.3 Hz, 1H), 11.06 (br. s, 1H); ^{19}F (DMSO-d_6, 376 MHz) δ -74.67; ^{13}C (DMSO-d_6, 100 MHz) δ 42.96, 110.72, 111.61, 117.63, 120.26, 124.52, 127.44, 127.95, 128.87, 142.24, 142.70, 145.26, 148.72, 150.28, 152.78, 152.93, 158.69, 159.04, 168.38; HRMS: $C_{19}H_{17}N_6O$ requires 345.1458 found 345.1458.

6.30. *N*-(4-(3-amino-1*H*-indazol-5-yl)pyridin-2-yl)-2-(3-pyridyl)acetamide 10

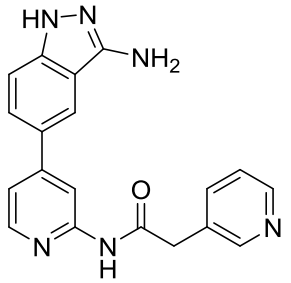

N-(4-chloropyridin-2-yl)-2-(2-pyridyl)acetamide (100 mg, 0.4 mmol), 5-(4,4,5,5-Tetramethyl-1,3,2-dioxaborolan-2-yl)-1*H*-indazol-3-amine (118 mg, 0.45 mmol), and Pd(dtbpf)Cl_2 (26 mg, 0.04 mmol) were placed in a 2-5 mL microwave vial which was sealed and purged with nitrogen for 5 mins. Ethanol (O_2-free, 1.12 mL) was added and the suspension stirred under nitrogen for a further 10 mins. K_3PO_4 (O_2-free, 1 M, 0.56 mL) was added and the solution stirred at 70 °C for 24 hours. Organics were extracted into ethyl acetate/methanol 9:1 (50 mL), washed with water and dried over magnesium sulphate, then adsorbed onto silica under reduced pressure. Chromatographic purification (Biotage SP4, 50 g cartridge, solvent system: ethyl acetate/methanol/1% Net_3, gradient: 0% 5CV; 0-2% 2CV; 2% 4CV) followed by HPLC purification yielded title compound as a bright yellow solid (as TFA salt) (87 mg, 47%) (LC-MS purity = 91.5%); ^{1}H (DMSO-d_6, 400 MHz) δ 4.08 (2, 2H), 7.46 (m, 2H), 7.76 (dd, *J* = 8.8 & 1.8 Hz, 1H), 7.92 (dd, *J* = 7.8 & 5.5 Hz, 1H), 8.29 (d, *J* = 0.8 Hz, 1H), 8.40 (m, 3H), 8.79 (d, *J* = 5 Hz, 1H), 8.86 (s, 1H), 11.08 (s, 1H); ^{19}F (DMSO-d_6, 376 MHz) δ -74.61; ^{13}C (DMSO-d_6, 100 MHz) δ 49.05, 110.72, 111.56, 117.56, 120.22, 127.84, 128.83, 134.89, 142.22, 142.75, 144.97, 145.25, 148.73, 150.24, 152.90, 158.77, 159.12, 169.29; HRMS: $C_{19}H_{17}N_6O$ requires 345.1458 found 345.1458.

6.31. *N*-(4-(3-amino-1*H*-indazol-5-yl)pyridin-2-yl)-2-(2-(trifluoromethyl)phenyl)acetamide 12

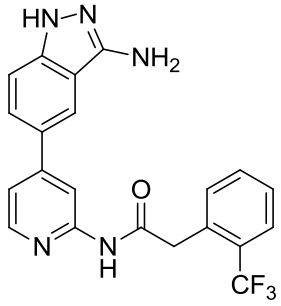

5-(4,4,5,5-Tetramethyl-1,3,2-dioxaborolan-2-yl)-1*H*-indazol-3-amine (118 mg, 0.45 mmol), *N*-(4-chloropyridin-2-yl)-2-(2-(trifluoromethyl)phenyl)acetamide (126 mg, 0.4 mmol) and Pd(dtbpf)Cl_2 (26 mg, 0.04 mmol) were placed in a 2-5 mL microwave vial which was sealed and purged with nitrogen for 5 mins. Ethanol (O_2-free, 1.12 mL) was added and the suspension stirred at 40 °C under nitrogen for a further 10 mins. K_3PO_4 (1 M, 0.56 mL) was added and the solution stirred at 70 °C for 24 hours. Reaction was quenched with water (5 mL) to yield a yellowish solid. Organics were extracted into ethyl acetate (50 mL) and adsorbed onto silica under reduced pressure. . Chromatographic purification (Biotage SP4, 50 g cartridge, solvent system: ethyl acetate/methanol, gradient: 0% 2CV; 0-2% 2CV; 2% 4CV) yielded title product as a pale yellow solid (94 mg, 57%) (LC-MS purity = 98.3%); ^{1}H (DMSO-d_6, 400 MHz) δ 4.07 (s, 2H), 5.52 (s, 2H), 7.33, (d, *J* = 8.8 Hz, 1H), 7.41 (dd, *J* = 5.3 & 1.8 Hz, 1H), 7.50 (t, *J* = 7.5 Hz, 1H), 7.56 (d, *J* = 7.5 Hz, 1H), 7.59 (dd, *J* = 8.8 & 1.8 Hz, 1H), 7.66 (t, *J* = 7.5 Hz, 1H), 7.72 (d, *J* = 7.8 Hz, 1H), 8.15 (d, *J* = 1 Hz, 1H), 8.36 (d, *J* = 5.3 Hz, 1H), 8.42 (s, 1H), 10.80 (s, 1H), 11.56 (br s, 1H); ^{13}C (DMSO-d_6, 100 MHz) δ 40.12, 110.48, 110.56, 115.14, 117.24, 119.59, 124.97 (d, *J* = 273.6 Hz), 125.47, 126.07 (d, *J* = 5.9 Hz), 127.31, 127.81, 128.15 (d, *J* = 30.2 Hz), 132.67, 134.11, 134.25, 142.00, 148.85, 150.46, 150.56, 153.25, 169.62. HRMS: $C_{21}H_{17}F_3N_5O$ requires 412.1380 found 412.1373.

6.32. *N*-(4-(3-amino-1*H*-indazol-5-yl)pyridin-2-yl)-2-(3-(trifluoromethyl)phenyl)acetamide 13

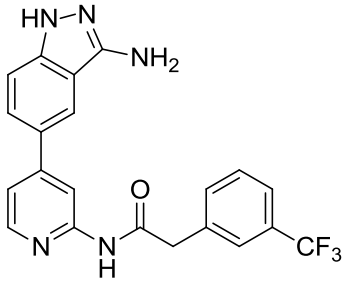

5-(4,4,5,5-Tetramethyl-1,3,2-dioxaborolan-2-yl)-1*H*-indazol-3-amine (118 mg, 0.45 mmol), *N*-(4-chloropyridin-2-yl)-2-(3-(trifluoromethyl)phenyl)acetamide (126 mg, 0.4 mmol) and Pd(dtbpf)Cl_2 (26 mg, 0.04 mmol) were placed in a 2-5 mL microwave vial which was sealed and purged with nitrogen for 5 mins. Ethanol (O_2-free, 1.12 mL) was added and the suspension stirred at 40 °C under nitrogen for a further 10 mins. K_3PO_4 (1 M, 0.56 mL) was added and the solution stirred at 70 °C for 24 hours. Reaction was quenched with water (5 mL) to yield a yellowish solid. Organics were extracted into ethyl acetate (50 mL) and adsorbed onto silica under reduced pressure. . Chromatographic purification (Biotage SP4, 50 g cartridge, solvent system: ethyl acetate/methanol, gradient: 0% 2CV; 0-2% 2CV; 2% 4CV) yielded title product as a pale yellow solid (71 mg, 43%) (LC-MS purity = 96.4%); ^{1}H (DMSO-d_6, 400 MHz) δ 3.91 (s, 2H), 5.53 (s, 2H), 7.33, (d, *J* = 8.5 Hz, 1H), 7.41 (dd, *J* = 5.3 & 1.8 Hz, 1H), 7.60 (m, 3H), 7.71 (s, 1H), 7.72 (s, 1H), 8.16 (d, *J* = 1 Hz, 1H), 8.35 (d, *J* = 5.3 Hz, 1H), 8.43 (s, 1H), 10.84 (s, 1H), 11.62 (br s, 1H); ^{13}C (DMSO-d_6, 100 MHz) δ 43.12, 110.62, 115.14, 117.43, 119.66, 124.86 (d, *J* = 271.6 Hz), 125.47, 125.58 (q, 3.7 Hz), 127.33, 127.85 (d, *J* = 31.2 Hz), 130.66 (2C), 130.80, 141.09, 142.00, 148.84, 150.46, 150.63, 153.16, 169.89; HRMS: $C_{21}H_{17}F_3N_5O$ requires 412.1380 found 412.1372.

6.33. *N*-(4-(3-amino-1*H*-indazol-5-yl)pyridin-2-yl)-2-(4-(trifluoromethyl)phenyl)acetamide 14

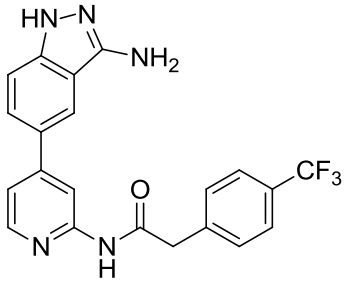

5-(4,4,5,5-Tetramethyl-1,3,2-dioxaborolan-2-yl)-1*H*-indazol-3-amine (118 mg, 0.45 mmol), *N*-(4-chloropyridin-2-yl)-2-(4-(trifluoromethyl)phenyl)acetamide (126 mg, 0.4 mmol) and Pd(dtbpf)Cl_2 (26 mg, 0.04 mmol) were placed in a 2-5 mL microwave vial which was sealed and purged with nitrogen for 5 mins. Ethanol (O_2-free, 1.12 mL) was added and the suspension stirred at 40 °C under nitrogen for a further 10 mins. K_3PO_4 (1 M, 0.56 mL) was added and the solution stirred at 70 °C for 24 hours. Reaction was quenched with water (5 mL) to yield a yellowish solid. Organics were extracted into ethyl acetate (50 mL) and adsorbed onto silica under reduced pressure. . Chromatographic purification (Biotage SP4, 50 g cartridge, solvent system: ethyl acetate/methanol, gradient: 0% 2CV; 0-2% 2CV; 2% 4CV) yielded title product as a pale yellow solid (78 mg, 47%) (LC-MS purity = 95.0%); ^{1}H (DMSO-d_6, 400 MHz) δ 3.92 (s, 2H), 5.53 (s, 2H), 7.34, (d, *J* = 8.8 Hz, 1H), 7.41 (dd, *J* = 5.3 & 1.8 Hz, 1H), 7.59 (m, 2H), 7.64 (d, *J* = 7.6 Hz, 1H), 7.68 (d, *J* = 7.6 Hz, 1H), 7.76 (s, 1H), 8.16 (d, *J* = 1 Hz, 1H), 8.36 (d, *J* = 5.3 Hz, 1H), 8.43 (s, 1H), 10.83 (s, 1H), 11.63 (br s, 1H); ^{13}C (DMSO-d_6, 100 MHz) δ 42.92, 110.59, 115.14, 117.43, 119.66, 123.87 (q, *J* = 3.7 Hz), 124.86 (d, *J* = 272.7 Hz), 125.50, 126.44 (q, *J* = 3.7 Hz), 127.32, 129.45 (d, *J* = 31.2 Hz), 129.78 (2C), 134.03, 137.60, 142.01, 148.84, 150.46, 150.64, 153.16, 170.01. HRMS: $C_{21}H_{17}F_3N_5O$ requires 412.1380 found 412.1374.

6.34. *N*-(4-(3-amino-1*H*-indazol-5-yl)pyridin-2-yl)-2-(3-aminophenyl)acetamide 15

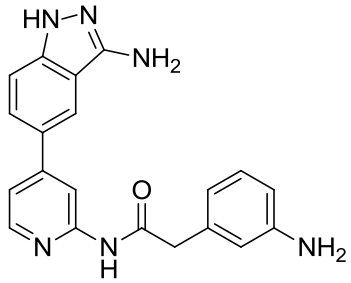

5-(4,4,5,5-Tetramethyl-1,3,2-dioxaborolan-2-yl)-1*H*-indazol-3-amine (118 mg, 0.45 mmol), *N*-(4-chloropyridin-2-yl)-2-(3-Boc-aminophenyl)acetamide (145.5 mg, 0.4 mmol) and Pd(dtbpf)Cl_2 (26 mg, 0.04 mmol) were placed in a 2-5 mL microwave vial which was sealed and purged with nitrogen for 5 mins. Ethanol (0_2-free, 1.12 mL) was added and the suspension stirred at 50 °C under nitrogen for a further 10 mins. K_3PO_4 (1 M, 0.56 mL) was added and the solution stirred at 70 °C for 24 hours. Reaction was quenched with water (50 mL) to yield a yellowish solid. This was sonicated for 30 mins and resultant solid was filtered and resuspended in 80% ethyl acetate/methanol (18 mL) and adsorbed onto silica. Product was obtained by chromatographic purification (Biotage SP4, 50 g cartridge, solvent system: ethyl acetate/methanol, gradient: 0% 2CV; 0-2% 2CV; 2% 6CV). Product was suspended in dichloromethane (3 mL) and trifluroacetic acid (1.5 mL) and stirred at room temperature for 8 hours. Solution was diluted with ethyl acetate (40 mL), washed with Na_2CO_3 (sat., 20 mL) and concentrated under reduced pressure to yield title product (55 mg, 39% over 2 steps). (LC-MS purity = 95.2%); ^{1}H (DMSO-d_6, 400 MHz) δ 3.58 (s, 2H), 5.02 (s, 2H), 5.52 (s, 2H), 6.44 (ddd, *J* = 8, 2.2 & 0.9 Hz, 1H), 6.52 (d, *J* = 7.5 Hz), 6.58 (m, 1H), 6.96 (t, *J* = 7.8 Hz, 1H), 7.34 (d, *J* = 8.5 Hz, 1H), 7.38 (dd, *J* = 5.3 & 1.8 Hz, 1H), 7.59 (dd, *J* = 8.8 & 1.8 Hz, 1H), 8.15 (d, *J* = 1 Hz, 1H), 8.34 (d, *J* = 5.3 Hz, 1H), 8.44 (s, 1H), 10.60 (s, 1H), 11.56 (s, 1H); ^{13}C (DMSO-d_6, 100 MHz) δ 43.83, 110.55, 110.58, 112.78, 115.09, 117.24, 117.28, 119.66, 125.50, 127.43, 129.22, 136.74, 142.00, 148.78, 149.09, 150.45, 150.57, 153.33, 170.83; HRMS: For $C_{20}H_{19}N_6O$ requires 359.1615 found 359.1609.

6.35. *N*-(4-(3-amino-1*H*-indazol-5-yl)pyridin-2-yl)-2-(4-aminophenyl)acetamide 16

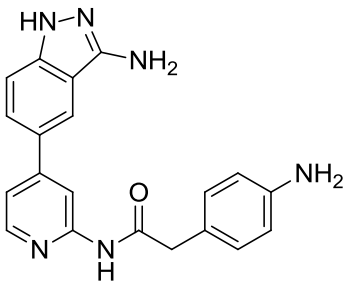

N-(4-(3-amino-1*H*-indazol-5-yl)pyridin-2-yl)-2-(4-Boc-aminophenyl)acetamide (25 mg, 0.07 mmol) was dissolved in dichloromethane (3 mL), methanol (0.3 mL) and trifluoroacetic acid (1 mL) and stirred at room temperature for 24 hours. TLC showed consumption of starting material so reaction was quenched with 1 M Na_2CO_3 solution (5 mL), product extracted into ethyl acetate (25 mL) and organics dried over magnesium sulphate, filtered and concentrated under reduced pressure to yield title compound as a brown solid (14 mg, 70%). (LC-MS purity = 86.4%); ^{1}H (DMSO-d_6, 400 MHz) δ 3.53 (s, 2H), 4.95 (br s, 2H), 5.55 (s, 2H), 6.52 (d, *J* = 8.5 Hz, 2H), 7.02 (d, *J* = 8.3 Hz, 2H), 7.33 (d, *J* = 8.8 Hz, 1H), 7.37 (dd, *J* = 5.3 & 1.8 Hz, 1H), 7.58 (dd, *J* = 8.8, 1.8 Hz, 1H), 8.14 (d, *J* = 1 Hz, 1H), 8.33 (d, *J* = 5 Hz, 1H), 8.42 (s, 1H), 10.55 (s, 1H), 11.57 (s, 1H); ^{13}C (DMSO-d_6, 150 MHz) δ 42.85, 110.51, 110.59, 114.33 (2C), 115.10, 117.24, 119.63, 123.09, 125.51, 127.45, 130.13 (2C), 141.99, 147.76, 148.77, 150.43, 150.54, 153.34, 171.48; HRMS: For $C_{20}H_{19}N_6O$ requires 359.1615 found 359.1612.

6.36. *N*-(4-(3-amino-1*H*-indazol-5-yl)pyridin-2-yl)-2-(3-Boc-aminophenyl)acetamide 18

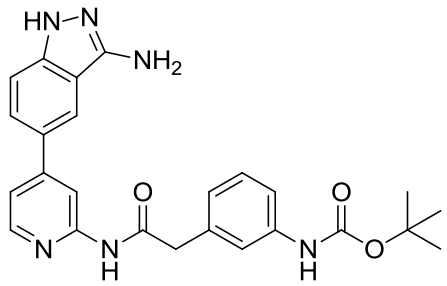

5-(4,4,5,5-Tetramethyl-1,3,2-dioxaborolan-2-yl)-1*H*-indazol-3-amine (120 mg, 0.46 mmol), *N*-(4-chloropyridin-2-yl)-2-(3-Boc-aminophenyl)acetamide (120 mg, 0.33 mmol) and Pd(dtbpf)Cl_2 (21.6 mg, 0.033 mmol) were placed in a 2-5 mL microwave vial which was sealed and purged with nitrogen for 5 mins. Ethanol (O_2-free, 1 mL) was added and the suspension stirred at 50 °C under nitrogen for a further 10 mins. K_3PO_4 (1 M, 0.5 mL) was added and the solution stirred at 70 °C for 24 hours. Reaction was quenched with water (50 mL) to yield a yellowish solid. This was sonicated for 30 mins and resultant solid was filtered and resuspended in 80% ethyl acetate/methanol (18 mL) and adsorbed onto silica. Chromatographic purification (Biotage SP4, 50 g cartridge, solvent system: ethyl acetate/methanol, gradient: 0% 2CV; 0-5% 3CV; 5% 6CV) yielded title product as a brown solid (30 mg, 20%) (LC-MS purity = 94.9%); (61 mg, 40%) (NMR purity ≈90%); ^{1}H (DMSO-d_6, 400 MHz) δ 1.47 (s, 9H), 3.71 (s, 2H), 5.52 (s, 2H), 6.98 (d, *J* = 7.5 Hz, 1H), 7.20 (t, *J* = 7.8 Hz, 1H), 7.27 (d, *J* = 8 Hz, 1H), 7.34 (d, *J* = 8.8 Hz, 1H), 7.39 (dd, *J* = 5.3 & 1.8 Hz, 1H), 7.55 (s, 1H), 7.59 (dd, *J* = 8.8, 1.8 Hz, 1H), 8.15 (d, *J* = 0.8 Hz, 1H), 8.34 (d, *J* = 5.5 Hz, 1H), 8.43 (s, 1H), 9.31 (s, 1H), 10.72 (s, 1H), 11.56 (s, 1H); ^{13}C (DMSO-d_6, 100 MHz) δ 28.59, 79.46, 110.59, 110.62, 115.10, 117.13, 117.36, 119.48, 119.64, 123.62, 125.54, 127.43, 128.96, 136.71, 139.95, 142.00, 148.83, 150.44, 150.57, 153.24, 153.28, 170.60; HRMS: For $C_{25}H_{27}N_5O_2$ requires 459.2139 found 459.2138

6.37. *N*-(4-(3-amino-1*H*-indazol-5-yl)pyridin-2-yl)-2-(4-Boc-aminophenyl)acetamide 19

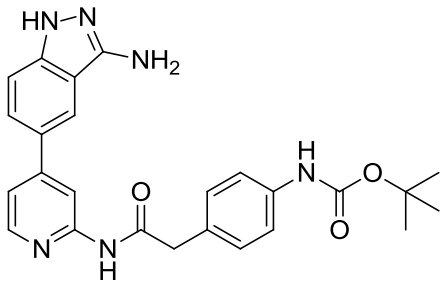

5-(4,4,5,5-Tetramethyl-1,3,2-dioxaborolan-2-yl)-1*H*-indazol-3-amine (110 mg, 0.42 mmol), *N*-(4-chloropyridin-2-yl)-2-(4-Boc-aminophenyl)acetamide (127 mg, 0.35 mmol) and Pd(dtbpf)Cl_2 (23 mg, 0.035 mmol) were placed in a 2-5 mL microwave vial which was sealed and purged with nitrogen for 5 mins. Ethanol (O_2-free, 1 mL) was added and the suspension stirred at 50 °C under nitrogen for a further 10 mins. K_3PO_4 (1 M, 0.5 mL) was added and the solution stirred at 70 °C for 24 hours. Reaction was quenched with water (5 mL) to yield a yellowish solid. Supernatant was removed and solid resuspended in 80% ethyl acetate/methanol (6 mL) and adsorbed onto silica under reduced pressure. Chromatographic purification (Biotage SP4, 50 g cartridge, solvent system: ethyl acetate/methanol, gradient: 0% 2CV; 0-5% 3CV; 5% 4CV) yielded title product as a brown solid (79 mg, 52%) (LC-MS purity = 100.0%); ^{1}H (DMSO-d_6, 400 MHz) δ 1.46 (s, 9H), 3.66 (s, 2H), 5.54 (s, 2H), 7.24 (d, *J* = 8.3 Hz, 2H), 7.33 (d, *J* = 8.8 Hz, 1H), 7.39 (m, 3H), 7.59 (dd, *J* = 8.3, 1.8 Hz, 1H), 8.14 (s, 1H), 8.33 (d, *J* = 4.8 Hz, 1H), 8.41 (s, 1H), 9.29 (s, 1H), 10.69 (s, 1H), 11.57 (s, 1H); ^{13}C (DMSO-d_6, 100 MHz) δ 28.60 (3C), 42.84, 110.52, 110.56, 115.11, 117.30, 118.63, 119.66, 125.50, 127.36, 129.78, 129.90 (2C), 138.56, 141.94, 148.81 (2C), 150.47, 150.56, 153.25, 153.29, 170.85* HRMS: For $C_{25}H_{27}N_5O_2$ requires 459.2139 found 459.2133.

*Peak expected ~79 ppm for **C**$(CH_3)_3$ not observed

6.38. *N*-(4-(3-amino-1*H*-indazol-5-yl)pyridin-2-yl)-2-(4-(methylthio)phenyl)acetamide 21

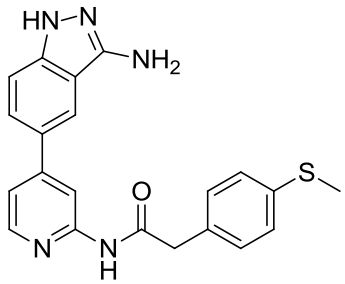

5-(4,4,5,5-Tetramethyl-1,3,2-dioxaborolan-2-yl)-1*H*-indazol-3-amine (110 mg, 0.42 mmol), *N*-(4-chloropyridin-2-yl)-2-(4-(methylthio)phenyl)acetamide (102 mg, 0.35 mmol) and Pd(dtbpf)Cl_2 (23 mg, 0.035 mmol) were placed in a 2-5 mL microwave vial which was sealed and purged with nitrogen for 5 mins. Ethanol (O_2-free, 1 mL) was added and the suspension stirred at 40 °C under nitrogen for a further 10 mins. K_3PO_4 (1 M, 0.5 mL) was added and the solution stirred at 70 °C for 24 hours. Reaction was quenched with water (5 mL) to yield a yellowish solid. Supernatant was removed and solid resuspended in 80% ethyl acetate/methanol (8 mL) and adsorbed onto silica under reduced pressure. Chromatographic purification (Biotage SP4, 50 g cartridge, solvent system: ethyl acetate/methanol, gradient: 0% 2CV; 0-5% 3CV; 5% 4CV) yielded title product as a brown solid (41 mg, 25%) (LC-MS purity = 93.8%); %); ^{1}H (DMSO-d_6, 400 MHz) δ 2.46 (s, 3H), 3.72 (s, 2H), 5.55 (s, 2H), 7.24 (m, 2H), 7.33 (m, 3H), 7.39 (dd, *J* = 5.3 & 1.8 Hz, 1H), 7.59 (dd, *J* = 8.8 & 1.8 Hz, 1H), 8.15 (d, *J* = 1 Hz, 1H), 8.34 (dd, *J* = 5.3 & 0.5 Hz, 1H), 8.42 (s, 1H), 10.75 (s, 1H), 11.58 (br s, 1H); ^{13}C (DMSO-d_6, 100 MHz) δ 15.44 (3H), 42.92 (2H), 110.57 (2C), 115.14, 117.34, 119.65, 125.48, 126.65 (2C), 127.38, 130.32 (2C), 133.00, 136.64, 141.99, 148.81, 150.45, 150.59, 153.25, 170.57; HRMS: $C_{21}H_{20}N_5OS$ requires 390.1383 found 390.1377.

6.39. *N*-(4-(3-amino-1*H*-indazol-5-yl)pyridin-2-yl)-2-(2-methoxyphenyl)acetamide 22

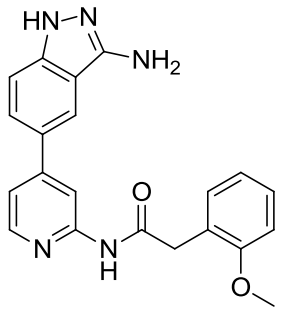

5-(4,4,5,5-Tetramethyl-1,3,2-dioxaborolan-2-yl)-1*H*-indazol-3-amine (110 mg, 0.42 mmol), *N*-(4-chloropyridin-2-yl)-2-(2-methoxyphenyl)acetamide (97 mg, 0.35 mmol) and Pd(dtbpf)Cl_2 (23 mg, 0.035 mmol) were placed in a 2-5 mL microwave vial which was sealed and purged with nitrogen for 5 mins. Ethanol (O_2-free, 1 mL) was added and the suspension stirred at 50 °C under nitrogen for a further 5 mins. K_3PO_4 (1 M, 0.5 mL) was added and the solution stirred at 70 °C for 24 hours. Reaction was quenched with water (5 mL) to yield a yellowish solid. Supernatant was removed and solid was resuspended in 80% ethyl acetate/methanol (6 mL) and adsorbed onto silica. Chromatographic purification (Biotage SP4, 50 g cartridge, solvent system: ethyl acetate/methanol, gradient: 0% 2CV; 0-5% 3CV; 5% 6CV) yielded title product as a pale brown solid (99 mg, 76%). (LC-MS purity = 97.6%); ^{1}H (DMSO-d_6, 400 MHz) δ 3.76 (s, 2H), 3.77 (s, 3H), 5.54 (br s, 2H), 6.91 (t, *J* = 7.3 Hz, 1H), 6.99 (d, *J* = 7.9 Hz, 1H), 7.24 (d, *J* = 7.5Hz, 2H), 7.32 (d, *J* = 8.3 Hz, 1H), 7.32 (dd, *J* = 5.3 & 1.8 Hz, 1H), 7.59 (d, *J* = 8.8 Hz 1H), 8.15 (s, 1H), 8.34 (d, *J* = 5.7 Hz, 1H), 8.44 (s, 1H), 10.55 (s, 1H), 11.57 (s, 1H); ^{13}C (DMSO-d_6, 100 MHz) δ 38.12, 55.89, 110.43, 110.54, 111.14, 115.11, 117.10, 119.61, 120.62, 124.44, 125.48, 127.36, 128.60, 131.56, 141.95, 148.81, 150.47, 153.36, 157.78, 170.61; HRMS: For $C_{21}H_{20}N_5O_2$ requires 374.1612 found 374.1606.

6.40. *N*-(4-(3-amino-1*H*-indazol-5-yl)pyridin-2-yl)-2-(3-methoxyphenyl)acetamide 23

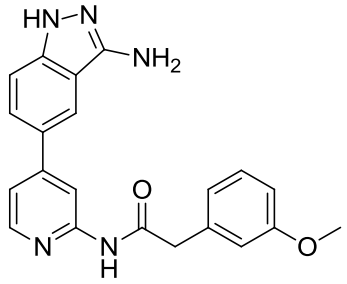

5-(4,4,5,5-Tetramethyl-1,3,2-dioxaborolan-2-yl)-1*H*-indazol-3-amine (110 mg, 0.42 mmol), *N*-(4-chloropyridin-2-yl)-2-(3-methoxyphenyl)acetamide (97 mg, 0.35 mmol) and Pd(dtbpf)Cl_2 (23 mg, 0.035 mmol) were placed in a 2-5 mL microwave vial which was sealed and purged with nitrogen for 5 mins. Ethanol (O_2-free, 1 mL) was added and the suspension stirred at 50 °C under nitrogen for a further 5 mins. K_3PO_4 (1 M, 0.5 mL) was added and the solution stirred at 70 °C for 24 hours. Reaction was quenched with water (5 mL) to yield a yellowish solid. Supernatant was removed and solid was resuspended in 80% ethyl acetate/methanol (6 mL) and adsorbed onto silica. Chromatographic purification (Biotage SP4, 50 g cartridge, solvent system: ethyl acetate/methanol, gradient: 0% 2CV; 0-5% 3CV; 5% 6CV) yielded title product as a pale brown solid (82 mg, 63%). (LC-MS purity = 90.1%); ^{1}H (DMSO-d_6, 400 MHz) δ 3.72 (s, 2H), 3.75 (s, 3H), 5.55 (s, 2H), 6.83 (d, *J* = 7.9 Hz, 1H), 6.94 (m, 2H), 7.24 (t, *J* = 7.7 Hz, 1H), 7.33 (d, *J* = 8.8 Hz, 1H), 7.39 (d, *J* = 5.3 Hz, 1H), 7.59 (d, *J* = 8.8 Hz, 1H), 8.15 (s, 1H), 8.34 (d, *J* = 5.3 Hz, 1H), 8.43 (s, 1H), 10.74 (s, 1H), 11.58 (br s, 1H); ^{13}C (DMSO-d_6, 100 MHz) δ 43.56, 55.44, 110.52, 110.57, 112.43, 115.11, 115.55, 117.34, 119.67, 121.96, 125.50, 127.34, 129.79, 137.70, 141.95, 148.83, 150.46, 150.59, 153.25, 159.66, 170.48; HRMS: For $C_{21}H_{20}N_5O_2$ requires 374.1612 found 374.1606.

6.41. *N*-(4-(3-amino-1*H*-indazol-5-yl)pyridin-2-yl)-2-(4-methoxyphenyl)acetamide 24

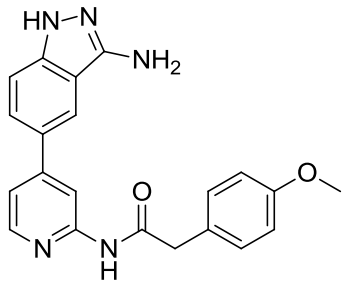

5-(4,4,5,5-Tetramethyl-1,3,2-dioxaborolan-2-yl)-1*H*-indazol-3-amine (110 mg, 0.42 mmol), *N*-(4-chloropyridin-2-yl)-2-(4-methoxyphenyl)acetamide (97 mg, 0.35 mmol) and Pd(dtbpf)Cl_2 (23 mg, 0.035 mmol) were placed in a 2-5 mL microwave vial which was sealed and purged with nitrogen for 5 mins. Ethanol (O_2-free, 1 mL) was added and the suspension stirred at 50 °C under nitrogen for a further 5 mins. K_3PO_4 (1 M, 0.5 mL) was added and the solution stirred at 70 °C for 24 hours. Reaction was quenched with water (5 mL) to yield a yellowish solid. Supernatant was removed and solid was resuspended in 80% ethyl acetate/methanol (6 mL) and adsorbed onto silica. Chromatographic purification (Biotage SP4, 50 g cartridge, solvent system: ethyl acetate/methanol, gradient: 0% 2CV; 0-5% 3CV; 5% 6CV) yielded title product as a pale brown solid (90 mg, 69%). (LC-MS purity = 98.4%); ^{1}H (DMSO-d_6, 400 MHz) δ 3.68 (s, 2H), 3.73 (s, 3H), 5.55 (br s, 2H), 6.91 (m, 2H), 7.29 (m, 2H), 7.34 (d, *J* = 8.8 Hz, 1H), 7.39 (dd, *J* = 5.4 & 1.6 Hz, 1H), 7.59 (dd, *J* = 8.8 & 1.8 Hz, 1H), 8.15 (s, 1H), 8.34 (d, *J* = 6.3 Hz, 1H), 8.43 (s, 1H), 10.70 (s, 1H), 11.59 (s, 1H); ^{13}C (DMSO-d_6, 100 MHz) δ 42.62, 55.5, 110.51, 110.57, 114.20 (2C), 115.11, 117.29, 119.66, 125.50, 127.36, 128.18, 130.73 (2C), 141.95, 148.81, 150.56, 153.31, 158.55, 170.99; HRMS: For $C_{21}H_{20}N_5O_2$ requires 374.1612 found 374.1606.

6.42. *N*-(4-(3-amino-1*H*-indazol-5-yl)pyridin-2-yl)-2-(3-(methylsulfonyl)phenyl)acetamide 25

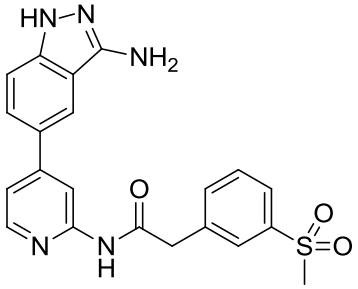

5-(4,4,5,5-Tetramethyl-1,3,2-dioxaborolan-2-yl)-1*H*-indazol-3-amine (118 mg, 0.45 mmol), *N*-(4-chloropyridin-2-yl)-2-(3-(methylsulfonyl)phenyl)acetamide (139 mg, 0.4 mmol) and Pd(dtbpf)Cl_2 (23 mg, 0.035 mmol) were placed in a 2-5 mL microwave vial which was sealed and purged with nitrogen for 5 mins. Ethanol (O_2-free, 1.12 mL) was added and the suspension stirred at 50 °C under nitrogen for a further 10 mins. K_3PO_4 (1 M, 0.56 mL) was added and the solution stirred at 70 °C for 24 hours. Reaction was quenched with water (5 mL) to yield a yellowish solid. Supernatant was removed and solid resuspended in 80% ethyl acetate/methanol (6 mL) and adsorbed onto silica under reduced pressure. Chromatographic purification (Biotage SP4, 50 g cartridge, solvent system: ethyl acetate/methanol, gradient: 0% 2CV; 0-5% 3CV; 5% 4CV) yielded title product as a greenish solid (61 mg, 34%). (LC-MS purity = 96.3%); ^{1}H (DMSO-d_6, 400 MHz) δ 3.23 (s, 3H), 3.93 (s, 2H), 5.53 (s, 2H), 7.34 (d, *J* = 8.5 Hz, 1H), 7.41 (dd, *J* = 5.3 & 1.8 Hz, 1H), 7.59 (dd, *J* = 8.8 & 1.8 Hz, 1H), 7.64 (t, *J* = 7.8 Hz, 1H), 7.73 (m, 1H), 7.85 (ddd, *J* = 7.6, 1.6 & 1.3 Hz, 1H), 7.97 (m, 1H), 8.16 (d, *J* = 1 Hz, 1H), 8.36 (dd, *J* = 5.3 & 0.5 Hz, 1H), 8.43 (s, 1H), 10.86 (s, 1H), 11.56 (s, 1H); ^{13}C (DMSO-d_6, 100 MHz) δ 42.92, 44.00, 110.56, 110.59, 115.11, 117.43, 119.68, 125.50, 125.80, 127.28, 128.04, 129.90, 135.10, 137.73, 141.30, 141.96, 148.87, 150.47, 150.62, 153.15, 169.92; HRMS: For $C_{21}H_{20}N_5O_3S$ requires 422.1281 found 422.1279.

6.43. *N*-(4-(3-amino-1*H*-indazol-5-yl)pyridin-2-yl)-2-(4-(methylsulfonyl)phenyl)acetamide 26

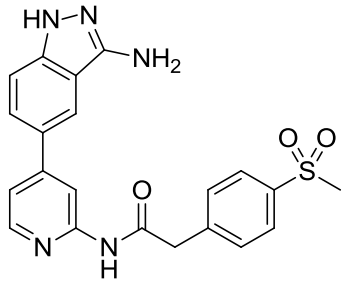

5-(4,4,5,5-Tetramethyl-1,3,2-dioxaborolan-2-yl)-1*H*-indazol-3-amine (118 mg, 0.45 mmol), *N*-(4-chloropyridin-2-yl)-2-(4-(methylsulfonyl)phenyl)acetamide (139 mg, 0.4 mmol) and Pd(dtbpf)Cl_2 (23 mg, 0.035 mmol) were placed in a 2-5 mL microwave vial which was sealed and purged with nitrogen for 5 mins. Ethanol (O_2-free, 1.12 mL) was added and the suspension stirred at 50 °C under nitrogen for a further 10 mins. K_3PO_4 (1 M, 0.56 mL) was added and the solution stirred at 70 °C for 24 hours. Reaction was quenched with water (5 mL) to yield a yellowish solid. Supernatant was removed and solid resuspended in 80% ethyl acetate/methanol (6 mL) and adsorbed onto silica under reduced pressure. Chromatographic purification (Biotage SP4, 50 g cartridge, solvent system: ethyl acetate/methanol, gradient: 0% 2CV; 0-5% 3CV; 5% 4CV) yielded title product as a greenish solid (30 mg, 17%). (LC-MS purity = 96.5%); ^{1}H (DMSO-d_6, 400 MHz) δ 3.21 (s, 3H), 3.93 (s, 2H), 5.52 (s, 2H), 7.34 (d, *J* = 8.8 Hz, 1H), 7.41 (dd, *J* = 5.3 & 1.8 Hz, 1H), 7.59 (dd, *J* = 8.7 & 1.6 Hz, 1H), 7.64 (d, *J* = 8.3 Hz, 2H), 7.91 (d, *J* = 8.4 Hz, 2H), 8.15 (d, *J* = 1 Hz, 1H), 8.36 (d, *J* = 5.5 Hz, 1H), 8.42 (s, 1H), 10.85 (s, 1H), 11.57 (s, 1H); ^{13}C (DMSO-d_6, 100 MHz) δ 43.18, 44.07, 110.61 (2C), 115.14, 117.45, 119.66, 125.47, 127.30, 127.45 (2C), 130.77 (2C), 139.70, 141.99, 142.27, 148.86, 150.45, 150.63, 153.13, 169.73; HRMS: $C_{21}H_{20}N_5O_3S$ requires 422.1281 found 422.1276.

6.44. *N*-(4-(3-amino-1*H*-indazol-5-yl)pyridin-2-yl)-2-(2-tolyl)acetamide 27

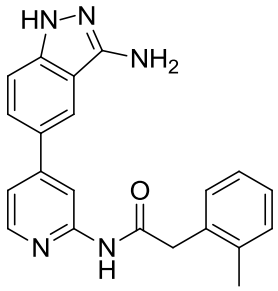

5-(4,4,5,5-Tetramethyl-1,3,2-dioxaborolan-2-yl)-1*H*-indazol-3-amine (85 mg, 0.325 mmol), *N*-(4-chloropyridin-2-yl)-2-(2-tolyl)acetamide (65 mg, 0.25 mmol) and Pd(dtbpf)Cl_2 (9 mg, 0.0125 mmol) were placed in a 2-5 mL microwave vial which was sealed and purged with nitrogen for 5 mins. Ethanol (O_2-free, 1 mL) was added and the suspension stirred at 50 °C under nitrogen for a further 5 mins. K_3PO_4 (1 M, 0.5 mL) was added and the solution stirred at 100 °C for 24 hours. Reaction was quenched with water (8 mL) to yield a brown solid which was filtered and further washed with water (15 x 10 mL) and hexane (8 x 10 mL). Solid was resuspended in 50% ethyl acetate/ methanol (20 mL), filtered and adsorbed onto silica. Chromatographic purification (Biotage SP4, 50 g cartridge, solvent system: 1% NEt_3 in ethyl acetate/methanol, gradient: 0% 3CV; 0-5% 2CV; 5% 4CV) yielded title product as a pale brown solid (59 mg, 66%). (LC-MS purity = 89.9%); ^{1}H (DMSO-d_6, 400 MHz) δ 2.32 (s, 3H), 3.81 (s, 2H), 5.55 (s, 2H), 7.16 (m, 3H), 7.28 (m, 1H), 7.32 (d, *J* = 8.8 Hz, 1H), 7.39 (dd, *J* = 5.1 & 1.5 Hz, 1H), 7.59 (dd, *J* = 8.8 & 1.3 Hz, 1H), 8.14 (s, 1H), 8.34 (d, *J* = 5.3 Hz, 1H), 8.43 (s, 1H), 10.74 (s, 1H), 11.57 (s, 1H); ^{13}C (DMSO-d_6, 150 MHz) δ 19.86, 41.20, 110.57, 110.61, 115.21, 117.28, 119.69, 125.53, 126.22, 127.20, 127.39, 130.35, 130.66, 134.98, 137.21, 141.97, 148.81, 150.49, 150.57, 153.29, 170.57; HRMS: For $C_{21}H_{19}N_5O$ requires 358.1662 found 358.1656.

6.45. *N*-(4-(3-amino-1*H*-indazol-5-yl)pyridin-2-yl)-2-(3-tolyl)acetamide 28

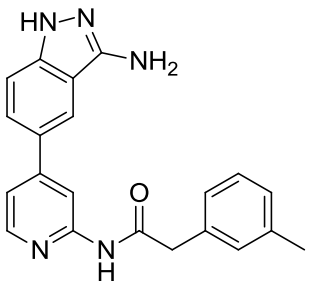

5-(4,4,5,5-Tetramethyl-1,3,2-dioxaborolan-2-yl)-1*H*-indazol-3-amine (85 mg, 0.325 mmol), *N*-(4-chloropyridin-2-yl)-2-(3-tolyl)acetamide (65 mg, 0.25 mmol) and Pd(dtbpf)Cl_2 (9 mg, 0.0125 mmol) were placed in a 2-5 mL microwave vial which was sealed and purged with nitrogen for 5 mins. Ethanol (O_2-free, 1 mL) was added and the suspension stirred at 50 °C under nitrogen for a further 5 mins. K_3PO_4 (1 M, 0.5 mL) was added and the solution stirred at 100 °C for 24 hours. Reaction was quenched with water (8 mL) to yield a brown solid which was filtered and further washed with water (15 x 10 mL) and hexane (8 x 10 mL). Solid was resuspended in 50% ethyl acetate/ methanol (20 mL), filtered and adsorbed onto silica. Chromatographic purification (Biotage SP4, 50 g cartridge, solvent system: 1% NEt_3 in ethyl acetate/methanol, gradient: 0% 3CV; 0-5% 2CV; 5% 4CV) yielded title product as a pale brown solid (35.8 mg, 40%). (LC-MS purity = 98.9%), ^{1}H (DMSO-d_6, 400 MHz) δ 2.30 (s, 3H), 3.71 (s, 2H), 5.55 (s, 2H), 7.06 (d, *J* = 7.5 Hz, 1H), 7.17 (m, 2H), 7.22 (t, *J* = 7.5 Hz, 1H), 7.33 (d, *J* = 8.8 Hz, 1H), 7.59 (dd, *J* = 5.3 & 1.8 Hz, 1H), 7.58 (d, *J* = 8.8 Hz, 1H), 8.34 (d, *J* = 5.3 Hz, 1H), 8.43 (s, 1H), 10.74 (s, 1H), 11.58 (s, 1H); ^{13}C (DMSO-d_6, 100 MHz) δ 20.95, 42.95, 110.05 (2C), 114.72, 116.81, 119.14, 124.98, 126.30, 127.18, 128.17, 128.14, 128.17, 129.86, 135.66, 137.29, 148.30, 150.07, 152.78, 170.15; HRMS: For $C_{21}H_{19}N_5O$ requires 358.1662 found 358.1656.

6.46. *N*-(4-(3-amino-1*H*-indazol-5-yl)pyridin-2-yl)-2-(4-tolyl)acetamide 29

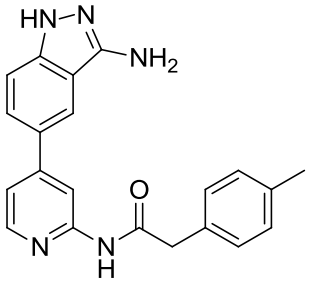

5-(4,4,5,5-Tetramethyl-1,3,2-dioxaborolan-2-yl)-1*H*-indazol-3-amine (110 mg, 0.42 mmol), *N*-(4-chloropyridin-2-yl)-2-(4-tolyl)acetamide (91 mg, 0.35 mmol) and Pd(dtbpf)Cl_2 (23 mg, 0.035 mmol) were placed in a 2-5 mL microwave vial which was sealed and purged with nitrogen for 5 mins. Ethanol (O_2-free, 1 mL) was added and the suspension stirred at 50 °C under nitrogen for a further 5 mins. K_3PO_4 (1 M, 0.5 mL) was added and the solution stirred at 70 °C for 24 hours. Reaction was quenched with water (5 mL) to yield a yellowish solid. Supernatant was removed and solid was resuspended in 80% ethyl acetate/methanol (6 mL) and adsorbed onto silica. Chromatographic purification (Biotage SP4, 50 g cartridge, solvent system: ethyl acetate/methanol, gradient: 0% 2CV; 2% 8CV) yielded title product as a pale brown solid (52 mg, 42%). (LC-MS purity = 97.4%); ^{1}H (DMSO-d_6, 400 MHz) δ 2.28 (s, 3H), 3.71 (s, 2H), 5.53 (s, 2H), 7.14 (d, *J* = 7.8 Hz, 2H), 7.28 (d, *J* = 8 Hz, 2H), 7.34 (d, *J* = 8.5 Hz, 1H), 7.39 (dd, *J* = 5.3 & 1.8 Hz, 1H), 7.59 (dd, *J* = 8.8 & 1.8 Hz, 1H), 8.15 (s, 1H), 8.34 (d, *J* = 5.5 Hz, 1H), 8.42 (2, 1H), 10.68 (s, 1H), 11.56 (s, 1H); ^{13}C (DMSO-d_6, 100 MHz) δ 21.12, 43.13, 110.56, 115.14, 117.31, 119.64, 125.49, 127.39, 129.32 (2C), 129.59 (2C), 133.22, 136.08, 141.99, 148.79, 150.45, 150.58, 153.29, 170.78; HRMS: For $C_{21}H_{19}N_5O$ requires 358.1662 found 358.1660.

6.47. 3-(2-(2-Phenylacetamido)pyridin-4-yl)benzamide 30

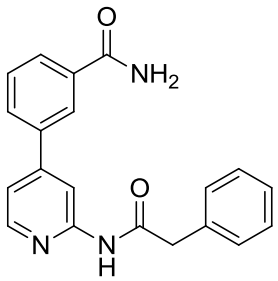

N-(4-chloropyridin-2-yl)-2-phenylacetamide (123 mg, 0.5 mmol), 3-aminocarbonylphenylboronic acid (99 mg, 0.6 mmol, 1.2 equiv.) and $Pd(dppf)Cl_2$ (26 mg, 0.05 mmol, 0.1 equiv.), were placed in a 2-5 mL microwave vial which was sealed and purged with nitrogen. Ethanol (1.5 mL) was added and the suspension brought to 90 °C with stirring before addition of K_3PO_4 (O_2-free, 1 M, 0.75 mL). Stirring continued for 24 hours. Reaction was quenched with water (5 mL) to yield a brown solid which was filtered and further washed with water (5 x 10 mL) and ethyl acetate/1% methanol (10 x 5 mL) to yield title product (80 mg, 48%). (LC-MS purity = > 99.9%); ^{1}H (DMSO-d_6, 400 MHz) δ 3.77 (s, 2H), 7.26 (m, 1H), 7.35 (m, 4H), 7.49 (d, *J* = 5.5 Hz, 2H), 7.60 (t, *J* = 7.8 Hz, 1H), 7.85 (d, *J* = 7.8 Hz, 1H), 7.97 (d, *J* = 7.8 Hz, 1H), 8.14 (s, 1H), 8.20 (s, 1H), 8.42 (br s, 2H), 10.83 (s, 1H); ^{13}C (DMSO-d_6, 100 MHz) δ 43.47, 111.23, 117.86, 126.28, 127.06, 128.72, 128.77 (2C), 129.72 (3C), 129.97, 135.66, 136.19, 138.13, 149.13, 149.19, 153.34, 167.90, 170.74; HRMS (ESI +ve): For $C_{20}H_{18}N_3O_2$ requires 332.1394 found 332.1388.

6.48. 4-(2-(2-Phenylacetamido)pyridin-4-yl)benzamide 31

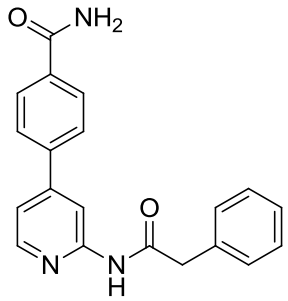

N-(4-chloropyridin-2-yl)-2-phenylacetamide (123 mg, 0.5 mmol), 4-aminocarbonylphenylboronic acid (99 mg, 0.6 mmol, 1.2 equiv.) and $Pd(dppf)Cl_2$ (26 mg, 0.05 mmol, 0.1 equiv.), were placed in a 2-5 mL microwave vial which was sealed and purged with nitrogen. Ethanol (1.5 mL) was added and the suspension brought to 90 °C with stirring before addition of K_3PO_4 (O_2-free, 1 M, 0.75 mL). Stirring continued for 24 hours. Reaction was quenched with water (5 mL) to yield a brown solid which was filtered and further washed with water (5 x 10 mL) and ethyl acetate/1% methanol (10 x 5 mL) to yield title product (27 mg, 17%). (LC-MS purity = 97.6%); ^{1}H (DMSO-*d*$_6$, 400 MHz) δ 3.77 (s, 2H), 7.26 (m, 1H), 7.35 (m, 4H), 7.44 (br s, 1H), 7.47 (dd, *J* = 5.1 & 1.6 Hz, 1H), 7.97 (d, *J* = 8.5 Hz, 2H), 8.01 (d, *J* = 8.3 Hz, 2H), 8.07 (br s, 1H), 8.42 (m, 2H), 10.84 (s, 1H); ^{13}C (DMSO-*d*$_6$, 100 MHz) δ 43.46, 111.20, 117.81, 127.07, 127.12 (2C), 128.77 (2C), 128.77 (2C), 128.82 (2C), 129.97 (2C), 135.28, 136.19, 140.58, 148.81, 149.18, 153.35, 167.75, 170.78; HRMS (ESI +ve): For $C_{20}H_{18}N_3O_2$ requires 332.1394 found 332.1388.

6.49. *N*-(4-(1H-benzo[*d*]imidazol-6-yl)pyridin-2-yl)-2-phenylacetamide 32

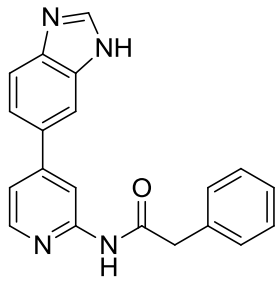

N-(4-chloropyridin-2-yl)-2-phenylacetamide (123 mg, 0.5 mmol), 1*H*-benzimidazole-5-boronic acid pinacol ester (146.5 mg, 0.6 mmol, 1.2 equiv.) and Pd(dppf)Cl_2 (26 mg, 0.05 mmol, 0.1 equiv.), were placed in a 2-5 mL microwave vial which was sealed and purged with nitrogen. Ethanol (1.5 mL) was added and the suspension brought to 90 °C with stirring before addition of K_3PO_4 (O_2-free, 1 M, 0.75 mL). Stirring continued for 24 hours. Resultant solution was cooled and quenched with water (5 mL) to yield a brown solid. Organics were extracted into ethyl acetate (100 mL), dried over magnesium sulphate and adsorbed onto silica under reduced pressure. Chromatographic purification (Biotage SP4, 50 g cartridge, solvent system: ethyl acetate/methanol, 0% 4CV; 0-2% 2CV; 2% 1CV; 2-5% 1CV; 5% 3CV; 2-10% 2CV; 10% 3 CV) yielded title product as a pale brown solid (16 mg, 10%). (LC-MS purity = 87.6%); 1H (DMSO-d6, 400 MHz) δ 3.77 (s, 1H), 6.57 (br s, 1H), 7.65 (m, 1H), 7.36 (m, 4H), 7.48 (d, J = 4 Hz, 1H), 7.56 (d, J = 6.5 Hz, 1H), 7.71 (m, 1H), 7.93 (m, 1H), 8.31 (s, 1H), 8.36 (d, J = 5.3 Hz, 1H), 8.45 (s, 1H), 10.77 (s, 1H), 12.59 (br s, 1H); HRMS (ESI +ve): For $C_{20}H_{16}N_4O$ requires 329.1397 found 329.1396.

6.50. *N*-(4-(4-((dimethylamino)methyl)phenyl)pyridin-2-yl)-2-phenylacetamide 33

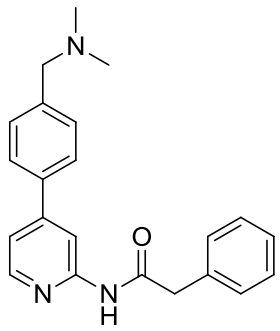

N-(4-chloropyridin-2-yl)-2-phenylacetamide (123 mg, 0.5 mmol), 4-((*N*,*N*-dimethylamino)methyl)phenylboronic acid pinacol ester (155 mg, 0.6 mmol, 1.2 equiv.) and Pd(dppf)Cl_2 (26 mg, 0.05 mmol, 0.1 equiv.), were placed in a 2-5 mL microwave vial which was sealed and purged with nitrogen. Ethanol (1.5 mL) was added and the suspension brought to 90 °C with stirring before addition of K_3PO_4 (O_2-free, 1 M, 0.75 mL). Stirring continued for 24 hours. Resultant solution was cooled and diluted in ethyl acetate, washed with water and adsorbed onto silica under reduced pressure. Chromatographic purification (Biotage SP4, 50 g cartridge, solvent system: ethyl acetate/methanol, 0% 4CV; 0-2% 2CV; 2% 3CV; 2-10% 1CV; 10% 2 CV) yielded title product as a sticky brown solid (116 mg, 67%). (LC-MS purity = 96.0%); ^{1}H (DMSO-d_6, 400 MHz) δ 2.16 (s, 6H), 3.44 (s, 2H), 3.75 (s, 2H), 7.25 (m, 1H), 7.34 (m, 4H), 7.42 (m, 3H), 7.66 (d, *J* = 7.9 Hz, 2H), 8.37 (m, 2H), 10.82 (s, 1H); ^{13}C (DMSO-d_6, 100 MHz) δ 43.50, 45.42 (2C), 63.39, 110.99, 117.53, 126.99 (2C), 127.03, 128.74 (2C), 129.69 (2C), 129.96 (2C), 136.24, 136.64, 140.75, 149.00, 149.51, 153.31, 170.69; HRMS (ESI +ve): For $C_{22}H_{23}N_3O$ requires 346.1914 found 346.1913.

6.51. 4-Bromo-*N*-phenethylpyridin-2-amine

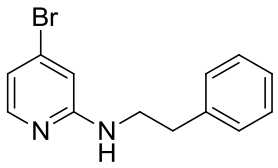

4-Bromo-2-fluoropyridine (0.10 mL, 1 mmol), phenethylamine (1.17 mL, 10 mmol) and ethanol (2 mL) were placed in a 2-5 mL microwave vial which was sealed and purged with nitrogen for 5 mins. Reaction mixture was microwaved at 140 °C for 40 mins then at 160 °C for 3 hours. Reaction was diluted with water (5 mL) and filtered, washing with a further 200 mL of water (20 x 10 mL) and hexane (8 x 10 mL) to yield title product as a pale yellow solid (223 mg, 80%). (LC-MS purity = 87.9%); ^{1}H (DMSO-d_6, 400 MHz) δ 2.81 (t, *J* = 7.5 Hz, 2H), 3.45 (q, *J* = 6.6 Hz, 2H), 6.65 (d, *J* = 4.8 Hz, 1H), 6.68 (s, 1H), 6.89 (m, 1H), 7.26 (m, 1H) 7.86 (d, *J* = 5.3 Hz, 1H); ^{13}C (DMSO-d_6, 100 MHz) δ 35.45, 42.80, 110.62, 114.64, 126.49, 128.77 (2C), 129.16 (2C), 132.08, 140.24, 149.56, 160.13.

6.52. 5-((2-Phenethylamino)pyridin-4-yl)-3-amino-1*H*-indazole 34

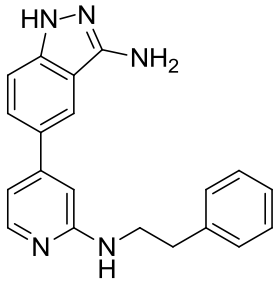

4-Bromo-*N*-phenethylpyridin-2-amine (111 mg, 0.4 mmol), 5-(4,4,5,5-Tetramethyl-1,3,2-dioxaborolan-2-yl)-1*H*-indazol-3-amine (110 mg, 0.42 mmol), Pd(dtbpf)Cl_2 (26 mg, 0.04 mmol) and ethanol (1.12 mL) were placed in a 2-5 mL microwave vial which was sealed and purged with nitrogen for 5 mins. K_3PO_4 (1 M, 0.56 mL) was added and the solution stirred at 70 °C for 24 hours. Organics were extracted into ethyl acetate (50 mL), washed with water and dried over magnesium sulphate. This was filtered and organics adsorbed onto silica. Chromatographic purification (Biotage SP4, 50 g cartridge, solvent system: ethyl acetate/methanol, 0% 2CV; 0-5% 3CV; 5% 4CV) yielded title product as a brown solid (58 mg, 44%). (LC-MS purity = 98.7%); ^{1}H (DMSO-d_6, 400 MHz) δ 2.88 (t, *J* = 7.4 Hz, 2H), 3.54 (q, *J* = 6.8 Hz, 2H), 5.47 (s, 2H), 6.55 (t, *J* = 5.5 Hz, 1H), 6.73 (s, 1H), 6.80 (dd, *J* = 5.3 & 1.5 Hz, 1H), 7.21 (m, 1H) 7.30 (m, 5H), 7.54 (dd, *J* = 8.8 & 1.8 Hz, 1H), 8.04 (d, *J* = 5.3 Hz, 1H), 8.09(d, *J* = 1 Hz, 1H), 11.52 (br s, 1H); ^{13}C (DMSO-d_6, 100 MHz) δ 35.80, 43.14, 104.99, 110.28, 110.32, 115.08, 119.06, 125.39, 126.41, 128.31, 128.76 (2C), 129.17 (2C), 141.05, 141.87, 148.60, 149.14, 150.29, 159.93; HRMS (ESI +ve): For $C_{20}H_{19}N_5$ requires 330.1713 found 330.1712.

6.53. *N*-(4-chloropyridin-2-yl)-3-phenylpropanamide

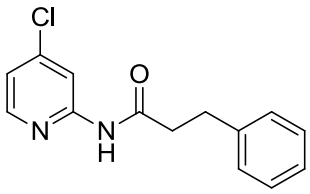

2-Amino-4-chloropyridine (167 mg, 1.3 mmol) and hydrocinnamic acid (150.2 mg, 1 mmol) were dissolved in THF (5 mL, anhydrous) to which triethylamine (0.54 mL, 4 mmol) was added. Stirring continued for 15 mins before addition of T3P (50% w/w in DMF, 1.16 mL, 2 mmol). Reaction mixture was stirred at room temperature for 28 hours. Reaction was quenched with water (50 mL), and organics extracted into ethyl acetate (250 mL). These were dried over magnesium sulphate, filtered and adsorbed onto silica under reduced pressure. Chromatographic purification (Biotage SP4, 50 g cartridge, solvent system: hexane/ethyl acetate, 30% 3CV; 30-50% 3CV; 50% 3CV) yielded title product as an off-white solid (78 mg, 30%). (LC-MS purity = ??.?%); ^{1}H (DMSO-d_6, 400 MHz) δ 2.73 (t-like, *J* = 7.6 Hz, 2H), 2.91 (t-like, *J* = 7.6 Hz, 2H), 7.23 (m, 6H), 8.19 (d, *J* = 1.8 Hz, 1H), 8.29 (d, *J* = 5.5 Hz, 1H), 10.76 (s, 1H); ^{13}C (DMSO-d_6, 100 MHz) δ 30.97, 38.10, 113.27, 119.71, 126.44, 128.73 (2C), 128.78 (2C), 141.42, 144.39, 149.88, 153.60, 172.34.

6.54. *N*-(4-(3-amino-1*H*-indazol-5-yl)pyridin-2-yl)-3-phenylpropanamide 35

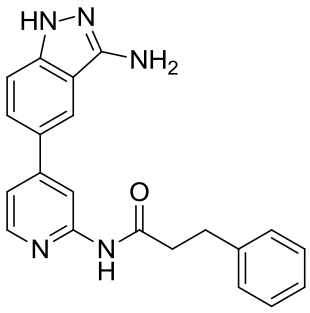

5-(4,4,5,5-Tetramethyl-1,3,2-dioxaborolan-2-yl)-1*H*-indazol-3-amine (43 mg, 0.17 mmol), *N*-(4-chloropyridin-2-yl)-3-phenylpropanamide (37 mg, 0.14 mmol) in ethanol (O_2-free, 0.4 mL) and Pd(dtbpf)Cl_2 (9 mg, 0.017 mmol) were placed in a 2-5 mL microwave vial which was sealed and purged with nitrogen for 5 mins. The suspension stirred at 50 °C under nitrogen for a further 5 mins. K_3PO_4 (1 M, 0.2 mL) was added and the solution stirred at 70 °C for 24 hours. Reaction was quenched with water (5 mL) and precipitate was filtered, washed with water (10 x 5 mL) and hexane (5 x 5 mL), dissolved in ethyl acetate and adsorbed onto silica under reduced pressure. Chromatographic purification (Biotage SP4, 50 g cartridge, solvent system: ethyl acetate/methanol, 0% 2CV; 0-5% 3CV; 5% 4CV) yielded title product as a grey/green solid (27 mg, 54%). (LC-MS purity = 97.3%); ^{1}H (DMSO-d_6, 400 MHz) δ 2.76 (t, *J* = 7.3 Hz, 2H), 2.94 (t, *J* = 7.8 Hz, 2H), 5.55 (s, 2H), 7.19 (m, 1H), 7.29 (m, 4H), 7.37 (m, 2H), 7.60 (dd, *J* = 8.8, 1.5 Hz, 1H), 8.17 (s, 1H), 8.32 (d, *J* = 5.3 Hz, 1H), 8.46 (s, 1H), 10.51 (s, 1H), 11.59 (br s, 1H); ^{13}C (DMSO-d_6, 100 MHz) δ 31.10, 38.10, 110.63, 115.16, 117.18, 119.66, 125.51, 126.42, 127.47, 128.75 (2C), 128.79 (2C), 141.59, 142.00, 148.75, 150.46, 150.56, 153.28, 171.92; HRMS (ESI +ve): For $C_{21}H_{19}N_5O$ requires 358.1662 found 358.1659.

6.55. 3-(Pyridine-4-yl)benzamide 36

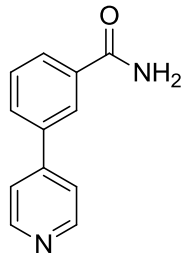

3-Carboxamidephenylboronic acid (165 mg, 1 mmol), 4-chloropyridine hydrochloride (119 mg, 0.8 mmol) and Pd(dtbpf)Cl_2 (26 mg, 0.04 mmol) were placed in a 10-20 mL microwave vial which was sealed and purged with nitrogen. Ethanol (3.2 mL) was added and the suspension brought to 90 °C with stirring before addition of K_3PO_4 (O_2-free, 1 M, 1.6 mL). Stirring continued for 24 hours. Resultant solution was diluted in ethyl acetate, washed with water and adsorbed onto silica under reduced pressure. Chromatographic purification (Biotage SP4, 50 g cartridge, solvent system: isocratic, ethyl acetate/0.5% triethylamine/10% methanol; 15 CV yielded product as a white solid. (130 mg, 82%). (LC-MS purity = 99.7%); ^{1}H (DMSO-d_6, 500 MHz) δ 7.49 (br s, 1H), 7.61 (t, *J* = 7.7 Hz, 1H), 7.77 (dd, *J* = 4.4 & 1.6 Hz, 2H), 7.95 (m, 2H), 8.15 (br s, 1H), 8.28 (t, *J* = 1.7 Hz, 1H), 8.66 (dd, *J* = 4.7 & 1.6 Hz, 2H); ^{13}C (DMSO-d_6, 125 MHz) δ 121.8, 126.23, 128.83, 129.74, 130.00, 135.66, 137.65, 146.92, 150.77, 167.93; HRMS (ESI +ve): For $C_{12}H_{11}N_2O$ requires 199.0866 found 199.0864.

6.56. 3'-Amino-[1,1'-biphenyl]-3-carboxamide 37

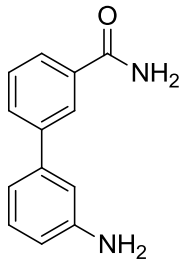

3-Carboxamidephenylboronic acid (165 mg, 1 mmol), 3-chloroaniline (84 µL, 0.8 mmol) and Pd(dtbpf)Cl_2 (26 mg, 0.04 mmol) were placed in a 10-20 mL microwave vial which was sealed and purged with nitrogen. Ethanol (3.2 mL) was added and the suspension brought to 90 °C with stirring before addition of K_3PO_4 (O_2-free, 1 M, 1.6 mL). Stirring continued for 24 hours. Resultant solution was diluted in ethyl acetate, washed with water and adsorbed onto silica under reduced pressure. Chromatographic purification (Biotage SP4, 50 g cartridge, solvent system: pet. ether/ethyl acetate, 20%, 2 CV; 20-80%, 1 CV; 80%, 4 CV; 100%, 6 CV) yielded product as a pale yellow solid (132 mg, 78%). (LC-MS purity = 99.1%); ^{1}H (DMSO-d_6, 500 MHz) δ 5.16 (s, 2H), 6.58 (dd, *J* = 8 & 1.4 Hz, 1H), 6.83 (d, *J* = 7.8 Hz, 1H), 6.89 (t, *J* = 1.7 Hz, 1H), 7.11 (t, *J* = 7.8 Hz, 1H), 7.38 (br s, 1H), 7.49 (t, *J* = 7.8 Hz, 1H), 7.49 (d, *J* = 7.8 Hz, 1H), 7.69 (d, *J* = 7.8 Hz, 1H), 7.82 (d, *J* = 7.8 Hz, 1H), 8.07 (m, 2 H); ^{13}C (DMSO-d_6, 125 MHz) δ 112.67, 113.88, 114.90, 126.06, 126.62, 129.16, 129.60, 129.92, 135.25, 140.77, 141.52, 149.64, 168.39; HRMS (ESI +ve): For $C_{13}H_{13}N_2O$ requires 213.1022 found 213.1021.

6.57. 3-(2-Aminopyridin-4-yl)benzamide 38

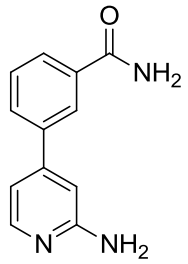

3-Carboxamidephenylboronic acid (165 mg, 1 mmol), 2-amino-4-chloropyridine (102 mg, 0.8 mmol) and Pd(dtbpf)Cl_2 (26 mg, 0.04 mmol) were placed in a 10-20 mL microwave vial which was sealed and purged with nitrogen. Ethanol (3.2 mL) was added and the suspension brought to 90 °C with stirring before addition of K_3PO_4 (O_2-free, 1 M, 1.6 mL). Stirring continued for 24 hours. Resultant solution was diluted in ethyl acetate, washed with water and adsorbed onto silica under reduced pressure. Chromatographic purification (Biotage SP4, 50 g cartridge, solvent system: pet. ether/ethyl acetate, 20%, 2 CV; 20-80%, 1 CV; 80%, 4 CV; 100%, 6 CV) yielded product as a pale yellow solid (42 mg, 25%) (LC-MS purity = 97.6%); ^{1}H (DMSO-d_6, 500 MHz) δ 5.98 (s, 2H), 6.76 (s, 1H), 6.84 (d, *J* = 4.4 Hz, 1H), 7.43 (s, 1H), 7.55 (t, *J* = 7.8 Hz, 1H), 7.77 (d, *J* = 7.8 Hz, 1H), 7.91 (d, *J* = 7.8 Hz, 1H), 8.00 (d, *J* = 4.7 Hz, 1H), 8.09 (s, 1H), 8.14 (s, 1H); ^{13}C (DMSO-d_6, 125 MHz) δ 105.66, 110.58, 125.99, 128.17, 129.49, 129.59, 135.46, 138.88, 148.07, 148.99, 160.95, 168.06; HRMS (ESI +ve): For $C_{12}H_{12}N_3O$ requires 214.0975 found 214.0973.

6.58. 3-(6-Aminopyrimidin-4-yl)benzamide 39

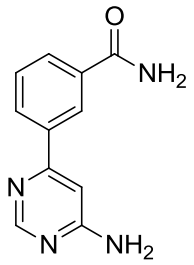

3-Carboxamidephenylboronic acid (165 mg, 1 mmol), 6-amino-4-chloropyrimidine (104 mg, 0.8 mmol) and Pd(dtbpf)Cl_2 (26 mg, 0.04 mmol) were placed in a 10-20 mL microwave vial which was sealed and purged with nitrogen. Ethanol (3.2 mL) was added and the suspension brought to 80 °C with stirring before addition of K_3PO_4 (O_2-free, 1 M, 1.6 mL). Stirring continued for 24 hours. Reaction was allowed to cool to room temperature before water (10 mL) was added. Resultant suspension was filtered, washing with small quantities of water, pet. ether and methanol to yield product as a pale yellow solid (66 mg, 39%) (LC-MS purity = 87.7%); ^{1}H (DMSO-d_6, 500 MHz) δ 6.93 (br s, 2H), 6.96 (br s, 1H), 7.42 (br s, 1H), 7.56 (m, 1H), 7.95 (d, *J* = 6 Hz, 1H), 8.11 (br s, 2H), 8.46 (br s, 2H); ^{13}C (DMSO-d_6, 125 MHz) δ 100.47, 126.06, 129.19, 129.31, 129.48, 135.30, 137.87, 159.13, 160.80, 164.92, 168.12; HRMS (ESI +ve): For $C_{11}H_{11}N_4O$ requires 215.0927 found 215.0925.

6.59. 3-(7*H*-pyrrolo[2,3-d]pyrimidin-4-yl)benzamide 40

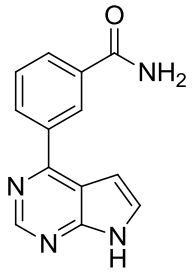

3-Carboxamidephenylboronic acid (165 mg, 1 mmol), 4-chloro-7*H*-pyrrolo[2,3-*d*]pyrimidine (123 mg, 0.8 mmol) and Pd(dtbpf)Cl_2 (26 mg, 0.04 mmol) were placed in a 10-20 mL microwave vial which was sealed and purged with nitrogen. Ethanol (3.2 mL) was added and the suspension brought to 80 °C with stirring before addition of K_3PO_4 (O_2-free, 1 M, 1.6 mL). Stirring continued for 24 hours. Reaction was allowed to cool to room temperature before water (10 mL) was added. Resultant suspension was filtered, washing with small quantities of water, pet. ether and methanol to yield product as a pale brown solid (136 mg, 71%). (LC-MS purity = 98.4%); ^{1}H (DMSO-d_6, 500 MHz) δ 6.90 (br s, 1H), 7.47 (br s, 1H), 7.68 (m, 2H), 8.03 (d, *J* = 6.3 Hz, 1H), 8.15 (br s, 1H), 8.30 (d, *J* = 6 Hz, 1H), 8.64 (br s, 1H), 8.86 (br s, 1H), 12.29 (br s, 1H); ^{13}C (DMSO-d_6, 125 MHz) δ 100.34, 115.06, 128.12, 128.41, 129.32 (2C), 131.66, 135.49, 138.48, 151.38, 153.11, 155.43, 168.18; HRMS (ESI +ve): For $C_{13}H_{11}N_4O$ requires 239.0927 found 239.0924.

6.60. 3-(1*H*-pyrrolo[2,3-*b*]pyridin-4-yl)benzamide 41

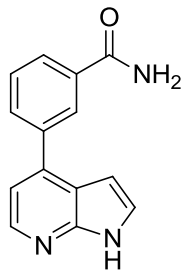

3-Carboxamidephenylboronic acid (165 mg, 1 mmol), 4-bromo-7*H*-pyrrolo[2,3-*b*]pyridine (157 mg, 0.8 mmol) and Pd(dtbpf)Cl_2 (26 mg, 0.04 mmol) were placed in a 10-20 mL microwave vial which was sealed and purged with nitrogen. Ethanol (3.2 mL) was added and the suspension brought to 70 °C with stirring before addition of K_3PO_4 (O_2-free, 1 M, 1.6 mL). Stirring continued for 24 hours. Reaction was allowed to cool to room temperature before water (10 mL) was added. Resultant suspension was filtered, washing with small quantities of water, pet. ether and methanol to yield product as a pale brown solid (144 mg, 76%). (LC-MS purity = >99.9%); ^{1}H (DMSO-d_6, 500 MHz) δ 6.61 (br s, 1H), 7.25 (d, *J* = 3.5 Hz, 1H), 7.45 (br s, 1H), 7.56 (br s, 1H), 7.63 (t, *J* = 6.6 Hz, 1H), 7.91 (d, *J* = 6.9 Hz, 1H), 7.95 (d, *J* = 6.6 Hz, 1H), 8.12 (br s, 1H), 8.25 (br s, 1H), 8.31 (d, *J* = 2.8 Hz, 1H), 11.82 (br s, 1H); ^{13}C (DMSO-d_6, 125 MHz) δ 99.37, 114.80, 117.70, 127.28, 127.68, 127.85, 129.44, 131.39, 135.57, 138.97, 140.11, 143.41, 149.63, 168.23; HRMS (ESI +ve): For $C_{14}H_{12}N_3O$ requires 238.0975 found 238.0972.

6.61. 3-(2-Amino-7*H*-pyrrolo[2,3-*d*]pyrimidin-4-yl)benzamide 42

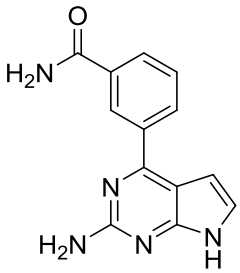

3-Carboxamidephenylboronic acid (165 mg, 1 mmol), 4-chloro-7*H*-pyrrolo[2,3-*d*]pyrimidin-2-amine (135 mg, 0.8 mmol) and Pd(dtbpf)Cl_2 (26 mg, 0.04 mmol) were placed in a 10-20 mL microwave vial which was sealed and purged with nitrogen. Ethanol (3.2 mL) was added and the suspension brought to 90 °C with stirring before addition of K_3PO_4 (O_2-free, 1 M, 1.6 mL). Stirring continued for 24 hours. Reaction was allowed to cool to room temperature before water (20 mL) was added. Resultant suspension was filtered, washing with water and pet. ether to yield product as a tan solid (189 mg, 93%). (LC-MS purity = 97.6%); ^{1}H (DMSO-d_6, 400 MHz) δ 6.16 (s, 2H), 6.57 (d, *J* = 2 Hz, 1H), 7.14 (br s, 1H), 7.43 (br s, 1H), 7.61 (t, *J* = 7.7 Hz, 1H), 7.98 (d, *J* = 7.8 Hz, 1H), 8.01 (br s, 1H), 8.18 (d, *J* = 7.8 Hz, 1H), 8.54 (s, 1H), 11.29 (br s, 1H); ^{13}C (DMSO-d_6, 100 MHz) δ100.32, 108.15, 123.61, 128.06, 128.78, 128.93, 131.40, 135.24, 139.03, 155.79, 156.59, 160.40, 168.31; HRMS (ESI +ve): For $C_{13}H_{12}N_5O$ requires 254.1036 found 254.1036.

6.62. 3-(2,6-Diaminopyrimidin-4-yl)benzamide 43

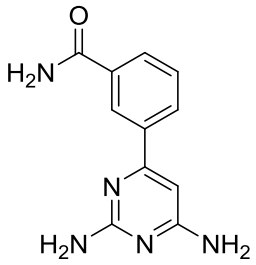

3-Carboxamidephenylboronic acid (165 mg, 1 mmol), 6-chloropyrimidine-2,4-diamine (116 mg, 0.8 mmol) and Pd(dtbpf)Cl_2 (26 mg, 0.04 mmol) were placed in a 10-20 mL microwave vial which was sealed and purged with nitrogen. Ethanol (3.2 mL) was added and the suspension brought to 90 °C with stirring before addition of K_3PO_4 (O_2-free, 1 M, 1.6 mL). Stirring continued for 24 hours. Reaction was allowed to cool to room temperature before water (20 mL) was added. Resultant suspension was filtered, washing with water and pet. ether to yield product as a tan solid (158 mg, 86%). (LC-MS purity = 87.5%); ^{1}H (DMSO-d_6, 400 MHz) δ 5.98 (s, 2H), 6.28 (s, 1H), 6.36 (br s, 2H), 7.39 (br s, 1H), 7.52 (t, *J* = 7.7 Hz, 1H), 7.91 (d, *J* = 7.8 Hz, 1H), 8.04 (m, 2H), 8.41 (s, 1H); ^{13}C (DMSO-d_6, 100 MHz) δ 91.28, 126.16, 128.62, 128.76, 129.34, 135.03, 138.93, 162.16, 164.16, 164.18, 165.72, 168.37; HRMS (ESI +ve): For $C_{11}H_{12}N_5O$ requires 230.1036 found 230.1037.

6.63. 4-Phenyl-7*H*-pyrrolo[2,3-*d*]pyrimidine 44

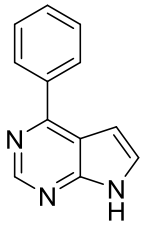

4-Chloro-7*H*-pyrrolo[2,3-*d*]pyrimidine (123 mg, 0.8 mmol), phenylboronic acid (122 mg, 1 mmol) and Pd(dtbpf)Cl_2 (26 mg, 0.04 mmol) were placed in a 2-5 mL microwave vial which was sealed and purged with nitrogen. Ethanol (3.2 mL) was added and stirring continued under nitrogen for a further 5 minutes. The suspension brought to 90 °C with stirring before addition of K_3PO_4 (O_2-free, 1 M, 1.6 mL). Stirring continued for 24 hours. Reaction was allowed to cool to room temperature before water (5 mL) was added. Precipitate was filtered, washing with water and pet. ether, to yield title compound as a pale orange solid (148 mg, 95%). (LC-MS purity = 91.5%); ^{1}H (DMSO-d_6, 400 MHz) δ 6.88 (d, *J* = 3.5 Hz, 1H), 7.57 (m, 3H), 7.65 (d, *J* = 3.5 Hz, 1H), 8.17 (m, 2H), 8.83 (s, 1H), 12.24 (br. s, 1H); ^{13}C (DMSO-d_6, 100 MHz) δ 99.89, 114.45, 127.64, 128.49 (2C), 128.77 (2C), 137.90, 150.88, 152.56, 155.49. HRMS (ESI +ve): For $C_{13}H_{10}N_3$ requires 196.1869 found 196.1868.

6.64. 4-(*m*-Tolyl)-7*H*-pyrrolo[2,3-*d*]pyrimidine 45

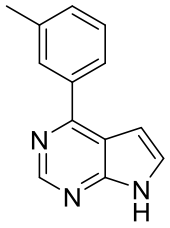

4-Chloro-7*H*-pyrrolo[2,3-*d*]pyrimidine (153 mg, 1 mmol), *m*-tolylboronic acid (136 mg, 1 mmol) and Pd(dtbpf)Cl_2 (26 mg, 0.04 mmol) were placed in a 2-5 mL microwave vial which was sealed and purged with nitrogen. Ethanol (3.2 mL) was added and stirring continued under nitrogen for a further 5 minutes. The suspension brought to 90 °C with stirring before addition of K_3PO_4 (O_2-free, 1 M, 1.6 mL). Stirring continued for 24 hours. Reaction was allowed to cool to room temperature before water (5 mL) was added. Precipitate was filtered, washing with water and pet. ether, to yield title compound as a pale orange solid (182 mg, 87%). ^{1}H (DMSO-d_6, 400 MHz) δ 2.44 (s, 3H), 6.88 (d, *J* = 3.5 Hz, 1H), 7.35 (d, *J* = 7.6 Hz, 1H), 7.46 (t, *J* = 7.6 Hz, 1H), 7.64 (d, *J* = 3.5 Hz, 1H), 7.96 (m, 2H), 8.81 (s, 1H), 12.22 (br. s, 1H); ^{13}C (DMSO-d_6, 100 MHz) δ 21.07, 100.00, 114.47, 125.71, 127.53, 128.66, 128.97, 130.58, 137.90, 137.99, 150.84, 152.53, 155.63. HRMS (ESI +ve): For $C_{13}H_{12}N_3$ requires 210.1026 found 210.1028.

6.65. 3-(7*H*-pyrrolo[2,3-*d*]pyrimidin-4-yl)aniline 46

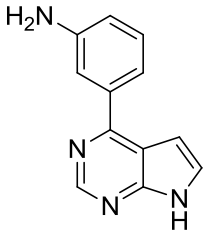

4-Chloro-7*H*-pyrrolo[2,3-*d*]pyrimidine (153 mg, 1 mmol), 3-aminophenylboronic acid (137 mg, 1.2 mmol) and Pd(dtbpf)Cl_2 (36 mg, 0.05 mmol) were placed in a 2-5 mL microwave vial which was sealed and purged with nitrogen. Ethanol (3 mL) was added and stirring continued under nitrogen for a further 5 minutes. The suspension brought to 85 °C with stirring before addition of K_3PO_4 (O_2-free, 1 M, 1.5 mL). Stirring continued for 24 hours. Reaction was allowed to cool to room temperature before water (5 mL) was added. Organics were extracted into ethyl acetate, washed with water and dried over magnesium sulphate. Solution was filtered and adsorbed onto silica. Chromatographic purification (Biotage SP4, 50 g cartridge, solvent system: pet. ether 40-60/ethyl acetate/1% triethylamine, 50%, 4 CV; 50-100%, 1 CV; 100%, 9 CV; ethyl acetate/1% triethylamine/methanol, 5%, 4 CV) yielded product as a pale yellow solid (82 mg, 39%). (LC-MS purity = > 99.9.%); ^{1}H (DMSO-d_6, 400 MHz) δ 5.28 (s, 2H), 6.71 (ddd, *J* = 7.8, 2.2 & 0.9 Hz, 1H), 6.94 (dd, *J* = 3.6 & 1.7 Hz, 1H), 7.19 (t, *J* = 7.7 Hz, 1H), 7.31 (dt, *J* = 7.5 & 0.9 Hz, 1H), 7.44 (t, *J* = 1.9 Hz, 1H), 7.60 (dd, *J* = 3.3 & 2.4 Hz, 1H), 8.77 (s, 1H), 12.15 (br s, 1H); ^{13}C (DMSO-d_6, 100 MHz) δ 100.22, 113.92, 114.37, 115.49, 116.15, 127.09, 129.12, 138.54, 149.01, 150.75, 152.50, 156.37; HRMS (ESI +ve): For $C_{12}H_{11}N_4$ requires 211.0978 found 211.0977.

6.66. 3-(7*H*-pyrrolo[2,3-*d*]pyrimidin-4-yl)phenol 47

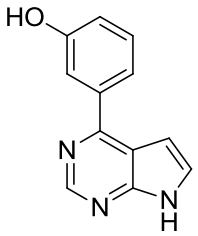

4-Chloro-7*H*-pyrrolo[2,3-*d*]pyrimidine (153 mg, 1 mmol), 3-hydroxyphenylboronic acid (164.3 mg, 1.2 mmol) and Pd(dtbpf)Cl_2 (36 mg, 0.05 mmol) were placed in a 2-5 mL microwave vial which was sealed and purged with nitrogen. Ethanol (3 mL) was added and stirring continued under nitrogen for a further 5 minutes. The suspension brought to 85 °C with stirring before addition of K_3PO_4 (O_2-free, 1 M, 1.5 mL). Stirring continued for 24 hours. Reaction was allowed to cool to room temperature before water (5 mL) was added. Organics were extracted into ethyl acetate, washed with water and dried over magnesium sulphate. Solution was filtered and adsorbed onto silica. Chromatographic purification (Biotage SP4, 50 g cartridge, solvent system: pet. ether 40-60/ethyl acetate/1% triethylamine, 100%, 15 CV) yielded product as a pale yellow solid (72 mg, 34%). (LC-MS purity = 98.5.%); ^{1}H (DMSO-d_6, 400 MHz) δ 6.84 (dd, *J* = 3.5 & 1 Hz, 1H), 6.94 (ddd, *J* = 8, 2.3 & 1.3 Hz, 1H), 7.38 (t, *J* = 7.9 Hz, 1H), 7.61 (m, 2H), 7.65 (dd, *J* = 3.4 & 2.1 Hz, 1H), 8.82 (s, 1H), 9.65 (s, 1H), 12.22 (br s, 1H); ^{13}C (DMSO-d_6, 100 MHz) δ 100.41, 114.91, 115.63, 117.51, 119.81, 128.02, 130.29, 139.71, 151.31, 153.06, 156.03, 158.13; HRMS (ESI +ve): For $C_{12}H_{10}N_4O$ requires 212.0818 found 212.0818.

6.67. (3-(7*H*-pyrrolo[2,3-*d*]pyrimidin-4-yl)phenyl)methanol 48

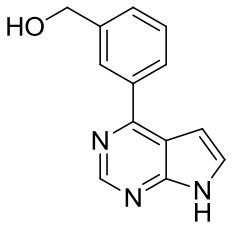

4-Chloro-7*H*-pyrrolo[2,3-*d*]pyrimidine (153 mg, 1 mmol), 3-(hydroxymethyl)phenylboronic acid (152 mg, 1.2 mmol) and Pd(dtbpf)Cl_2 (36 mg, 0.05 mmol) were placed in a 2-5 mL microwave vial which was sealed and purged with nitrogen. Ethanol (3 mL) was added and stirring continued under nitrogen for a further 5 minutes. The suspension brought to 85 °C with stirring before addition of K_3PO_4 (O_2-free, 1 M, 1.5 mL). Stirring continued for 24 hours. Reaction was allowed to cool to room temperature before water (5 mL) was added. Organics were extracted into ethyl acetate, washed with water and dried over magnesium sulphate. Solution was filtered and adsorbed onto silica. Chromatographic purification (Biotage SP4, 50 g cartridge, solvent system: pet. ether 40-60/ethyl acetate, 70-100%, 3 CV; 100%, 13 CV) yielded product as an off-white solid (26 mg, 12%). (LC-MS purity = >99.9%); ^{1}H (DMSO-d_6, 400 MHz) δ 4.65 (d, *J* = 5.5 Hz, 2H), 5.33 (t, *J* = 5.8 Hz, 1H), 6.90 (d, *J* = 3.5 Hz, 1H), 7.48 (m, 1H), 7.54 (t, *J* = 7.5 Hz, 1H), 7.66 (d, *J* = 3.5 Hz, 1H), 8.05 (dt, *J* = 7.7 & 1.4 Hz, 1H), 8.17 (d, *J* = 0.5 Hz, 1H), 8.84 (s, 1H), 12.24 (br s, 1H); ^{13}C (DMSO-d_6, 100 MHz) δ 63.27, 100.49, 114.98, 126.99, 127.36, 128.07, 128.49, 129.02, 138.26, 143.70, 151.37, 153.07, 156.16; HRMS (ESI +ve): For $C_{13}H_{12}N_3O$ requires 226.0975 found 226.0972.

6.68. 3-(7*H*-pyrrolo[2,3-*d*]pyrimidin-4-yl)benzonitrile 49

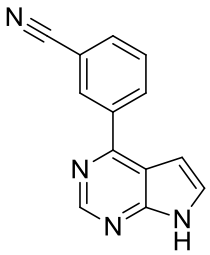

4-Chloro-7*H*-pyrrolo[2,3-*d*]pyrimidine (153 mg, 1 mmol), 3-cyanophenylboronic acid (147 mg, 1.2 mmol) and Pd(dtbpf)Cl_2 (36 mg, 0.05 mmol) were placed in a 2-5 mL microwave vial which was sealed and purged with nitrogen. Ethanol (3 mL) was added and stirring continued under nitrogen for a further 5 minutes. The suspension brought to 85 °C with stirring before addition of K_3PO_4 (O_2-free, 1 M, 1.5 mL). Stirring continued for 24 hours. Reaction was allowed to cool to room temperature before water (5 mL) was added. Organics were extracted into ethyl acetate, washed with water and dried over magnesium sulphate. Solution was filtered and adsorbed onto silica. Chromatographic purification (Biotage SP4, 50 g cartridge, solvent system: pet. ether 40-60/ethyl acetate, 70-100%, 4 CV; 100%, 7 CV; ethyl acetate/methanol, 10%, 6 CV) yielded product as a white solid (82 mg, 37%). (LC-MS purity = 98.4%); ^{1}H (DMSO-d_6, 400 MHz) δ 6.99 (d, *J* = 3.5 Hz, 1H), 7.73 (d, *J* = 3.5 Hz, 1H), 7.81 (td, *J* = 7.8 & 0.5 Hz, 1H), 8.03 (dt, *J* = 7.9 & 1.3 Hz, 1H), 8.52 (m, 2H), 8.89 (2, 1H), 12.38 (br s, 1H); ^{13}C (DMSO-d_6, 100 MHz) δ 100.20, 112.61, 115.11, 119.02, 128.97, 130.70, 132.26, 133.64, 133.94, 139.47, 151.34, 153.27, 153.62; HRMS (ESI +ve): For $C_{13}H_9N_4$ requires 221.0822 found 221.0819.

6.69. 3-(7*H*-pyrrolo[2,3-*d*]pyrimidin-4-yl)benzoic acid 50

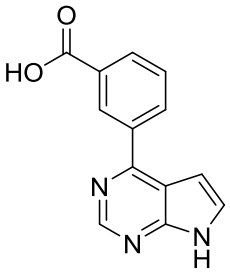

4-Chloro-7*H*-pyrrolo[2,3-*b*]pyridine (123 mg, 0.8 mmol), 3-boronobenzoic acid (166 mg, 1 mmol) and Pd(dtbpf)Cl_2 (26 mg, 0.04 mmol) were placed in a 2-5 mL microwave vial which was sealed and purged with nitrogen. Ethanol (3.2 mL) was added and stirring continued under nitrogen for a further 5 minutes. The suspension brought to 90 °C with stirring before addition of K3PO4 (O2-free, 1 M, 1.6 mL). Stirring continued for 24 hours. Reaction was allowed to cool to room temperature before water (5 mL) was added. Precipitate was filtered, washing with water and pet. ether, to yield title compound as a pale orange solid (183 mg, 96%). (LC-MS purity = 97.5%); ^{1}H (DMSO-d_6, 400 MHz) δ 6.87 (dd, *J* = 3.5 & 1.8 Hz, 1H), 7.71 (m, 2H), 8.10 (dt, *J* = 7.8 & 1.3 Hz, 1H), 8.41 (dt, *J* = 7.9 & 1.4 Hz, 1H), 8.76 (t, *J* = 1.6Hz, 1H), 8.87 (s, 1H), 12.32 (br s, 1H), 13.19 (br s, 1H); ^{13}C (DMSO-d_6, 100 MHz) δ 99.60, 114.48, 128.13, 129.19, 129.27, 130.58, 131.46, 132.63, 138.16, 150.90, 152.99, 154.69, 154.37, 167.01; HRMS (ESI +ve): For $C_{13}H_{10}N_3O_2$ requires 240.0768 found 240.0768.

6.70. 1-(3-(7*H*-pyrrolo[2,3-*d*]pyrimidin-4-yl)phenyl)urea 51

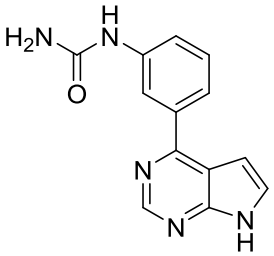

3-(7*H*-pyrrolo[2,3-*d*]pyrimidin-4-yl)aniline (42 mg, 0.2 mmol) and potassium cyanate (52 mg, 0.6 mmol) were diluted in acetic acid (9 mL) and water (1 mL) and stirred at room temperature for 24 hours. Solution was diluted in water and organics were extracted into ethyl acetate before solvent was removed under reduced pressure to yield title compound as a pale brown solid (18 mg, 36%). (LC-MS purity = 95.0%); ^{1}H (DMSO-d_6, 400 MHz) δ 5.89 (s, 2H), 6.90 (d, *J* = 3.5 Hz, 1H), 7.41 (t, *J* = 7.7 Hz, 1H), 7.50 (ddd, *J* = 8.0, 2.2 & 1 Hz, 1H), 7.64 (d, *J* = 3 Hz, 1H), 7.72 (dt, *J* = 7.8 & 1.3 Hz, 1H), 8.36 (t, *J* = 1.9 Hz, 1H), 8.80 (s, 1H), 8.81 (s, 1H), 12.21 (br s, 1H); ^{13}C (DMSO-d_6, 100 MHz) δ 100.01, 114.44, 117.96, 119.18, 121.18, 127.48, 128.98, 138.18, 140.94, 150.79, 152.58, 155.59, 156.03; HRMS (ESI +ve): For $C_{13}H_{12}N_5O$ requires 254.1036 found 254.1035.

6.71. 3-(1*H*-pyrrolo[2,3-*b*]pyridin-4-yl)benzenesulfonamide 52

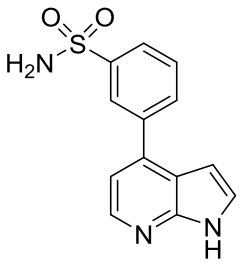

4-Chloro-7*H*-pyrrolo[2,3-*b*]pyridine (38 mg, 0.25 mmol), (3-sulfamoylphenyl)boronic acid (50 mg, 0.25 mmol) and Pd(dtbpf)Cl_2 (16.3 mg, 0.025 mmol) were placed in a 2-5 mL microwave vial which was sealed and purged with nitrogen. Dioxane (1.5 mL) was added and stirring continued under nitrogen for a further 5 minutes. The suspension brought to 110 °C with stirring before addition of K_2CO_3 (O_2-free, 2 M, 0.5 mL, 1 mmol). Stirring continued for 24 hours. Reaction was allowed to cool to room temperature before water (5 mL) was added. Organics were extracted into ethyl acetate, washed with water and dried over magnesium sulphate. Solution was filtered and adsorbed onto silica. Chromatographic purification (Biotage SP4, 10 g cartridge, solvent system: ethyl acetate, 100%, 10 CV) yielded product as a pale brown solid (25 mg, 37%). (LC-MS purity = 96.3%); ^{1}H (DMSO-d_6, 400 MHz) δ 6.64 (dd, *J* = 3.3 & 1.8 Hz, 1H), 7.23 (d, *J* = 5.1 Hz, 1H), 7.46 (s, 2H), 7.61 (t, *J* = 3 Hz, 1H), 7.75 (t, *J* = 7.6 Hz, 1H), 7.91 (d, *J* = 7.8 Hz, 1H), 7.99 (d, *J* = 7.8 Hz, 1H), 8.22 (s, 1H), 8.33 (d, *J* = 4.8 Hz, 1H), 11.88 (br s, 1H); ^{13}C (DMSO-d_6, 100 MHz) δ 98.66, 114.16, 117.04, 125.19, 125.34, 127.16, 129.80, 131.40, 138.61, 139.10, 142.99, 144.77, 149.16; HRMS (ESI -ve): For $C_{13}H_{10}N_3O_2S$ requires 272.0499 found 272.0504.

6.72. *N*-(3-(dimethylamino)propyl)-3-(7*H*-pyrrolo[2,3-*d*]pyrimidin-4-yl)benzamide 53

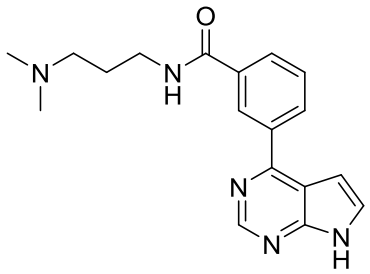

3-(7*H*-pyrrolo[2,3-*d*]pyrimidin-4-yl)benzoic acid (120 mg, 0.5 mmol), *N*,*N*-dimethylpropane-1,3-diamine (81 µL, 0.65 mmol) and triethylamine (0.27 mL, 2 mmol) were stirred in THF (8 mL) under nitrogen for 5 mins after which T3P (50% w/w in DMF, 0.58 mL, 1 mmol) was added and the solution stirred at room temperature for 24 hours. Solution was diluted in water, extracted into ethyl acetate and dried over magnesium sulphate. Solution was filtered and solvent removed under reduced pressure. Solids were triturated with ethyl acetate (2 mL) and oven dried to yield title product as a white solid (51 mg, 32%) (LC-MS purity = 86.0%); ^{1}H (DMSO-d_6, 400 MHz) δ 1.73 (qu, *J* = 7.1 Hz, 2H), 2.26 (s, 6H), 2.42 (t, *J* = 6.9 Hz, 2H), 3.34 (m, 2H), 6.91 (dd, *J* = 3.5 & 1.5 Hz, 1H), 7.96 (m, 2H), 8.00 (dt, *J* = 8 & 1.3 Hz, 1H), 8.31 (dt, *J* = 7.8 & 1.4 Hz, 1H), 8.62 (t, *J* = 1.6 Hz, 1H), 8.73 (t, *J* = 5.5 Hz, 1H), 8.88 (s, 1H), 12.31 (br s, 1H); ^{13}C (DMSO-d_6, 100 MHz) δ 27.07, 38.17, 45.20, 57.14, 100.33, 115.05, 127.65, 128.45, 129.06, 129.38, 131.51, 135.78, 138.49, 151.39, 153.13, 155.38, 166.35; HRMS (ESI +ve): For $C_{18}H_{22}N_5O$ requires 324.1819 found 324.1822.

6.73. *N*-(3-methoxypropyl)-3-(7*H*-pyrrolo[2,3-*d*]pyrimidin-4-yl)benzamide 54

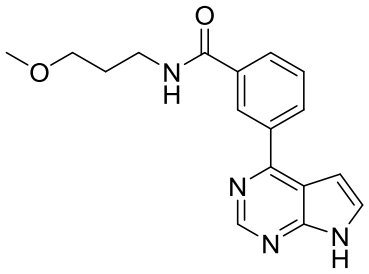

3-(7*H*-pyrrolo[2,3-*d*]pyrimidin-4-yl)benzoic acid (120 mg, 0.5 mmol), 3-methoxypropylamine (76 µL, 0.75 mmol) and triethylamine (0.27 mL, 2 mmol) were stirred in THF (8 mL) under nitrogen for 5 mins after which T3P (50% w/w in DMF, 0.58 mL, 1 mmol) was added and the solution stirred at room temperature for 24 hours. Solution was diluted in water, extracted into ethyl acetate and dried over magnesium sulphate. Solution was filtered and solvent removed under reduced pressure. Solids were triturated with diethyl ether (2 mL) and oven dried to yield title product as an off-white solid (58 mg, 37%) (LC-MS purity = 97.2%); ^{1}H (DMSO-d_6, 400 MHz) δ 1.80 (qu, *J* = 6.7 Hz, 2H), 3.31 (s, 3H), 3.36 (q, *J* = 6.8 Hz, 2H), 3.41 (t, *J* = 6.3 Hz, 2H), 6.91 (dd, *J* = 3.5 & 1.5 Hz, 1H), 7.69 (m, 2H), 8.00 (dt, *J* = 7.9 & 1.3 Hz, 1H), 8.31 (dt, *J* = 7.8 & 1.4 Hz, 1H), 8.62 (t, *J* = 1.6 Hz, 1H), 8.65 (t, *J* = 5.5 Hz, 1H), 8.88 (s, 1H), 12.31 (br s, 1H); ^{13}C (DMSO-d_6, 100 MHz) δ29.69, 37.18, 58.41, 70.27, 100.35, 115.06, 127.72, 128.42, 129.10, 129.38, 131.52, 135.83, 138.48, 151.41, 153.13, 155.40, 166.41; HRMS (ESI +ve): For $C_{17}H_{19}N_4O_2$ requires 311.1503 found 311.1504.

6.74. *N*-isopentyl-3-(7*H*-pyrrolo[2,3-*d*]pyrimidin-4-yl)benzamide 55

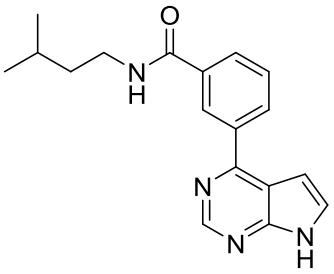

3-(7*H*-pyrrolo[2,3-*d*]pyrimidin-4-yl)benzoic acid (120 mg, 0.5 mmol), 3-methylbutan-1-amine (88 µL, 0.75 mmol) and triethylamine (0.27 mL, 2 mmol) were stirred in THF (8 mL) under nitrogen for 5 mins after which T3P (50% w/w in DMF, 0.58 mL, 1 mmol) was added and the solution stirred at room temperature for 24 hours. Solution was diluted in water, extracted into ethyl acetate and dried over magnesium sulphate. Solution was filtered and solvent removed under reduced pressure. Solids were triturated with diethyl ether (2 mL) and oven dried to yield title product as an off-white solid (60 mg, 39%) (LC-MS purity = 96.8%); ^{1}H (DMSO-d_6, 400 MHz) δ 0.92 (s, 3H), 0.94 (s, 3H) 1.47 (q, *J* = 6.9 Hz, 2H), 1.47 (sept, *J* = 6.6 Hz, 1H), 3.34 (m, 2H), 6.91 (d, *J* = 3.5 Hz, 1H), 7.68 (m, 2H), 8.00 (dt, *J* = 7.9 & 1.3 Hz, 1H), 8.30 (dt, *J* = 7.7 & 1.3 Hz, 1H), 8.60 (m, 2H), 8.88 (s, 1H), 12.31 (br s, 1H); ^{13}C (DMSO-d_6, 100 MHz) δ 22.95, 25.84, 38.06, 38.59, 100.33, 115.06, 127.72, 128.47, 129.09, 129.35, 131.46, 135.93, 138.47, 151.40, 153.13, 155.43, 166.27; HRMS (ESI +ve): For $C_{18}H_{21}N_4O$ requires 309.1710 found 309.1704.

6.75. 4-Chloro-1*H*-pyrrolo[2,3-*b*]pyridine-3-carbaldehyde 90

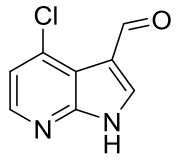

4-Chloro-1*H*-pyrrolo[2,3-*b*]pyridine (1.83 g, 12 mmol) and hexamethylenetetramine (2.52 g, 18 mmol) were suspended in 33% acetic acid (75 mL) and stirred at reflux for 18 h. Suspension was added to cold water (200 mL) and filtered to yield title compound as an off-white solid (1.973 g, 91%). ^{1}H (DMSO-d_6, 400 MHz) δ 7.40 (d, *J* = 5.3 Hz, 1H), 8.29 (d, *J* = 5.3 Hz, 1H), 8.47 (s, 1H), 10.27 (s, 1H), 13.07 (s, 1H); ^{13}C (DMSO-d_6, 100 MHz) δ 116.21, 116.74, 119.28, 135.52, 136.54, 145.24, 150.83, 184.56.

6.76. (4-Chloro-1*H*-pyrrolo[2,3-*b*]pyridin-3-yl)methanol 91

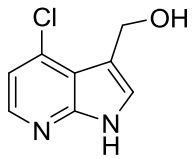

4-Chloro-1*H*-pyrrolo[2,3-*b*]pyridine-3-carbaldehyde (180 mg, 1 mmol), sodium borohydride (76 mg, 2 mmol) and acetic acid (70 µL, 1.25 mmol) were dissolved in DCM/ethanol (15 mL, 2:1) and stirred at room temperature under nitrogen for 24 hours. Water (80 mL) was added and the precipitate filtered and dried to yield product as a whitish solid (101 mg, 55%). ^{1}H (DMSO-d_6, 400 MHz) δ 4.77 (m, 2H), 4.84 (m, 1H), 7.12 (d, *J* = 5.3 Hz, 1H), 7.45 (d, *J* = 2.3 Hz, 1H), 8.12 (d, *J* = 5.3 Hz, 1H), 11.80 (br s, 1H); ^{13}C (DMSO-d_6, 100 MHz) δ 55.73, 114.85, 115.70, 116.00, 125.43, 134.37, 143.04, 149.72; LRMS (ESI -ve): 181.06, 183.06 (100:29) ($C_8H_6ClN_2O$, $[M-1]^-$)

6.77. 4-Chloro-1*H*-pyrrolo[2,3-*b*]pyridine-3-carbaldehyde oxime 92

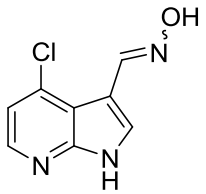

4-Chloro-1*H*-pyrrolo[2,3-*b*]pyridine-3-carbaldehyde (903 mg, 5 mmol), hydroxylamine hydrochloride (834 mg, 12 mmol, pyridine (1.4 mL, 18 mmol), THF (5 mL) and methanol (2.5 mL) were placed in a 10-20 mL microwave vial which was sealed and purged with nitrogen. Solution was stirred at 70 °C for 4 h before cooling and diluting with water. Precipitate was filtered to yield product as a white solid (511 mg, 52%). ^{1}H (DMSO-d_6, 400 MHz) δ 7.30 (d, *J* = 5.3 Hz, 1H), 8.19 (s, 1H), 8.24 (d, *J* = 5 Hz, 1H), 8.54 (s, 1H), 11.54 (s, 1H), 12.53 (br s, 1H); ^{13}C (DMSO-d_6, 100 MHz) δ 105.77, 115.40, 118.02, 113.13, 134.91, 137.85, 144.43, 149.00.

6.78. 4-Chloro-1*H*-pyrrolo[2,3-*b*]pyridine-3-carbonitrile 93

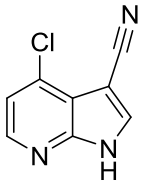

4-Chloro-1*H*-pyrrolo[2,3-*b*]pyridine-3-carbaldehyde oxime (400 mg, 2.05 mg) was suspended in DCM (10 mL) and $SOCl_2$ (1.5 mL, 20.5 mmol) added under nitrogen. Suspension was stirred at room temperature for 24 hours before addition of water (50 mL) and filtering to yield product as a white solid (310 mg, 84%). ^{1}H (DMSO-d_6, 400 MHz) δ 7.41 (d, *J* = 5.3 Hz, 1H), 8.34 (d, *J* = 5.1 Hz, 1H), 8.55 (d, *J* = 2.3 Hz, 1H), 13.15 (br s, 1H); ^{13}C (DMSO-d_6, 100 MHz) δ 82.56, 115.31, 116.50, 118.18, 134.66, 137.31 145.73, 148.23; LRMS (ESI +ve) found 178.2, 180.2 (3:1) ($C_8H_5ClN_3$, $[M+1]^+$); IR major peaks (cm^{-1}): 1311.59, 1334.74, 1396.46, 1454.33, 1512.19, 1571.99, 2227.78, 2831.50-3138.18.

6.79. 3-(3-Cyano-1*H*-pyrrolo[2,3-*b*]pyridin-4-yl)benzamide 56

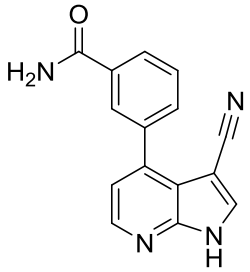

4-Chloro-1*H*-pyrrolo[2,3-*b*]pyridine-3-carbonitrile (89 mg, 0.5 mmol), 3-carboxamidephenylboronic acid (99 mg, 0.6 mmol) and Pd(dtbpf)Cl_2 (24 mg, 0.037 mmol) were placed in a 2-5 mL microwave vial which was sealed and purged with nitrogen. Ethanol (1.5 mL) was added and stirring continued under nitrogen for a further 5 minutes. The suspension brought to 80 °C with stirring before addition of K_3PO_4 (O_2-free, 1 M, 0.75 mL). Stirring continued for 24 hours. Solution was allowed to cool to room temperature before water (5 mL) was added. Organics were extracted into ethyl acetate/methanol 9:1, dried over magnesium sulfate and adsorbed onto silica. Chromatographic purification (Biotage SP4, 50 g cartridge, solvent system: ethyl acetate isocratic 6 CV) yielded product as an off-white solid (133 mg, >99%). (LC-MS purity = 95.0%); ^{1}H (DMSO-d_6, 500 MHz) δ 7.30 (d, *J* = 4.4 Hz, 1H), 7.44 (s, 1H), 7.61 (t, *J* = 7.5 Hz, 1H), 7.77 (d, *J* = 7.8 Hz, 1H), 7.99 (d, *J* = 7.5 Hz, 1H), 8.03 (s, 1H), 8.12 (s, 1H), 8.46 (d, *J* = 4.7 Hz, 1H), 8.52 (s, 1H), 13.01 (br s, 1H); ^{13}C (DMSO-d_6, 125 MHz) δ 83.57, 116.04, 116.34, 118.60, 128.45, 128.59, 128.77, 132.39, 134.89, 136.67, 137.70, 142.15, 145.58, 148.69, 167.93; HRMS (ESI -ve): For $C_{15}H_9N_4O$ requires 261.0771 found 261.0785. IR major peaks (cm^{-1}): 1321.24, 1336.67, 1386.82, 1413.82, 1485.19, 1514.12, 1566.20, 2214.28, 3014.74-3086.11, 3115.04, 3192.19, 3425.58.

6.80. 3-(3-Formyl-1*H*-pyrrolo[2,3-*b*]pyridin-4-yl)benzamide 57

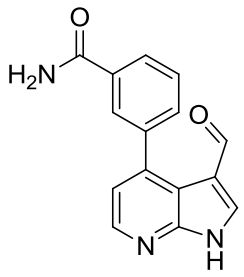

4-Chloro-1*H*-pyrrolo[2,3-*b*]pyridine-3-carbaldehyde (542 mg, 3 mmol), 3-carboxamidephenylboronic acid (693 mg, 4.2 mmol) and Pd(dtbpf)Cl_2 (98 mg, 0.15 mmol) were placed in a 10-20 mL microwave vial which was sealed and purged with nitrogen. Dioxane (7 mL) and K_2CO_3 (O_2-free, 2 M, 3 mL, 6 mmol) were added and the solution heated under microwave conditions to 120 °C for 2 hours. Organics were extracted into ethyl acetate, washed with water and dried over magnesium sulphate. Solution was filtered and adsorbed onto silica. Chromatographic purification (Biotage SP4, 50 g cartridge, solvent system: pet. ether 40-60/ethyl acetate, 50%, 6 CV; 50-80%, 4 CV; 80%, 4 CV; 80-100%, 4CV; 100%, 2 CV; ethyl acetate/methanol, 0-10%, 4 CV; 10%, 16 CV; 15%, 11 CV) yielded product as a pale brown solid (395 mg, 50%). (LC-MS purity = 95.1%); ^{1}H (DMSO-d_6, 400 MHz) δ 7.26 (d, *J* = 5.3 Hz, 1H), 7.41 (br s, 1H), 7.57 (t, *J* = 7.5 Hz, 1H), 7.65 (d, *J* = 7.5 Hz, 1H), 8.00 (d, *J* = 7.8 Hz, 1H), 8.03 (s, 1H), 8.08 (br s, 1H), 8.43 (d, *J* = 4.8 Hz, 1H), 8.46 (s, 1H), 9.56 (s, 1H), 13.05 (br s, 1H); ^{13}C (DMSO-d_6, 100 MHz) δ 115.26, 117.29, 119.48, 127.90, 128.30, 128.59, 132.07, 134.52, 137.20, 139.87, 143.10, 144.80, 150.50, 168.01, 184.00. HRMS (ESI +ve): For $C_{15}H_{12}N_4O_2$ requires 266.0924 found 266.0912.

6.81. 3-(3-(Hydroxymethyl)-1*H*-pyrrolo[2,3-*b*]pyridin-4-yl)benzamide 58

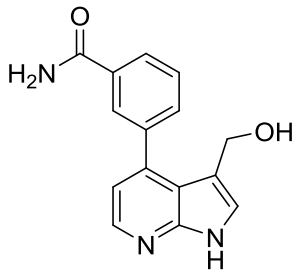

(4-Chloro-1*H*-pyrrolo[2,3-*b*]pyridin-3-yl)methanol (91 mg, 0.5 mmol), 3-carboxamidephenylboronic acid (99 mg, 0.6 mmol) and Pd(dtbpf)Cl_2 (16.3 mg, 0.025 mmol) were placed in a 2-5 mL microwave vial which was sealed and purged with nitrogen. Ethanol (1.5 mL) was added and stirring continued under nitrogen for a further 5 minutes. The suspension brought to 80 °C with stirring before addition of K_3PO_4 (O_2-free, 1 M, 0.75 mL). Stirring continued for 24 hours. Solution was cooled, extracted into ethyl acetate, dried over magnesium sulfate and adsorbed onto silica. Chromatographic purification (Biotage SP4, 50 g cartridge, solvent system: ethyl acetate/methanol; 0% 6 CV; 0-2% 4 CV; 2% 2 CV; 2-5% 2 CV; 5% 2 CV; 5-10% 2 CV; 10% 10 CV) yielded product as a white solid (40 mg, 30%). (LC-MS purity = 98.4%); ^{1}H (DMSO-d_6, 500 MHz) δ 4.18 (d, *J* = 5 Hz, 2H), 4.71 (t, *J* = 5.3 Hz, 1H), 6.98 (d, *J* = 4.7 Hz, 1H), 7.42 (m, 2H), 7.57 (t, *J* = 7.5 Hz, 1H), 7.68 (dt, *J* = 7.7 & 1.2 Hz, 1H), 7.94 (dt, *J* = 7.8 & 1.4 Hz, 1H), 8.05 (t, *J* = 2.0 Hz, 1H), 8.24 (d, *J* = 5.0 Hz, 1H), 11.65 (br s, 1H); ^{13}C (DMSO-d_6, 125 MHz) δ 56.98, 115.46, 116.01, 116.56, 125.55, 127.58, 128.13, 128.69, 131.78, 134.53, 139.84, 142.03, 142.82, 149.83, 168.17; HRMS (ESI +ve): For $C_{15}H_{14}N_3O_2$ requires 268.1081 found 268.1079.

6.82. 6-Bromoindoline

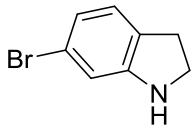

6-Bromoindole (1.96 g, 10 mmol) and sodium cyanoborohydride (2.5 g, 40 mmol) were stirred in glacial acetic acid (50 mL) at room temperature under an inert atmosphere for 2 h. Solution was poured into cold water and neutralised with sodium hydroxide. Organics were extracted into ethyl acetate , dried over magnesium sulfate and isolated *in vacuo* to yield title compound as a brown solid (601 mg, 30%). ^{1}H (DMSO-d_6, 500 MHz) δ 2.89 (t, *J* = 8.5 Hz, 2H), 3.47 (t, *J* = 8.5 Hz, 2H), 6.62 (d, *J* = 1.5 Hz, 1H), 6.65 (dd, *J* = 7.7 & 1.8 Hz, 1H), 6.96 (d, *J* = 7.6 Hz, 1H); ^{13}C (DMSO-d_6, 125 MHz) δ 28.49, 46.63, 110.38, 118.68, 119.74, 125.65, 128.25, 154.47; LRMS (ESI +ve): 198.13, 200.13 (50:48) (C_8H_9BrN, $[M+1]^+$)

6.83. 4-(Indolin-1-yl)-7*H*-pyrrolo[2,3-*d*]pyrimidine 63

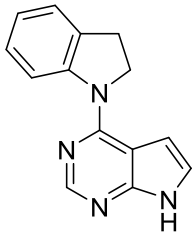

4-Chloro-7*H*-pyrrolo[2,3-*d*]pyrimidine (153 mg, 1 mmol), indoline (274 µL, 2 mmol) were stirred in dioxane (1 mL) under microwave conditions at 130 °C for 2 hours. The suspension was filtered and washed with water to yield title compound as an off-white solid (206 mg, 87%). (LC-MS purity > 99.9%); ^{1}H (DMSO-d_6, 400 MHz) δ 3.29 (t, *J* = 8.5 Hz, 2H), 4.53 (t, *J* = 8.5 Hz, 2H), 6.73 (d, *J* = 3.5 Hz, 1H), 6.95 (td, *J* = 7.4 & 1 Hz, 1H), 7.19 (td, *J* = 7.8 & 1 Hz, 1H), 7.26 (dd, *J* = 7.3 & 0.8 Hz, 1H), 7.30 (d, *J* = 3.5 Hz, 1H), 8.34 (s, 1H), 8.57 (d, *J* = 7.8 Hz, 1H), 11.88 (br s, 1H); ^{13}C (DMSO-d_6, 100 MHz) δ 28.23, 50.52, 101.67, 104.15, 117.02, 122.26, 122.55, 125.07, 127.22, 132.23, 144.72, 150.78, 152.43, 153.98; HRMS (ESI +ve): For $C_{14}H_{13}N_4$ requires 237.1135 found 237.1134.

6.84. 4-(6-Bromoindolin-1-yl)-7*H*-pyrrolo[2,3-*d*]pyrimidine 64

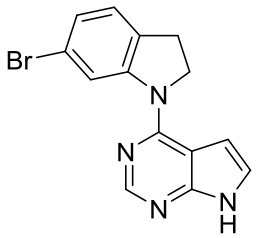

4-Chloro-7*H*-pyrrolo[2,3-*d*]pyrimidine (153 mg, 1 mmol) and 6-bromoindoline (198 mg, 1 mmol) were stirred in IPA (2 mL) and dioxane (1 mL) under microwave conditions at 130 °C for 2 hours. Solvent was removed *in vacuo* to yield title compound as a blue solid (315 mg, >99%). (LC-MS purity = 96.3.%); ^{1}H (DMSO-d_6, 400 MHz) δ 3.24 (t, *J* = 8.6 Hz, 2H), 4.56 (t, *J* = 8.6 Hz, 2H), 6.75 (dd, *J* = 3.5 & 1.8 Hz, 1H), 7.11 (dd, *J* = 7.8 & 1.8 Hz, 1H), 7.20 (d, *J* = 7.8 Hz, 1H), 7.33 (m, 1H), 8.42 (s, 1H), 8.77 (d, *J* = 1.8 Hz, 1H), 12.04 (br s, 1H); ^{13}C (DMSO-d_6, 100 MHz) δ 27.26, 50.62, 101.35, 103.84, 118.98, 119.33, 122.70, 124.35, 126.15, 131.58, 145.61, 149.51, 150.79, 153.27; LRMS (ESI +ve) found 315.0, 317.0 (50:50) ([M+1]$^{+}$); HRMS (ESI -ve): For $C_{14}H_{10}N_4Br$ requires 313.0094 found 313.0096.

6.85. 3-(1-(7*H*-pyrrolo[2,3-*d*]pyrimidin-4-yl)indolin-6-yl)prop-2-yn-1-ol 65

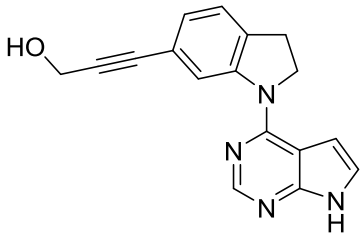

Bis(triphenylphosphine)palladium (II) dichloride (70 mg, 0.1 mmol) and copper iodide (38 mg, 0.2 mmol) were stirred under nitrogen in dry DMF (1mL) for 10 minutes. A solution of 4-(6-bromoindolin-1-yl)-7*H*-pyrrolo[2,3-*d*]pyrimidine (314 mg, 1 mmol) and propargyl alcohol (87 µL, 1.5 mmol) in diisopropylamine (560 µL, 4 mmol) and DMF (1 mL) were added and reaction mixture stirred at 60 °C for 24 hours. HPLC purification yielded title product as a white TFA salt (40 mg, 10%). (LC-MS purity = 99.1%); ^{1}H (DMSO-d_6, 400 MHz) δ 3.31 (t, *J* = 8.5 Hz, 2H), 4.58 (t, *J* = 8.5 Hz, 2H), 6.78 (dd, *J* = 3.4 & 1.6 Hz, 1H), 7.05 (dd, *J* = 7.7 & 1.4 Hz, 1H), 7.28 (d, *J* = 7.8 Hz, 1H), 7.35 (dd, *J* = 3.5 & 2.5 Hz, 1H), 8.46 (s, 1H), 8.65 (d, *J* = 1.3 Hz, 1H), 12.06 (br s, 1H); ^{13}C (DMSO-d_6, 100 MHz) δ28.18, 49.98, 50.70, 85.02, 89.07, 101.63, 119.39, 121.15, 122.82, 125.24, 125.49, 132.48, 133.25, 144.89, 150.75, 152.51, 153.91; HRMS (ESI -ve): For $C_{17}H_{13}N_4O$ requires 289.1095 found 289.1093.

6.86. 4-(1-(7*H*-pyrrolo[2,3-*d*]pyrimidin-4-yl)indolin-6-yl)but-3-yn-1-ol 66

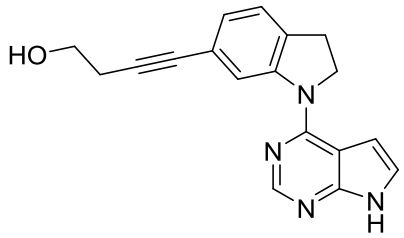

Bis(triphenylphosphine)palladium (II) dichloride (70 mg, 0.1 mmol) and copper iodide (38 mg, 0.2 mmol) were stirred under nitrogen in dry DMF (1mL) for 10 minutes. A solution of 4-(6-bromoindolin-1-yl)-7*H*-pyrrolo[2,3-*d*]pyrimidine (314 mg, 1 mmol) and but-3-yn-1-ol (114 µL, 1.5 mmol) in diisopropylamine (560 µL, 4 mmol) and DMF (1 mL) were added and reaction mixture stirred at 60 °C for 24 hours. Chromatographic purification (Biotage SP4, 50 g cartridge, solvent system: pet. ether 60-80/ethyl acetate, 50%, 3 CV; 50-100%, 6 CV; 100%, 10 CV) yielded title product as an off-white solid (40 mg, 13%). (LC-MS purity = 99.4%); ^{1}H (DMSO-d_6, 400 MHz) δ 2.57 (t, *J* = 6.8 Hz, 2H), 3.28 (t, *J* = 8.5 Hz, 2H), 3.60 (td, *J* = 6.8 & 5.5 Hz, 2H), 4.55 (t, *J* = 8.7 Hz, 2H), 4.92 (t, *J* = 5.5 Hz, 1H), 6.73 (dd, *J* = 3.6 & 1.9 Hz, 1H), 6.99 (dd, *J* = 7.5 & 1.5 Hz, 1H), 7.22 (d, *J* = 7.5 Hz, 1H), 7.31 (dd, *J* = 3.5 & 2.5 Hz, 1H), 8.38 (s, 1H), 8.61 (d, *J* = 1.3 Hz, 1H), 11.92 (br s, 1H); ^{13}C (DMSO-d_6, 100 MHz) δ 23.26, 27.63, 50.21, 59.78, 81.84, 87.14, 101.14, 118.90, 121.42, 122.27, 124.59, 125.13, 132.12, 144.29, 150.26, 151.98, 153.40; HRMS (ESI -ve): For $C_{18}H_{15}N_4O$ requires 303.1251 found 303.1252.

6.87. 4-(1-(7*H*-pyrrolo[2,3-*d*]pyrimidin-4-yl)indolin-6-yl)-2-methylbut-3-yn-2-ol

67

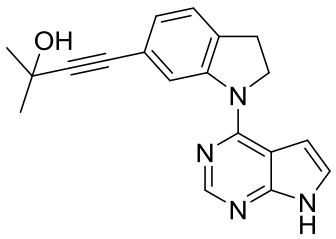

Bis(triphenylphosphine)palladium (II) dichloride (70 mg, 0.1 mmol) and copper iodide (38 mg, 0.2 mmol) were stirred under nitrogen in dry DMF (1mL) for 10 minutes. A solution of 4-(6-bromoindolin-1-yl)-7*H*-pyrrolo[2,3-*d*]pyrimidine (314 mg, 1 mmol) and 2-methylbut-3-yn-2-ol (145 µL, 1.5 mmol) in diisopropylamine (560 µL, 4 mmol) and DMF (1 mL) were added and reaction mixture stirred at 60 °C for 24 hours. HPLC purification yielded title product as a white TFA salt (42 mg, 10%). (LC-MS purity = 98.3%); ^{1}H (DMSO-d_6, 400 MHz) δ 1.49 (s, 6H), 3.30 (t, *J* = 8.4 Hz, 2H), 4.57 (t, *J* = 8.5 Hz, 2H), 6.78 (dd, *J* = 3.5 & 1.8 Hz, 1H), 7.01 (dd, *J* = 7.5 & 1.5 Hz, 1H), 7.26 (d, *J* = 7.8 Hz, 1H), 7.35 (dd, *J* = 3.4 & 2.4 Hz, 1H), 8.44 (s, 1H), 8.59 (d, *J* = 1.3 Hz, 1H), 12.04 (br s, 1H); ^{13}C (DMSO-d_6, 100 MHz) δ 27.63, 31.66 (2C), 50.22, 59.70, 63.58, 81.23, 94.72, 101.15, 118.69, 120.84, 122.30, 124.68, 125.13, 132.47, 144.33, 150.24, 151.99, 153.40; HRMS (ESI +ve): For $C_{19}H_{17}N_4O$ requires 317.1408 found 317.1405

6.88. 4-(1*H*-indol-1-yl)-7*H*-pyrrolo[2,3-*d*]pyrimidine 68

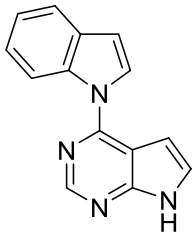

4-(indolin-1-yl)-7*H*-pyrrolo[2,3-*d*]pyrimidine (118 mg, 0.5 mmol) and DDQ (136 mg, 0.6 mmol) were stirred in 1,4-dioxane at 80 °C for 24 hours. Resultant solution was adsorbed onto silica and chromatographic purification (Biotage SP4, 10 g cartridge, solvent system: pet. ether 60-80/ethyl acetate; isocratic, 30% ethyl acetate, 8CV) yielded title compound as a pale tan solid (114 mg, 97%). (LC-MS purity > 99.9%); ^{1}H (DMSO-d_6, 400 MHz) δ 6.88 (dd, *J* = 3.6 & 1.9 Hz, 1H), 6.89 (dd, *J* = 3.5 & 0.8 Hz, 1H), 7.25 (m, 1H), 7.32 (m, 1H), 7.66 (dd, *J* = 3.5 & 2.5 Hz, 1H), 7.70 (dt, *J* = 7.9 & 0.9 Hz, 1H), 8.18 (d, *J* = 3.8 Hz, 1H), 8.57 (dd, *J* = 8.4 & 0.9 Hz, 1H), 8.75 (s, 1H), 12.42 (br s, 1H); ^{13}C (DMSO-d_6, 100 MHz) δ 99.63, 106.88, 106.90, 115.23, 120.79, 121.94, 123.20, 126.79, 127.12, 129.82, 135.16, 150.27, 153.50*; HRMS (ESI +ve): For $C_{14}H_{11}N_4$ requires 235.1978 found 235.0976

*1 peak missing - not found through JMOD/HSQC/HMBC.

6.89. 4-(6-Bromo-1*H*-indol-1-yl)-7*H*-pyrrolo[2,3-*d*]pyrimidine 69

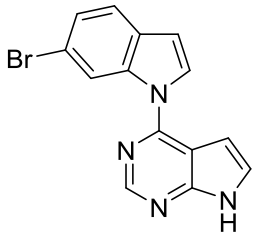

4-(6-Bromo-1*H*-indolin-1-yl)-7*H*-pyrrolo[2,3-*d*]pyrimidine (945 mg, 3 mmol) and DDQ (816 mg, 3.6 mmol) were stirred in 1,4-dioxane at 80 °C for 24 hours. Resultant solution was adsorbed onto silica and chromatographic purification (Biotage SP4, 10 g cartridge, solvent system: pet. ether 60-80/ethyl acetate; isocratic, 30% ethyl acetate, 8CV) yielded title compound as a pale brown solid (396 mg, 42%). (LC-MS purity = 83.4%); ^{1}H (DMSO-d_6, 400 MHz) δ 6.92 (m, 2H), 7.40 (dd, *J* = 8.3 & 1.8 Hz, 1H), 7.68 (m, 2H), 8.24 (d, *J* = 3.5 Hz, 1H), 8.79 (s, 1H), 8.84 (d, *J* = 1.8 Hz, 1H), 12.47 (br s, 1H); ^{13}C (DMSO-d_6, 100 MHz) δ 99.53, 106.70, 106.94, 114.38, 117.97, 122.51, 124.85, 127.11, 128.01, 129.51, 135.80, 150.21, 153.57*; LRMS (ESI +ve) found 311.0, 313.0 (50:50) ($[M+1]^+$); HRMS (ESI -ve): For $C_{14}H_8N_4Br$ requires 310.9938 found 310.9937.

*1 peak missing - not found through JMOD/HSQC/HMBC.

6.90. 3-(1-(7*H*-pyrrolo[2,3-*d*]pyrimidin-4-yl)-1*H*-indol-6-yl)prop-2-yn-1-ol 70

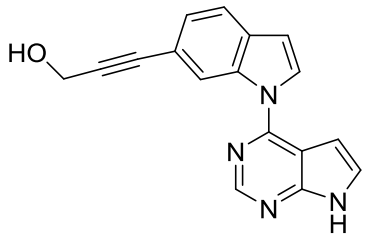

Bis(triphenylphosphine)palladium (II) dichloride (21 mg, 0.03 mmol) and copper iodide (11.4 mg, 0.06 mmol) were stirred under nitrogen in dry DMF (2mL) for 10 minutes. A solution of 4-(6-bromoindol-1-yl)-7*H*-pyrrolo[2,3-*d*]pyrimidine (94 mg, 0.3 mmol) and propargyl alcohol (35 µL, 0.6 mmol) in diisopropylamine (168 µL, 1.2 mmol) and DMF (2 mL) were added and reaction mixture stirred at 80 °C for 18 hours. Chromatographic purification (Biotage SP4, 10 g cartridge, solvent system: pet. ether 60-80/ethyl acetate; 50%, 8CV; 50-100%, 4.5 CV; 100%, 6 CV) followed by HPLC purification yielded title product as a white TFA salt (1.5 mg, 2%). (LC-MS purity = 97.1%); ^{1}H (DMSO-d_6, 400 MHz) δ 4.34 (s, 2H), 6.92 (m, 2H), 7.28 (dd, *J* = 8 & 1.5 Hz, 1H), 7.70 (m, 2H), 8.29 (d, *J* = 3.8 Hz, 1H), 8.72 (s, 1H), 8.80 (s, 1H), 12.49 (br s, 1H); ^{13}C (DMSO-d_6, 100 MHz) δ 49.53, 84.87, 88.69, 90.08, 99.55, 107.08, 110.55, 116.94, 118.54, 121.08, 125.05, 127.03, 128.62, 129.85, 134.74, 150.52, 153.55; HRMS (ESI -ve): For $C_{17}H_{11}N_4O$ requires 287.0938 found 287.0937.

6.91. 4-(1-(7*H*-pyrrolo[2,3-*d*]pyrimidin-4-yl)-1*H*-indol-6-yl)but-3-yn-1-ol 71

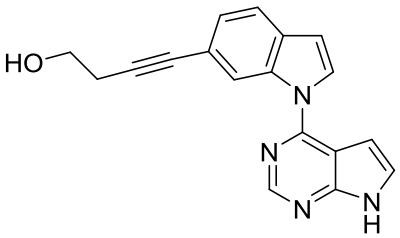

Bis(triphenylphosphine)palladium (II) dichloride (21 mg, 0.03 mmol) and copper iodide (11.4 mg, 0.06 mmol) were stirred under nitrogen in dry DMF (2mL) for 10 minutes. A solution of 4-(6-bromoindol-1-yl)-7*H*-pyrrolo[2,3-*d*]pyrimidine (94 mg, 0.3 mmol) and but-3-yn-1-ol (45 µL, 0.6 mmol) in diisopropylamine (168 µL, 1.2 mmol) and DMF (2 mL) were added and reaction mixture stirred at 80 °C for 18 hours. Chromatographic purification (Biotage SP4, 10 g cartridge, solvent system: pet. ether 60-80/ethyl acetate; 50%, 8CV; 50-100%, 4.5 CV; 100%, 6 CV) followed by HPLC purification yielded title product as a white TFA salt (5 mg, 5%). (LC-MS purity = 95.7%); ^{1}H (DMSO-d_6, 400 MHz) δ 2.59 (t, *J* = 6.8 Hz, 2H), 3.62 (t, *J* = 6.9 Hz, 2H), 6.90 (m, 2H), 7.25 (dd, *J* = 8 & 1.3 Hz, 1H), 7.66 (d, *J* = 8 Hz, 1H), 7.68 (dd, *J* = 3.4 & 2.4 Hz, 1H), 8.25 (d, *J* = 3.5 Hz, 1H), 8.66 (s, 1H), 8.79 (s, 1H), 12.46 (br s, 1H); ^{13}C (DMSO-d_6, 100 MHz) δ 23.35, 59.84, 82.18, 87.23, 99.56, 106.78, 107.05, 110.26, 117.80, 118.36, 120.91, 125.28, 126.98, 128.77, 129.46, 134.77, 150.26, 153.54; HRMS (ESI -ve): For $C_{18}H_{13}N_4O$ requires 301.1095 found 301.1096.

6.92. 4-(1-(7*H*-pyrrolo[2,3-*d*]pyrimidin-4-yl)-1*H*-indol-6-yl)-2-methylbut-3-yn-2-ol 72

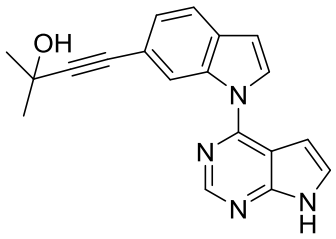

Bis(triphenylphosphine)palladium (II) dichloride (21 mg, 0.03 mmol) and copper iodide (11.4 mg, 0.06 mmol) were stirred under nitrogen in dry DMF (2mL) for 10 minutes. A solution of 4-(6-bromoindol-1-yl)-7*H*-pyrrolo[2,3-*d*]pyrimidine (94 mg, 0.3 mmol) and 2-methylbut-3-yn-2-ol (58 µL, 0.6 mmol) in diisopropylamine (168 µL, 1.2 mmol) and DMF (2 mL) were added and reaction mixture stirred at 80 °C for 18 hours. Chromatographic purification (Biotage SP4, 10 g cartridge, solvent system: pet. ether 60-80/ethyl acetate; 50%, 8CV; 50-100%, 4.5 CV; 100%, 6 CV) followed by HPLC purification yielded title product as a white TFA salt (3 mg, 2%). (LC-MS purity = 98.4%); ^{1}H (DMSO-d_6, 400 MHz) δ 1.50 (s, 6H), 6.92 (m, 2H), 7.25 (dd, *J* = 8.2 & 1.4 Hz, 1H), 7.68 (m, 2H) 8.26 (d, *J* = 3.5 Hz, 1H), 8.65 (s, 1H), 8.80 (s, 1H), 12.46 (br s, 1H); ^{13}C (DMSO-d_6, 150 MHz) δ 31.27 (2C), 63.64, 81.58, 94.88, 99.56, 106.65, 107.07, 117.16, 118.25, 121.02, 125.19, 127.35, 128.82, 129.68, 134.74, 150.48, 153.54*; HRMS (ESI -ve): For $C_{18}H_{13}N_4O$ requires 315.1251 found 315.1251.

*1 peak missing - not found through JMOD/HSQC/HMBC.

6.93. 6-Bromo-1-(pyrimidin-4-yl)indoline

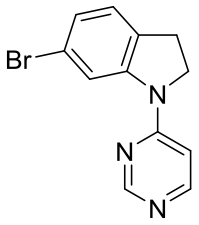

4-Chloropyrimidine dihydrochloride (188 mg, 1 mmol) and 6-bromoindoline (198 mg, 1 mmol) were dissolved in isopropyl alcohol (2 mL) and dioxane (1 mL) in a 2-5 mL microwave vial and heated to 140 °C for 2 hours under microwave conditions. Water (3 mL) was added and organics extracted into ethyl acetate. Solvent was removed under reduced pressure then resolubilised in a minimum of ethyl acetate, sonicated and precipitated from pet. ether to yield title product as a pale brown solid (305 mg, 87%). ^{1}H (DMSO-d_6, 500 MHz) δ 3.20 (t, *J* = 8.7 Hz, 2H), 4.08 (t, *J* = 8.7 Hz, 2H), 6.88 (d, *J* = 6.1 Hz, 1H), 7.13 (dd, *J* = 7.9, 1.8 Hz, 1H), 7.22 (d, *J* = 7.8 Hz, 1H), 8.47 (d, *J* = 6.1 Hz, 1H), 8.65 (d, *J* = 1.5 Hz, 1H), 8.81 (s, 1H); ^{13}C (DMSO-d_6, 125 MHz) δ 26.90, 49.03, 106.66, 118.69, 119.94, 124.97, 126.93, 132.50, 145.11, 156.79, 157.95, 158.77.

6.94. 6-(6-Bromoindolin-1-yl)pyrimidin-4-amine

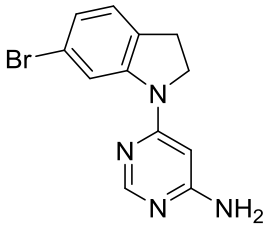

4-Chloropyrimidin-2-amine (194 mg, 1.5 mmol) and 6-bromoindoline (297 mg, 1.5 mmol) were dissolved in ethanol (2 mL) and dioxane (1 mL) in a 2-5 mL microwave vial and heated to 140 °C for 2 hours under microwave conditions. Water (3 mL) was added and the resulting precipitate filtered to yield title product as a beige coloured solid (312 mg, 71%). ^{1}H (DMSO-d_6, 400 MHz) δ 3.18 (t, *J* = 8.5 Hz, 2H), 4.00 (t, *J* = 8.5 Hz, 2H), 5.84 (s, 1H), 7.15 (dd, *J* = 8 & 1.8 Hz, 1H), 7.22 (d, *J* = 8 Hz, 1H), 7.62 (br s, 2H), 8.44 (s, 1H), 8.50 (d, *J* = 1.8 Hz, 1H); ^{13}C (DMSO-d_6, 150 MHz) δ 26.43, 48.95, 84.28, 118.53, 119.52, 124.93, 126.58, 132.20, 144.47, 151.73, 158.02, 158.17.

6.95. 4-(6-Bromoindolin-1-yl)pyrimidin-2-amine

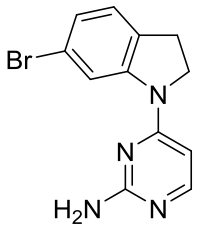

4-Chloropyrimidin-2-amine (194 mg, 1.5 mmol) and 6-bromoindoline (297 mg, 1.5 mmol) were dissolved in ethanol (2 mL) and dioxane (1 mL) in a 2-5 mL microwave vial and heated to 140 °C for 2 hours under microwave conditions. Water (3 mL) was added and the resulting precipitate filtered to yield title product as a beige coloured solid (313 mg, 72%). ^{1}H (DMSO-d_6, 400 MHz) δ 3.17 (t, *J* = 8.5 Hz, 2H), 4.10 (t, *J* = 8.5 Hz, 2H), 6.27 (d, *J* = 6.8 Hz, 1H), 7.20 (m, 2H), 7.43 (br s, 2H), 8.03 (d, *J* = 6.8 Hz, 1H), 8.70 (d, *J* = 1.5 Hz, 1H); ^{13}C (DMSO-d_6, 150 MHz) δ 26.32, 49.08, 96.50, 119.43, 119.73, 125.73, 126.38, 132.54, 144.00, 129.80, 158.01, 159.59.

6.96. 6-(6-Bromoindolin-1-yl)pyrimidine-2,4-diamine

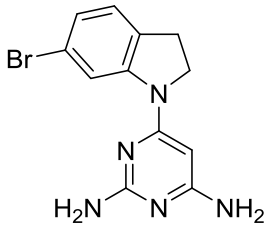

6-Chloropyrimidine-2,4-diamine (72 mg, 0.5 mmol) and 6-bromoindoline (99 mg, 0.5 mmol) were dissolved in isopropyl alcohol (2 mL) and dioxane (1 mL) in a 2-5 mL microwave vial and heated to 160 °C for 2 hours under microwave conditions. Water (3 mL) was added and organics extracted into ethyl acetate. Solvent was removed under reduced pressure then resolubilised in a minimum of ethyl acetate, sonicated and precipitated from pet. ether to yield title product as a brown solid (131 mg, 86%). ^{1}H (DMSO-*d*$_6$, 500 MHz) δ 3.16 (t, *J* = 8.5 Hz, 2H), 3.97 (t, *J* = 8.6 Hz, 2H), 5.25 (s, 1H), 5.77 (s, 1H), 6.37 (br s, 2H), 6.65 (br s, 2H), 7.07 (d, *J* = 7.9 Hz, 1H), 7.17 (d, *J* = 7.3 Hz, 1H), 8.62 (s, 1H); LRMS (ESI +ve) found 306.1, 308.0 (50:50) ($C_{12}H_{13}BrN_5$, $[M+1]^+$).

6.97. 6-(6-Bromoindolin-1-yl)-9*H*-purine

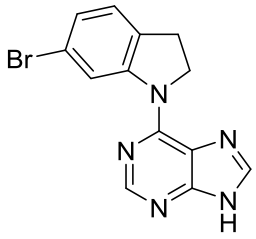

6-Chloro-9*H*-purine (154 mg, 1 mmol) and 6-bromoindoline (219 mg, 1.1 mmol) were stirred in ethanol (2 mL) and dioxane (1 mL) under microwave conditions at 140 °C for 2 hours. Water was added and precipitate filtered to yield title product as a pale brown solid (295 mg, 93%). ^{1}H (DMSO-d_6, 400 MHz) δ 3.23 (t, *J* = 8.5 Hz, 2H), 4.83 (t, *J* = 8.5 Hz, 2H), 7.15 (dd, *J* = 7.8 & 1.8 Hz, 1H), 8.30 (s, 1H), 8.50 (s, 1H), 8.84 (d, *J* = 1.8 Hz, 1H), 13.30 (br s, 1H); ^{13}C (DMSO-d_6, 150 MHz) δ 27.34, 51.37, 118.94, 119.35, 119.83, 124.59, 126.25, 126.27, 131.77, 145.41, 150.90, 151.38, 152.09.

6.98. 4-(6-Bromoindolin-1-yl)-7*H*-pyrrolo[2,3-*d*]pyrimidin-2-amine

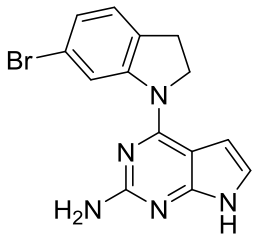

4-Chloro-7*H*-pyrrolo[2,3-*d*]pyrimidin-2-amine (82 mg, 0.5 mmol) and 6-bromoindoline (99 mg, 0.5 mmol) were dissolved in isopropyl alcohol (2 mL) and dioxane (1 mL) in a 2-5 mL microwave vial and heated to 160 °C for 2 hours under microwave conditions. Water (3 mL) was added and the resulting precipitate filtered to yield title product as a brown solid (280 mg, 85%). ^{1}H (DMSO-d_6, 500 MHz) δ 3.23 (t, *J* = 8.5 Hz, 2H), 4.52 (t, *J* = 8.5 Hz, 2H), 6.63 (br s, 1H), 6.97 (br s, 1H), 7.19 (d, *J* = 8 Hz, 1H), 7.23 (d, *J* = 8 Hz, 1H), 8.77 (s, 1H).

6.99. 2-Methyl-4-(1-(pyrimidin-4-yl)indolin-6-yl)but-3-yn-2-ol 73

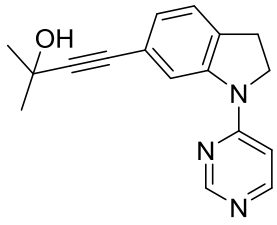

6-Bromo-1-(pyrimidin-4-yl)indoline (110 mg, 0.4 mmol), copper iodide (15.2 mg, 0.08 mmol) and Pd(dppf)Cl_2 (33 mg, 0.04 mmol) were stirred under argon in DMF (1 mL) in a sealed 0.5-2 mL microwave vial. DIPA (225 µL, 1.6 mmol) and 2-methylbut-3-yn-2-ol (78 µL, 0.8 mmol) were added before heating to 90 °C with stirring for 24 hours. HPLC purification yielded title product as a brown TFA salt (35 mg, 19%). (LC-MS purity = 95.5%); ^{1}H (DMSO-d_6, 500 MHz) δ 1.48 (s, 6H), 3.29 (t, *J* = 8.3 Hz, 2H), 4.17 (t, *J* = 8.3 Hz, 2H), 5.63 (d, *J* = 15.9 Hz, 1H), 6.14 (d, *J* = 16.0 Hz, 1H), 7.14 (m, 2H), 7.33 (d, *J* = 7.6 Hz, 1H), 8.50 (s, 1H); ^{13}C (DMSO-d_6, 125 MHz) δ 27.26, 32.10, 49.62, 64.09, 81.09, 95.90, 105.63, 117.47, 119.86, 21.80, 125.96, 127.81, 134.63, 142.55, 152.30, 158.76; HRMS (ESI +ve): For $C_{17}H_{18}N_3O$ requires 280.1444 found 280.1441.

6.100. 4-(1-(6-Aminopyrimidin-4-yl)indolin-6-yl)-2-methylbut-3-yn-2-ol 74

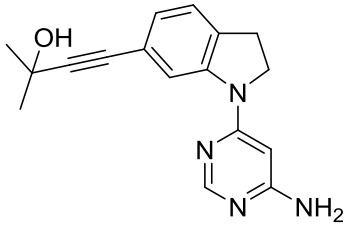

6-(6-Bromoindolin-1-yl)pyrimidin-4-amine (73 mg, 0.25 mmol), copper iodide (9.3 mg, 0.05 mmol) and Pd(dppf)Cl_2 (20.4 mg, 0.025 mmol) were stirred under argon in DMF (1 mL) in a sealed 0.5-2 mL microwave vial. DIPA (140 µL, 1 mmol) and 2-methylbut-3-yn-2-ol (24 µL, 0.25 mmol) were added before heating to 90 °C with stirring for 24 hours. HPLC purification yielded title product as a white TFA salt. (28 mg, 27%). (LC-MS purity = 96.4%); ^{1}H (DMSO-d_6, 500 MHz) δ 1.47 (br s, 6H), 3.24 (t, *J* = 7.78 Hz, 2H), 4.01 (t, *J* = 7.86 Hz, 2H), 5.85 (br s, 1H), 7.04 (d, *J* = 7.32 Hz, 1H), 7.27 (d, *J* = 7.17 Hz, 1H), 7.81 (br s, 2H), 8.31 (br s, 1H), 8.50 (br s, 1H); ^{13}C (DMSO-d_6, 125 MHz) δ 27.28, 32.12 (2C), 49.32, 64.10, 81.26, 84.45, 95.97, 119.04, 121.72, 125.78, 126.79, 133.91, 143.25, 151.22, 157.17, 158.61; HRMS (ESI +ve): For $C_{17}H_{19}N_4O$ requires 295.1553 found 295.1550.

6.101. 4-(1-(2-Aminopyrimidin-4-yl)indolin-6-yl)-2-methylbut-3-yn-2-ol[195] 75

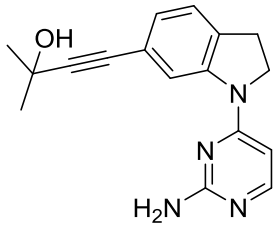

4-(6-Bromoindolin-1-yl)pyrimidin-2-amine (73 mg, 0.25 mmol), copper iodide (9.3 mg, 0.05 mmol) and Pd(dppf)Cl_2 (20.4 mg, 0.025 mmol) were stirred under argon in DMF (1 mL) in a sealed 0.5-2 mL microwave vial. DIPA (140 µL, 1 mmol) and 2-methylbut-3-yn-2-ol (24 µL, 0.25 mmol) were added before heating to 90 °C with stirring for 24 hours. HPLC purification yielded title product as a white TFA salt. (24 mg, 24%). (LC-MS purity = 96.6%); ^{1}H (DMSO-d_6, 500 MHz) δ 1.50 (s, 1H), 3.24 (t, *J* = 7.9 Hz, 2H), 4.19 (t, *J* = 8.1 Hz, 2H), 5.42 (br s, 1H), 6.47 (d, *J* = 6.4 Hz, 1H), 7.15 (d, *J* = 7.5 Hz, 1H), 7.31 (d, *J* = 7.3 Hz, 1H), 8.05 (br s, 1H), 8.17 (br s, 2H), 8.48 (br s, 1H); ^{13}C (DMSO-d_6, 125 MHz) δ 27.15, 32.12, 49.89, 64.18, 81.23, 96.08, 98.03, 120.41, 122.04, 125.82, 128.68, 134.81, 142.23, 144.45, 155.16, 160.05; HRMS (ESI +ve): For $C_{17}H_{19}N_4O$ requires 295.1553 found 295.1556.

6.102. 4-(1-(2,6-Diaminopyrimidin-4-yl)indolin-6-yl)-2-methylbut-3-yn-2-ol 76

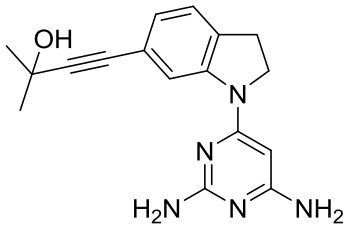

6-(6-Bromoindolin-1-yl)pyrimidine-2,4-diamine (impure, 122 mg, assumed 0.4 mmol), copper iodide (19 mg, 0.1 mmol) and Pd(dppf)Cl_2 (36.5 mg, 0.05 mmol) were stirred under argon in DMF:dioxane (3 mL, 2:1) in a sealed 2-5 mL microwave vial. DIPA (280 µL, 2 mmol) and 2-methylbut-3-yn-2-ol (97 µL, 1 mmol) were added before heating to 90 °C with stirring for 24 hours. HPLC purification yielded title product as an off-white TFA salt (106 mg, 63% over 2 steps). (LC-MS purity = 93.8%); ^{1}H (DMSO-*d*$_6$, 500 MHz) δ 1.49 (s, 6H), 3.18 (t, *J* = 8.4 Hz, 2H), 3.98 (t, *J* = 8.5 Hz, 2H), 5.33 (br s, 1H), 7.02 (dd, *J* = 7.6 & 1.1 Hz, 1H), 7.23 (d, *J* = 7.8 Hz, 1H), 7.59 (br s, 2H), 7.72 (br s, 2H), 8.32 (br s, 1H); ^{13}C (DMSO-*d*$_6$, 150 MHz) δ 27.16, 32.13, 49.37, 64.16, 75.45, 81.50, 95.68, 121.82, 125.56, 127.03, 128.78, 133.85, 143.30, 153.88, 159.09, 160.42; HRMS (ESI +ve): For $C_{17}H_{20}N_5O$ requires 310.1662 found 310.1659.

6.103. 4-(1-(9*H*-purin-6-yl)indolin-6-yl)-2-methylbut-3-yn-2-ol 77

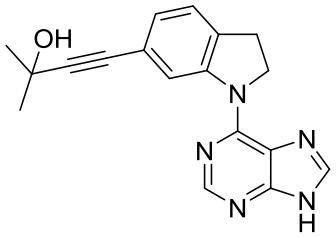

6-(6-Bromoindolin-1-yl)-9*H*-purine (47 mg, 0.15 mmol), copper iodide (5.6 mg, 0.03 mmol) and Pd(dppf)Cl_2 (12.3 mg, 0.015 mmol) were stirred under argon in DMF (1 mL) in a sealed 2-5 mL microwave vial. DIPA (84 µL, 0.6 mmol) and 2-methylbut-3-yn-2-ol (37 µL, 0.3 mmol) were added before heating to 90 °C with stirring for 24 hours. HPLC purification yielded title product as an off-white TFA salt (7 mg, 11%). (LC-MS purity = 93.2%); ^{1}H (DMSO-d_6, 500 MHz) δ 1.49 (s, 6H), 3.28 (t, *J* = 8.9 Hz, 2H), 4.81 (t, *J* = 8.4 Hz, 2H), 7.02 (d, *J* = 7.5 Hz, 1H), 7.27 (d, *J* = 7.6 Hz, 1H), 8.29 (s, 1H), 8.54 (br s, 1H), 8.65 (s, 1H); ^{13}C not obtained- signal suppression due to nitrogen; HRMS (ESI +ve): For $C_{18}H_{17}N_5O$ requires 320.1506 found 320.1501.

6.104. 4-(1-(2-Amino-7*H*-pyrrolo[2,3-*d*]pyrimidin-4-yl)indolin-6-yl)-2-methylbut-3-yn-2-ol 78

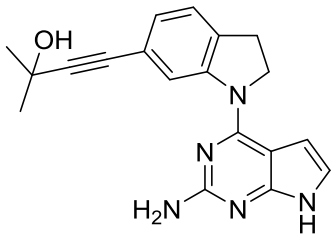

4-(6-Bromoindolin-1-yl)-7*H*-pyrrolo[2,3-*d*]pyrimidin-2-amine (132 mg, 0.4 mmol), copper iodide (15.2 mg, 0.08 mmol) and Pd(dppf)Cl_2 (33 mg, 0.04 mmol) were stirred under argon in DMF (1 mL) in a sealed 0.5-2 mL microwave vial. DIPA (225 µL, 1.6 mmol) and 2-methylbut-3-yn-2-ol (78 µL, 0.8 mmol) were added before heating to 90 °C with stirring for 24 hours. Product was adsorbed onto celite and chromatographic purification (Biotage SP4, 10 g cartridge, solvent system: pet. ether/ethyl acetate, 50% 6CV; 50-100% 6CV; 100% 10CV) yielded title product as a pale brown solid (43 mg, 32%). (LC-MS purity = 92.6%); ^{1}H (DMSO-d_6, 500 MHz) δ 1.49 (s, 6H), 3.24 (t, *J* = 8.5 Hz, 2H), 4.45 (t, *J* = 8.5 Hz, 2H), 5.39 (s, 1H), 6.02 (br s, 1H), 6.51 (br s, 2H), 6.88 (d, *J* = 2.9 Hz, 1H), 6.95 (d, *J* = 7.5 Hz, 1H), 7.20 (d, *J* = 7.5 Hz, 1H), 8.53 (s, 1H); ^{13}C (DMSO-d_6, 125 MHz) δ 28.05, 32.16, 50.75, 64.14, 81.94, 95.27, 97.87, 102.24, 118.92, 119.52, 121.51, 125.06, 125.72, 132.94, 144.77, 153.77, 154.54, 158.84; HRMS (ESI +ve): For $C_{19}H_{20}N_5O$ requires 334.1662 found 334.1662.

6.105. 4-(9*H*-carbazol-9-yl)pyrimidin-2-amine 79

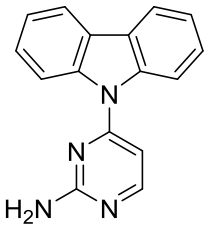

9*H*-carbazole (167 mg, 1 mmol) and NaH (40 mg, 1 mmol, 60% dispersion in oil) were stirred in anhydrous DMF (1 mL) and stirred under argon at 0 °C in a 2-5 mL microwave vial. 4-chloropyrimidin-2-amine (129 mg, 1 mmol) was added and the solution stirred at 100 °C for 24 hours. Water (30 mL) was added and the resulting precipitate filtered to yield title product as a white solid (41 mg, 16%). (LC-MS purity = 84.9%); ^{1}H (DMSO-d_6, 500 MHz) δ 6.96 (d, *J* = 5.5 Hz, 1H), 6.98 (s, 2H), 7.36 (t, *J* = 7.4 Hz, 2H), 7.50 (t, *J* = 7.4 Hz, 2H), 8.13 (d, *J* = 8.4 Hz, 2H), 8.23 (d, *J* = 7.6 Hz, 2H), 8.43 (d, *J* = 5.5 Hz, 1H); ^{13}C (DMSO-d_6, 125 MHz) δ 102.83, 113.55, 120.78, 122.13, 124.69, 127.00, 138.74, 158.71, 160.74, 164.48; HRMS (ESI +ve): For $C_{16}H_{13}N_4$ requires 261.1135 found 261.1134.

6.106. 4-(2-Bromo-9*H*-carbazol-9-yl)pyrimidin-2-amine 80

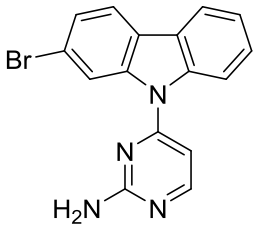

2-Bromo-9*H*-carbazole (492 mg, 2 mmol) and NaH (85 mg, 2.125 mmol, 60% dispersion in oil) were stirred in anhydrous DMF (2 mL) and stirred under argon at 0 °C in a 2-5 mL microwave vial. 4-chloropyrimidin-2-amine (259 mg, 2 mmol) was added and the solution stirred at 100 °C for 24 hours. Water (30 mL) was added and the resulting precipitate filtered to yield title product as a white solid (188 mg, 28%). (LC-MS purity = 99.9%); ^{1}H (DMSO-d_6, 500 MHz) δ 6.94 (d, *J* = 5.3 Hz, 1H), 7.07 (s, 2H), 7.38 (t, *J* = 7.4 Hz, 1H), 7.52 (m, 2H), 8.02 (d, *J* = 8.4 Hz, 1H), 8.18 (d, *J* = 8.2 Hz, 1H), 8.24 (d, *J* = 7.6 Hz, 1H), 8.30 (d, *J* = 1.4 Hz, 1H), 8.45 (d, *J* = 5.3 Hz, 1H); ^{13}C (DMSO-d_6, 125 MHz) δ 102.97, 113.33, 116.18, 119.73, 121.07, 122.47, 122.50, 123.77, 123.98, 125.00, 127.53, 138.82, 139.55, 158.28, 161.10, 164.49; LRMS (ESI +ve) found 339.0, 341.0 (50:50) ($[M+1]^+$); HRMS (ESI +ve): For $C_{16}H_{12}N_4Br$ requires 339.0240 found 339.0240.

6.107. 4-(9-(2-Aminopyrimidin-4-yl)-9*H*-carbazol-2-yl)-2-methylbut-3-yn-2-ol 81

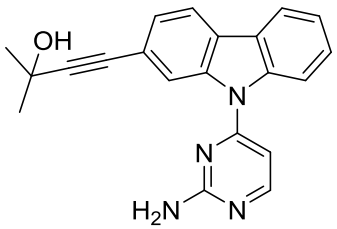

4-(2-Bromo-9*H*-carbazol-9-yl)pyrimidin-2-amine (85 mg, 0.25 mmol), copper iodide (9.3 mg, 0.05 mmol) and Pd(dppf)Cl_2·CH_2Cl_2 (20.4 mg, 0.025 mmol) were stirred under argon in DMF (1 mL) in a sealed 0.5-2 mL microwave vial. DIPA (140 µL, 1 mmol) and 2-methylbut-3-yn-2-ol (50 µL, 0.5 mmol) were added before heating to 100 °C with stirring for 18 hours. Product was adsorbed onto silica and chromatographic purification (Biotage SP4, 10 g cartridge, solvent system: pet. ether/ethyl acetate, 60% 8CV; 60-100% 4CV; 100% 4CV) yielded title product as a pale brown solid (60 mg, 70%). (LC-MS purity = 90.7%); ^{1}H (DMSO-d_6, 500 MHz) δ 1.51 (s, 6H), 5.49 (s, 1H), 6.94 (d, *J* = 3.4 Hz, 1H), 7.07 (br s, 2H), 7.37 (m, 2H), 7.51 (t, *J* = 7.7 Hz, 1H), 8.05 (m, 2H), 8.21 (d, *J* = 8.2 Hz, 1H), 8.23 (d, *J* = 8.2 Hz, 1H), 8.52 (s, 1H); ^{13}C (DMSO-d_6, 125 MHz) δ 32.14 (2C), 64.19, 81.77, 96.54, 103.37, 113.33, 115.77, 120.90, 121.09, 121.11, 122.39, 124.13, 124.42, 125.38, 127.51, 138.43, 139.29, 158.40, 160.99, 164.61; HRMS (ESI +ve): For $C_{21}H_{19}N_4O$ requires 343.1553 found 343.1553.

6.108. *N*-(3-iodophenyl)-7*H*-pyrrolo[2,3-*d*]pyrimidin-4-amine

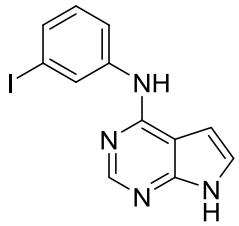

4-Chloro-7*H*-pyrrolo[2,3-*d*]pyrimidine (153 mg, 1 mmol) and 3-iodoaniline (219 mg, 1 mmol) were dissolved in ethanol (2 mL) and dioxane (1 mL) in a 2-5 mL microwave vial and heated to 140 °C for 2 hours under microwave conditions. Water (3 mL) was added and the resulting precipitate filtered to yield title product as an indigo coloured solid (151 mg, 45%). ^{1}H (DMSO-d_6, 400 MHz) δ 6.81 (dd, *J* = 3.5 & 2 Hz, 1H), 7.14 (t, *J* = 8 Hz, 1H), 7.27 (dd, *J* = 3.4 & 2.4 Hz, 1H), 7.36 (ddd, *J* = 7.8, 1.6 & 0.9 Hz, 1H), 7.96 (ddd, *J* = 8.3, 2 & 1 Hz, 1H), 8.33 (s, 1H), 8.40 (t, *J* = 1.9 Hz, 1H), 9.39 (s, 1H); ^{13}C (DMSO-d_6, 150 MHz) δ 94.36, 98.69, 103.85, 119.09, 122.59, 127.85, 130.25, 130.50, 141.93, 150.43, 150.81, 153.01.

6.109. N^4-(3-iodophenyl)pyrimidine-4,6-diamine

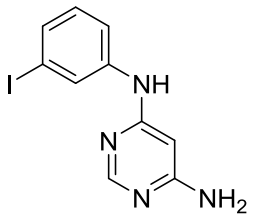

6-Chloropyrimidin-4-amine (129 mg, 1 mmol) and 3-iodoaniline (219 mg, 1 mmol) were dissolved in ethanol (2 mL) and dioxane (1 mL) in a 2-5 mL microwave vial and heated to 140 °C for 2 hours under microwave conditions. Water (3 mL) was added, organics extracted into ethyl acetate and dried over magnesium sulfate. Solvent was removed under reduced pressure then resolubilised in a minimum of ethyl acetate, sonicated and precipitated from pet. ether to yield title product as an off-white solid (70 mg, 22%). ^{1}H (DMSO-d_6, 400 MHz) δ 3.18 (s, 2H), 5.97 (d, *J* = 0.8 Hz, 1H), 7.18 (t, *J* = 8 Hz, 1H), 7.48 (m, 2H), 7.67 (s, 1H), 7.93 (s, 1H), 8.38 (s, 1H); ^{13}C not obtained- signal suppression due to nitrogen, no more available material.

6.110. N^4-(3-iodophenyl)pyrimidine-2,4-diamine

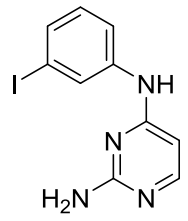

4-Chloropyrimidin-2-amine (129 mg, 1 mmol) and 3-iodoaniline (219 mg, 1 mmol) were dissolved in ethanol (2 mL) and dioxane (1 mL) in a 2-5 mL microwave vial and heated to 140 °C for 2 hours under microwave conditions. Water (3 mL) was added and the resulting precipitate filtered to yield title product as an off-white solid (73 mg, 23%). ^{1}H (DMSO-d_6, 400 MHz) δ 6.39 (d, J = 7.3 Hz, 1H), 7.18 (t, J = 8 Hz, 1H), 7.53 (dq, J = 7.8 & 0.8 Hz, 1H), 7.87 (m, 2H), 8.09 (s, 1H), 10.85 (s, 1H); ^{13}C (DMSO-d_6, 150 MHz) δ 94.58, 98.89, 120.60, 129.25, 130.76, 130.09, 139.42, 142.41, 155.31, 161.36.

6.111. *N*-(3-iodophenyl)-9*H*-purin-6-amine

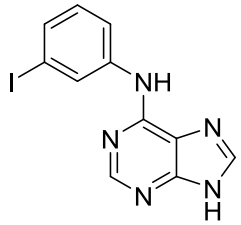

6-Chloro-9*H*-purine (154 mg, 1 mmol) and 3-iodoaniline (219 mg, 1 mmol) were dissolved in ethanol (2 mL) and dioxane (1 mL) in a 2-5 mL microwave vial and heated to 140 °C for 2 hours under microwave conditions. Water (3 mL) was added and the resulting precipitate filtered to yield title product as an off-white solid (260 mg, 77%). ^{1}H (DMSO-d_6, 400 MHz) δ 7.13 (t, *J* = 8.0 Hz, 1H), 7.37 (d, *J* = 8.3 Hz, 1H), 7.99 (dd, *J* = 8.3, 1.3 Hz, 1H), 8.32 (s, 1H), 8.43 (s, 1H), 8.52 (t, *J* = 1.8 Hz, 1H), 9.93 (s, 1H), 13.25 (br s, 1H); ^{13}C (DMSO-d_6, 150 MHz) δ 94.25, 119.58, 128.27, 130.35, 130.64, 141.47, 150.59, 151.49, 151.70*

*2 peaks missing - not found through JMOD/HSQC/HMBC.

6.112. 4-(3-((7*H*-pyrrolo[2,3-*d*]pyrimidin-4-yl)amino)phenyl)-2-methylbut-3-yn-2-ol 82

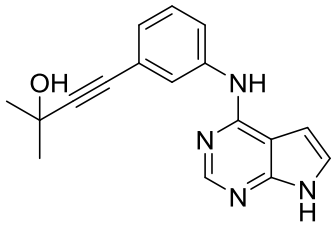

Copper iodide (7.4 mg, 0.04 mmol) and tetrakis(triphenylphosphine)palladium(0) (12 mg, 0.02 mmol) were stirred under nitrogen in DMF (1 mL) in a sealed 0.5-2 mL microwave vial. *N*-(3-iodophenyl)-7*H*-pyrrolo[2,3-*d*]pyrimidin-4-amine (66 mg, 0.2 mmol) and 2-methylbut-3-yn-2-ol (39 µL, 0.4 mmol) were added in a solution of DIPA (112 µL, 0.8 mmol) and DMF (1 mL) and the solution stirred at 100 °C for 18 hours. Resultant solution was diluted in ethyl acetate and washed with water before removing solvent under reduced pressure. HPLC purification yielded product as a white TFA salt (10 mg, 12%); (LC-MS purity = 99.1%); ^{1}H (DMSO-d_6, 400 MHz) δ 1.48 (s, 6H), 6.82 (s, 1H), 7.13 (d, *J* = 7.3 Hz, 1H), 7.34 (d, *J* = 3 Hz, 1H), 7.38 (t, *J* = 7.9 Hz, 1H), 7.81 (d, *J* = 7.8 Hz, 1H), 7.94 (d, *J* = 7.94 Hz, 1H), 8.39 (s, 1H); ^{13}C (DMSO-d_6, 150 MHz) δ 32.07, 64.10, 80.77, 96.57, 99.65, 100.22, 122.00, 123.57, 123.91, 124.48, 126.83, 129.75, 139.53, 149.63, 150.90, 152.58; HRMS (ESI +ve): For $C_{17}H_{17}N_4O$ requires 293.1397 found 293.1395.

6.113. 4-(3-((6-Aminopyrimidin-4-yl)amino)phenyl)-2-methylbut-3-yn-2-ol 83

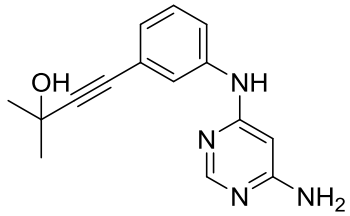

Copper iodide (7.4 mg, 0.04 mmol), Pd(dppf)Cl_2 (16.3 mg, 0.02 mmol) and N^4-(3-iodophenyl)pyrimidine-4,6-diamine (62 mg, 0.2 mmol) were placed in a 2-5 mL microwave vial which was sealed and purged with argon. DMF (anhy., 1 mL) and DIPA (112 µL, 0.8 mmol) were added and the solution heated to 90 °C before addition of 2-methylbut-3-yn-2-ol (39 µL, 0.4 mmol) and stirring for 24 hours. HPLC purification yielded title product as an off-white TFA salt (12 mg, 16%). (LC-MS purity = 94.9%); ^{1}H (DMSO-d_6, 500 MHz) δ 1.47 (s, 6H), 5.93 (s, 1H), 7.15 (d, J = 7 Hz, 1H), 7.38 (m, 2H), 7.51 (br s, 1H), 7.73 (br s, 2H) 8.38 (br s, 1H), 10.02 (s, 1H); ^{13}C (DMSO-d_6, 150 MHz) δ 31.53, 63.58, 79.98, 82.97, 96.34, 121.71, 123.30, 124.14, 126.95, 129.43, 129.45, 138.53, 149.06, 151.33; HRMS (ESI +ve): For $C_{15}H_{17}N_4O$ requires 269.1397 found 269.1392.

6.114. 4-(3-((2-Aminopyrimidin-4-yl)amino)phenyl)-2-methylbut-3-yn-2-ol 84

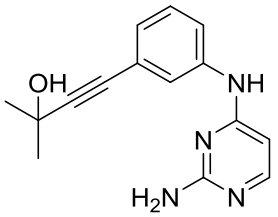

Copper iodide (7.4 mg, 0.04 mmol), Pd(dppf)Cl_2 (16.3 mg, 0.02 mmol) and N^4-(3-iodophenyl)pyrimidine-2,4-diamine (62 mg, 0.2 mmol) were placed in a 2-5 mL microwave vial which was sealed and purged with argon. DMF (anhy., 1 mL) and DIPA (112 µL, 0.8 mmol) were added and the solution heated to 90 °C before addition of 2-methylbut-3-yn-2-ol (39 µL, 0.4 mmol) and stirring for 24 hours. HPLC purification yielded title product as an off-white TFA salt (15 mg, 20%). (LC-MS purity = 94.9%); ^{1}H (DMSO-d_6, 500 MHz) δ 1.48 (s, 6H), 3.17 (t, *J* = 8.5 Hz, 2H), 4.10 (t, 8.5 Hz, 2H), 6.27 (d, *J* = 6.8 Hz, 1H), 7.20 (m, 2H), 7.43 (br s, 2H), 8.03 (d, *J* = 6.8 Hz, 1H), 8.70 (d, *J* = 1.5 Hz, 1H); ^{13}C (DMSO-d_6, 100 MHz) δ 32.04, 64.11, 80.41, 96.97, 123.72, 127.98, 129.82, 138.54, 143.32, 155.89, 161.99; HRMS (ESI +ve): For $C_{15}H_{17}N_4O$ requires 269.1397 found 269.1395.

6.115. 4-(3-((9*H*-purin-6-yl)amino)phenyl)-2-methylbut-3-yn-2-ol 85

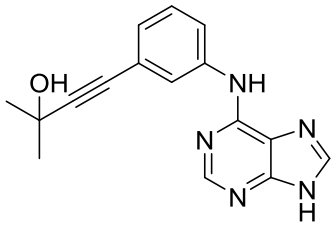

Copper iodide (7.4 mg, 0.04 mmol), $Pd(dppf)Cl_2$ (16.3 mg, 0.02 mmol) and *N*-(3-iodophenyl)-9*H*-purin-6-amine (70 mg, 0.24 mmol) were placed in a 2-5 mL microwave vial which was sealed and purged with argon. DMF (anhy., 1 mL) and DIPA (112 µL, 0.8 mmol) were added and the solution heated to 90 °C before addition of 2-methylbut-3-yn-2-ol (39 µL, 0.4 mmol) and stirring for 24 hours. HPLC purification yielded title product as an off-white TFA salt (22 mg, 23%). (LC-MS purity = 99.9%); ^{1}H (DMSO-d_6, 500 MHz) δ 1.48 (br s, 6H), 7.08 (d, *J* = 7.3 Hz, 1H), 7.34 (t, *J* =7.7 Hz, 1 H), 7.86 (d, J=7.8 Hz, 1 H), 8.08 (br s, 1 H), 8.39 (br s, 1 H), 8.48 (br s, 1 H), 10.01 (br s, 1 H); ^{13}C not obtained- signal suppression due to nitrogen; HRMS (ESI +ve): For $C_{16}H_{16}N_5O$ requires 294.1349 found 294.1347.

6.116. 4-Chloro-5-iodo-7*H*-pyrrolo[2,3-*d*]pyrimidine 97

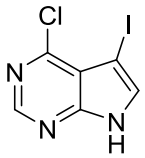

4-Chloro-7*H*-pyrrolo[2,3-*d*]pyrimidine (400 mg, 2.62 mmol) and *N*-iodosuccinimide (646 mg, 2.88 mmol) were suspended in DCM (20 mL) and stirred at room temperature for 16 hours. Solvent was removed under reduced pressure and solids stirred in saturated sodium thiosulfate (50 mL) for 5 minutes. Suspension was filtered, washed with water and pet. ether to yield title product as a pale tan solid (687 mg, 91%). ^{1}H (DMSO-d_6, 500 MHz) δ 7.94 (s, 1H), 8.60 (s, 1H), 12.96 (br s, 1H);); ^{13}C (DMSO-d_6, 125 MHz) δ 52.13, 116.26, 134.35, 150.96, 151.21, 152.00.

6.117. 4-Chloro-7*H*-pyrrolo[2,3-*d*]pyrimidine-5-carbaldehyde 98

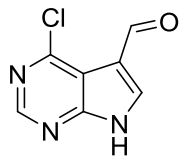

4-Chloro-5-iodo-7*H*-pyrrolo[2,3-*d*]pyrimidine (2.23 g, 8 mmol) was stirred in anhydrous THF (50 mL) under argon at -78 °C for 5 minutes. n-butyllithium (2M in hexanes, 8.8 mL, 17.6 mmol) was added slowly and solution was stirred for 1 hour. Anhydrous DMF (0.62 mL, 8 mmol) was added and stirring continued for 30 minutes before warming to room temperature and stirring for a further 1 hour. Water (2 mL) was added and solvent removed under reduced pressure. Solids were solubilised in ethyl acetate, washed with sat. ammonium chloride solution and dried over magnesium sulfate. Product was adsorbed to silica and chromatographic purification (Biotage SP4, 10 g cartridge, solvent system: pet. ether/ethyl acetate, 10%, 15CV) yielded an analytically pure sample of title compound. ^{1}H (DMSO-d_6, 500 MHz) δ 8.60 (s, 1H), 8.75 (s, 1H), 10.25 (s, 1H), 13.55 (br s, 1H); ^{13}C (DMSO-d_6, 125 MHz) δ 114.29, 116.04, 137.75, 151.67, 152.18, 154.24, 184.37.

6.118. 4-Chloro-7*H*-pyrrolo[2,3-*d*]pyrimidine-5-carbaldehyde oxime 99

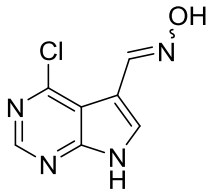

4-Chloro-7*H*-pyrrolo[2,3-*d*]pyrimidine-5-carbaldehyde (171 mg, 0.94 mmol), sodium carbonate (212 mg, 2 mmol) and hydroxylamine hydrochloride (244 mg, 3.5 mmol) were solubilised in ethanol (9 mL) and water (1 mL) and stirred at room temperature for 2 hours. Solvent was removed under reduced pressure and solids sonicated in water for 2 minutes. Suspension was filtered and washed with water and pet. ether to yield title product as a pale tan solid (178 mg, 96%, 5:7 mixture of isomers by ^{1}H NMR). ^{1}H (DMSO-d_6, 500 MHz) δ 8.02 and 8.10 (s, 1H), 8.52 and 8.58 (s, 1H), 8.63 and 8.67 (s, 1H), 11.08 and 11.80 (s, 1H); ^{13}C (DMSO-d_6, 125 MHz) δ 107.93, 114.25, 126.54, 141.35, 150.83, 151.10, 152.78 and 105.32, 113.93, 133.66, 136.94, 150.76, 151.43, 152.00; LC-MS R_t = 4.84 (m/z = 197.0 (100%) and 198.9 (40%)) and 4.70 minutes (m/z = 196.9 (100%) and 199.1 (20%)) ($C_7H_6ClN_4O$, $[M+1]^+$).

6.119. 4-Chloro-7*H*-pyrrolo[2,3-*d*]pyrimidine-5-carbonitrile 99

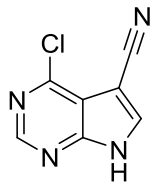

4-Chloro-7*H*-pyrrolo[2,3-*d*]pyrimidine-5-carbaldehyde oxime (158 mg, 0.8 mmol) and $SOCl_2$ (580 µL, 8 mmol) were solubilised in DCM (10 mL) and stirred at room temperature for 16 hours. Solvent was removed under reduced pressure and residual $SOCl_2$ was azeotroped with toluene. Solids were stirred in sat. sodium bicarbonate for 5 minutes before filtering and washing with water and pet. ether to yield title compound as a pale brown solid (71 mg, 50%). ^{1}H (DMSO-d_6, 500 MHz) δ 8.69 (s, 1H), 8.79 (s, 1H), 13.65 (br s, 1H); ^{13}C (DMSO-d_6, 125 MHz) δ 85.81, 114.73, 115.50, 139.00, 151.30, 152.18, 152.87; IR major peaks (cm^{-1}): 1236.4, 1560.4, 1604.8, 2239.4, 2816.1, 2955.0m 3074.5; LRMS (ESI -ve) found 177.0, 179.0 (100:35) ($C_7H_2ClN_4$, $[M-1]^-$).

6.120. 4-(6-Bromoindolin-1-yl)-7*H*-pyrrolo[2,3-*d*]pyrimidine-5-carbonitrile

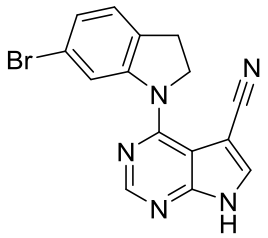

4-Chloro-7*H*-pyrrolo[2,3-*d*]pyrimidine-5-carbonitrile (65 mg, 0.33 mol) and 6-bromoindoline (61 mg, 0.33 mmol) were dissolved in isopropyl alcohol (2 mL) and dioxane (1 mL) in a 10-20 mL microwave vial and heated to 175 °C for 3 hours under microwave conditions. Water (10 mL) was added and the resulting precipitate filtered, washing with water to yield title product as a brown solid (98mg, 87%). ^{1}H (DMSO-d_6, 400 MHz) δ 3.24 (t, *J* = 8.3 Hz, 2H), 4.56 (t, *J* = 8.3 Hz, 2H), 7.16 (dd, *J* = 7.9 & 1.9 Hz), 7.25 (d, *J* = 7.6 Hz, 1H), 8.30 (d, *J* = 1.8 Hz, 1H), 8.47 (s, 1H), 8.51 (s, 1H), 13.13 (br s, 1H);); ^{13}C (DMSO-d_6, 150 MHz) δ 28.22, 52.88, 84.21, 102.89, 117.78, 119.61, 119.84, 125.43, 126.78, 132.48, 136.32, 145.98, 152.11, 153.28, 153.76; LRMS (ESI +ve) found 340.0, 342.0 (50:50) ($C_{15}H_{11}BrN_5$, $[M+1]^+$).

6.121. 4-(6-(3-Hydroxy-3-methylbut-1-yn-1-yl)indolin-1-yl)-7*H*-pyrrolo[2,3-*d*]pyrimidine-5-carbonitrile 86

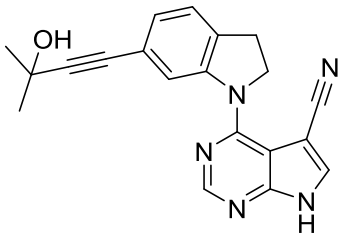

4-(6-Bromoindolin-1-yl)-7*H*-pyrrolo[2,3-*d*]pyrimidine-5-carbonitrile (85 mg, 0.25 mmol), copper iodide (9.5 mg, 0.05 mmol) and Pd(dppf)Cl_2 (19 mg, 0.025 mmol) were stirred under argon in DMF (1 mL) in a sealed 0.5-2 mL microwave vial. DIPA (140 µL, 1 mmol) and 2-methylbut-3-yn-2-ol (98 µL, 1 mmol) were added before heating to 90 °C with stirring for 18 hours. Product was adsorbed onto silica and chromatographic purification (Biotage SP4, 10 g cartridge, solvent system: pet. ether/ethyl acetate, 10%, 8 CV; 10-100%, 8 CV; 100%, 8 CV) followed by HPLC purification yielded title product as a white TFA salt (8 mg, 9%) (LC-MS purity = 96.5%); ^{1}H (DMSO-d_6, 500 MHz) δ 1.47 (s, 6H), 3.28 (t, *J* = 8.2 Hz, 2H), 4.55 (t, *J* = 8.3 Hz, 2H), 7.03 (dd, *J* = 7.6 & 0.9 Hz, 1H), 7.28 (d, *J* = 7.6 Hz, 1H), 8.13 (s, 1H), 8.45 (s, 1H), 8.50 (s, 1H), 13.10 (br s, 1H); ^{13}C (DMSO-d_6, 125 MHz) δ 28.68, 32.14, 52.72, 64.10, 81.49, 84.28, 95.45, 102.84, 117.90, 119.86, 121.23, 125.41, 126.49, 133.59, 136.19, 144.46, 152.18, 153.28, 154.01; HRMS (ESI +ve): For $C_{20}H_{18}N_5O$ requires 344.1506 found 334.1490.

6.122. 2-Amino-4-(6-bromoindolin-1-yl)-7*H*-pyrrolo[2,3-*d*]pyrimidine-5-carbonitrile

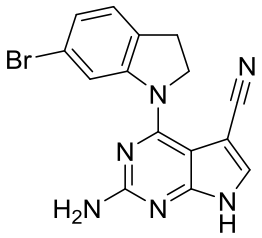

N-(4-chloro-5-cyano-6,7-dihydro-5*H*-pyrrolo[2,3-*d*]pyrimidin-2-yl)pivalamide (36 mg, 0.13 mmol) and 6-bromoindoline (26 mg, 0.13 mmol) were dissolved in isopropyl alcohol (2 mL) and dioxane (1 mL) in a 10-20 mL microwave vial and heated to 175 °C for 3 hours under microwave conditions. Brine (10 mL) was added and the resulting precipitate filtered, washing with water to yield title product as a brown solid (38mg, 82%). ^{1}H (DMSO-d_6, 500 MHz) δ 3.17 (t, *J* = 8.3 Hz, 2H), 4.43 (t, *J* = 8.3 Hz, 2H), 7.09 (dd, *J* = 7.8 & 1.8 Hz, 1H), 7.19 (d, *J* = 7.9 Hz, 1H), 7.98 (s, 1H), 8.14 (d, *J* = 1.7 Hz, 1H); ^{13}C (DMSO-d_6, 125 MHz) δ 28.09, 52.68, 84.25, 96.03, 118.38, 119.40, 119.89, 124..98, 126.58, 132.17, 133.15, 141.39, 146.41, 154.49, 178.57; LRMS (ESI +ve) found 355.0, 356.9 (50:50) ($C_{15}H_{12}BrN_6$, $[M+1]^+$).

6.123. 2-Amino-4-(6-(3-hydroxy-3-methylbut-1-yn-1-yl)indolin-1-yl)-7*H*-pyrrolo[2,3-*d*]pyrimidine-5-carbonitrile 87

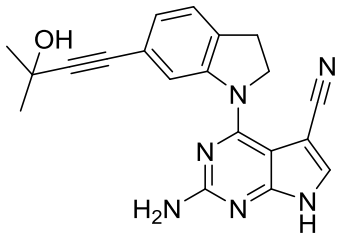

2-Amino-4-(6-bromoindolin-1-yl)-7*H*-pyrrolo[2,3-*d*]pyrimidine-5-carbonitrile (35.5 mg, 0.1 mmol), copper iodide (1.9 mg, 0.02 mmol) and Pd(dppf)Cl_2 (7.3 mg, 0.01 mmol) were stirred under argon in DMF (1 mL) in a sealed 0.5-2 mL microwave vial. DIPA (56 µL, 0.4 mmol) and 2-methylbut-3-yn-2-ol (29 µL, 0.3 mmol) were added before heating to 100 °C with stirring for 18 hours. Product was adsorbed onto silica and chromatographic purification (Biotage SP4, 10 g cartridge, solvent system: pet. ether/ethyl acetate, 50% 6CV; 50-100% 6CV; 100% 10CV) yielded title product as a brown solid (13 mg, 36%). (LC-MS purity = 95.0%); ^{1}H (DMSO-d_6, 500 MHz) δ 1.47 (s, 6H), 3.21 (t, *J* = 8.1 Hz, 2H), 4.40 (t, *J* = 8.1 Hz, 2H), 5.40 (s, 1H), 6.21 (br s, 2H), 6.95 (d, *J* = 7.3 Hz, 1H), 7.22 (d, *J* = 7.5 Hz, 1H), 7.88 (s, 1H), 7.98 (s, 1H), 12.19 (br s, 1H); ^{13}C (DMSO-d_6, 125 MHz) δ 28.55, 32.16 (2C), 52.48, 64.11, 81.75, 84.18, 95.27, 96.33, 118.41, 118.88, 121.37, 125.18, 125.78, 132.93, 133.16, 145.14, 154.78, 156.14, 160.17; LRMS (ESI +ve): 359.1 ([M+1]$^+$); HRMS (ESI +ve): For $C_{20}H_{19}N_6O$ requires 359.1615 found 196.0695 (M^{2+}+NH_4^+)

6.124. 4-Chloro-5-(cyclopropylethynyl)-7*H*-pyrrolo[2,3-*d*]pyrimidine

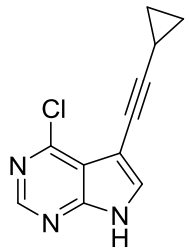

4-Chloro-5-iodo-7*H*-pyrrolo[2,3-*d*]pyrimidine (140 mg, 0.5 mmol), $Pd(PPh_3)_2Cl_2$ (36 mg, 0.05 mmol) and CuI (19 mg, 0.1 mmol) were stirred under argon in DMF (2 mL) in a sealed 10-20 mL microwave vial. DIPA (280 µL, 2 mmol) and ethynylcyclopropane (160 µL, 2 mmol) was added and the reaction stirred at r.t. for 72 hours. Product was adsorbed onto celite and chromatographic purification (Biotage SP4, 10 g cartridge, solvent system: pet. ether/ethyl acetate; 10%, 6CV; 10-50%, 4 CV; 50%, 4 CV) yielded title compound as a yellowy solid (56 mg, 52%). ^{1}H (DMSO-d_6, 500 MHz) δ 0.74 (m, 2H), 0.89 (m, 2H), 1.57 (m, 1H), 7.90 (s, 1H), 8.59 (s, 1H), 12.76 (br s, 1H); ^{13}C (DMSO-d_6, 125 MHz) δ 0.02, 8.08 (2C), 67.66, 95.11, 95.87, 115.62, 131.90, 151.08, 151.17; LRMS (ESI +ve): 218.1, 220.1 (100:30) ($C_{11}H_9ClN_3$, $[M+1]^+$).

6.125. 4-(6-Bromoindolin-1-yl)-5-(cyclopropylethynyl)-7*H*-pyrrolo[2,3-*d*]pyrimidine

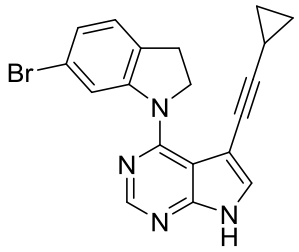

4-Chloro-5-(cyclopropylethynyl)-7*H*-pyrrolo[2,3-*d*]pyrimidine (43 mg, 0.2 mmol) and 6-bromoindoline (44 mg, 0.22 mmol) were stirred in isopropyl alcohol (2 mL) and dioxane (1 mL) under microwave conditions at 175 °C for 2 hours. Organics were adsorbed to celite and chromatographic purification (Biotage SP4, 10 g cartridge, solvent system: pet. ether/ethyl acetate; 0%, 4 CV; 0-50%, 6 CV; 50%, 6 CV, 50-100%, 4 CV; 100%, 6 CV) yielded impure title compound (38 mg, 56% pure by LC) LRMS (ESI +ve): 379.0, 381.0 (50:50) ($C_{19}H_{16}BrN_4$, $[M+1]^+$).

6.126. 4-(1-(5-(Cyclopropylethynyl)-7*H*-pyrrolo[2,3-*d*]pyrimidin-4-yl)indolin-6-yl)-2-methylbut-3-yn-2-ol 88

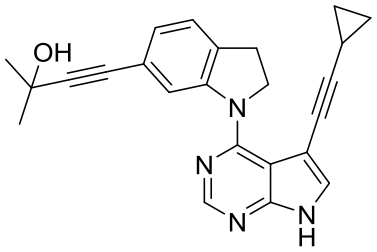

Impure 4-(6-bromoindolin-1-yl)-5-(cyclopropylethynyl)-7*H*-pyrrolo[2,3-*d*]pyrimidine (30 mg, 0.08 mmol), $Pd(PPh_3)_2Cl_2$ (2.8 mg, 400 µmol) and CuI (1.5 mg, 800 µmol) were stirred under argon in DMF (1 mL) in a sealed 0.5-2 mL microwave vial. DIPA (25 µL, 0.32 mmol) and 2-methylbut-3-yn-2-ol (32 µL, 0.32 mmol) were added and the reaction stirred at 90 °C for 16 hours. HPLC purification yielded title product as a white TFA salt (6 mg, 3% over 2 steps). (LC-MS purity = 98.4%). ^{1}H (DMSO-d_6, 500 MHz) δ 0.13 (m, 2H), 0.46 (m, 2H), 0.89 (m, 1H), 1.44 (s, 6H), 3.12 (t, *J* = 7.9 Hz, 2H), 4.22 (t, *J* = 8.1 Hz, 2H), 6.89 (d, *J* = 7.5 Hz, 1H), 6.99 (s, 1H), 7.23 (d, *J* = 7.5 Hz, 1H), 7.40 (s, 1H), 8.31 (d, *J* = 2.1 Hz, 1H), 8.50 (s, 1H), 12.65 (br s, 1H); LRMS (ESI +ve): 383.1 ($C_{24}H_{23}N_5O$, $[M+1]^+$) and 401.1 ($C_{24}H_{25}N_5O_2$, $[M+H_3O]^+$)

d. Biochemical assays

IKK biochemical assay

Recombinant IKKα (active) 37 nM or recombinant IKKβ (active) 37 nM, (Millipore, Dundee, UK) were incubated with IκBα (Ser32), biotinylated peptide substrate (0.375 µM or 0.18 µM respectively) (New England Biolabs, Hitchin, UK) and ATP (40 µM or 10 µM respectively) in assay buffer (40 mM Tris-HCl (pH 7.5), 20 mM $MgCl_2$, EDTA 1 mM, DTT 2 mM and BSA 0.01 mg/mL) in a V-bottom 96-well plate in the presence and absence of test compound or standard.

The assay plate was then incubated for 1 hour at 30 °C, after which the kinase reaction was quenched by the addition of 50 mM EDTA, pH8. The resulting mixture was transferred to a streptavidin coated 96-well plate (Perkin Elmer, Beaconsfield, UK) and incubated for 1 hour at 30 °C to immobilise the substrate peptide. After three washes with wash buffer (0.01 M PBS, 0.05% Tween-20, pH 7.4), p-IκBα (Ser32/36) mouse mAb (New England Biolabs, Hitchin, UK) (1:1000 dilution with 1% BSA in wash buffer) (40 µL) was added and incubated at 37 °C for 2 hours.

After a further three washes, a secondary europiated antibody (Eu-N1 labelled anti-mouse IgG, (Perkin Elmer, Beaconsfield, UK) diluted 1:500 with 1% BSA in wash buffer) (40 µL) was added and incubated at 30 °C for 30 minutes. After a further five washes, DELFIA enhancement solution (Perkin Elmer, Beaconsfield UK) was added and allowed to incubate for 10 min at room temperature, protected from light. The relative fluorescence units (RFU) signal were measured on a Wallac Victor2 1420 multilabel counter (Perkin Elmer, Beaconsfield, UK), in time-resolved fluorescence mode. The counter was set at an excitation wavelength of 340 nm with a 400 µs delay before detecting emitted light at 615 nm.

The apparent K_i was calculated for each compound using the Cheng-Prusoff Equation.[145]

NIK biochemical assay

Recombinant human NIK (active) 5 nM (Promega, USA) was added to MBP 0.1 mg/mL (Promega, USA) and 5 µM ATP in assay buffer (40 mM Tris-HCl (pH 7.5 ± 0.05), 20 mM $MgCl_2$, BSA 0.1 mg/mL and DTT (50 µM) in a white half well 96-well plate (Greiner Bio One GmbH, Germany), in the presence and absence of test compound, to a total volume of 20 µL. Plate was covered with a lid, wrapped in cling film and placed in a foil bag (previously stored streptavidin coated plate (Perkin Elmer, UK)) and shaken on a Stuart microplate shaker (Bibby Scientific Ltd, UK) at 850 rpm for 1 minute before incubating at 30 °C for 1 hour. Plate was removed from foil bag and allowed to equilibrate to 21 °C for 15 minutes before addition of Kinase-Glo® reagent (Promega, USA) (20 µL). Mixture was incubated in the dark for 10 minutes and luminescence was detected on a Wallac Victor^2 1420 multilabel counter (Perkin Elmer, UK).

The apparent K_i was calculated for each compound using the Cheng-Prusoff Equation.[145]

e. Computational methods

Docking methods

Structures to be docked were first drawn in ChemDraw[245] and prepared using Pipeline Pilot[246] to “add hydrogens”, “minimize molecule” and calculate “3D co-ordinates”. Protein crystal structures were downloaded from the PDB and prepared in Discovery Studio[247] by removing crystallisation artefacts and non-structural waters. Prepared compounds were docked using CCDC GOLD software.[248] Chemscore_kinase was used as the template and any structural water or crystallised ligand extracted and reloaded. Binding sites were defined as a centroid around the approximate centre of the orthosteric binding site and residues within 10 Å made available for interaction. Compounds were given the freedom for amides and protonated carboxylic acids to flip, as were planar nitrogens. Pyramidal nitrogens were also allowed to invert. ChemPLP with default parameters was used as the scoring function and no early termination was allowed. Compounds were docked either 10 or 100 times with diverse solutions requested for library docking prior to synthesis.

7. References

(1) NIH National Cancer Institute. What Is Cancer? http://www.cancer.gov/about-cancer/understanding/what-is-cancer (accessed Jul 4, 2016).

(2) Organisation, W. H. *World Cancer Report 2014*, 1st ed.; Stewart, B. W., Wild, C. P., Eds.; International Agency for Research on Cancer, 2014.

(3) Hanahan, D.; Weinberg, R. A. The Hallmarks of Cancer. *Cell* **2000**, *100* (1), 57–70.

(4) Hanahan, D.; Weinberg, R. A. Hallmarks of Cancer: The next Generation. *Cell* **2011**, *144* (5), 646–674.

(5) World Cancer Research Fund International. Cancer facts and figures http://www.wcrf.org/int/cancer-facts-figures/data-specific-cancers/pancreatic-cancer-statistics (accessed Mar 30, 2016).

(6) Cancer Research UK. Survival statistics for Pancreatic Cancer http://www.cancerresearchuk.org/about-cancer/type/pancreatic-cancer/treatment/statistics-and-outlook-for-pancreatic-cancer (accessed Jul 22, 2016).

(7) Cancer Research UK. Types of pancreatic cancer http://www.cancerresearchuk.org/about-cancer/type/pancreatic-cancer/about/types-of-pancreatic-cancer (accessed Jul 22, 2016).

(8) Perkins, G. L.; Slater, E. D.; Sanders, G. K.; Prichard, J. G. Serum Tumor Markers. *Am. Fam. Physician* **2003**, *68* (6), 1075–1082.

(9) Maestranzi, S.; Przemioslo, R.; Mitchell, H.; Sherwood, R. A. The Effect of Benign and Malignant Liver Disease on the Tumour Markers CA19-9 and CEA. *Ann. Clin. Biochem.* **1998**, *35* (1), 99–103.

(10) Cancer Research UK. Tests for pancreatic cancer http://www.cancerresearchuk.org/about-cancer/type/pancreatic-cancer/diagnosis/tests-for-pancreatic-cancer (accessed Jul 22, 2016).

(11) Cancer Research UK. The stages of pancreatic cancer

http://www.cancerresearchuk.org/about-cancer/type/pancreatic-cancer/treatment/the-stages-of-pancreatic-cancer#number (accessed Jul 22, 2016).

(12) Cancer Research UK. Types of treatment for pancreatic cancer http://www.cancerresearchuk.org/about-cancer/type/pancreatic-cancer/treatment/which-treatment-for-pancreatic-cancer (accessed Jul 22, 2016).

(13) Cerqueira, N. M. F. S. A.; Fernandes, P. A.; Ramos, M. J. Understanding Ribonucleotide Reductase Inactivation by Gemcitabine. *Chem. - A Eur. J.* **2007**, *13* (30), 8507–8515.

(14) Oettle, H.; Post, S.; Neuhaus, P.; Gellert, K.; Langrehr, J.; Ridwelski, K.; Schramm, H.; Fahlke, J.; Zuelke, C.; Burkart, C.; Gutberlet, K.; Kettner, E.; Schmalenberg, H.; Weigang-Koehler, K.; Bechstein, W.-O.; Niedergethmann, M.; Schmidt-Wolf, I.; Roll, L.; Doerken, B.; Riess, H. Vs Observation in Patients Undergoing Curative-Intent Resection of Pancreatic Cancer. *J. Am. Med. Assoc.* **2007**, *297* (3), 267–277.

(15) Ahmad, S. I.; Kirk, S. H.; Eisenstark, A. Thymine Metabolism and Thymineless Death in Prokaryotes and Eukaryotes. *Annu. Rev. Microbiol.* **1998**, *52* (1), 591–625.

(16) Nicolson, M.; Webb, A.; Cunningham, D.; Norman, A.; O'Brien, M.; Hill, A.; Hickish, T. Cisplatin and Protracted Venous Infusion 5-Fluorouracil (CF)--Good Symptom Relief with Low Toxicity in Advanced Pancreatic Carcinoma. *Ann. Oncol.* **1995**, *6* (8), 801–804.

(17) Rao, S.; Cunningham, D. Advanced Pancreatic Cancer--5 Years on. *Ann. Oncol.* **2002**, *13* (8), 1165–1168.

(18) World Cancer Research Fund International. Cancer facts and figures http://www.wcrf.org/int/cancer-facts-figures/data-specific-cancers/prostate-cancer-statistics (accessed Apr 4, 2016).

(19) Cancer Research UK. Prostate cancer symptoms http://www.cancerresearchuk.org/about-cancer/type/prostate-cancer/about/prostate-cancer-symptoms (accessed Apr 4, 2016).

(20) Sanford, M. T.; Greene, K. L.; Carroll, P. R. The Argument for Palliative Care in Prostate Cancer. *Transl. Androl. Urol.* **2013**, *2* (4), 278–280.

(21) Seruga, B.; Ocana, A.; Tannock, I. F. Drug Resistance in Metastatic Castration-Resistant Prostate Cancer. *Nat. Rev. Clin. Oncol.* **2011**, *8* (1), 12–23.

(22) Ahmed, A.; Ali, S.; Sarkar, F. H. Advances in Androgen Receptor Targeted Therapy for Prostate Cancer. *J. Cell. Physiol.* **2014**, *229* (3), 271–276.

(23) Farmer, R. Prostate Cancer: Epidemiology and Risk Factors. *Trends Urol. Gynaecol. Sex. Heal.* **2008**, *13* (3), 32–34.

(24) Crawford, E. D. Epidemiology of Prostate Cancer. *Urology* **2003**, *62* (6 SUPPL. 1), 3–12.

(25) Collin, S. M.; Martin, R. M.; Metcalfe, C.; Gunnell, D.; Albertsen, P. C.; Neal, D.; Hamdy, F.; Stephens, P.; Lane, J. A.; Moore, R.; Donovan, J. Prostate-Cancer Mortality in the USA and UK in 1975-2004: An Ecological Study. *Lancet Oncol.* **2008**, *9* (5), 445–452.

(26) Suzman, D. L.; Antonarakis, E. S. Castration-Resistant Prostate Cancer: Latest Evidence and Therapeutic Implications. *Ther. Adv. Med. Oncol.* **2014**, *6* (4), 167–179.

(27) Prostate Cancer UK. Treatments http://prostatecanceruk.org/prostate-information/treatments?category=6606 (accessed Jan 5, 2016).

(28) Magon, N. Gonadotropin Releasing Hormone Agonists: Expanding Vistas. *Indian Journal of Endocrinology and Metabolism*. 2011, pp 261–267.

(29) Cook, T.; Sheridan, W. P. Development of GnRH Antagonists for Prostate Cancer: New Approaches to Treatment. *Oncologist* **2000**, *5* (2), 162–168.

(30) Akaza, H. Combined Androgen Blockade for Prostate Cancer: Review of Efficacy, Safety and Cost-Effectiveness. *Cancer Sci.* **2011**, *102* (1), 51–56.

(31) FDA. FDA approves new treatment for a type of late stage prostate cancer http://www.fda.gov/NewsEvents/Newsroom/PressAnnouncements/ucm317838.htm (accessed Apr 12, 2016).

(32) Shore, N. D.; Chowdhury, S.; Villers, A.; Klotz, L.; Siemens, D. R.; Phung, D.; van Os, S.; Hasabou, N.; Wang, F.; Bhattacharya, S.; Heidenreich, A. Efficacy and Safety of Enzalutamide versus Bicalutamide for Patients with Metastatic Prostate Cancer

(TERRAIN): A Randomised, Double-Blind, Phase 2 Study. *Lancet Oncol.* **2016**, *2045* (15), 1–11.

(33) Drugs.com. Drug price database http://www.drugs.com/price-guide (accessed Apr 12, 2016).

(34) Petrylak, D. P.; Tangen, C. M.; Hussain, M. H. A.; Lara, P. N.; Jones, J. A.; Taplin, M. E.; Burch, P. A.; Berry, D.; Moinpour, C.; Kohli, M.; Benson, M. C.; Small, E. J.; Raghavan, D.; Crawford, E. D. Docetaxel and Estramustine Compared with Mitoxantrone and Prednisone for Advanced Refractory Prostate Cancer. *N. Engl. J. Med.* **2004**, *351* (15), 1513–1520.

(35) Tannock, I. F.; de Wit, R.; Berry, W. R.; Horti, J.; Pluzanska, A.; Chi, K. N.; Oudard, S.; Théodore, C.; James, N. D.; Turesson, I.; Rosenthal, M. A.; Eisenberger, M. A. Docetaxel plus Prednisone or Mitoxantrone plus Prednisone for Advanced Prostate Cancer. *N. Engl. J. Med.* **2004**, *351* (15), 1502–1512.

(36) Small, E. J.; Tchekmedyian, N. S.; Rini, B. I.; Fong, L.; Lowy, I.; Allison, J. P. A Pilot Trial of CTLA-4 Blockade with Human Anti-CTLA-4 in Patients with Hormone-Refractory Prostate Cancer. *Clin. Cancer Res.* **2007**, *13* (6), 1810–1815.

(37) Kwon, E. D.; Drake, C. G.; Scher, H. I.; Fizazi, K.; Bossi, A.; Van den Eertwegh, A. J. M.; Krainer, M.; Houede, N.; Santos, R.; Mahammedi, H.; Ng, S.; Maio, M.; Franke, F. A.; Sundar, S.; Agarwal, N.; Bergman, A. M.; Ciuleanu, T. E.; Korbenfeld, E.; Sengeløv, L.; Hansen, S.; Logothetis, C.; Beer, T. M.; McHenry, M. B.; Gagnier, P.; Liu, D.; Gerritsen, W. R. Ipilimumab versus Placebo after Radiotherapy in Patients with Metastatic Castration-Resistant Prostate Cancer That Had Progressed after Docetaxel Chemotherapy (CA184-043): A Multicentre, Randomised, Double-Blind, Phase 3 Trial. *Lancet Oncol.* **2014**, *15* (7), 700–712.

(38) Joyce, D. D. CD28 and CTLA-4 Have Opposing Effects on the Response of T Cells to Stimulation. *J. Exp. Med.* **1996**, *43* (2), 329–375.

(39) Brahmer, J. R.; Drake, C. G.; Wollner, I.; Powderly, J. D.; Picus, J.; Sharfman, W. H.; Stankevich, E.; Pons, A.; Salay, T. M.; McMiller, T. L.; Gilson, M. M.; Wang, C.; Selby, M.; Taube, J. M.; Anders, R.; Chen, L.; Korman, A. J.; Pardoll, D. M.; Lowy, I.; Topalian, S. L. Phase I Study of Single-Agent Anti-Programmed Death-1 (MDX-1106)

in Refractory Solid Tumors: Safety, Clinical Activity, Pharmacodynamics, and Immunologic Correlates. *J. Clin. Oncol.* **2010**, *28* (19), 3167–3175.

(40) Topalian, S. L.; Hodi, F. S.; Brahmer, J. R.; Gettinger, S. N.; Smith, D. C.; McDermott, D. F.; Powderly, J. D.; Carvajal, R. D.; Sosman, J. A.; Atkins, M. B.; Leming, P. D.; Spigel, D. R.; Antonia, S. J.; Horn, L.; Drake, C. G.; Pardoll, D. M.; Chen, L.; Sharfman, W. H.; Anders, R. A.; Taube, J. M.; McMiller, T. L.; Xu, H.; Korman, A. J.; Jure-Kunkel, M.; Agrawal, S.; McDonald, D.; Kollia, G. D.; Gupta, A.; Wigginton, J. M.; Sznol, M. Safety, Activity, and Immune Correlates of Anti–PD-1 Antibody in Cancer. *N. Engl. J. Med.* **2012**, *366* (26), 2443–2454.

(41) Wolchok, J. D.; Kluger, H.; Callahan, M. K.; Postow, M. a; Rizvi, N. a; Lesokhin, A. M.; Segal, N. H.; Ariyan, C. E.; Gordon, R.-A.; Reed, K.; Burke, M. M.; Caldwell, A.; Kronenberg, S. a; Agunwamba, B. U.; Zhang, X.; Lowy, I.; Inzunza, H. D.; Feely, W.; Horak, C. E.; Hong, Q.; Korman, A. J.; Wigginton, J. M.; Gupta, A.; Sznol, M. Nivolumab plus Ipilimumab in Advanced Melanoma. *N. Engl. J. Med.* **2013**, *369* (2), 122–133.

(42) Garg, A.; Aggarwal, B. B. REVIEW Nuclear Transcription Factor- Kappa B as a Target for Cancer Drug Development. *Nature* **2002**, *16* (6), 1053–1068.

(43) Bassères, D. S.; Baldwin, A. S. Nuclear Factor-kappaB and Inhibitor of kappaB Kinase Pathways in Oncogenic Initiation and Progression. *Oncogene* **2006**, *25* (51), 6817–6830.

(44) Escárcega, R. O.; Fuentes-Alexandro, S.; García-Carrasco, M.; Gatica, A.; Zamora, A. The Transcription Factor Nuclear Factor-Kappa B and Cancer. *Clin. Oncol.* **2007**, *19* (2), 154–161.

(45) Sun, S.-C. The Noncanonical NF-κB Pathway. *Immunol. Rev.* **2012**, *246* (1), 125–140.

(46) Thu, Y. M.; Richmond, A. NF-κB Inducing Kinase: A Key Regulator in the Immune System and in Cancer. *Cytokine Growth Factor Rev.* **2010**, *21* (4), 213–226.

(47) Beinke, S.; Ley, S. C. Functions of NF-kappaB1 and NF-kappaB2 in Immune Cell Biology. *Biochem. J.* **2004**, *382* (2), 393–409.

(48) Viatour, P.; Merville, M. P.; Bours, V.; Chariot, A. Phosphorylation of NF-kB and IkB

Proteins: Implications in Cancer and Inflammation. *Trends Biochem. Sci.* **2005**, *30* (1), 43–52.

(49) Sakurai, H.; Suzuki, S.; Kawasaki, N.; Nakano, H.; Okazaki, T.; Chino, A.; Doi, T.; Saiki, I. Tumor Necrosis Factor-α-Induced IKK Phosphorylation of NF-κB p65 on Serine 536 Is Mediated through the TRAF2, TRAF5, and TAK1 Signaling Pathway. *J. Biol. Chem.* **2003**, *278* (38), 36916–36923.

(50) Jacobs, M. D.; Harrison, S. C. Structure of an IκBα/NF-κB Complex. *Cell* **1998**, *95*, 749–758.

(51) Perkins, N. D. Integrating Cell-Signalling Pathways with NF-κB and IKK Function. *Nat. Rev. Mol. Cell Biol.* **2007**, *8* (1), 49–62.

(52) Woronicz, J. D.; Gao, X.; Cao, Z.; Rothe, M.; Goeddel, D. V. IkappaB Kinase-Beta: NF-kappaB Activation and Complex Formation with IkappaB Kinase-Alpha and NIK. *Science (80-.).* **1997**, *278* (5339), 866–870.

(53) Liu, J.; Sudom, A.; Min, X.; Cao, Z.; Gao, X.; Ayres, M.; Lee, F.; Cao, P.; Johnstone, S.; Plotnikova, O.; Walker, N.; Chen, G.; Wang, Z. Structure of the Nuclear Factor κB-Inducing Kinase (NIK) Kinase Domain Reveals a Constitutively Active Conformation. *J. Biol. Chem.* **2012**, *287* (33), 27326–27334.

(54) Treiber, D. K.; Shah, N. P. Ins and Outs of Kinase DFG Motifs. *Chem. Biol.* **2013**, *20* (6), 745–746.

(55) Tao, Z.; Ghosh, G. Understanding NIK Regulation from Its Structure. *Structure* **2012**, *20* (10), 1615–1617.

(56) Wharry, C. E.; Haines, K. M.; Carroll, R. G.; May, M. J. Constitutive Non-Canonical NFkappaB Signaling in Pancreatic Cancer Cells. *Cancer Biol. Ther.* **2009**, *8* (16), 1567–1576.

(57) Baud, V.; Karin, M. Is NF-kappaB a Good Target for Cancer Therapy? Hopes and Pitfalls. *Nat. Rev. Drug Discov.* **2009**, *8* (1), 33–40.

(58) Odqvist, L.; Sánchez-Beato, M.; Montes-Moreno, S.; Martín-Sánchez, E.; Pajares, R.; Sánchez-Verde, L.; Ortiz-Romero, P. L.; Rodriguez, J.; Rodríguez-Pinilla, S. M.; Iniesta-

Martínez, F.; Solera-Arroyo, J. C.; Ramos-Asensio, R.; Flores, T.; Palanca, J. M.; Bragado, F. G.; Franjo, P. D.; Piris, M. a. NIK Controls Classical and Alternative NF-κB Activation and Is Necessary for the Survival of Human T-Cell Lymphoma Cells. *Clin. Cancer Res.* **2013**, *19* (9), 2319–2330.

(59) Claudio, E.; Brown, K.; Park, S.; Wang, H.; Siebenlist, U. BAFF-Induced NEMO-Independent Processing of NF-κB2 in Maturing B Cells. *Nat. Immunol.* **2002**, *3* (10), 958–965.

(60) Baldwin, A. S. Control of Oncogenesis and Cancer Therapy Resistance by the Transcription Factor NF-κB. *J. Clin. Invest.* **2001**, *107* (3), 241–246.

(61) Karin, M.; Cao, Y.; Greten, F. R.; Li, Z.-W. NF-kappaB in Cancer: From Innocent Bystander to Major Culprit. *Nat. Rev. Cancer* **2002**, *2* (4), 301–310.

(62) Döppler, H.; Liou, G.-Y.; Storz, P. Downregulation of TRAF2 Mediates NIK-Induced Pancreatic Cancer Cell Proliferation and Tumorigenicity. *PLoS One* **2013**, *8* (1), e53676.

(63) Lessard, L.; Bégin, L. R.; Gleave, M. E.; Mes-Masson, A.-M.; Saad, F. Nuclear Localisation of Nuclear Factor-kappaB Transcription Factors in Prostate Cancer: An Immunohistochemical Study. *Br. J. Cancer* **2005**, *93* (9), 1019–1023.

(64) O'Reilly, E.; Santocanale, C.; Szegezdi, E.; Higgins, P. J. Molecular Targets for Novel Drug Development in Pancreatic Cancer. *Ann. Cancer Res.* **2015**, *2* (3), 1–11.

(65) Flohr, S.; Naumann, T. PYRAZOLOISOQUINOLINE DERIVATIVES FOR INHIBITING NFKAPPAB-INDUCING KINASE (NIK). CA20032490571 20030620, 2004.

(66) Storz, P. Targeting the Alternative NF-κB Pathway in Pancreatic Cancer: A New Direction for Therapy? *Expert Rev. Anticancer Ther.* **2013**, *13* (5), 501–504.

(67) Mortier, J.; Frederick, R.; Ganeff, C.; Remouchamps, C.; Talaga, P.; Pochet, L.; Wouters, J.; Piette, J.; Dejardin, E.; Masereel, B. Pyrazolo[4,3-C]isoquinolines as Potential Inhibitors of NF-κB Activation. *Biochem. Pharmacol.* **2010**, *79* (10), 1462–1472.

(68) Manna, S. K.; Babajan, B.; Raghavendra, P. B.; Raviprakash, N.; Sureshkumar, C.

Inhibiting TRAF2-Mediated Activation of NF-kB Facilitates Induction of AP-1. *J. Biol. Chem.* **2010**, *285* (15), 11617–11627.

(69) Ninomiya-Tsuji, J.; Kishimoto, K.; Hiyama, a; Inoue, J.; Cao, Z.; Matsumoto, K. The Kinase TAK1 Can Activate the NIK-I kappaB as Well as the MAP Kinase Cascade in the IL-1 Signalling Pathway. *Nature* **1999**, *398* (6724), 252–256.

(70) Melisi, D.; Xia, Q.; Paradiso, G.; Ling, J.; Moccia, T.; Carbone, C.; Budillon, A.; Abbruzzese, J. L.; Chiao, P. J. Modulation of Pancreatic Cancer Chemoresistance by Inhibition of TAK1. *J. Natl. Cancer Inst.* **2011**, *103* (15), 1190–1204.

(71) Ninomiya-Tsuji, J.; Kajino, T.; Ono, K.; Ohtomo, T.; Matsumoto, M.; Shiina, M.; Mihara, M.; Tsuchiya, M.; Matsumoto, K. A Resorcylic Acid Lactone, 5Z-7-Oxozeaenol, Prevents Inflammation by Inhibiting the Catalytic Activity of TAK1 MAPK Kinase Kinase. *J. Biol. Chem.* **2003**, *278* (20), 18485–18490.

(72) Tan, L.; Nomanbhoy, T.; Gurbani, D.; Patricelli, M.; Hunter, J.; Geng, J.; Herhaus, L.; Zhang, J.; Pauls, E.; Ham, Y.; Choi, H. G.; Xie, T.; Deng, X.; Buhrlage, S. J.; Sim, T.; Cohen, P.; Sapkota, G.; Westover, K. D.; Gray, N. S. Discovery of Type II Inhibitors of Tgfβ-Activated Kinase 1 (TAK1) and Mitogen-Activated Protein Kinase Kinase Kinase Kinase 2 (MAP4K2). *J. Med. Chem.* **2015**, *58* (1), 183–196.

(73) Bang, D.; Wilson, W.; Ryan, M.; Yeh, J. J.; Baldwin, A. S. GSK-3a Promotes Oncogenic KRAS Function in Pancreatic Cancer via TAK1-TAB Stabilization and Regulation of Noncanonical NF-kB. *Cancer Discov.* **2013**, *3* (6), 690–703.

(74) Nadiminty, N.; Chun, J. Y.; Lou, W.; Lin, X.; Gao, A. C. NF-κB2/p52 Enhances Androgen-Independent Growth of Human LNCaP Cells via Protection from Apoptotic Cell Death and Cell Cycle Arrest Induced by Androgen-Deprivation. *Prostate* **2008**, *68* (16), 1725–1733.

(75) Nadiminty, N.; Lou, W.; Sun, M.; Chen, J.; Yue, J.; Kung, H. J.; Evans, C. P.; Zhou, Q.; Gao, A. C. Aberrant Activation of the Androgen Receptor by NF-κB2/p52 in Prostate Cancer Cells. *Cancer Res.* **2010**, *70* (8), 3309–3319.

(76) Ammirante, M.; Luo, J.-L.; Grivennikov, S.; Nedospasov, S.; Karin, M. B-Cell-Derived Lymphotoxin Promotes Castration-Resistant Prostate Cancer. *Nature* **2010**, *464*

(7286), 302–305.

(77) Luo, J.-L.; Tan, W.; Ricono, J. M.; Korchynskyi, O.; Zhang, M.; Gonias, S. L.; Cheresh, D. a; Karin, M. Nuclear Cytokine-Activated IKKalpha Controls Prostate Cancer Metastasis by Repressing Maspin. *Nature* **2007**, *446* (7136), 690–694.

(78) Yamamoto, Y.; Verma, U. N.; Prajapati, S.; Kwak, Y.-T.; Gaynor, R. B. Histone H3 Phosphorylation by IKK-Alpha Is Critical for Cytokine-Induced Gene Expression. *Nature* **2003**, *423* (6940), 655–659.

(79) Hoberg, J. E.; Popko, A. E.; Ramsey, C. S.; Mayo, M. W. IκB Kinase a-Mediated Derepression of SMRT Potentiates Acetylation of RelA/p65 by p300. *Mol. Cell. Biol.* **2006**, *26* (2), 457–471.

(80) Rossetto, D.; Avvakumov, N.; Côté, J. Histone Phosphorylation: A Chromatin Modification Involved in Diverse Nuclear Events. *Epigenetics* **2012**, *7* (10), 1098–1108.

(81) Liao, G.; Chen, L. Y.; Zhang, A.; Godavarthy, A.; Xia, F.; Ghosh, J. C.; Li, H.; Chen, J. D. Regulation of Androgen Receptor Activity by the Nuclear Receptor Corepressor SMRT. *J. Biol. Chem.* **2003**, *278* (7), 5052–5061.

(82) Song, L.-N.; Coghlan, M.; Gelmann, E. P. Antiandrogen Effects of Mifepristone on Coactivator and Corepressor Interactions with the Androgen Receptor. *Mol. Endocrinol.* **2004**, *18* (1), 70–85.

(83) Lessard, L.; Saad, F.; Le Page, C.; Diallo, J. S.; P??ant, B.; Delvoye, N.; Mes-Masson, A. M. NF-kB2 Processing and p52 Nuclear Accumulation after Androgenic Stimulation of LNCaP Prostate Cancer Cells. *Cell. Signal.* **2007**, *19* (5), 1093–1100.

(84) Gonzalez-Suarez, E.; Jacob, A. P.; Jones, J.; Miller, R.; Roudier-Meyer, M. P.; Erwert, R.; Pinkas, J.; Branstetter, D.; Dougall, W. C. RANK Ligand Mediates Progestin-Induced Mammary Epithelial Proliferation and Carcinogenesis. *Nature* **2010**, *468* (7320), 103–107.

(85) Schramek, D.; Leibbrandt, A.; Sigl, V.; Kenner, L.; Pospisilik, J. a; Lee, H. J.; Hanada, R.; Joshi, P. a; Aliprantis, A.; Glimcher, L.; Pasparakis, M.; Khokha, R.; Ormandy, C. J.; Widschwendter, M.; Schett, G.; Penninger, J. M. Osteoclast Differentiation Factor

RANKL Controls Development of Progestin-Driven Mammary Cancer. *Nature* **2010**, *468* (7320), 98–102.

(86) Cao, Y.; Bonizzi, G.; Seagroves, T. N.; Greten, F. R.; Johnson, R.; Schmidt, E. V.; Karin, M. IKKα Provides an Essential Link between RANK Signaling and Cyclin D1 Expression during Mammary Gland Development. *Cell* **2001**, *107* (6), 763–775.

(87) Zou, Z.; Anisowicz, A.; Hendrix, M.; Thor, A.; Neveu, M.; Sheng, S.; Rafidi, K.; Seftor, E.; Sager, R. Maspin, a Serpin with Tumor-Suppressing Activity in Human Mammary Epithelial Cells. *Science (80-.).* **1994**, *263* (5146), 526–529.

(88) Scheidereit, C. IkappaB Kinase Complexes: Gateways to NF-kappaB Activation and Transcription. *Oncogene* **2006**, *25* (51), 6685–6705.

(89) FDA. FDA Approves Denosumab http://www.fda.gov/Drugs/InformationOnDrugs/ApprovedDrugs/ucm356667.htm (accessed Jun 4, 2016).

(90) National Institutes of Health. Study of Denosumab vs. Zoledronic Acid to Treat Bone Metastases in Men With Hormone-refractory Prostate Cancer https://clinicaltrials.gov/ct2/show/NCT00321620 (accessed Jun 4, 2016).

(91) Castellano, D.; Sepulveda, J. M.; García-Escobar, I.; Rodriguez-Antolín, A.; Sundlöv, A.; Cortes-Funes, H. The Role of RANK-Ligand Inhibition in Cancer: The Story of Denosumab. *Oncologist* **2011**, *16* (2), 136–145.

(92) Huang, W.-C.; Hung, M.-C. Beyond NF-κB Activation : Nuclear Functions of IκB Kinase α. *J. Biomed. Sci.* **2013**, *20* (3), 1–13.

(93) Llona-Minguez, S.; Baiget, J.; Mackay, S. P. Small-Molecule Inhibitors of IκB Kinase (IKK) and IKK-Related Kinases. *Pharm. Pat. Anal.* **2013**, *2* (4), 481–498.

(94) Baldwin, I. R.; Bamborough, P.; Christopher, J. A.; Hamadi, A. M.; Lackey, K. E. Pyrrolo-Pyridine Derivatives for the Treatment of Disorders Associated with Inapporpriate IKK1 Activity. WO2008110508, 2008.

(95) Christopher, J. A.; Jung, D. K.; Lackey, K. E. 1H-Indazole-3-Amine Compounds as IKK1 Inhibitors. WO/2008/132121, 2008.

(96) Gupta, S.; Takebe, N.; Lorusso, P. Targeting the Hedgehog Pathway in Cancer. *Ther Adv Med Oncol* **2010**, *2* (4), 237–250.

(97) Chen, W. Activity-Dependent Internalization of Smoothened Mediated by β-Arrestin 2 and GRK2. *Science (80-.).* **2004**, *306* (5705), 2257–2260.

(98) Rubin, L. L.; de Sauvage, F. J. Targeting the Hedgehog Pathway in Cancer. *Nat. Rev. Drug Discov.* **2006**, *5* (12), 1026–1033.

(99) Chen, J. K.; Taipale, J.; Young, K. E.; Maiti, T.; Beachy, P. a. Small Molecule Modulation of Smoothened Activity. *Proc. Natl. Acad. Sci. U. S. A.* **2002**, *99* (22), 14071–14076.

(100) Williams, J. A.; Guicherit, O. M.; Zaharian, B. I.; Xu, Y.; Chai, L.; Wichterle, H.; Kon, C.; Gatchalian, C.; Porter, J. A.; Rubin, L. L.; Wang, F. Y. Identification of a Small Molecule Inhibitor of the Hedgehog Signaling Pathway: Effects on Basal Cell Carcinoma-like Lesions. *Proc. Natl. Acad. Sci. U. S. A.* **2003**, *100* (8), 4616–4621.

(101) Tremblay, M. R.; Lescarbeau, A.; Grogan, M. J.; Tan, E.; Lin, G.; Austad, B. C.; Yu, L. C.; Behnke, M. L.; Nair, S. J.; Hagel, M.; White, K.; Conley, J.; Manna, J. D.; Alvarez-Diez, T. M.; Hoyt, J.; Woodward, C. N.; Sydor, J. R.; Pink, M.; MacDougall, J.; Campbell, M. J.; Cushing, J.; Ferguson, J.; Curtis, M. S.; McGovern, K.; Read, M. A.; Palombella, V. J.; Adams, J.; Castro, A. C. Discovery of a Potent and Orally Active Hedgehog Pathway Antagonist (IPI-926). *J. Med. Chem.* **2009**, *52* (14), 4400–4418.

(102) FDA. FDA approves new treatment for most common type of skin cancer http://www.fda.gov/NewsEvents/Newsroom/PressAnnouncements/ucm289545.htm (accessed Jul 4, 2016).

(103) FDA. FDA approves new treatment for most common form of advanced skin cancer http://www.fda.gov/NewsEvents/Newsroom/PressAnnouncements/ucm455862.htm (accessed Jul 4, 2016).

(104) A Biomarker Study to Identify Predictive Signatures of Response to LDE225 (Hedgehog Inhibitor) In Patients With Resectable Pancreatic Cancer https://clinicaltrials.gov/ct2/show/record/NCT01911416 (accessed Jul 4, 2016).

(105) Gemcitabine + Nab-paclitaxel With LDE-225 (Hedgehog Inhibitor) as Neoadjuvant

Therapy for Pancreatic Adenocarcinoma https://clinicaltrials.gov/ct2/show/NCT01431794 (accessed Jul 4, 2016).

(106) Catenacci, D. V. T.; Junttila, M. R.; Karrison, T.; Bahary, N.; Horiba, M. N.; Nattam, S. R.; Marsh, R.; Wallace, J.; Kozloff, M.; Rajdev, L.; Cohen, D.; Wade, J.; Sleckman, B.; Lenz, H.-J.; Stiff, P.; Kumar, P.; Xu, P.; Henderson, L.; Takebe, N.; Salgia, R.; Wang, X.; Stadler, W. M.; de Sauvage, F. J.; Kindler, H. L. Randomized Phase Ib/II Study of Gemcitabine Plus Placebo or Vismodegib, a Hedgehog Pathway Inhibitor, in Patients With Metastatic Pancreatic Cancer. *J. Clin. Oncol.* **2015**, *33* (36), 4284–4292.

(107) Fruman, D. A.; Rommel, C. PI3K and Cancer: Lessons, Challenges and Opportunities. *Nat. Rev. Drug Discov.* **2014**, *13* (2), 140–156.

(108) Liu, P.; Cheng, H.; Roberts, T. M.; Zhao, J. J. Targeting the Phosphoinositide 3-Kinase Pathway in Cancer. *Nat. Rev. Drug Discov.* **2009**, *8* (8), 627–644.

(109) FDA. FDA Approves Trametinib http://www.fda.gov/Drugs/InformationOnDrugs/ApprovedDrugs/ucm354478.htm (accessed Jul 4, 2016).

(110) Germann, U.; Furey, B.; Roix, J.; Markland, W.; Hoover, R.; Aronov, A.; Hale, M.; Chen, G.; Martinez-Botella, G.; Alargova, R.; Fan, B.; Sorrell, D.; Meshaw, K.; Shapiro, P.; Wick, M. J.; Benes, C.; Garnett, M.; DeCrescenzo, G.; Namchuk, M.; Saha, S.; Welsch, D. J. Abstract 4693: The Selective ERK Inhibitor BVD-523 Is Active in Models of MAPK Pathway-Dependent Cancers, Including Those with Intrinsic and Acquired Drug Resistance. *Cancer Res.* **2015**, *75* (15 Supplement), 4693–4693.

(111) Bhat, M.; Robichaud, N.; Hulea, L.; Sonenberg, N.; Pelletier, J.; Topisirovic, I. Targeting the Translation Machinery in Cancer. *Nat. Rev. Drug Discov.* **2015**, *14* (4), 261–278.

(112) Akinleye, A.; Avvaru, P.; Furqan, M.; Song, Y.; Liu, D. Phosphatidylinositol 3-Kinase (PI3K) Inhibitors as Cancer Therapeutics. *J. Hematol. Oncol.* **2013**, *6* (1), 88.

(113) Carver, B. S.; Chapinski, C.; Wongvipat, J.; Hieronymus, H.; Chen, Y.; Chandarlapaty, S.; Arora, V. K.; Le, C.; Koutcher, J.; Scher, H.; Scardino, P. T.; Rosen, N.; Sawyers, C. L. Reciprocal Feedback Regulation of PI3K and Androgen Receptor Signaling in PTEN-

Deficient Prostate Cancer. *Cancer Cell* **2011**, *19* (5), 575–586.

(114) Kaarbø, M.; Mikkelsen, O. L.; Malerød, L.; Qu, S.; Lobert, V. H.; Akgul, G.; Halvorsen, T.; Maelandsmo, G. M.; Saatcioglu, F. PI3K-AKT-mTOR Pathway Is Dominant over Androgen Receptor Signaling in Prostate Cancer Cells. *Cell. Oncol.* **2010**, *32* (1–2), 11–27.

(115) Wullaert, A.; Bonnet, M. C.; Pasparakis, M. NF-κB in the Regulation of Epithelial Homeostasis and Inflammation. *Cell Res.* **2011**, *21* (1), 146–158.

(116) Mustapha, S.; Kirshner, A.; De Moissac, D.; Kirshenbaum, L. A. A Direct Requirement of Nuclear Factor-Kappa B for Suppression of Apoptosis in Ventricular Myocytes. *Am. J. Physiol. Heart Circ. Physiol.* **2000**, *279* (3), H939-45.

(117) Beg, A. A.; Sha, W. C.; Bronson, R. T.; Ghosh, S.; Baltimore, D. Embryonic Lethality and Liver Degeneration in Mice Lacking the RelA Component of NF-Kappa B. *Nature*. 1995, pp 167–170.

(118) Pannicke, U.; Baumann, B.; Fuchs, S.; Henneke, P.; Rensing-Ehl, A.; Rizzi, M.; Janda, A.; Hese, K.; Schlesier, M.; Holzmann, K.; Borte, S.; Laux, C.; Rump, E.-M.; Rosenberg, A.; Zelinski, T.; Schrezenmeier, H.; Wirth, T.; Ehl, S.; Schroeder, M. L.; Schwarz, K. Deficiency of Innate and Acquired Immunity Caused by an IKBKB Mutation. *N. Engl. J. Med.* **2013**, *369* (26), 2504–2514.

(119) Kumar, S.; O'Rahilly, S. *Insulin Resistance*; Kumar, S., O'Rahilly, S., Eds.; John Wiley & Sons, Ltd: Chichester, UK, 2004.

(120) Adli, M.; Merkhofer, E.; Cogswell, P.; Baldwin, A. S. IKKα and IKKβ Each Function to Regulate NF-κB Activation in the TNF-Induced/canonical Pathway. *PLoS One* **2010**, *5* (2), 1–7.

(121) Cohen, P.; Alessi, D. R. Kinase Drug Discovery--What's next in the Field? *ACS Chem. Biol.* **2013**, *8* (1), 96–104.

(122) Morphy, R. Selectively Nonselective Kinase Inhibition: Striking the Right Balance. *J. Med. Chem.* **2010**, *53* (4), 1413–1437.

(123) Visiongain. *Kinase Inhibitors for Treating Cancer: Industry Analysis, R&D Trends and*

World Market Forecasts 2014-2024; 2014.

(124) Wu, P.; Nielsen, T. E.; Clausen, M. H. FDA-Approved Small-Molecule Kinase Inhibitors. *Trends Pharmacol. Sci.* **2015**, *36* (7), 422–439.

(125) Cox, K. J.; Shomin, C. D.; Ghosh, I. Tinkering Outside the Kinase ATP Box: Allosteric (Type IV) and Bivalent (Type V) Inhibitors of Protein Kinases. *Future Med. Chem.* **2011**, *3* (1), 29–43.

(126) Lamba, V.; Ghosh, I. New Directions in Targeting Protein Kinases: Focusing Upon True Allosteric and Bivalent Inhibitors. *Curr. Pharm. Des.* **2012**, *18* (20), 2936–2945.

(127) Wu, P.; Nielsen, T. E.; Clausen, M. H. Small-Molecule Kinase Inhibitors: An Analysis of FDA-Approved Drugs. *Drug Discov. Today* **2016**, *21* (1), 5–10.

(128) Okamoto, K.; Ikemori-Kawada, M.; Jestel, A.; Von K??nig, K.; Funahashi, Y.; Matsushima, T.; Tsuruoka, A.; Inoue, A.; Matsui, J. Distinct Binding Mode of Multikinase Inhibitor Lenvatinib Revealed by Biochemical Characterization. *Med. Chem. Lett.* **2015**, *6* (1), 89–94.

(129) Lovering, F.; Bikker, J.; Humblet, C. Escape from Flatland: Increasing Saturation as an Approach to Improving Clinical Success. *J. Med. Chem.* **2009**, *52* (21), 6752–6756.

(130) Fabbro, D. 25 Years of Small Molecular Weight Kinase Inhibitors : Potentials and Limitations. *Mol. Pharmacol.* **2015**, *10* (May), 766–775.

(131) Szakacs, G.; Paterson, J. K.; Ludwig, J. A.; Booth-Genthe, C.; Gottesman, M. M.; Szakács, G.; Paterson, J. K.; Ludwig, J. A.; Booth-Genthe, C.; Gottesman, M. M. Targeting Multidrug Resistance in Cancer. *Nat. Rev. Drug Discov.* **2006**, *5* (3), 219–234.

(132) Hammer, S. M.; Squires, K. E.; Hughes, M. D.; Grimes, J. M.; Demeter, L. M.; Currier, J. S.; Eron, J. J.; Feinberg, J. E.; Balfour, H. H.; Deyton, L. R.; Chodakewitz, J. A.; Fischl, M. A.; Phair, J. P.; Pedneault, L.; Nguyen, B.-Y.; Cook, J. C. A Controlled Trial of Two Nucleoside Analogues plus Indinavir in Persons with Human Immunodeficiency Virus Infection and CD4 Cell Counts of 200 per Cubic Millimeter or Less. *N. Engl. J. Med.* **1997**, *337* (11), 725–733.

(133) Hooft van Huijsduijnen, R.; Sauer, W. H. B.; Bombrun, A.; Swinnen, D. Prospects for Inhibitors of Protein Tyrosine Phosphatase 1B as Antidiabetic Drugs. *J. Med. Chem.* **2004**, *35* (43), 4142–4146.

(134) Erbe, D. V; Wang, S.; Zhang, Y.-L.; Harding, K.; Kung, L.; Tam, M.; Stolz, L.; Xing, Y.; Furey, S.; Qadri, A.; Klaman, L. D.; Tobin, J. F. Ertiprotafib Improves Glycemic Control and Lowers Lipids via Multiple Mechanisms. *Mol. Pharmacol.* **2005**, *67* (1), 69–77.

(135) Shrestha, S.; Bhattarai, B. R.; Cho, H.; Choi, J. K.; Cho, H. PTP1B Inhibitor Ertiprotafib Is Also a Potent Inhibitor of IkB Kinase B (IKK-B). *Bioorganic Med. Chem. Lett.* **2007**, *17* (10), 2728–2730.

(136) Deininger, M. Imatinib–an Overview. *Hematol. Rep.* **2005**, *1* (8), 20–27.

(137) Milojkovic, D.; Apperley, J. F. Mechanisms of Resistance to Imatinib and Second-Generation Tyrosine Inhibitors in Chronic Myeloid Leukemia. *Clin. Cancer Res.* **2009**, *15* (24), 7519–7527.

(138) Shah, N. P.; Tran, C.; Lee, F. Y.; Chen, P.; Norris, D.; Sawyers, C. L. Overriding Imatinib Resistance with a Novel ABL Kinase Inhibitor. *Science (80-.).* **2004**, *305* (5682), 399–401.

(139) Hughes, J. P.; Rees, S. S.; Kalindjian, S. B.; Philpott, K. L. Principles of Early Drug Discovery. *Br. J. Pharmacol.* **2011**, *162* (6), 1239–1249.

(140) Anderson, N. L.; Anderson, N. G. Proteome and Proteomics: New Technologies, New Concepts, and New Words. *Electrophoresis* **1998**, *19* (11), 1853–1861.

(141) Patrick, G. L. Pharmacokinetics and Related Topics. In *An Introduction to Medicinal Chemistry*; Oxford University Press, 2005; p 134.

(142) Cyprotex PLC. Everything You Need to Know about ADME. 2015, pp 1–78.

(143) Broekman, F. Tyrosine Kinase Inhibitors: Multi-Targeted or Single-Targeted? *World J. Clin. Oncol.* **2011**, *2* (2), 80.

(144) McLellan, B.; Kerr, H. Cutaneous Toxicities of the Multikinase Inhibitors Sorafenib and Sunitinib. *Dermatol. Ther.* **2011**, *24* (4), 396–400.

(145) Cheng, Y.; Prusoff, W. H. Relationship between the Inhibition Constant (K1) and the Concentration of Inhibitor Which Causes 50 per Cent Inhibition (I50) of an Enzymatic Reaction. *Biochem. Pharmacol.* **1973**, *22*, 3099–3108.

(146) BLAST sequence alignment of IKKa and CDK2 https://goo.gl/R6HqZf (accessed Jun 30, 2016).

(147) Altschul, S. F.; Gish, W.; Miller, W.; Myers, E. W.; Lipman, D. J. Basic Local Alignment Search Tool. *J. Mol. Biol.* **1990**, *215* (3), 403–410.

(148) De Wit, P.; Pespeni, M. H.; Ladner, J. T.; Barshis, D. J.; Seneca, F.; Jaris, H.; Therkildsen, N. O.; Morikawa, M.; Palumbi, S. R. The Simple Fool's Guide to Population Genomics via RNA-Seq: An Introduction to High-Throughput Sequencing Data Analysis. *Mol. Ecol. Resour.* **2012**, *12* (6), 1058–1067.

(149) Jaffe, H. H. A Re-Examination of the Hammett Equation. *Chem. Rev.* **1953**, *53* (2), 191–261.

(150) Fujita, T.; Iwasa, J.; Hansch, C. A New Substituent Constant, Π, Derived from Partition Coefficients. *J. Am. Chem. Soc.* **1964**, *86* (23), 5175–5180.

(151) Lin, G.; Liu, Y.-C.; Wu, Y.-G.; Lee, Y.-R. Ortho Effects in Quantitative Structure Activity Relationships for Lipase Inhibition by Aryl Carbamates. *QSAR Comb. Sci.* **2003**, *22* (8), 852–858.

(152) Schultz, W. T.; Cajina-Quezada, M. Structure-Activity Relationships for Mono-Alkylated or Halogenated Phenols. *Toxicol. Lett.* **1987**, *37* (2), 121–130.

(153) Craig, P. N. Interdependence between Physical Parameters and Selection of Substituent Groups for Correlation Studies. *J. Med. Chem.* **1971**, *14* (8), 680–684.

(154) Yamazaki, T.; Taguchi, T.; Ojima, I.; Matsumura, Y.; Nakazato, A.; Sinisi, R.; Jagodzinska, M.; Candiani, G.; Huguenot, F.; Sani, M.; Volonterio, A.; Maffezzoni, R.; Zanda, M.; Pepe, A.; Kuznetsova, L.; Sun, L.; Begue, J.-P.; Bonnet-Delpon; Maruyama, T.; Ikejiri, M.; Izawa, K.; Onishi, T. *Fluorine in Medicinal Chemistry and Chemical Biology*; Ojima, I., Ed.; John Wiley & Sons, Inc., 2009.

(155) Hansch, C.; Leo, A.; Taft, R. W. A Survey of Hammett Substituent Constants and

Resonance and Field Parameters. *Chem. Rev.* **1991**, *91* (2), 165–195.

(156) Hansch, C.; Leo, A. *Substituent Constants For Correlation Analysis in Chemistry and Biology*; John Wiley & Sons, Inc.: California, 1979.

(157) Thompson, H. W.; Steel, G. The Correlation of Vibrational Band Intensities with Reactivity: The CN Group. *Trans. Faraday Soc.* **1956**, *52*, 1451.

(158) Cresset. Torch. Litlington, Cambridgeshire, UK.

(159) Cheeseright, T.; Mackey, M.; Rose, S.; Vinter, A. Molecular Field Extrema as Descriptors of Biological Activity: Definition and Validation. *J. Chem. Inf. Model.* **2006**, *46* (2), 665–676.

(160) Meanwell, N. A. Synopsis of Some Recent Tactical Application of Bioisosteres in Drug Design. *J. Med. Chem.* **2011**, *54* (8), 2529–2591.

(161) Montalbetti, C. A. G. N.; Falque, V. Amide Bond Formation and Peptide Coupling. *Tetrahedron* **2005**, *61* (46), 10827–10852.

(162) Jursic, B. S.; Zdravkovski, Z. A Simple Preparation of Amides from Acids and Amines by Heating of Their Mixture. *Synth. Commun.* **1993**, *23* (19), 2761–2770.

(163) Valeur, E.; Bradley, M. Amide Bond Formation: Beyond the Myth of Coupling Reagents. *Chem. Soc. Rev.* **2009**, *38* (2), 606–631.

(164) Hickman, A. J.; Sanford, M. S. High-Valent Organometallic Copper and Palladium in Catalysis. *Nature* **2012**, *484* (7393), 177–185.

(165) Mori, K.; Mizoroki, T.; Ozaki, A. Arylation of Olefin with Iodobenzene Catalyzed by Palladium. *Bull. Chem. Soc. Jpn.* **1973**, *46* (5), 1505–1508.

(166) Dieck, H. A.; Heck, R. F. Organophosphinepalladium Complexes as Catalysts for Vinylic Hydrogen Substitution Reactions. *J. Am. Chem. Soc.* **1974**, *96* (4), 1133–1136.

(167) Murahashi, S.; Yamamura, M.; Yanagisawa, K.; Mita, N.; Kondo, K. Stereoselective Synthesis of Alkenes and Alkenyl Sulfides from Alkenyl Halides Using Palladium and Ruthenium Catalysts. *J. Org. Chem.* **1979**, *44* (14), 2408–2417.

(168) Nicholas, P. P. Amidation of Chloroalkenes Catalyzed by Tertiary Phosphine

Complexes of palladium(0). *J. Org. Chem.* **1987**, *52* (23), 5266–5272.

(169) Littke, A. F.; Fu, G. C. Eine Bequeme Und Allgemein Anwendbare Methode Für Pd-Katalysierte Suzuki- Kreuzkupplungen von Arylchloriden Und Arylboronsäuren. *Angew. Chemie* **1998**, *110* (24), 3586–3587.

(170) Zapf, A.; Ehrentraut, A.; Beller, M. A New Highly Efficient Catalyst System for the Coupling of Nonactivated and Deactivated Aryl Chlorides with Arylboronic Acids **. *Angew. Chem. Int. Ed. Engl.* **2000**, *39* (22), 4153–4155.

(171) Shelby, Q.; Kataoka, N.; Mann, G.; Hartwig, J. Unusual in Situ Ligand Modification to Generate a Catalyst for Room Temperature Aromatic C−O Bond Formation. *J. Am. Chem. Soc.* **2000**, *122* (43), 10718–10719.

(172) Wolfe, J. P.; Singer, R. a.; Yang, B. H.; Buchwald, S. L. Highly Active Palladium Catalysts for Suzuki Coupling Reactions. *J. Am. Chem. Soc.* **1999**, *121* (41), 9550–9561.

(173) Johansson Seechurn, C. C. C.; Kitching, M. O.; Colacot, T. J.; Snieckus, V. Palladium-Catalyzed Cross-Coupling: A Historical Contextual Perspective to the 2010 Nobel Prize. *Angew. Chemie* **2012**, *51* (21), 5062–5085.

(174) Littke, A. F.; Fu, G. C. Palladium-Catalyzed Coupling Reactions of Aryl Chlorides. *Angew. Chem. Int. Ed. Engl.* **2002**, *41* (22), 4176–4211.

(175) Billingsley, K. L.; Barder, T. E.; Buchwald, S. L. Palladium-Catalyzed Borylation of Aryl Chlorides: Scope, Applications, and Computational Studies. *Angew. Chem. Int. Ed. Engl.* **2007**, *46* (28), 5359–5363.

(176) Smith, G. B.; Dezeny, G. C.; Hughes, D. L.; King, A. O.; Verhoeven, T. R. Mechanistic Studies of the Suzuki Cross-Coupling Reaction. *J. Org. Chem.* **1994**, *59* (26), 8151–8156.

(177) Miyaura, N.; Suzuki, A. Palladium-Catalyzed Cross-Coupling Reactions of Organoboron Compounds. *Chem. Rev.* **1995**, *95* (7), 2457–2483.

(178) Uenishi, J.; Beau, J. M.; Armstrong, R. W.; Kishi, Y. Dramatic Rate Enhancement of Suzuki Diene Synthesis. Its Application to Palytoxin Synthesis. *J. Am. Chem. Soc.*

1987, *109* (15), 4756–4758.

(179) Hsiao, K.; Alves, J.; Goueli, S. A.; Zegzouti, H. NIK Kinase Assay. Promega: Madison 2012, pp 1–2.

(180) Ghosh, S.; Karin, M. Missing Pieces in the NF-κB Puzzle. *Cell* **2002**, *109* (2), S81–S96.

(181) Turner, R. S.; Chou, C. H. J.; Mazzei, G. J.; Dembure, P.; Kuo, J. F. Phospholipid-Sensitive Ca2+ -Dependent Protein Kinase Preferentially Phosphorylates Serine-115 of Bovine Myelin Basic Protein. *J. Neurochem.* **1984**, *43* (5), 1257–1264.

(182) Turner, R. S.; Kemp, B. E.; de Su, H.; Kuo, J. F. Substrate Specificity of phospholipid/Ca2+-Dependent Protein Kinase as Probed with Synthetic Peptide Fragments of the Bovine Myelin Basic Protein. *J. Biol. Chem.* **1985**, *260* (21), 11503–11507.

(183) Kim, S.-J.; Kim, H.; Pillion, D. J. Insulin-Sensitive Myelin Basic Protein Phosphorylation on Tyrosine Residues. *Biochem. Biophys. Res. Commun.* **1991**, *179* (1), 392–400.

(184) Sanghera, J. S.; Aebersold, R.; Morrison, H. D.; Bures, E. J.; Pelech, S. L. Identification of the Sites in Myelin Basic Protein That Are Phosphorylated by Meiosis-Activated Protein Kinase p44mpk. *FEBS Lett.* **1990**, *273* (1–2), 223–226.

(185) Signalchem. Using Myelin Basic Protein (MBP) for Effective Cell Signaling Research http://www.signalchem.com/resources/technical_bulletin/MBP.pdf (accessed Aug 31, 2016).

(186) de Leon-Boenig, G.; Bowman, K. K.; Feng, J. a; Crawford, T.; Everett, C.; Franke, Y.; Oh, A.; Stanley, M.; Staben, S. T.; Starovasnik, M. a; Wallweber, H. J. a; Wu, J.; Wu, L. C.; Johnson, A. R.; Hymowitz, S. G. The Crystal Structure of the Catalytic Domain of the NF-κB Inducing Kinase Reveals a Narrow but Flexible Active Site. *Structure* **2012**, *20* (10), 1704–1714.

(187) Zhang, J.-H.; Chung, T. D. Y.; Oldenburg, K. R. A Simple Statistical Parameter for Use in Evaluation and Validation of High Throughput Screening Assays. *Journal of Biomolecular Screening*. 1999, pp 67–73.

(188) Congreve, M.; Carr, R.; Murray, C.; Jhoti, H. A “Rule of Three” for Fragment-Based

Lead Discovery? *Drug Discov. Today* **2003**, *8* (19), 876–877.

(189) Erlanson, D. A.; McDowell, R. S.; O'Brien, T. Fragment-Based Drug Discovery. *J. Med. Chem.* **2004**, *47* (14), 3463–3482.

(190) Pajouhesh, H.; Lenz, G. R. Medicinal Chemical Properties of Successful Central Nervous System Drugs. *Neurotherapeutics* **2005**, *2* (4), 541–553.

(191) Kuntz, I. D.; Chen, K.; Sharp, K. a; Kollman, P. a. The Maximal Affinity of Ligands. *Proc. Natl. Acad. Sci.* **1999**, *96* (18), 9997–10002.

(192) Aronov, A. M.; McClain, B.; Moody, C. S.; Murcko, M. A. Kinase-Likeness and Kinase-Privileged Fragments: Toward Virtual Polypharmacology. *J. Med. Chem.* **2008**, *51* (5), 1214–1222.

(193) Mayo, S. L.; Olafson, B. D.; Iii, W. a G.; Eb, E.; El, E. a E. T. DREIDING: A Generic Force Field for Molecular Simulations. *J. Phys. Chem.* **1990**, *94* (26), 8897–8909.

(194) Li, K.; McGee, L. R.; Fisher, B.; Sudom, A.; Liu, J.; Rubenstein, S. M.; Anwer, M. K.; Cushing, T. D.; Shin, Y.; Ayres, M.; Lee, F.; Eksterowicz, J.; Faulder, P.; Waszkowycz, B.; Plotnikova, O.; Farrelly, E.; Xiao, S.-H.; Chen, G.; Wang, Z. Inhibiting NF-κB-Inducing Kinase (NIK): Discovery, Structure-Based Design, Synthesis, Structure-Activity Relationship, and Co-Crystal Structures. *Bioorg. Med. Chem. Lett.* **2013**, *23* (5), 1238–1244.

(195) Chen, G.; Cushing, T. D.; Fisher, B.; He, X.; Li, K.; Li, Z.; McGee, L. R.; Pattaropong, V.; Faulder, P.; Seganish, J. L.; Shin, Y. Alkynyl Alcohols as Kinase Inhibitors. WO2009158011, 2009.

(196) Mortier, J.; Masereel, B.; Remouchamps, C.; Ganeff, C.; Piette, J.; Frederick, R. NF-kappaB Inducing Kinase (NIK) Inhibitors: Identification of New Scaffolds Using Virtual Screening. *Bioorg. Med. Chem. Lett.* **2010**, *20* (15), 4515–4520.

(197) Pandey, A.; Scarborough, R. M.; Matsuno, K.; Ichimura, M.; Nomoto, Y.; Fujiwara, S.; Ide, S.; Tsukuda, E.; Irie, J.; Oda, S. Nitrogeneous Heterocyclic Compounds. WO0216360, 2002.

(198) Gogoll, A.; Oernebro, J.; Grennberg, H.; Baeckvall, J.-E. Mechanism of Apparent Pi-

Allyl Rotation in (Pi-Allyl)palladium Complexes with Bidentate Nitrogen Ligands. *J. Am. Chem. Soc.* **1994**, *116* (8), 3631–3632.

(199) Kang, B.; Kim, M.; Lee, J.; Do, Y.; Chang, S. Trimanganese Complexes Bearing Bidentate Nitrogen Ligands as a Highly Efficient Catalyst Precursor in the Epoxidation of Alkenes. *J. Org. Chem.* **2006**, *71* (18), 6721–6727.

(200) van Asselt, R.; Elsevier, C. J.; Smeets, W. J. J.; Spek, A. L. Zerovalent Palladium and Platinum Complexes Containing Rigid Bidentate Nitrogen Ligands and Alkenes: Synthesis, Characterization, Alkene Rotation and Substitution Reactions. X-Ray Crystal Structure of [Bis((2,6-Diisopropylphenyl)imino)acenaphthene](maleic. *Inorg. Chem.* **1994**, *33* (7), 1521–1531.

(201) Ferro, R.; Milione, S.; Caruso, T.; Grassi, A. Iron(III) Complexes of Bidentate Nitrogen Ligands as Catalysts in Reverse Atom Transfer Radical Polymerization of Styrene. *J. Mol. Catal. A Chem.* **2009**, *307* (1–2), 128–133.

(202) Duff, J. C.; Bills, E. J. 282. Reactions between Hexamethylenetetramine and Phenolic Compounds. Part II. Formation of Phenolic Aldehydes. Distinctive Behaviour of P-Nitrophenol. *J. Chem. Soc.* **1934**, 1305.

(203) Duff, J. C.; Bills, E. J. 273. Reactions between Hexamethylenetetramine and Phenolic Compounds. Part I. A New Method for the Preparation of 3- and 5-Aldehydosalicylic Acids. *J. Chem. Soc.* **1932**, 1987.

(204) Holladay, M. W.; Liu, G.; Rowbottom, M. W. Biaryl Acetamide Compounds and Methods of Use Thereof Related Application. WO2015031613 A1, 2014.

(205) Karuvalam, R. P.; Pakkath, R.; Haridas, K. R.; Rishikesan, R.; Kumari, N. S. Synthesis, Characterization, and SAR Studies of New (1H-Indol-3-Yl)alkyl-3-(1H-Indol-3-Yl)propanamide Derivatives as Possible Antimicrobial and Antitubercular Agents. *Med. Chem. Res.* **2013**, *22* (9), 4437–4454.

(206) Brough, P.; Drysdale, M. 1H-Pyrrolo[2,3-B]pyridine Derivatives Useful as HSP90 Inhibitors. WO2008025947 A1, 2006.

(207) Beckmann, E. Zur Kenntniss Der Isonitrosoverbindungen. *Berichte der Dtsch. Chem. Gesellschaft* **1886**, *19* (1), 988–993.

(208) De Luca, L.; Giacomelli, G.; Porcheddu, A. Beckmann Rearrangement of Oximes under Very Mild Conditions. *J. Org. Chem.* **2002**, *67* (17), 6272–6274.

(209) Clayden, J.; Greeves, N.; Warren, S.; Wothers, P. *Organic Chemistry*, 1st ed.; Rogers, M., Ed.; Oxford University Press, 2001.

(210) Hartwig, J. F. Palladium-Catalyzed Amination of Aryl Halides and Sulfonates. In *Modern Amination Methods*; Wiley-VCH Verlag GmbH: Weinheim, Germany; pp 195–262.

(211) Yang, B. H.; Buchwald, S. L. Palladium-Catalyzed Amination of Aryl Halides and Sulfonates. *J. Organomet. Chem.* **1999**, *576* (1–2), 125–146.

(212) Terrier, F. Rate and Equilibrium Studies in Jackson-Meisenheimer Complexes. *Chem. Rev.* **1982**, *82* (2), 77–152.

(213) Artamkina, G. A.; Egorov, M. P.; Beletskaya, I. P. *Some Aspects of Anionic σ-Complexes*; 1982; Vol. 82.

(214) Caldwell, J. J.; Davies, T. G.; Donald, A.; McHardy, T.; Rowlands, M. G.; Aherne, G. W.; Hunter, L. K.; Taylor, K.; Ruddle, R.; Raynaud, F. I.; Verdonk, M.; Workman, P.; Garrett, M. D.; Collins, I. Identification of 4-(4-Aminopiperidin-1-Yl)-7H-pyrrolo[2,3-D]pyrimidines as Selective Inhibitors of Protein Kinase B through Fragment Elaboration. *J. Med. Chem.* **2008**, *51* (7), 2147–2157.

(215) Caldwell, J. J.; Cheung, K.-M.; Collins, I. Synthesis of 4-(Cyclic Dialkylamino)-7-Azaindoles by Microwave Heating of 4-Halo-7-Azaindoles and Cyclic Secondary Amines. *Tetrahedron Lett.* **2007**, *48* (9), 1527–1529.

(216) Borror, A. L.; Chinoporos, E.; Filosa, M. P.; Herchen, S. R.; Petersen, C. P.; Stern, C. A.; Onan, K. D. Regioselectivity of Electrophilic Aromatic Substitution: Syntheses of 6- and 7-Sulfamoylindolines and -Indoles. *J. Org. Chem.* **1988**, *53* (9), 2047–2052.

(217) Glaser, C. Beiträge Zur Kenntniss Des Acetenylbenzols. *Berichte der Dtsch. Chem. Gesellschaft* **1869**, *2* (1), 422–424.

(218) Sonogashira, K.; Tohda, Y.; Hagihara, N. A Convenient Synthesis of Acetylenes: Catalytic Substitutions of Acetylenic Hydrogen with Bromoalkenes, Iodoarenes and

Bromopyridines. *Tetrahedron Lett.* **1975**, *16* (50), 4467–4470.

(219) Dieck, H. A.; Heck, F. R. Palladium Catalyzed Synthesis of Aryl, Heterocyclic and Vinylic Acetylene Derivatives. *J. Organomet. Chem.* **1975**, *93* (2), 259–263.

(220) Cassar, L. Synthesis of Aryl- and Vinyl-Substituted Acetylene Derivatives by the Use of Nickel and Palladium Complexes. *J. Organomet. Chem.* **1975**, *93* (2), 253–257.

(221) Sonogashira, K. Development of Pd-Cu Catalyzed Cross-Coupling of Terminal Acetylenes with sp2-Carbon Halides. *J. Organomet. Chem.* **2002**, *653* (1–2), 46–49.

(222) Chinchilla, R.; Najera, C. Recent Advances in Sonogashira Reactions. *Chem. Soc. Rev.* **2011**, *40* (10), 5084–5121.

(223) Migawa, M. T.; Hinkley, J. M.; Hoops, G. C.; Townsend, L. B. A Two Step Synthesis of the Nucleoside Q Precursor 2-Amino-5-cyanopyrrolo[2,3-D]Pyrimidin 4-One (PreQo). *Synth. Commun.* **1996**, *26* (17), 3317–3322.

(224) Klepper, F.; Gutsmiedl, K.; Carell, T. A Short and Efficient Synthesis of the tRNA Nucleosides PreQ0 and Archaeosine. *Org. Biomol. Chem.* **2007**, *5* (23), 3821.

(225) Klepper, F.; Polborn, K.; Carell, T. Robust Synthesis and Crystal-Structure Analysis of 7-Cyano-7-Deazaguanine (PreQ0 Base) and 7-(Aminomethyl)-7-Deazaguanine (PreQ1 Base). *Helv. Chim. Acta* **2005**, *88* (10), 2610–2616.

(226) Gangjee, A.; Vidwans, A.; Elzein, E.; McGuire, J. J.; Queener, S. F.; Kisliuk, R. L. Synthesis, Antifolate, and Antitumor Activities of Classical and Nonclassical 2-Amino-4-Oxo-5-Substituted-pyrrolo[2,3- D]Pyrimidines. *J. Med. Chem.* **2001**, *44* (12), 1993–2003.

(227) Llona-Minguez, S.; Mackay, S. P. Stereoselective Synthesis of Carbocyclic Analogues of the Nucleoside Q Precursor (PreQ0). *Beilstein J. Org. Chem.* **2014**, *10*, 1333–1338.

(228) Ju, J.; Kim, D. H.; Bi, L.; Meng, Q.; Bai, X.; Li, Z.; Li, X.; Marma, M. S.; Shi, S.; Wu, J.; Edwards, J. R.; Romu, A.; Turro, N. J. Four-Color DNA Sequencing by Synthesis Using Cleavable Fluorescent Nucleotide Reversible Terminators. *Proc. Natl. Acad. Sci. U. S. A.* **2006**, *103* (52), 19635–19640.

(229) Corbett, M. S.; Kauffman, G. S.; Freeman-Cook, K. D.; Lippa, B. S.; Luzzio, M. J.;

Morris, J. Amine Derivatives Useful as Anticancer Agents and Their Preparation, Pharmaceutical Compositions and Use in the Treatment of Neoplasm. 2008012635 A2, 2008.

(230) Ren, P.; Liu, Y.; Wilson, T. E.; Li, L.; Chan, K.; Rommel, C. Preparation of 1,2-dihydroisoquinolin-1(2H)-one Derivatives as Modulators of PI3 Kinase. 20090312319 A1, 2009.

(231) Cossrow, J.; Guan, B.; Ishchenko, A.; Jones, J. H.; Kumaravel, G.; Lugovskoy, A.; Peng, H.; Powell, N.; Raimundo, B. C.; Tanaka, H.; Vessels, J.; Wynn, T.; Xin, Z. Heterocyclic Compounds Useful as Raf Kinase Inhibitors and Their Preparation, and Use in the Treatment of Raf-mediated Diseases. 20090005359 A1, 2009.

(232) Shimanouchi, T. Tables of Molecular Vibrational Frequencies: Part 6. *Journal of Physical and Chemical Reference Data*. 1973, pp 121–162.

(233) Link, J. O.; Taylor, J. G.; Xu, L.; Mitchell, M.; Guo, H.; Liu, H.; Kato, D.; Kirschberg, T.; Sun, J.; Squires, N.; Parrish, J.; Keller, T.; Yang, Z. Y.; Yang, C.; Matles, M.; Wang, Y.; Wang, K.; Cheng, G.; Tian, Y.; Mogalian, E.; Mondou, E.; Cornpropst, M.; Perry, J.; Desai, M. C. Discovery of Ledipasvir (GS-5885): A Potent, Once-Daily Oral NS5A Inhibitor for the Treatment of Hepatitis C Virus Infection. *J. Med. Chem.* **2014**, *57* (5), 2033–2046.

(234) Li, X.; Tu, Z.; Li, H.; Liu, C.; Li, Z.; Sun, Q.; Yao, Y.; Liu, J.; Jiang, S. Biological Evaluation of New Largazole Analogues: Alteration of Macrocyclic Scaffold with Click Chemistry. *ACS Med. Chem. Lett.* **2013**, *4* (1), 132–136.

(235) Zhao, Y. H.; Le, J.; Abraham, M. H.; Hersey, A.; Eddershaw, P. J.; Luscombe, C. N.; Boutina, D.; Beck, G.; Sherborne, B.; Cooper, I. A. N.; Platts, J. A. Evaluation of Human Intestinal Absorption Data and Subsequent Derivation of a Quantitative Structure-Activity Relationship (QSAR) with the Abraham Descriptors. *J. Pharm. Sci.* **2001**, *90* (6), 749–784.

(236) Cyprotex PLC. Microsomal stability assay http://www.cyprotex.com/admepk/in-vitro-metabolism/microsomal-stability (accessed Jul 12, 2016).

(237) Zhang, Y.; Gupta, A.; Wang, H.; Zhou, L.; Vethanayagam, R. R.; Unadkat, J. D.; Mao,

Q. BCRP Transports Dipyridamole and Is Inhibited by Calcium Channel Blockers. *Pharm. Res.* **2005**, *22* (12), 2023–2034.

(238) *Anti-Inflammatory Drug Discovery*; Levin, J. I., Laufer, S., Eds.; Royal Society of Chemistry, 2012.

(239) Haupt, V. J.; Daminelli, S.; Schroeder, M. Drug Promiscuity in PDB: Protein Binding Site Similarity Is Key. *PLoS One* **2013**, *8* (6).

(240) Savoie, P. R.; Welch, J. T. Preparation and Utility of Organic Pentafluorosulfanyl-Containing Compounds. *Chem. Rev.* **2015**, *115*, 1130–1190.

(241) Blaquiere, N.; Burch, J.; Castanedo, G.; Feng, J. A.; Hu, B.; Lin, X.; Staben, S.; Wu, G.; Yuen, P. Alkynyl Alcohols and Methods of Use. WO2015025026, 2015.

(242) Liu, Q.; Batt, D. G.; Lippy, J. S.; Surti, N.; Tebben, A. J.; Muckelbauer, J. K.; Chen, L.; An, Y.; Chang, C.; Pokross, M.; Yang, Z.; Wang, H.; Burke, J. R.; Carter, P. H.; Tino, J. A. Design and Synthesis of Carbazole Carboxamides as Promising Inhibitors of Bruton's Tyrosine Kinase (BTK) and Janus Kinase 2 (JAK2). *Bioorganic Med. Chem. Lett.* **2015**, *25* (19), 4265–4269.

(243) Giraud, F.; Akué-Gédu, R.; Nauton, L.; Candelon, N.; Debiton, E.; Théry, V.; Anizon, F.; Moreau, P. Synthesis and Biological Activities of 4-Substituted pyrrolo[2,3-A]carbazole Pim Kinase Inhibitors. *Eur. J. Med. Chem.* **2012**, *56*, 225–236.

(244) Martin, S.; Sauvêtre, R.; Normant, J.-F. Reaction of Perhalostyrenes with Organolithium Compounds. Preparation of 1-aryl-1-alkynes Involving the Intermediacy of Aryl Fluoro Acetylenes. *Tetrahedron Lett.* **1982**, *23* (42), 4329–4332.

(245) PerkinElmer. ChemDraw. 2015.

(246) Dassault Systemes Biovia Corp. Pipeline Pilot. 2016.

(247) Accelrys Software Inc. Discovery Studio 4.0. 2013.

(248) Jones, G.; Willett, P.; Glen, R. C.; Leach, A. R.; Taylor, R. Development and Validation of a Genetic Algorithm for Flexible Docking. *J. Mol. Biol.* **1997**, *267* (3), 727–748.

8. Appendix I

In order to explore differences between to the two IKK isoforms, we built a homology model of the IKKα kinase domain based on the crystal structure of IKKβ (chain B, residues 1-309, PDB entry 4KIK), keeping the inhibitor (KSA700 in the pdb file) and water molecules found within 6 Å of the protein-inhibitor complex (**Figure 1**). Both IKK kinase domains were solvated then subjected to extended molecular dynamics, with an average structure generated for the last 21 ns (IKKα) or 26 ns (IKKβ) and subsequently minimised.

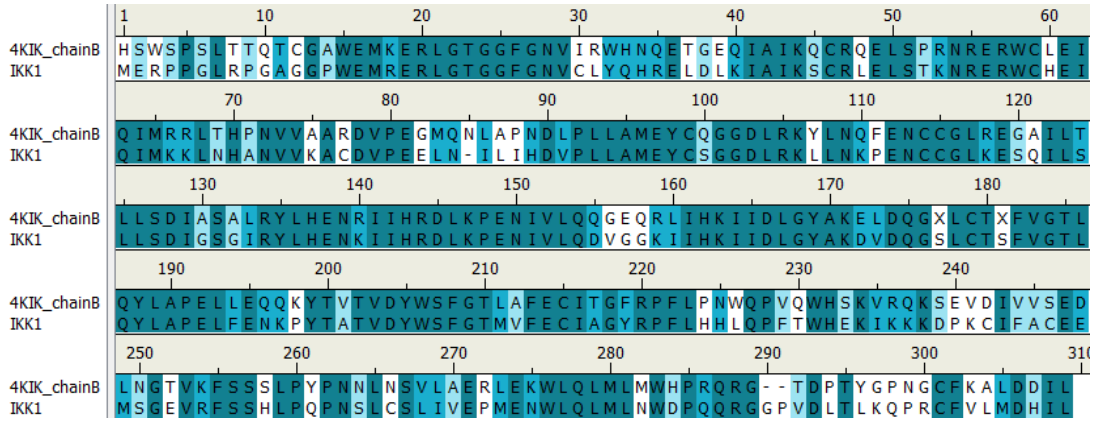

Figure 1. Sequence alignment for the kinase domains of IKKα (IKK1) and IKKβ (IKK2) (4KIK_chainB) showing 61 % of identical residues (coloured in turquoise), a further 14 %

similar residues (polar for polar, hydrophobic for hydrophobic; in light blue) and 25 % non-similar residues (white).

When superimposing the pre-simulated structures of both IKK isoforms, it was striking to see how regions making up the ATP-binding pocket were essentially identical (**Figure 2; Left**). However, analysis of descriptors of motion extracted from their MD trajectories such as residual fluctuation, revealed dynamic differences between the two isoforms that could be exploited in an inhibitor design programme.

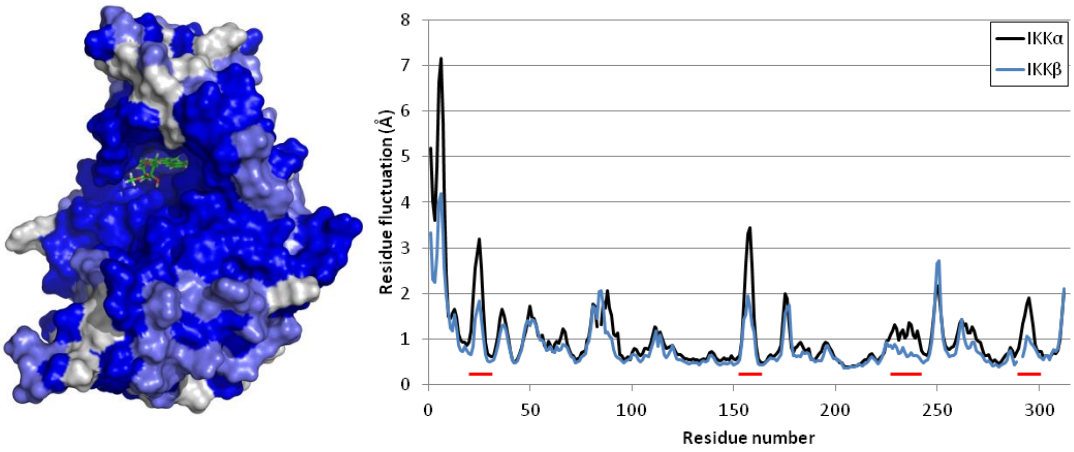

Figure 2 Left: Minimized average structure of IKKβ highlighting residues that are identical (dark blue), similar (light blue) or different (white) with IKKα. The staurosporine analogue present in the PDB file (entry 4KIK, stick model) marks the ATP binding site and is surrounded by dark blue residues. **Right:** Residual fluctuations of IKKα (black line) and IKKβ (blue line) arising during the MD simulations. Several areas were found to be more flexible in IKKα (red underline).

Residual fluctuations obtained from the MD trajectories highlighted areas of the IKKs that acted differently during the simulations (**Figure 2; Right**). Overall, the two isoforms behaved very similarly, but IKKα appeared more flexible in several key areas around the ATP binding site, particularly at the G-loop (residues 22-27) above the site entrance and the loop located just adjacent to the hinge (residues 155-159 in IKKα (VGGKI) and residues 156-160 in IKKβ (GEQRL)). Two residues could account for the differences observed with the G-loop: Pro52 and Gln48 in IKKβ (Thr52 and Leu52 in IKKα) induce a tension at the tip of the first α-helix through proline's intrinsic structure and the engagement of the glutamine side chain in a reciprocal H-bond dimer arrangement with the side chain amide of Asn28 (**Figure 3**). This asparagine is located at the end of the G-loop and its interaction with Gln48 restrained the G-loop movement by more than 1 Å in IKKβ when compared with IKKα. A different dynamic behaviour was observed with IKKα, as the equivalent residues do not impose restraints on the G-loop movements: Thr52 has no rigid turn capability like Pro52 in IKKβ and the side chain of Leu48 seeks a hydrophobic environment and will not engage in H-bond formation with Asn28, leaving the side chain of this latter residue free to make

interactions in the ATP binding site of IKKα (as opposed to being sequestered by Gln48 in IKKβ) (**Figure 3**). The other interesting difference was related to the VGGKI (residues 155-159) loop in IKKα (residues GEQRL (number 156-160) in IKKβ). In this case, one residue is responsible for the change observed in residual fluctuation: Lys158 in IKKα is replaced by Arg159 in IKKβ. The slightly longer arginine side chain and its bifurcate H-bonding capacity forms a reciprocal H-bond dimer with the side chain carboxylate of Asp128 in IKKβ that is maintained throughout the simulation, whilst the equivalent lysine in IKKα never engages in a strong interaction with the equivalent Asp127 in IKKα (**Figure 4**). This interaction in IKKβ is responsible for tethering the 156-160 loop to α-helix 3 (Asp128 is located in the middle of this helix), thus reducing its flexibility compared with IKKα.

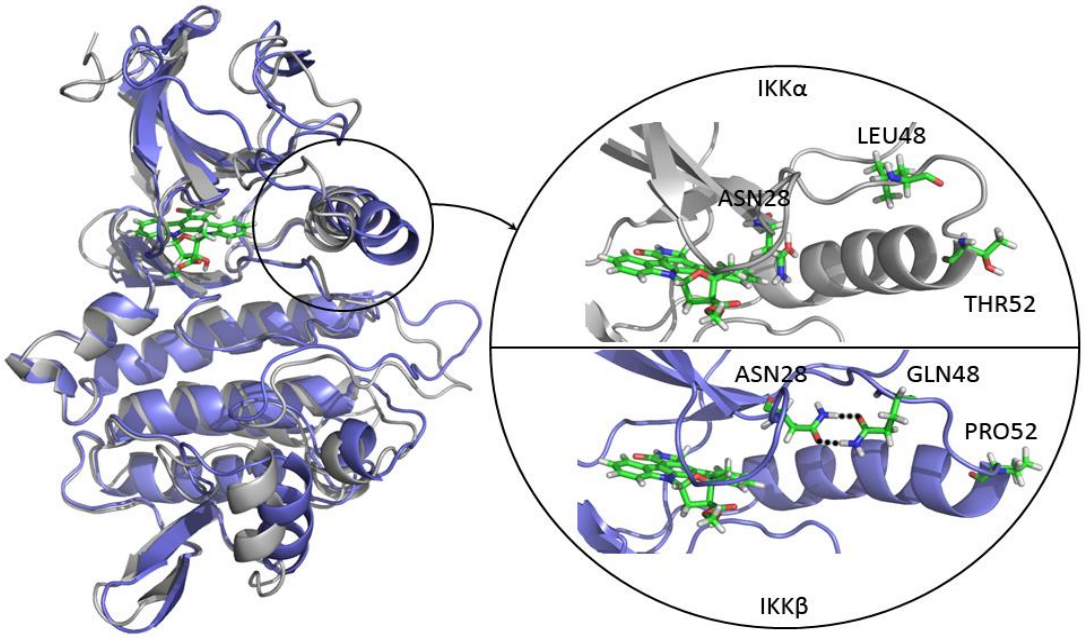

Figure 3. Superimposition of IKKα (white) and IKKβ (blue) highlighting the differences near/in the ATP binding site (marked by the staurosporine analogue as a stick model) between the two isoforms. The expanded area shows equivalent residues in IKKα (ASN28, LEU48 and THR52) and IKKβ (ASN28, GLN48 and PRO52) engaged in different interactions/structural effects resulting in ASN28 being available to interact with putative ligands in the binding pocket of IKKα but not IKKβ.

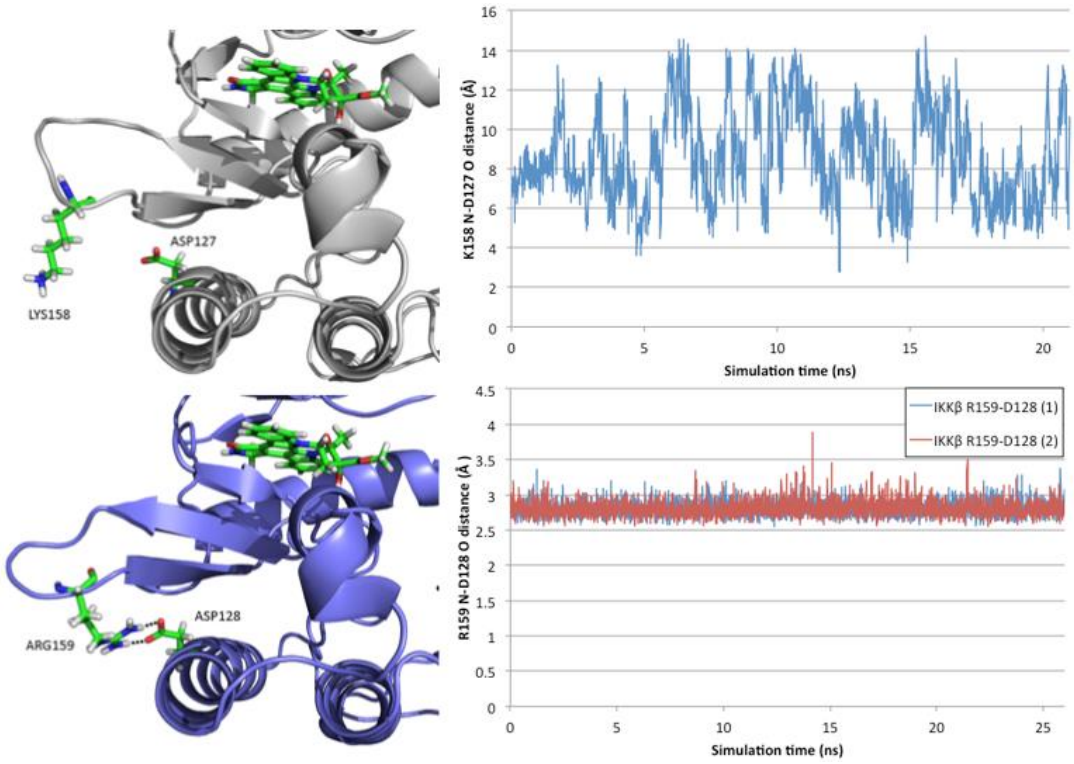

Figure 4. **Left:** Structure of the loop located below the active site in IKKα (white) and IKKβ (blue) and its relationship with α-helix 3 residue ASP127 (IKKα)/ASP128 (IKKβ). In IKKβ, ARG159 makes a reciprocal hydrogen bond dimer interaction with ASP128, whereas in IKKα, LYS158 has no close interactions with ASP127. **Right:** Side chain amine nitrogen (LYS158 (IKKα)/ARG159 (IKKβ)) to side chain acid oxygen (ASP127 (IKKα)/ASP128 (IKKβ)) distance throughout the equilibrated phase of the simulation.

With respect to putative inhibitor binding, the implications for isoform selectivity of these two sets of differences in the ATP site are two-fold: firstly, it should be possible to design small molecules that target the free Asn28 side chain amide presented at the back of the IKKα pocket that is otherwise engaged in IKKβ (Figure 3); and secondly, because the ATP binding pocket has greater flexibility in IKKα, it has the potential to accommodate larger substituents, particularly below the G-loop.